

MULTISPECTRAL REFLECTANCE AND IMAGE TEXTURAL SIGNATURES
OF ARID ALLUVIAL GEOMORPHIC SURFACES IN THE CASTLE DOME MOUNTAINS
AND PIEDMONT, SOUTHWESTERN ARIZONA

by

Ernest Hsiao Hsin Shih

A Thesis Submitted to the Faculty of the
DEPARTMENT OF GEOSCIENCES
In Partial Fulfillment of the Requirements
For the Degree of
MASTER OF SCIENCE
In the Graduate College
THE UNIVERSITY OF ARIZONA

1 9 8 2

Copyright 1982 Ernest Hsiao Hsin Shih

Call No.

BINDING INSTRUCTIONS

INTERLIBRARY INSTRUCTIONS

E9791
1982
533

Author: Shih, E.

Title:

COLOR:

M.S.

Dept.

RUSH _____

PERMABIND _____

PAMPHLET _____

GIFT _____

POCKET FOR MAP _____

COVERS

Front _____ Both _____

REFERENCE _____

Other _____

Special Instructions - Bindery or Repair

5/4/84

L-279

Call No.

BINDING INSTRUCTIONS

INTERLIBRARY INSTRUCTIONS

E9791
1982
533

Author: Shih, E.

Title:

COLOR:

M.S.

Dept.

RUSH _____

PERMABIND _____

PAMPHLET _____

GIFT _____

POCKET FOR MAP _____

COVERS

Front _____ Both _____

REFERENCE _____

Other _____

Special Instructions - Bindery or Repair

5/4/84


L-279

STATEMENT BY AUTHOR

This thesis has been submitted in partial fulfillment of requirements for an advanced degree at The University of Arizona and is deposited in the University Library to be made available to borrowers under rules of the Library.

Brief quotations from this thesis are allowable without special permission, provided that accurate acknowledgment of source is made. Requests for permission for extended quotation from or reproduction of this manuscript in whole or in part may be granted by the copyright holder.

SIGNED: _____



APPROVAL BY THESIS DIRECTOR

This thesis has been approved on the date shown below:

Vinton R. Baker
V. R. BAKER

Professor of Geosciences

14 Dec. 1982

Date

ACKNOWLEDGMENTS

I would like to thank my parents for their past and continuing unconditional support and constant encouragement, without which this thesis would not have been possible.

Dr. Robert Schowengerdt was my instructor in image processing applied to remote sensing. Without his constant support, consultation and prodding, this work would not have been completed.

Dr. William B. Bull was responsible for introducing me to the fascinating geomorphic peculiarities of the desert in southwestern Arizona. His systematic approach to the classification of arid alluvial deposits paved the way for my research efforts.

From the initial stages of my research to the completion of my writing, the Applied Remote Sensing Program of the Office of Arid Lands Studies constantly supported my efforts by providing research assistantships, acquiring image data, and supporting my efforts in the field. They provided me with an office, which was an invaluable refuge for my thesis writing. For this I thank Dr. Charles Hutchinson, present Director, and Dr. Dave Mouat, past Director, of the Applied Remote Sensing Program. In addition, I would like to thank all the ARSP staff for helpful discussions concerning remote sensing.

I am indebted to Dr. Robert Hunt, Director of DIAL (Digital Image Analysis Laboratory), for allowing me to use the Laboratory. My computer

programming benefitted greatly from contact with image processing students working at the Laboratory. Robin Strickland, Rob Gray, and Tom Bruegge were particularly helpful.

I am particularly grateful to Dr. P. N. Slater for use of the Microdensitometer and Integrating Sphere Reflectometer (ISR) at Optical Sciences. Mike Jacobsen and R. D. Lamoreaux graciously took the time to train me in the use of the ISR.

The Geological Society of America Grant No. 2528-79 provided the initial funding for this project. The research was partially supported by Grant No. 14-08-0001-G-664 from the U.S. Geological Survey, EROS program. Field work on the Kofa Game Range was made possible by permission of the U.S. Department of the Interior, Fish and Wildlife Service, and was supported in part by the Department of Geosciences, University of Arizona.

I would like to thank my first advisor, Dr. William B. Bull and my present advisors, Dr. Victor Baker, Prof. Terah Smiley, and Dr. Robert Schowengerdt for taking the time to review and comment on this thesis.

TABLE OF CONTENTS

| | Page |
|--|-------|
| LIST OF ILLUSTRATIONS | .viii |
| LIST OF TABLES | xii |
| ABSTRACT | .xiii |
| CHAPTER | |
| 1. INTRODUCTION | 1 |
| Objectives | 2 |
| The Study | 6 |
| Image Data | 7 |
| The Study Area | 9 |
| Physiography | 9 |
| Climate | 12 |
| Vegetation | 13 |
| Geology | 15 |
| Geologic/Geomorphic Sketch Map | 17 |
| Arid Soils and Geomorphic Surfaces | 22 |
| Desert Pavement | 24 |
| Desert Varnish | 26 |
| Geomorphic Classification | 29 |
| The Idealized Cycle of Desert Pavement Formation and its Influence on Soil Reflectances | 30 |
| Landsat Remote Sensing | 34 |
| The Landsat System | 34 |
| Landsat MSS Radiance Measurements | 36 |
| Scattering | 38 |
| Causes of Color | 39 |
| Rock Reflectance | 42 |
| Soil Reflectance | 42 |
| Plant Reflectance | 46 |
| Mixed Reflectance Components within the Resolution Cell | 48 |
| Radar Remote Sensing | 51 |
| SLAR Systems | 53 |
| SAR Systems | 57 |
| Polarization | 61 |

TABLE OF CONTENTS -- Continued

| | Page |
|---|---------|
| Parameters of Radar Backscatter | 62 |
| Surface Slope and Geometry | 64 |
| Surface Roughness | 65 |
| Dielectric Constant and Radar Penetration | 68 |
| Geometric and Cavity Resonance | 69 |
| 2. FIELD AND LABORATORY INVESTIGATIONS | 71 |
| Geomorphic Reconnaissance | 73 |
| Site Location and Field Descriptors | 78 |
| Site Descriptions | 81 |
| Site 1. Q4 Stream Channel | 81 |
| Site 2. Q2pd Erosional Bedrock Basin | 82 |
| Site 3. Q3/Q4 Mountain Wash | 84 |
| Site 4. Q2c Pavement | 85 |
| Site 5. Q2b Dissected Desert Pavement | 87 |
| Site 6. Q2a Dissected Pavement | 89 |
| Site 7. Q2pd Degraded Desert Pavement | 92 |
| Site 8. Q2pd Degraded Desert Pavement | 93 |
| Site 9. Q2c Pavement | 95 |
| Site 1B. Q2pd Fine-Grain Disturbed Pavement | 96 |
| Site B1. Q3/4 Sandy Alluvial Flat | 98 |
| Site 61B. Q3a Lightly Varnished Flat Pavement | 99 |
| Site 65.35. Q2c Dark Pavement with Encroaching Vegetation | 101 |
| Site 70.25. Q2c Dark Pavement with Intermediate Volcanic Composition | 102 |
| Site 70+P. Q2c Dark Pavement in Intermediate Volcanics | 102 |
| Site 70+D. Q3/4 Coarse Erosional Surface | 103 |
| Site 83.7. Q2c Dark Pavement | 105 |
| Laboratory Reflectance of Desert Varnish | 106 |
| Varnish Reflectance and Oxide Abundance | 115 |
| Field Spectral Radiometer Readings | 119 |
| Field Spectral Reflectances | 123 |
| Summary and Correlation of Field Data | 132 |
| 3. IMAGE INVESTIGATIONS | 138 |
| Preprocessing | 138 |
| Landsat | 138 |
| Radar | 139 |
| Registration | 139 |
| Image Site Investigation | 140 |
| Landsat, Field Correlations | 142 |

TABLE OF CONTENTS -- Continued

| | Page |
|--|------|
| Radar, Field Correlations | 153 |
| Radar-Roughness Map | 158 |
| Image Texture | 162 |
| LEAD Texture Extraction | 164 |
| Textural Features | 167 |
| Image Classification | 170 |
| Supervised Bayesian Classification | 171 |
| Spectral/Geomorphic Classes | 172 |
| Classification Training and Feature Selection | 175 |
| Classification Results | 176 |
| 4. SUMMARY AND CONCLUSIONS | 184 |
| APPENDIX A: IMAGE SOURCES AND SPECIFICATIONS | 189 |
| APPENDIX B: FIELD DATA | 194 |
| Lithology Determination | 195 |
| Particle Size Distribution Determination | 205 |
| APPENDIX C: RADIOMETRIC INSTRUMENTATION AND DATA | 212 |
| Integrating Sphere Reflectometer | 213 |
| RMR-10 | 218 |
| Spectral Radiometer Data | 219 |
| Spectral Plots Output from Program PLOTS | 233 |
| APPENDIX D: SOFTWARE AND IMAGE DATA | 242 |
| Software Summary | 243 |
| Output from TRAINS: Site Information | 245 |
| Scene Light/Dark Correction | 274 |
| REFERENCES CITED | 275 |

LIST OF ILLUSTRATIONS

| Figure | Page |
|--------|---|
| 1. | Band 5 of Landsat scene E-1194-17391-501 8 |
| 2. | SAR data, USAF flight 665-079 pass 11 8 |
| 3. | Location of study area 10 |
| 4. | Portion of Wilson's 1933 map containing thesis study area 16 |
| 5. | Geologic/geomorphic sketch map 19 |
| 6. | Hypothetical surface of reflectance as a function of age and lithology in arid alluvial surfaces 31 |
| 7. | The effect of particle size on reflectance as illustrated by the bidirectional reflection spectra from four different particle sizes of the mineral beryl 41 |
| 8. | Reflectance of 4 rock types 43 |
| 9. | Three types of soil reflectance curves 45 |
| 10. | Examples of the errors introduced when the MSS scans bars of different radiance with a width of 69 m 50 |
| 11. | The microwave atmosphere and common radar frequencies . . . 52 |
| 12. | Basic geometry of a SLAR system 55 |
| 13. | Block diagram of a SAR system 59 |
| 14. | Azimuth and range discrimination in an unfocused SAR . . . 60 |
| 15. | Orthophotoquad mosaic with outline of study area and location of field sites 72 |
| 16. | A generalized cross-section illustrating the terrace relationships in the mountain valleys 74 |

LIST OF ILLUSTRATIONS -- Continued

| Figure | Page |
|--|------|
| 17. A generalized cross-section illustrating the alluvial geomorphic surfaces across the valley bottom | 74 |
| 18. Site 1, Q4 stream channel | 83 |
| 19. View east overlooking site 2, erosional bedrock basin . . . | 83 |
| 20. View west overlooking site 3 | 86 |
| 21. Site 4, Q2c pavement | 86 |
| 22. View NW from site 5, Q2b pavement, to tuff hill | 90 |
| 23. View NE from site 6, Q2a pavement | 90 |
| 24. Surface of site 7 (Q2pd), degraded pavement | 94 |
| 25. Surface of site 8 (Q2pd), degraded pavement | 94 |
| 26. Surface of site 9, Q2c pavement | 97 |
| 27. Surface of site B1, sandy alluvial flat (Q3/Q4) | 100 |
| 28. Site 65.35, Q2c dark pavement | 100 |
| 29. Site 70+P, dark Q2c pavement | 104 |
| 30. Site 70+D, Q3/4 coarse erosional surface | 104 |
| 31. Spectral plot of Colorado River andesite (#1) | 109 |
| 32. Spectral plot of Colorado River amphibolite (#2) | 110 |
| 33. Spectral plot of Pinecate basalt (#3) | 111 |
| 34. Spectral plot of Sheep Mountain quartz monzonite (#4) . . . | 112 |
| 35. Spectral plot of Sheep Mountain amphibolite (#5) | 113 |
| 36. Radiometrics RMR-10 multispectral radiometer shown in field operation | 120 |
| 37. Field spectral signature of volcanic bedrock | 125 |

LIST OF ILLUSTRATIONS -- Continued

| Figure | Page |
|---|------|
| 38. Field spectral signature of older Pleistocene pavements . . | 126 |
| 39. Field spectral signature of young Pleistocene pavements . . | 128 |
| 40. Field spectral signature of disturbed pavements | 129 |
| 41. Field spectral signature of modern alluvial surfaces . . . | 131 |
| 42. The relationship between field reflectance and average particle size | 135 |
| 43. Band 4, 5, 6 false color composite with field sites outlined | 141 |
| 44. Registered radar with field sites outlined | 141 |
| 45. Linear regression between Band 4 field and Landsat data . . | 146 |
| 46. Linear regression between Band 5 field and Landsat data . . | 147 |
| 47. Linear regression between Band 6 field and Landsat data . . | 148 |
| 48. Linear regression between Band 7 field and Landsat data . . | 149 |
| 49. Influence of shadowing on reflectance with a 31° solar elevation | 151 |
| 50. Linear regression between RADN and 2P+3V | 157 |
| 51. Radar roughness map | 159 |
| 52. LEAD texture extraction | 165 |
| 53. TCC display of 7x7 radar textural feature | 168 |
| 54. TCC display of 9x9 Landsat textural feature | 168 |
| 55. Grey level plots of classes 2, 4, 5, 6 and 7 | 178 |
| 56. Grey level plots of classes 1 and 10 | 178 |
| 57. S4 map | 181 |
| 58. STL4 map | 181 |

LIST OF ILLUSTRATIONS -- Continued

| Figure | Page |
|------------------------|------|
| 59. STL7 map | 182 |
| 60. STR4 map | 182 |

LIST OF TABLES

| Table | Page |
|-------|---|
| 1. | Geologic/geomorphic classes of sketch map 20 |
| 2. | Correlations between reflectance and oxide abundance for fresh rock surfaces (bnF), varnished surfaces (bnV), and fresh and varnished surfaces combined (bnV+F) 117 |
| 3. | Spectral and compositional data for correlation analysis 117 |
| 4. | Summary table of field descriptors 133 |
| 5. | Image data from field sites 143 |
| 6. | Landsat corrected DN (Bn), radiometer reflectance (aRn), and linear regression for 12 sites 145 |
| 7. | Ranked mean radar DN (RADN), particle size (P), and vegetation density (V) correlations 155 |
| 8. | Classes of radar roughness map 160 |
| 9. | Spectral/geomorphic class descriptions used in classifications 173 |
| 10. | Performance based on training site statistics 177 |

ABSTRACT

Landsat Multispectral Scanner (MSS) and airborne Synthetic Aperture Radar (SAR) data can be used, in digital format, to directly map arid geomorphic surfaces if significant field parameters are correlated with image attributes.

Data obtained in the laboratory and field indicate that the shape and amplitude of desert reflectance curves vary systematically as a function of geomorphic age, particle size and lithology. Desert varnish is characterized by two reflectance curves which are highly correlated with SiO and FeO abundances. SAR backscatter from alluvial geomorphic surfaces, when averaged, is highly correlated to a weighted addition of particle size and vegetation density.

Image texture is extracted with an algorithm which measures the local density of thresholded high (spatial) frequency elements. Several supervised statistical classifications using original spectral and extracted textural data sets produced several image maps. The classification with seven Landsat spectral and textural features produced the best results.

CHAPTER 1

INTRODUCTION

The arid terrain is one of elemental nakedness and geometric elegance. Unlike its humid temperate counterparts the desert is not softened by its biology, but rather its rugged rock faces, stream channels and valley flats record the logic, the rhythm and the interplay of terrestrial forces. To understand the pattern of rock weathering and erosion, to grasp the geometry of alluvial deposits and soil formation is to learn about the past and present environment.

The warm desert environment is one of extremes in temperature and precipitation. Seemingly interminable cycles of cold nights and scorchingly hot days are broken only by short bursts of often violent storms. Under such rigors plants either adapt or disappear. To map plant community and distribution is to map the specific conditions to which they are keyed.

The desert may be likened to a system composed of mineral and biologic elements. Powered by the forces of natural process and shaped by the response of its elements to these processes, the desert possesses an architecture which is the sum product of past and present processes.

As development pressures begin to affect arid lands in this country and abroad, the need for detailed knowledge of arid soil, terrain and vegetation conditions becomes increasingly important. While

modern development patterns are often ill-designed and poorly adapted to natural conditions, the desert is and has been a self-regulating system marked by beauty, economy and balance. To understand the desert, its processes, its morphologic and biologic adaptations is to learn how to live with aridity.

This study is an attempt to understand, in part, this system, the natural warm desert, by using the radiant energy reflectance patterns of its elements to -- in effect -- map themselves. Using modern society's high-technology tools, satellite scanners, airborne imaging radar, and computer processing, and guided by the natural science tradition of empirical and intuitive reasoning, I, above all, produce this study as a modern homage to the primitive, the pristine and intricately complex arid landscape.

Objectives

Due to the lack of moisture and vegetation, the surface morphology, color and mechanical texture of arid alluvial surfaces are indicators of soil development and relative age. In southwestern Arizona, a suite of alluvial geomorphic surfaces ranging in age from early Pleistocene to late Holocene have been identified and correlated on the basis of surface morphology, sedimentology, and soil development (Bull, in preparation; Schenker, 1977; Fleischhauer, 1978; McHargue, 1981).

While diagnostic horizons for the dating of desert soils cannot be observed on the surface, surficial features such as surface roughness, relief, the darkness of "desert varnish," the formation and degradation

of "desert pavement," and the abundance and type of vegetation are features which are observable and can be related to the age of the surface, its soil properties, and the geomorphic activity of the surface.

Sparse and uneven distribution of vegetation allows the use of vegetation to map certain age deposits. Dense riparian vegetation, for example, is indicative of active ephemeral channels. The lack of vegetation on desert pavement, which is related to the high alkalinity of the soil (Musick, 1975) is an expression of a certain maturity of soil development. The combination of the two in paved areas is proportional to the amount of dissection active on that surface. Desert surfaces which are degraded are often littered with calcium carbonate clasts. These tend to lighten the overall reflectance of the surface. Older surfaces which are deeply dissected have a topography which characteristically appear as ridge and ravine or hill and valley terrains. These are strongly contrasted in terms of image texture, surface roughness, image shadow content, and surface bidirectional reflectance characteristics to the flat dark pavement surfaces which tend to have a lower reflectance and surface roughness. They also differ from other surfaces by their characteristic vegetative communities.

In short, arid alluvial geomorphic surfaces have specific surficial and reflectance properties which are related to pedologic, ecologic and sedimentologic parameters of geomorphic, land use and resource management significance.

Landsat multispectral scanner (MSS) imagery is sensitive to vegetation, rock and soil color (McGinnies et al., 1974; Sabins, 1978) while synthetic aperture side-looking radar (SAR) is sensitive to slope, particle size, surface roughness, and surface geometry (Schaber, Berlin and Brown, 1976; Daily et al., 1978). If the assemblage of surficial parameters defining the response of the individual picture element (PIXEL) on MSS and SAR data can be differentiated from each other and correlated with morphogenetically significant classes, then these image signatures can be exploited for alluvial geomorphic mapping purposes.

Several of the mapping informational criteria such as local topography, drainage density, vegetation density and distribution are manifested in image data as tonal variation, structure and pattern. The addition of Landsat-derived image textural features to spectral features allows for the differentiation of classes spectrally similar but texturally dissimilar. Due to the high resolution of SAR imaging systems and its sensitivity to surface terrain parameters, geologic and vegetation classes in SAR imagery are often defined by texture-tone attributes rather than by tone alone (Estes et al., 1975; MacDonald, 1969; Simonett, 1968). Consideration of this characteristic of SAR data coupled with the significance of surface morphology in arid alluvial surfaces suggests the use of textural features derived from SAR data as another valuable secondary image data source for geomorphic mapping.

A digital multispectral approach to image analysis allows the use of imagery not only as a photo-interpretable end product but also

as an "n" dimensional matrix of individually accessible data elements amenable to transformations and manipulations like any group of real numbers. Images with relatively coarse resolution for photo-interpretation are in fact a dense grid of sample measurement vectors when considered from the digital remote sensing viewpoint.

The addition of secondary features such as texture feature images in effect increases the magnitude of the measurement vector. If these features are relatively uncorrelated with the original spectral features but are sensitive to significant geologic or vegetative information features then increases in computer classification accuracy are the result.

Digital image processing applied to remote sensing incorporates two different approaches to the treatment of image data: image enhancement, and image classification. Image enhancement is the manipulation of image data sets to enhance various image attributes for either photo-interpretation or image classification. Computer image classification is the classifying of "n" dimensional data sets in a manner prescribed by the classification algorithm.

The primary advantage of the digital classification approach lies in its speed, precision, uniformity, objectivity, repeatability, and in its ability to "see" multi-dimensionally. Disadvantages are that suitable algorithms for the utilization of image shape, size, pattern, shadow and association elements, parallax viewing, and collateral information-- all attributes used by human interpreters--

do not exist.¹ On the other hand, human interpreters vary greatly from one another and are subjected to psychological biases, fatigue, and limited tonal range discrimination (Estes and Simonett, 1975; Colwell, 1978).

The objectives of this thesis are to investigate and isolate specific geologic and geomorphic-ecologic variables which control the spectral signatures of desert alluvial geomorphic surfaces in Landsat MSS data and in X band SAR imagery; to use these signatures as guidelines in the application of image enhancement techniques for photo-interpretation and for statistical image classification; and to extract and use textural features as well as tonal features in a multivariate maximum likelihood Bayesian classification to produce detailed, accurate and morphogenetically significant maps of alluvial geomorphic surfaces in the study area.

The Study

The study is divided into two parts: the first part described in Chapter 2 is the acquisition and analysis of field and laboratory data which forms the basis for understanding the nature of desert surface reflectance patterns and their morphological significance. Generally these investigations involve the qualitative and quantitative description of each surface site, the spectral reflectances of their constituents and their plant, soil and terrain characteristics. An integrating sphere spectral radiometer and a portable spectral radio-

1. Many studies in texture feature classification have been performed, but no overall satisfactory techniques developed. These are reviewed in later sections. Recently contextual classifiers have been reported by Siegel, Swain and Smith (1980) and Tilton, Swain and Vardeman (1980).

meter were used to obtain spectral signatures of soil, plant and surface constituent. Details concerning radiometric instrumentation used are provided in Appendix C.

Standard geomorphic, pedologic, and botanical descriptions with emphasis on variables to which Landsat and SAR sensors are most sensitive to were used to characterize and classify the surface. Investigations on the density of plant communities, the particle size of soil surface clasts and the variability of the surface were made to test the sensitivity of Landsat, SAR and their secondary images to variations in these parametric measurements.

The second part, described in Chapter 3, is the analysis and manipulation of computer-formatted Landsat and SAR imagery and the secondary image products produced from them.

The remainder of this first chapter outlines the larger geographical and multi-disciplinary context of this study. The closing chapter, Chapter 4, discusses the methodologies and conclusions of this thesis in light of possible future applications.

Image Data

Aside from orthophotoquads used for photointerpretation and location, two types of imagery were used: the four-band Landsat MSS data (Figure 1) and the declassified U.S. Air Force synthetic aperture airborne side-looking radar (SAR) (Figure 2). The Landsat MSS scene used in this study is scene E-1194-17391 taken on February 2, 1973 with a solar azimuth of 143° and a sun elevation of 31° . The image was obtained on computer-



Figure 1. Band 5 of Landsat scene E-1194-17391-501.



Figure 2. SAR data, USAF flight 665-079 pass 11.

compatible tape (CCT) from EROS data center, Sioux Falls, South Dakota. Band 5 of the scene is photographically reproduced with the thesis site outlined in Figure 1.

The Radar data was obtained as a film transparency from the repository of USAF radar imagery at Goodyear Aerospace, Litchfield Park, Arizona. The data was acquired on November 5, 1964, flight 665-079, pass 11 with a radar look to the south at a depression angle of 8 to 4 degrees. The radar is synthetic aperture, X band, HH polarized with a resolution of about 15m (50 ft) at the film scale of 1:480,000. The film contains an initial ground sweep geometric correction and has been photographically reproduced with the thesis site outlined in Figure 2. Additional information on image specifications and sources are provided in Appendix A.

The Study Area

The thesis study site is an area of approximately 296 square kilometers (110 miles²) located in the hot arid desert of southwest Arizona (Figure 3). The site is centered at approximately 114° W. longitude and 33° 05' N. latitude and ranges in elevation from a height of 743m (2439 ft) to a low of 213m (700 ft) above sea level.

Physiography

Located within the Kofa Game range boundaries, the site is situated in a large NW-SE elongated basin which opens south into the Gila river valley. Forming the southwestern and western boundaries of the basin are the Castle Dome mountains. These mountains are a blocky, irregular mass of steep-sided ridges, peaks, spires and towers, the

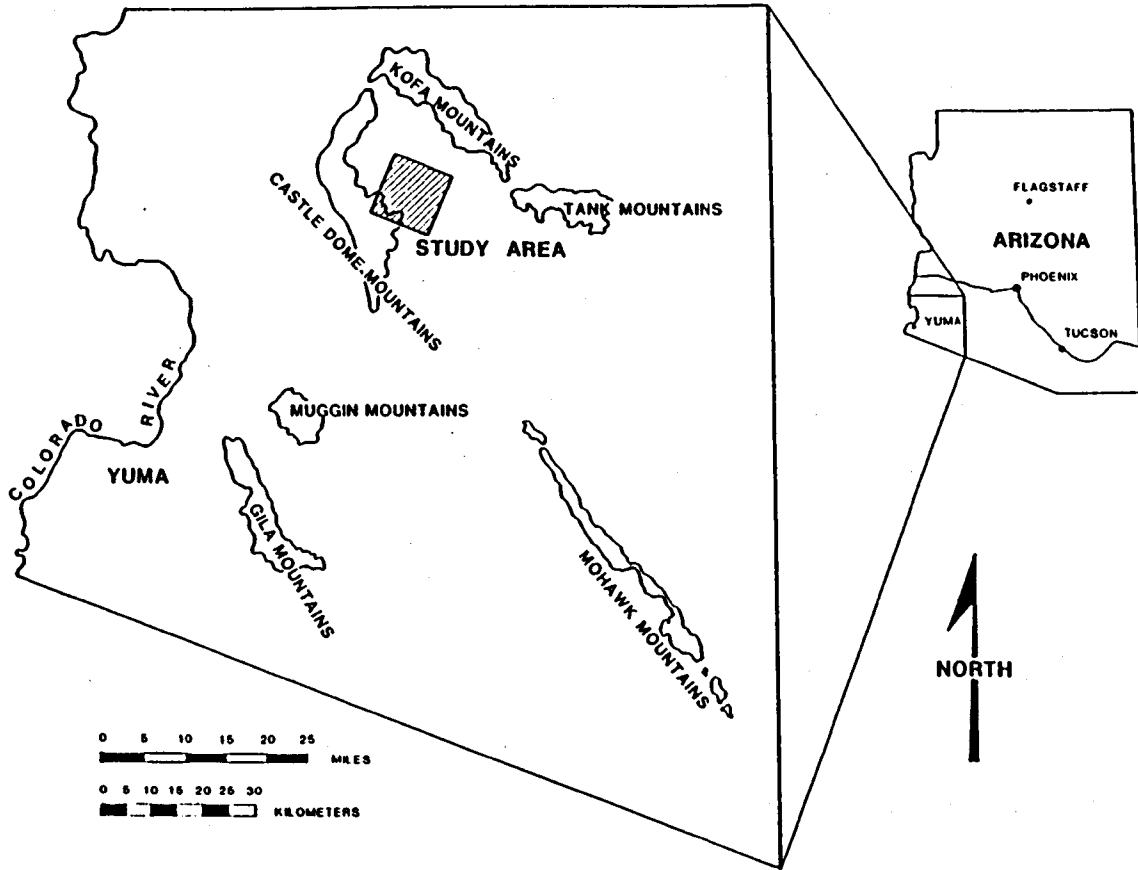


Figure 3. Location of study area.

highest of which, at an elevation of 1156m (3792 ft) is the Castle Dome peak. The Castle Dome mountains present an irregular mountain front to the northeast where the juncture with its north sloping pediment plain is articulated by a series of canyon and valley reentrances, large dissected channels and isolated pediment inselbergs.

To the northeast, the basin is bounded by the Kofa mountains. These mountains, capped by the 1472m (4828 ft) Kofa Peak appear strikingly monolithic at its northernmost point. This monolithic facade is broken only by short, structurally controlled, steep walled canyons some of which contain Arizona's only native palm trees. In contrast to the Castle Dome mountains, the Kofa mountains present a smooth linear mountain front to the basin with small valley reentrances, a steep short pediment plain, and few inselbergs. The mountain front, however, becomes more irregular toward the southern end of the range as the mountain mass itself becomes more dissected and irregular.

The basin closes to the northwest in a wide semi-circular arc formed by the northern Castle Dome mountains, the Kofa mountains, and the low rounded Livingston hills which nearly bridges the two large ranges. Thus constricted, the basin plain ranges in elevation from 610m (2000 ft) at the head of the watershed to 183m (600 ft) where it opens into the Gila river valley.

The study site is situated near the middle of the basin mostly on the northeast pediment plain of the central Castle Dome mountains. Contained in the study site are part of the Castle Dome mountains, the

pediment plain and several inselbergs, and a portion of King valley, the basin axial stream system.

Instead of a dendritic pattern, the axial stream system, for most of its length is a bundle of anastomosing channels with little apparent contribution by tributaries. The complex of small tributaries draining both pediment plains join the King valley system at large angle confluences, often at 90 degrees. Topographic contour lines in the basin express this fact by a pattern of segmented lines rather than a continuous curve across the valley with one line segment for each pediment slope and a line segment for the slope of the axial stream. This pattern disappears near the head of the watershed and at its mouth. The dendritic pattern at the head of the watershed suggests that most of the water and sediment load carried by the stream system is derived from the large semi-circular head of the watershed with little apparent contribution from small mountain front watersheds. The change from dendritic to braided stream system is probably a function of increasing sediment load relative to discharge in the downstream direction.

Climate

The study site is located in the hot subtropic Sonoran desert at the boundary between the extremely arid and arid desert as classified by Meigs (1953). With a rainfall average ranging from 109

to 185 mm (4.3 to 7.3 inches) and an average mean annual temperature of 22 degrees C (72 F), the climate is both hot and dry².

As is typical of hot arid deserts the climate is characterized by extremes in temperature and precipitation. High summer temperatures can reach 48 C (118 F) with a diurnal temperature range of 16 C (30 F) (Sellers and Hill, 1974). Rainfall can be very localized in both time and space such that a single rainfall in one locality may equal the entire mean annual precipitation while nearby localities receive little or no rain.

Nevertheless, there is a seasonality in precipitation with about half of the rain falling in the winter and the remainder falling in the late summer (Sellers and Hill, 1974). The winter rains originate from Pacific air masses and are usually steady and penetrating. Summer rains originate from the Gulf of Mexico and the Gulf of California and are characterized by short, torrential thunderstorms associated with heavy runoff (Kearny and Peebles, 1960).

Vegetation

Brown (1973) has mapped the area as falling into two subdivisions of the Sonoran Desertscrub Natural Vegetative community: The Arizona Upland subdivision and the Lower Colorado subdivision. These two subdivisions interdigitate with the primarily creosote

2. The average rainfall range and the average mean annual temperature are respectively interpolated from, and averaged from summary data for the three nearest stations as reported in Sellers and Hill (1974). These are: 6.15 inches/yr and 72.9 F at altitude 1775 ft in the Kofa mountains; 3.52 inches/yr and 73.5 F at altitude 324 ft in Yuma Proving Grounds; and 3.84 inches/yr and 69.5 F at altitude 324 ft in Tacna.

(Larrea tridentata) -bursage (Ambrosia dumosa) Lower Colorado desert-scrub in the sandy soils of the valley and plain and the primarily paloverde (Cercidium sp.) -saguaro (Carnegiea gigantea) or paloverde-cactus Arizona Upland desertscrub on the rocky slopes and ranges (Lowe and Brown, 1973).

Most of the vegetation is restricted to riparian settings either in very dense communities along the flanks of major stream channels, in more open communities within wide upland drainageways or along small surface dissection runnels on desert pavement. These differ in density and character. In the major stream riparian setting, primarily along the basin axial stream channels, the community is dominated by paloverde (Cercidium sp.), jojoba (Simmondsia chinensis), acacia (Acacia sp.), mesquite (Prosopis glandulosa), and ironwood (Olneya tesota). In the more open upland drainageways, saguaro (Carnegiea gigantea), and smoketree (Dalea spinosa) are added to the more dominant species along with smaller shrubs. Along surface dissection runnels, cacti, shrubs and ocotillo (Fouquieria splendens) tend to be more dominant although paloverde and jojoba are still quite common. In the flat sandier alluvial plains, evenly spaced creosote plants (Larrea tridentata) form almost pure stands. In less sandy alluvial plains a mixture of shrubs, primarily brittlebush (Encelia farinosa), bursage (Ambrosia dumosa) and shrubby coldenia (Tiquilia canescens), along with ocotillo and creosote, are found. Where there is desert pavement almost no plants are found. In large pavement areas plants are found in dissection runnels or in circular sandy patches within desert pavement but which are free from pavement. On bedrock and

very rocky slopes, primarily cacti, saguaro, brittlebush and ocotillo are found, with sometimes rather thick stands of teddy bear cholla (Opuntia bigelovii). More detailed descriptions of plant communities are given in individual site descriptions in Chapter 2.

Geology

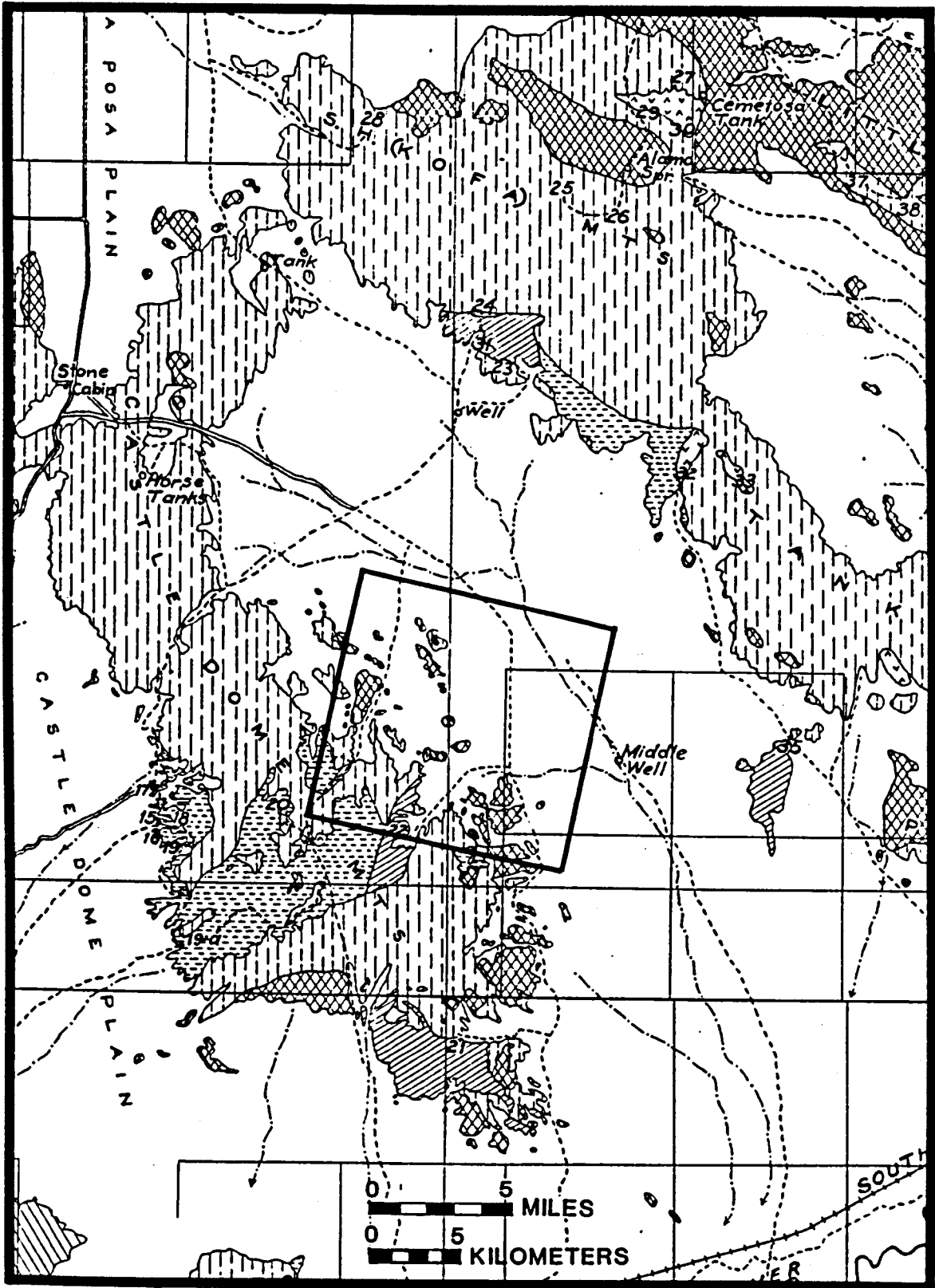
The study site falls within the Basin and Range physiographic province as defined by Fenneman (1931). Both the Castle Dome mountains and the Kofa mountains are typical of basin and range mountains in that they are oriented NW-SE, bounded by high-angle normal faults, and are separated by sloping pediment plains and alluvial basins. The NE-trending Livingston hills and the northern Castle Dome mountains may be an expression of a transverse structural trend in the middle Basin and Range which is also seen in the Chocolate mountains, the Harcurvar mountains, and the Harquahala mountains.

Little is known about the geology of southwest Arizona. The only published geologic investigation of the Castle Dome mountains was a reconnaissance study by E. D. Wilson which was included in his Geology and Mineral Deposits of Southern Yuma County (Wilson, 1933). The geologic map which accompanied this work, with slight revisions, has been the basis for all subsequent geologic maps of the area.

The portion of Wilson's 1933 map containing the study area is reproduced in Figure 4 of this text. In it he interprets the Castle Dome mountains as primarily composed of undifferentiated Tertiary volcanic rocks with a core of older sedimentary, metamorphic and some granitic

Figure 4. Portion of Wilson's 1933 map containing thesis study area.





rocks in the south central part of the range. Younger than the Tertiary volcanic rocks are what he calls "Quaternary basalts" and undifferentiated alluvial deposits. All these lithologies except for the granitic rocks are represented and have been observed in this writer's thesis area.

In later maps, the 1960 Geologic Map of Yuma County (Wilson, 1960) and the 1969 Geologic Map of Arizona (Wilson, Moore and Cooper, 1969), both at smaller scales, Wilson leaves the outcrop pattern basically unchanged but makes some age reassignments which in light of recent work should be revised. Stratigraphic and isotopic studies in the region by Eberly and Stanley (1978), Shafiqullah et al. (1980) and by Crowe (1978) in nearby California all suggest a middle Tertiary (25-15 MYBP) age for the tilted acid-intermediate volcanic rocks of the Castle Dome mountains. Moreover, rocks originally mapped as Quaternary basalts are probably basaltic andesite in composition (Lynch, personal communication, 1979) and late Tertiary (18-6 MYBP) in age.

Shafiqullah et al. (1980) have obtained radiometric dates for the Kofa mountain volcanics which are 18.3 MYBP for the oldest flat-lying volcanic flows (basaltic andesites) and 21.5 MYBP for the youngest tilted volcanic flows (olivine basalt). If the same age for tilting is assumed in the Castle Dome mountains, then these ages are probably very reasonable dates for the tilted and non-tilted Tertiary volcanic rocks found in the field study area.

Geologic/Geomorphic Sketch Map

On the basis of reconnaissance and photo interpretation, a

generalized geologic/geomorphic sketch map of the study area was produced (Figure 5). This map is classified into 10 classes defined in the accompanying table (Table 1).

Generally, the site can be divided into three major regions trending southeast to northwest. From southwest to northeast these are the mountain mass, the alluvium-mantled pediment plain, and the axial stream complex valley floor.

The mountain mass consists of a Mesozoic sedimentary core overlain by Tertiary acidic volcanics. While most of the rock exposures in the study site are Tertiary volcanic rocks, the sedimentary core is exposed in the very southwest portion of the study area. It consists of sandstones, limestones, conglomerates, and slates, most of which have been metamorphosed. Although they have not been directly compared to the Livingstone Hills formation found just north and west of here, they are similar to descriptions of that formation as given by Harding (1980) and are more than likely correlative.

Overlying these rocks in places are hypabyssal or porphyritic rhyolites. These rocks are rhyolitic in composition but have a crystalline porphyritic texture. They are near surface or very shallow-depth igneous intrusions, of late Mesozoic or early Tertiary age. To the east of the Mesozoic sedimentary rocks are Mesozoic schists. In false color composites, the Mesozoic rocks are spectrally differentiated from other rocks by their blue signature. The volcanic rocks have signatures more closely associated with their varnishing and weathering characteristics.

The oldest of the Tertiary volcanic rocks are a thick series of

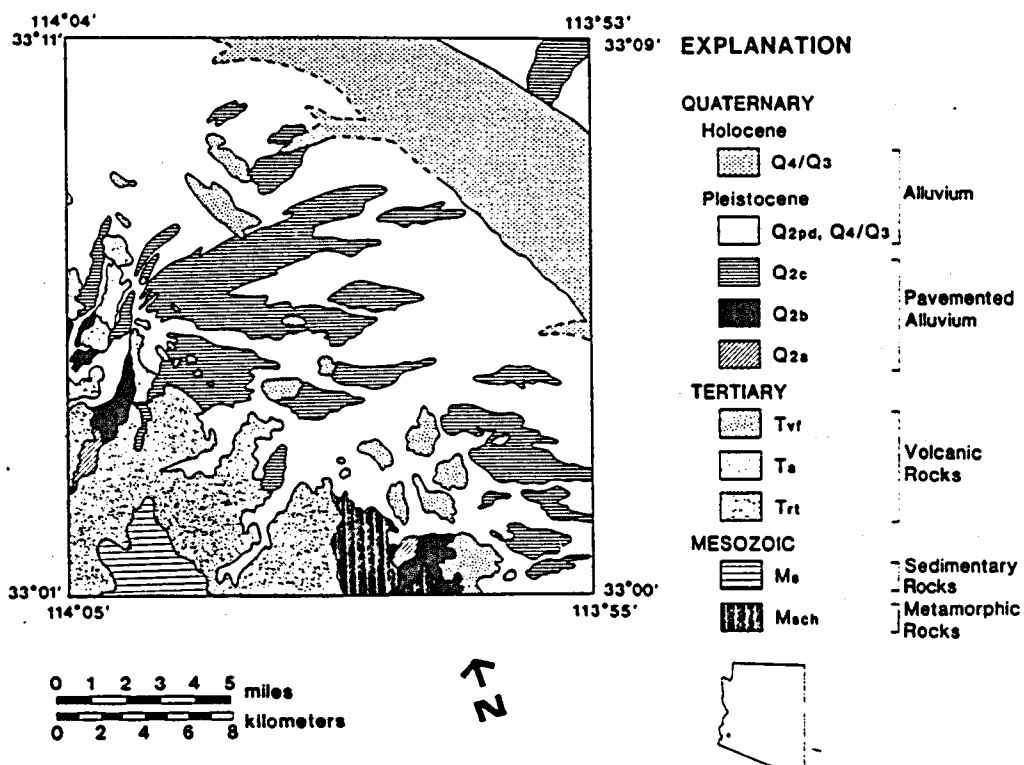


Figure 5. Geologic/geomorphic sketch map (refer to Table 1 for description of geologic units).

Table 1. Geologic/geomorphic classes of sketch map.

| Class | Description |
|-------------------|--|
| <u>Quaternary</u> | |
| Q4/Q3 | Modern alluvium, stream channels, flood plains, overbank deposits. |
| Q2/pd, Q4/Q3 | Complex of Pleistocene and Modern alluvium: stable and partially or fully degraded or dissected pavement. |
| Q2c | Late Pleistocene alluvium. Flat, stable desert pavement. |
| Q2b | Middle Pleistocene alluvium. Moderately dissected desert pavement, ridge and ravine topography. |
| Q2a | Middle Pleistocene alluvium, highly dissected, with remnants of desert pavement. Hill and valley topography. |
| <u>Tertiary</u> | |
| Tvf | Acid to acid-intermediate volcanic flow and pyroclastics. |
| Ta | Basaltic andesites. |
| Trt | Rhyolitic ash-flow tuffs and banded rhyolites, faulted and tilted. |
| <u>Mesozoic</u> | |
| Ms | Sedimentary and low-grade metamorphic rocks of sedimentary origin, slates, limestones, conglomerates, sandstones and quartzites. |
| Msch | Mesozoic schists. |

rhyolitic ash-flow tuffs which have been tilted and faulted. At the base of the tuffs are flow-banded rhyolites. Flow-banded rhyolites are only locally exposed in the study area, but large exposures of flow-banded rhyolites can be seen elsewhere in the north central Castle Dome mountains. The tuff flows can be divided into two major units, the older unit which is light-colored, does not varnish, and forms slopes; and the younger unit which is dark, dense, forms a dark varnish, and is a cliff-former. These two units are represented by samples EH #1 and site 2 #1 described in Appendix B. The older unit can be divided into approximately 12 individual welded units while the younger one, because of its density and darkness of desert varnish, appears as one unit. Overlying the younger tuff unit is a basaltic andesite which contains olivine.

Elevated middle Pleistocene age (1.0-.05 MYBP) geomorphic surfaces are primarily found within the mountain mass region on remnant middle Pleistocene alluvial fans. Late Pleistocene pavements (.05-.01 MYBP) as well as Holocene geomorphic surfaces (< 10,000 YBP) are found in the major valleys within the mountain mass area but are for the most part not differentiated on the map.

The alluvium-mantled pediment plain, the middle region, is composed of inselbergs, alluvial surfaces, and ephemeral washes. Late Pleistocene dark paved surfaces (Q2c) are quite widespread, although Holocene fluvial activity has reduced the once-continuous fan of dark stable desert pavement into a complex of interdigitated stable desert pavements (Q2c), vertically degraded desert pavements (Q2pd), and modern erosional surfaces (Q4/Q3). Degraded pavements are those surfaces which

are recognized as vertically eroded desert pavements by diagnostic horizons in their truncated soils and by stratigraphic considerations. Modern erosional surfaces have no evidence of soil development and show signs of fluvial erosional activity.

Desert varnish makes bedrock inselbergs and desert alluvial pavements dark in color. These classes are differentiated on satellite images by the shadowed and illuminated slope textures associated with inselbergs and a grainy mottled texture associated with dark desert pavements. Dissected desert pavements have a grainy mottling texture along with numerous fine filaments created by dissection channels. Degraded pavements have an even light tone whereas erosional surfaces are recognized by uneven light tones.

The axial stream complex, the third region, is composed of anastomosing sand-and-gravel channels and dense riparian vegetation. Between the channels are flat overbank deposits of sand and silt, often covered with creosote bush (Larrea diveracata). The entire region is generalized in the sketch map as Q4/Q3.

Arid Soils and Geomorphic Surfaces

In arid soils, low soil moistures prevent the complete leaching of salts, causing an accumulation of calcium carbonates and calcium sulfate salts to form in the soil profile. Much of these salts, as well as silt and clay are derived from eolian sources (Yaalon and Ganor, 1973; Yaalon and Dan, 1974; Goudie, 1978). In young soils the salts tend to accumulate near the surface. In the desert pavement soils of southwestern

Arizona, these calcium carbonates, along with fine sands, silts and coarse clays, form what is known as a vesicular horizon just under the rock mantle. Older soils have calcium concentrations both near surface in the vesicular horizon, and in a calcic horizon which progressively thickens with age. Gile, Peterson and Grossman (1966) have identified four major stages of calcium carbonate accumulation morphologies in arid soils, allowing for the use of CaCO_2 depositional morphology in the C horizon as a relative measure of age.

The amount of clay production and translocation in the formation of an argillic B horizon is proportional to the amount of time the soil has been exposed to conditions of greater effective moisture than is found in the region today. Since the presence of calcium cations tends to flocculate clays, calcium must be largely removed from the upper part of the pedon before the translocation and accumulation of clays can occur (Birkeland, 1974). Also, the in situ formation of clays from minerals requires chemical weathering under relatively moist conditions. Therefore, soils with argillic horizons in the arid region today were formed at a time when the amount of effective moisture was great enough to produce clays, leach calcium salts, and translocate the clays. In the study area, soils with argillic B horizons are older soils whose formation dates from Pleistocene "pluvial periods."

These two pedologic variables, the amount of calcium in the C horizon, and the amount of clay in the B horizon, have been used in this thesis as the diagnostic criteria for the determination of the relative age of soils in the study area. The surface morphology and degree of

desert varnish in conjunction with subsurface pedologic criteria have been used for field recognition of relative soil ages.

Desert Pavement

One of the most striking aspects of geomorphic surfaces in arid regions is the development of "desert pavement" and "desert varnish." Desert pavement, also called stone pavement or hamada, is a stony surface mantle which when best developed forms a dark planar surface of size-sorted stones so well fitted together that the surface has an appearance of a rock mosaic. Typically the pavement develops on gravelly alluvium and is only one to two stones thick. The stones are darkened by a coating of desert varnish which is brown to black on the top surface, orange red on the subsurface with usually a ring of darker varnish just at the intersection of the subsurface and surface. Beneath the stone pavement is usually found the vesicular horizon which is from 2 to 4 cm thick and light orange in color. Soils associated with the best-developed desert pavements in this area are the late Pleistocene soils with well-developed stage III calcic horizons (Gile et al., 1966) and some illuviated clays.³

Desert pavements have been found and described in most of the arid regions of the world (Beaumont, 1968; Blake, 1904; Cooke, 1970; Jessup, 1960; Sharon, 1962; Symmons and Heming, 1968; Springer, 1958). Three mechanisms have been suggested for the formation of desert pavement:

3. In gravelly parent material, stage III denotes a plugged calcic horizon: all grains are coated with carbonate, voids filled with carbonate.

(1) wind deflation; (2) water sorting; (3) upward migration of stones. Cooke and Warren (1973) have reviewed much of the literature on this subject. While arguments for the operation of all three mechanisms either singly or in concert are plausible, the dominant process operating in this region is probably selective sorting of particle sizes by water action with some loss of fine particles by wind deflation (Sharon, 1962; Lowdermilk and Sundling, 1950; McHargue, 1981).

Both wind deflation and the washing and compaction of particles by raindrop impact (McIntyre, 1958) could play minor roles in the initial formation of desert pavements. However, most of the work (removal of fines) is probably due to the effects of surface sheetwash. Sharon (1962) has shown that under specific conditions sheetwash alone could account for the formation of a pavement in the space of only a few years.

The amount of time required for the formation of a desert pavement is variable and is dependent on the particle sizes of the original alluvial material and that of the stable pavement configuration. A detailed analysis of particle size distribution changes between the pavement and the unaltered subsurface alluvium by McHargue (1981) suggests that regardless of original size distribution, the distribution of particle sizes in desert pavement tends to converge toward a preferred distribution which is dependent on local environmental parameters. Alluvium which is coarse and similar to the stable pavement distribution will stabilize (form a pavement) relatively quickly (3,000 to 5,000 years in the Aguila mountains, southwest, Arizona). Alluvium which is far from that convergent distribution such as fine sands or silts will form a pavement only

if it contains some gravelly material and will require removal of much more material.

Once formed, the pavement is both aerodynamically and hydraulically stable (Cooke and Warren, 1973). The surficial accumulation of rocks inhibits further deflation while the tight fit of rocks and the presence of fine sand, silts, and carbonates in the vesicular horizon inhibits infiltration. Chepil (1950) was first to suggest a critical surface roughness at which the height and width between clasts is such that soil erosion by the wind ceases. Infiltration rate measurements and soil analysis by Musick (1975) led him to conclude that slow infiltration rates of desert pavements are due primarily to high amounts of exchangeable salts which are located near the surface in the vesicular horizon.

With time, the pavement becomes better fitted as the particles readjust during each surface flow event (Denny, 1965). As the pavement approaches the convergent distribution, removal of fines up to granule size (2-4 mm) by sheetwash is offset somewhat by addition of fines through eolian deposition and physical weathering of larger clasts (McHargue, 1981). The relatively stabilized surface crust allows for the textural development of the vesicular horizon. Additions to the vesicular horizon either from dustfall or sheetwash deposition changes the texture from pebbly sand to a partly indurated silt or clay loam (McHargue, 1981).

Desert Varnish

The term desert varnish refers to the dark patination often found

as coatings on rocks in arid regions. When fully developed, the varnish attains a thickness on the order of tens of microns and has an appearance characterized by a dark "greasy" brownish black patina on top and a bright orange patina on its bottom side. In the thesis site, varnish tends to be best developed on resistant bedrock surfaces and on the flat younger Pleistocene pavement surfaces.

Since the discovery of desert varnish by the scientific community, numerous investigations into its nature, chemistry, and occurrence have been undertaken (Merrill, 1898; Laudermilk, 1931; Hunt, 1954; Engel and Sharp, 1958; Hunt, 1961; Hooke, Yang and Weiblen, 1969; Potter and Rossman, 1977; Allen, 1978; Perry and Adams, 1978). While not yet fully understood, it has been determined that desert varnish forms at a variable rate which ranges from 1000 to tens of thousands of years, depending on the environment (Hunt, 1961; Engel and Sharp, 1958). It is a heterogeneous surface coating composed of clays enriched in Si, Mg, Mn, and Fe oxides with generally decreasing enrichment with distance from the surface (Engel and Sharp, 1958; Potter and Rossman, 1977). Structurally, it has been reported that the surface coating is composed of cyclical layers with alternating color and chemistry (Perry and Adams, 1978). Detrital grains are commonly admixed in the layers such that the layering often becomes botryoidal (Perry and Adams, 1978). The source of materials to form the varnish is undoubtedly from without and probably from atmospheric sources (Allen, 1978; Perry and Adams, 1978; and Potter and Rossman, 1977).

The exact mechanism involved in the formation of desert varnish is

still not completely resolved. It is generally agreed that desert dew and eolian materials play important roles in the formation of desert varnish and that the pH, eH, and redox potential of the chemical micro-environment are constraints on the formation and rate of growth. Potter and Rossman (1977) have argued that the clay may act as an active agent, first serving as a medium for varnish solutions then acting as a manganese fixing agent. Others (Scheffer, Meyer and Kalk, 1963; Perry and Adams, 1978; Bauman, 1976; Dorn, 1980) have argued that it is a product of chemolithotropic oxidation by microorganisms. Proponents of the biologic origin theories cite the presence of growth centers, the cyclical nature of the varnish, the ubiquity of desert microfauna, and the identification of organisms living on the varnish as support for this hypothesis. Recently Dorn and Oberlander (1981) claimed to have produced desert varnish by cultivating Metallogenium and Pedomiccobium-like bacteria obtained from natural varnish sites in a medium of agar, sodium acetate, manganous sulfate, oxidized iron sulfate, and a vitamin mixture.

Archaeologists and geomorphologists have long been intrigued by the possibility of using desert varnish as a tool for absolute dating of materials in the arid region. Goodwin (1960) has reviewed much of this literature. As a relative dating device, desert varnish has been frequently used to date artifacts, pictographs, and geomorphic surfaces. Hayden (1976) based much of his pre-altithermal stratigraphy in the Sierra Pinacates, Sonora, Mexico, on desert varnish stratigraphy. Bard, Asaro and Heizer (1978) attempted to date desert varnish by trace element analysis. Their method sought to establish trace element signatures for

varnish of different ages as determined by stylistic considerations in artifacts rather than to establish some systematic trace element variation with time. Dorn and Oberlander (1981) suggested that varnish micromorphology and chemical profiles may indicate environmental fluctuations through time. To this writer's knowledge, no work has been published which seeks to spectrally quantify the darkness of desert varnish in order to determine the relationship between age and color of desert varnish. This has been particularly studied in the context of the larger goals of this thesis and is reported on in the next chapter.

Geomorphic Classification

Bull (personal communication, 1978) has suggested an outline for the evolution of gravelly arid alluvial surfaces from deposition, to formation of desert pavement, to the destruction of the pavement and erosion of the alluvial deposit for climatic fans in tectonically stable areas of southwest Arizona. Within the framework of this evolutionary sequence Bull has developed a general classification for different alluvial piedmont surfaces ranging in age from oldest Pleistocene to youngest Holocene. These units are designated Q1, Q2, Q3, and Q4. These are oldest Pleistocene (and perhaps latest Pliocene) (2.5-1.0 MYBP), middle to youngest Pleistocene (1.0-.01 MYBP), early Holocene (10,000-2,000 YBP), and modern (late Holocene) (2,000 to present), respectively (Fleischhauer, 1978). The designated units can be further subdivided by the addition of a lower case alpha character. For example, in this thesis, Q2 is subdivided into Q2a, Q2b, and Q2c, which are from oldest to youngest, respectively.

The classification system may be considered a morphostratigraphic system in the sense used by Frye and Willman (1962). Subdivisions of the alluvial geomorphic surfaces as classified by Bull (1974) are based on the sedimentology and stratigraphy of the deposit, and the genetic and morphologic characteristics of the surface and soil which have evolved since deposition ceased.

The Idealized Cycle of Desert Pavement Formation and its Influence on Soil Reflectances

For the purposes of geomorphic mapping from remote sensing data bases, it is useful to consider the evolution of alluvial surficial deposits (in regard to their surface morphology and color) as an idealized cycle of desert pavement formation and destruction. The influence of this cycle on average reflectance properties, along with another major controlling factor, lithology as it affects weathering characteristics, is hypothetically depicted in Figure 6, the hypothetical surface of averaged reflectance over the visible portion of the electromagnetic spectrum (EMS) as a function of age and lithology.

In the idealized cycle, a recent alluvial deposit is left as an elevated terrace due to renewed channel incision. The soil is not developed and the surface retains the bar and channel surface morphology of the original channel deposit. The active channel is designated Q4 and the stream terrace is Q3.

Initially both Q4 and Q3 surfaces would be quite similar and indistinguishable except for differences in surface elevation. If

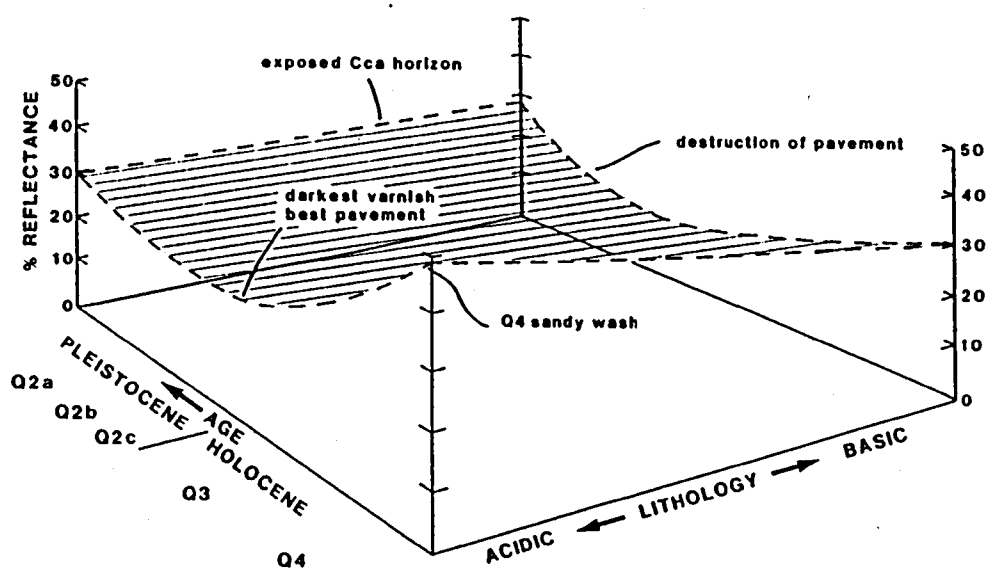


Figure 6. Hypothetical surface of reflectance as a function of age and lithology in arid alluvial surfaces.

composed of leucocratic rocks, the surfaces would have a high reflectance in the visible, which would be attenuated somewhat by the presence of riparian vegetation. If the alluvial material is primarily composed of melanocratic rocks, then the reflectance over the visible EMS would be lower but still higher than the original rock material.

As the processes of renewed channel incision continues with time, more terraces are formed such that a suite of Q3 terraces creates a stepped ephemeral stream terrace system. These terraces can be subdivided into Q3a, Q3b, Q3c, and sometimes Q3d. The suite of Q3 terraces would range as a function of age from greatest (Q3a) to least (Q3d) soil and surface development. The surface of the youngest terrace would be most like the Q4 channel except perhaps for the distribution of vegetation. Going from youngest to oldest, the rocks become darker with varnish, pavement better developed, and the vegetation diminishing in both density and type. The original bar and channel morphology is subdued by the processes of pavement formation so that it becomes a more gentle bar and swale surface. The vesicular horizon is formed and the calcic C horizon begins to form. The overall effect is to darken and flatten the surface so that the original unsorted, irregular light-colored alluvial deposit is now darker, moderately paved, better sorted, with less vertical micro-relief.

Continuation of the process darkens the varnish even more so that the surface is now dark brown to black, very flat, with little or no vegetation. This is recognized as the youngest Q2 surface, a dark, flat terrace with a strongly developed soil. Soils of Q2 age and older bear

the imprint of past climatic regimes. The diagnostic criteria for the Q2 deposit is based on the presence of clay in the textural B horizon which is indicative of soil formation under a climatic regime of greater effective moisture than is available in the region today.

In Q2 soils, the calcic horizon development ranges from stage II, continuous pebble coatings, to stage III and IV, the formation of a plugged horizon and laminar carbonate deposits. Variations in clay and carbonate development from area to area are due to variations in local climatic and lithologic conditions.

Usually by Q2a stage, and certainly by Q1 stage, the surface has been stranded by trunk stream channel entrenchment for a sufficiently long time so that a dendritic pattern of streams originating on the surface forms and begins to substantially degrade the surface. At this point of the cycle, the dark pavement is slowly destroyed and lighter rocks, especially calcium carbonate from the calcic horizon, are exposed. The topography increases in relief and begins to transform from that of a flat pavement to flat-topped ridges and ravines, to finally a knobby rolling hills handscape. The surface color is generally lighter in color due to exposure of unvarnished rocks from the subsurface, calcium-coated rocks and clasts of petracalcic material. Surfaces composed originally of melanocratic rocks are, in this stage, not much darker and perhaps lighter than those composed primarily of leucocratic rocks. The reason is that these rocks contain more original calcium and therefore may have more prominent, pedogenic petracalcic clasts littering the surface. Also, concurrent with continuing erosion, there is a solution and redeposition

of pedogenic carbonates, which coats the gravel that will next be exposed at the surface. Another factor is that the greater relief of the topography will exercise more control over the average reflectance of the surface due to the effects of shadowing and vegetation components than in previous stages.

It must be noted that this idealized cycle is only applicable to rocky alluvial material in the tectonically stable arid piedmonts of southwest U.S. Fine-grained alluvial deposits are subject to different processes and different rates. They are also generally found in parts of the basin that are, on the whole, aggradational rather than degradational. The cycle is idealized and basically Davisian and as such is subject to the influence of a host of other geomorphic parameters. Especially important are the effects of climatic and tectonic perturbations which are manifested locally as variations in the sedimentology and pedology of the deposits; and in the distribution, extent, and pattern of occurrence of the various Q surfaces. Locally, many Q surfaces may be non-existent or may be below the spatial resolution of the imaging systems used. Other surfaces may be subdivided more finely than is mentioned here. Nevertheless, the idealized cycle provides a basis for the remote sensing morphogenetic classification of arid alluvial deposits.

Landsat Remote Sensing

The Landsat System

Landsat MSS data has been obtained from multispectral scanner systems onboard Landsats 1, 2, and 3. The Landsat satellites are earth-

imaging satellites designed for use in earth resources applications. They provide systematic, repetitive earth coverage in a circular, sun-synchronous, near-polar orbit at an altitude of 918 km (494 nautical miles). The satellite repeats its coverage once every 18 days, always at the same local time between 9:30 and 10:00 AM (NASA, 1972).

The MSS is a mechanically scanning optical instrument which images the earth simultaneously in four spectral bands referred to by convention as bands 4, 5, 6, and 7. These bands are sensitive to the visible green spectral region (.5-.6 μm), the visible red spectral region (.6-.7 μm), and two near-infrared regions (.7-.8 μm , .8-1.1 μm), respectively. The instantaneous field of view (IFOV) of the Landsat MSS corresponds to approximately 76 m² on the ground. This is often referred to as one pixel. A typical Landsat scene is composed of approximately 7.5 million pixels per band.

Upwelling radiant flux from the earth is reflected by the scanner mirror through the optics to an array of 24 fiber optic detectors. Radiant flux intercepted by the optic fibers is transmitted through a spectral filter and then onto either a photomultiplier tube (4, 5, 6) or a silicon photo detector (7). An analog signal is produced at the detector, and converted to a digital value for transmission to a ground receiving station or stored on onboard recorders for later transmission. Once on the ground, the data is formatted and processed for use. Additional specifications on the Landsat satellite and the MSS sensor are given in Appendix A. More detailed information on satellite and sensor characteristics is available from NASA (1972), Taranik (1978), and Slater (1980b).

Landsat MSS Radiance Measurements

The relationship between the target surface radiance and the irradiance at the MSS detector can be modeled using the camera equation, which in its simplest form is:

$$E = \frac{\pi L_o}{4N^2} \quad (1)$$

where

E = the irradiance at the detector measured in W/m^2

L_o = the total path radiant flux density at the entrance pupil
in $W/st\ cm^2$

N = f number of the lens

The total radiant flux density, L_o , at the satellite is composed of two components: L_s , the radiant flux density due to the target surface; and L_a , the radiant flux density due to the upwelling atmospheric backscatter. Therefore:

$$L_o = L_s + L_a \quad (2)$$

The average radiant flux emitted from the earth due to black body radiation approximates the flux due to a Planckian black body at $300^\circ K$. The spectral curve of this radiator peaks at about $10.0\ \mu m$ and is effectively at zero value by $1.0\ \mu m$. Since the solar flux approximates a black body radiator at $6000^\circ K$ with a peak in the visible green spectral region, $.5\ \mu m$, it can be assumed that all the radiant flux, L_s , is due to reflected solar flux rather than from earth material black body radiation for wavelengths in the visible and near-infrared (VNIR) regions of the EMS (Slater, 1980b).

If we assume that the natural surface approximates a perfectly diffuse reflecting surface (i.e., a Lambertian surface), then the radiant flux density of the surface for a particular wavelength is:

$$L_s = \rho_\lambda E / \pi \quad (3)$$

where

ρ_λ = the reflectance of the material at the wavelength λ

$1/\pi$ = the portion reflected into the upper hemisphere above a Lambertian surface

E = the irradiance due to sun and sky. For direct sunlight:

$$E = \sin B \int_{\lambda_1}^{\lambda_2} E(\lambda) T_B(\lambda) d\lambda \quad (4)$$

for solar elevation B , atmospheric transmissivity T_B , and wavelength λ_1 to λ_2 .

The Lambertian assumption is not unreasonable for most natural surfaces illuminated at high solar elevations and viewed from a nadir-viewing sensor (Janza, 1975).

Considering the effects of atmospheric scatter and absorption (for relatively non-absorbing portions of the EMS) and integrating over the wavelength interval λ_1 to λ_2 :

$$L_s = 1/\pi \int_{\lambda_1}^{\lambda_2} E_\lambda \rho_\lambda T_A(\lambda) d\lambda \quad (5)$$

where

$T_A(\lambda)$ is the wavelength-dependent atmospheric transmittance

Substituting Equation (5) into Equation (1) we have the simplified expression of the irradiance at the detector as:

$$E = \frac{1}{4N^2} \int_{\lambda_1}^{\lambda_2} (E_{\lambda} \rho_{\lambda} T_A(\lambda) + \pi L_{a\lambda}) d\lambda \quad (6)$$

Thus it can be seen that the MSS radiance values are due to the atmospheric attenuated solar light as reflected by the target surface combined with the solar light as backscattered by the atmosphere.

The expression is simplified because the effects due to optics, e.g., vignetting, lens design, off-axis irradiance dropoff, etc., and electronics such as S/N ratios, integration time, etc. are not considered. For expanded treatment of this subject, see Slater (1980b) and Reeves (1975).

Scattering

The two terms $T_A(\lambda)$, the path atmospheric transmittance and $L_a(\lambda)$, the upwelling atmospheric path radiance are functions of the atmospheric absorption and scattering properties. For generally, non-absorbing spectral regions of the atmosphere, as in the MSS wavebands, the effects of absorption are negligible (Slater, 1980a). The effects of scattering are, however, significant and can be attributed to three mechanisms: (1) Rayleigh (scattering due to particles $< .1\lambda$, i.e., that caused by air molecules); (2) Mie (due to particles $.1-10\lambda$, i.e., atmospheric aerosols); and (3) that scattering which is due to non-selective (not wavelength-dependent in the VNIR) particles such as clouds, dust, fog.

While the atmosphere does not ever behave as the theoretical Rayleigh atmosphere (i.e., only scattered by air molecules) (Curcio, 1961),

studies on atmospheric correction for clear skies in the San Carlos Indian reservation (Slater, 1980a), Arizona, suggest that for classification purposes, on clear days and in arid areas, the atmosphere can be considered a Rayleigh atmosphere without compromising the classification results.

In this viewpoint, then, scattering only affects the contrast and brightness of the target radiance. For a Rayleigh atmosphere, scattering increases with decreasing wavelength so that that part of the radiance as measured by the satellite, attributed to the upwelling atmospheric path radiance, increases for shorter wavelengths. While many quite often elaborate correction techniques have been developed (Slater, 1980b; Sabins, 1978), in this study atmospheric scattering is corrected by calibration of image data to ground reflectance measurements.

Causes of Color

Due to the diversity of phenomenon affecting the spectral reflectance characteristics of rocks and minerals in the visible and near infrared (VNIR) spectral region, the quantitative analysis of physical-chemical features controlling VNIR spectral features in natural materials is a particularly complex and unresolved field of research. For expanded discussion and detailed bibliographies well beyond the scope of this thesis, the reader is referred to Burns and Fyfe (1967), Salisbury and Hunt (1974), Hunt (1977), and Nassau (1980).

With the exception of geometrical and physical optic mechanisms, all the causes of color in the VNIR can be attributed to the interaction

of light with electrons. These can be grouped into 5 major types of mechanisms: (1) vibrational processes; (2) crystal field effects; (3) charge transfer; (4) color centers; and (5) conductor bands (Hunt, 1977). Geometrical and physical optic mechanisms include dispersive refraction, scattering, interference and molecular diffraction grating (Nassau, 1980).

Difficulties in attributing VNIR spectral features to specific rocks and minerals arise from the fact that any number of the above light interaction mechanisms can be operative at the same time; most of the principal constituents of rock-forming minerals display no intrinsic features in this spectral range (Salisbury and Hunt, 1974); spectral features are broad and not sharp and are often masked by opaque minerals; most natural materials are not homogeneous (chemically pure) at resolutions common to remote sensing systems; and that the particle sizes and geometry strongly affect both the absolute reflectance and the spectral contrast of rocks and mineral spectral features (Hunt, 1977). The latter point is illustrated in Figure 7 which shows the change in spectral reflectance of the mineral beryl at 4 different particle sizes.

In the VNIR the vast majority of spectral features can be attributed to just two substances--iron and water (Salisbury and Hunt, 1974). Other transitional elements such as Ni, Cr, Co, etc. are also important since their unfilled outer electron shells can be easily influenced by interaction with light energy.

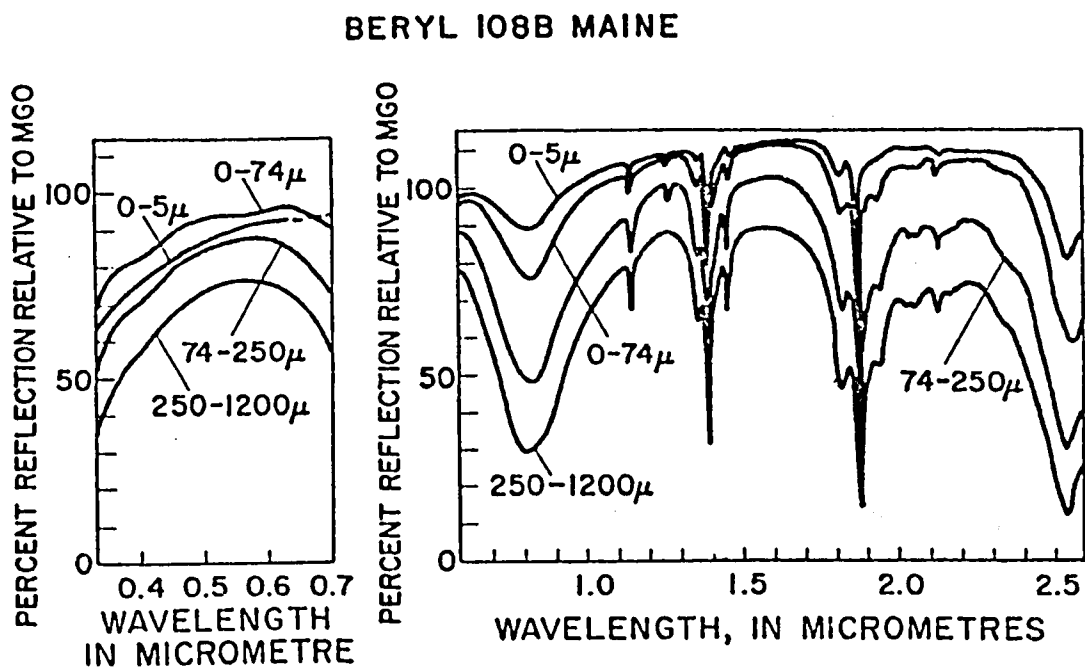


Figure 7. The effect of particle size on reflectance as illustrated by the bidirectional reflection spectra from four different particle sizes of the mineral beryl (taken from Hunt, 1977).

Rock Reflectance

Several typical spectral curves of various rock types are plotted in Figure 8. Generally, fresh surface rocks do not display strong spectral features in the VNIR from .4 to 1.1 μm . The flattest curves are usually associated with igneous rocks (except perhaps some tuffs). The presence of transparent and light-colored felsitic minerals produce a relatively high reflectance in acidic rocks. Basic rocks are darker, primarily due to the presence of magnetite and other opaque minerals. Basalts, due to their plentiful magnetite content, tend to be very flat and dark. The presence of mafic minerals such as pyroxenes, amphiboles and olivine, produce spectral absorption features in the .7 and 1.1 μm region due to their iron content. These are most clearly seen in ultrabasic rocks such as dunite or pyroxenite (Salisbury and Hunt, 1974).

Pure quartz sandstone and white limestone have high reflectances and fairly flat spectral curves. The addition of carbonaceous, argillaceous, ferric and ferrous materials will both darken and decrease the contrast of the spectral signature.

In Figure 8 both the limestone and arkose show a drop in reflectance from .6 to .5 μm , which is characteristic of iron oxides. Metamorphic rocks are similarly affected by these constituents but because of their greater crystallinity, metamorphic rocks tend to show more spectral contrast than sedimentary rocks of similar composition (Salisbury and Hunt, 1974).

Soil Reflectance

Soil reflectance values in the VNIR are influenced by composition,

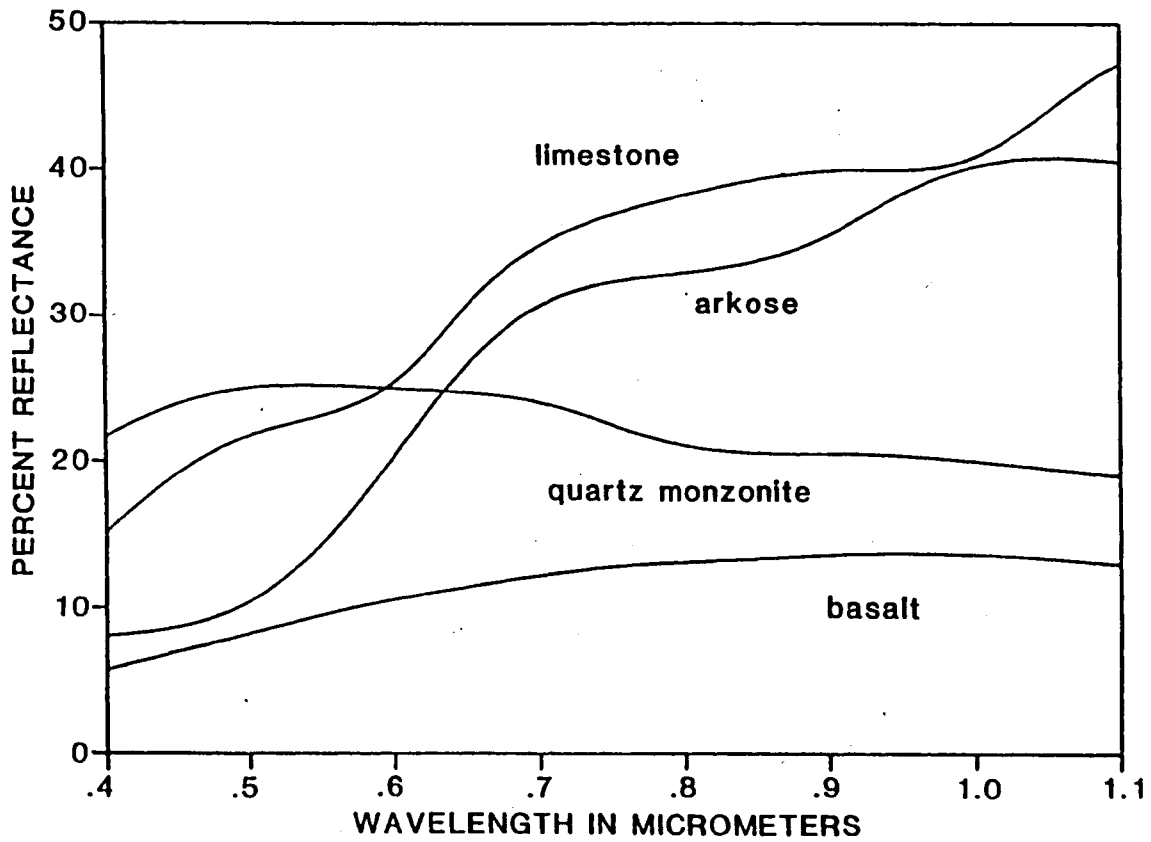


Figure 8. Reflectance of 4 rock types (from Goertz, 1976 and own data).

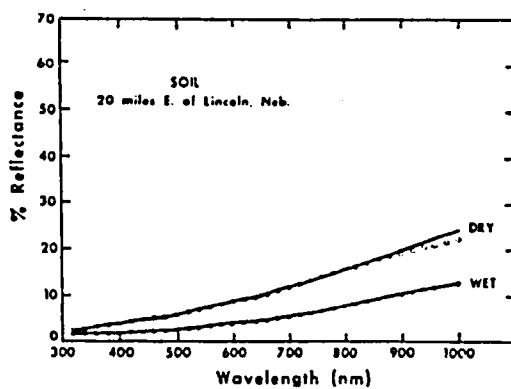
particle size and moisture content. Piech and Walker (1974) suggest that both an increase in moisture content and an increase in average particle size will generally darken the tone of a soil element. Exceptions to this rule are found in such soils as wet bog soils, where the opaque FeS minerals tend to darken with decreasing particle size (Piech and Walker, 1974).

In a study of 285 samples from 36 different states in the U.S., Condit (1970) determined that there are three basic types of spectral curves for American soils: the chernozem type, pedalfer type, and the laterite or red soil type (Figure 9).⁴

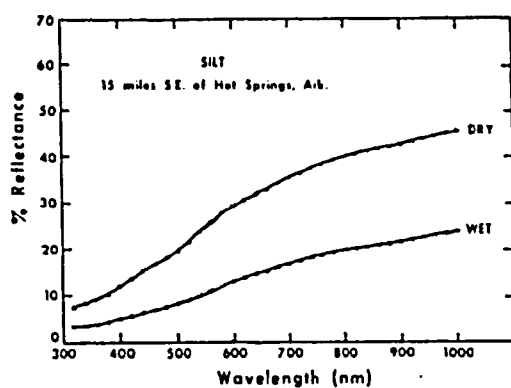
Observations of numerous spectral curves, both for wet and dry soils (Condit, 1970), indicated that in every case the wet curve is similar in shape to the dry curve but has a lower slope. Differences between wet and dry curves in absolute percent reflectance ranged from 5 to 30% in the 1.0 μm region to 2 to 5% in the .4 μm region.

Since most surface texture and roughness sizes are much larger than the wavelength of VNIR light, soil surfaces tend to behave in a Lambertian fashion. Surfaces which are rough, however, may have reflectance values which are sensitive to variations in illumination angles because these surfaces have high soil micro-shadow components. However, Janza (1975) reported that the shadow areas are almost fully compensated by the higher brightness of sloping surfaces exposed to full sunlight.

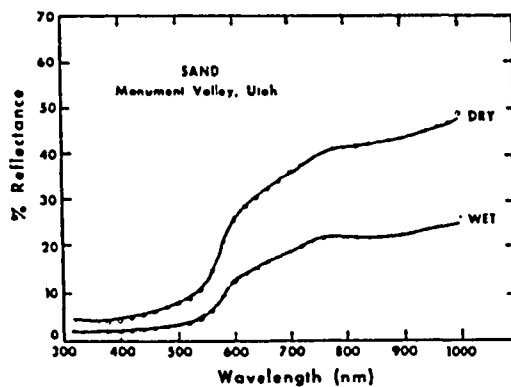
4. In the terminology of the recently adopted Soil Taxonomy (United States Department of Agriculture, 1975), these generally correspond to: (1) mollisols; (2) many groups of soils lacking calcium; and (3) oxisols and many ultisols, respectively.



Type 1. Chernozem



Type 2. Pedalfer



Type 3. Laterite

Figure 9. Three types of soil reflectance curves (from Condit, 1970).

Due to the multiplicity of factors affecting soil reflectance and the lack of strong spectral features for earth-forming materials in the VNIR, studies relating soil reflectance with composition have met with limited success. Numerous workers have noted qualitative relationships between soil organic matter and iron content with reflectance. Among them are Bowers and Hanks, 1965; Baumgardner, Johannsen and Kristoff, 1969; Crown and Pawluck, 1974; and Mathews, Cunningham and Peterson, 1973. Schreier (1977) reported significant negative correlation between soil carbon, exchangeable Mg and soil iron content with spectral reflectance. Using a curvilinear fit for the carbon and magnesium and a linear regression for the iron, he was able to predict chemical variations across farm fields from airborne spectral data.

Kristoff and Zachary (1974) warned that many soils cannot be adequately differentiated by spectral means due to the fact that soils are conventionally differentiated by subsurface criteria which have no relationship with surficial properties. This is probably less true for arid soils than for many other types of soils since the surface morphology and reflectance of arid soils can be more directly related to subsurface horizons than are soils found in humid and humid-temperature zones.

Plant Reflectance

Plant interaction with VNIR light occurs at both the leaf and plant surfaces and within plant internal tissue structures. In the visible wavelengths from .4 to .7 μm , plant reflectances are dominantly

controlled by chlorophyll absorption bands at .4 and .6 μm (Hoffer and Johannsen, 1969). Differences in pigmentation of the leaf drastically alters the reflectance signatures of plants in the visible but does not affect the NIR reflectance.

The NIR reflectance of plants is more related to plant turgor, maturity and phenology. In the NIR, plant reflectances are dominantly controlled by internal tissue structure. In plant leaves, high infrared reflectances are caused by high internal reflectances in either the wall-air interfaces of spongy mesophyll tissue (Gates et al., 1965) or in the palisade tissue (Sinclair, Shreiber and Hoffer, 1973).

Desert plants tend to have high overall reflectances. In a study of 5 different ecological groups, Billings and Morris (1951) found that desert plants had the highest reflectance of any group. This is most often attributed to the tendency toward high pubescence and sclerophylly in desert plants. Ehleringer and Björkman (1978) have shown that in the common Sonoran desert plant, Encelia farinosa, the VNIR leaf reflectance increases with pubescence with the largest increase in the NIR. A decrease in water content of desert shrubs also increases the reflectance. Mooney, Ehleringer and Bjorkman (1977) have shown this to be true for Atriplex hymenelytra while Ehleringer and Björkman (1978) report that the dried pubescent Encelia farinosa leaves have the highest reflectance of all Encelia leaves.

It is unfortunate that while most plant reflectance studies have concentrated on plant leaf reflectance, desert plants are for the most part microphyllous, drought-deciduous, or photosynthesize primarily

through green trunks (palo verde, cacti). The lack of study of other plant parts is, for the most part, due to the physical difficulty of studying body parts which are not flat and easily detached.

Mixed Reflectance Components Within the Resolution Cell

At almost any resolution size, most natural classes are composed of a complex mixture of components which differ in reflectance values. Musick et al. (1973) recognized that in a typical desert plant community, the components of a cell are composed of (1) plant tissue, (2) completely bare ground, (3) ground covered with litter, algae crust or small living plants, and (4) shadows of the larger plants.

The simplified expected reflectance for surfaces with mixed reflectance components is:

$$R_T = \frac{A_1 R_1 + A_2 R_2 + A_3 R_3 \dots A_N R_N}{A_T} \quad (7)$$

where

R_T = total reflectance

N = individual component

$A_N R_N$ = area reflectance of component

A_T = total area of resolution element (Landsat = 4761 square meters)

This expression assumes that each component is a Lambertian reflector and that there are not interaction effects between components.

When individual components behave in a non-Lambertian fashion such as in the case of a small bright specular reflecting object, it

can saturate the entire resolution element and produce a reflectance comparable to the reflectance from a large white diffuse surface. This was proven by Evans (1974) when he successfully saturated on Landsat pixel by reflecting the sun from a small mirror only 56 cm (22 inches) in diameter toward the satellite at the time of overpass. The resulting digital value had a contrast of 2:1 with neighboring pixels.

The reflectance within a resolution cell is also affected by the size of homogeneous groups within the cell and by the reflectance of neighboring cells. To study these errors Norwood (1974) observed the errors introduced by the MSS scanner when scanning across fields of homogeneous classes. With a field width of 69 m, a .87 factor of the instantaneous field of view (IFOV = 1 pixel) (Figure 10), it was seen that the errors introduced by the scanner, known as MTF or modulation transfer function, tended to average adjacent contrasting fields by a factor of up to 7%. She concluded that two factors characterized the MTF error: (1) as the field size increases the error diminishes; and (2) as the radiant contrast between adjacent pixels diminishes, the error also diminishes.

In addition to the system MTF error which, as Norwood (1974) showed was a function of the natural surface size and brightness, Everett and Simonett (1976) defined an environmental modulation transfer function (EMTF) which they express as:

$$E = f(C_R, S_R, T_R, A_R \dots X_R) \quad (8)$$

where

C_R = number of distinct land-use or mapping categories present

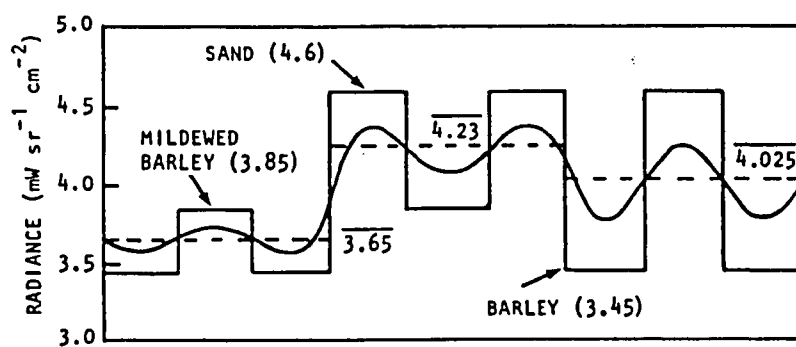


Figure 10. Examples of the errors introduced when the MSS scans bars of different radiance with a width of 69 m (after Norwood, 1974).

(dependent on classification scheme)

S_R = size and spatial arrangement of the homogeneous categories comprising an area

T_R = a measure of the time-variable nature of the environment

A_R = a measure of atmospheric constraints on sensing, e.g., cloud cover

X_R = other aspects of the environment

In other words, the more complex and variable the environment and classification scheme is, the larger the EMTF error.

Radar Remote Sensing

Imaging radar sensing systems are active sensors which transmit and receive microwave energy. The term radar is an acronym for radio detection and ranging. The direction and amount of microwave energy reflected from any object is known as radar detection, while radar ranging is based on the time lag between the transmission and reception of that energy. The strength of the radar return signal controls the image tone at that point and is a complex function of the geometry of interaction between the transmitted microwave pulse and the terrain.

Most modern radars operate in the microwave region extending from 7 mm to 1 m in wavelength (Moore, 1975). Within this spectral region, the atmosphere is remarkably free from attenuation by atmospheric water and oxygen (Figure 11). Atmospheric attenuation by water molecules decreases from very high values in the mm range to almost zero (completely transparent) at about 5 cm while the attenuation due to oxygen peaks at

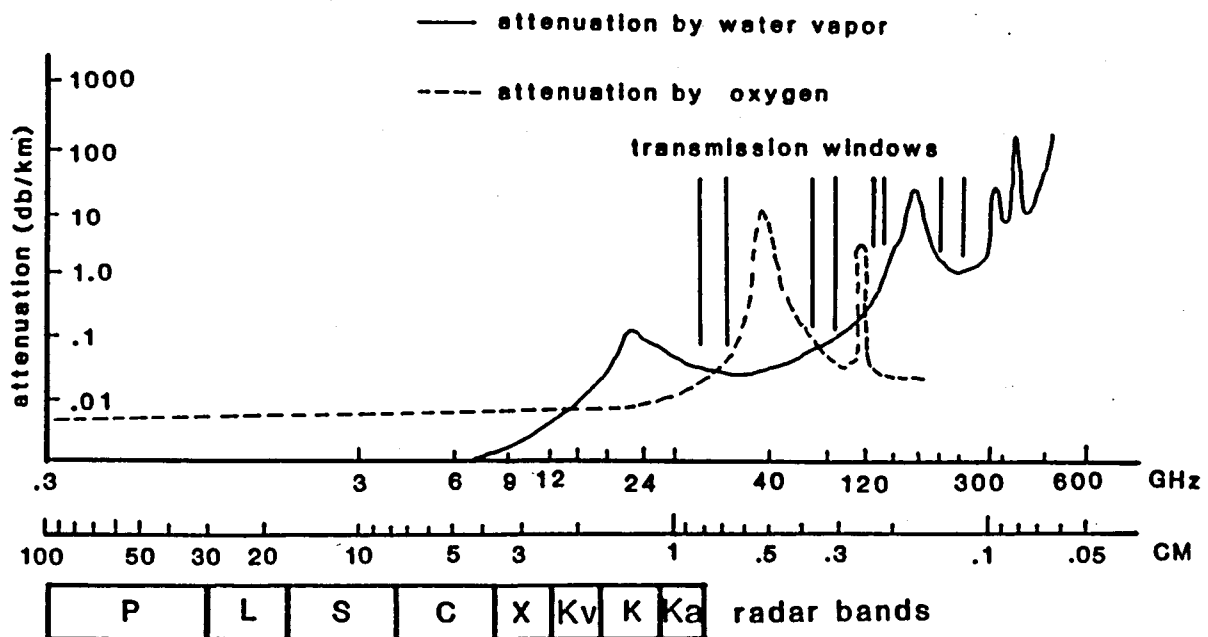


Figure 11. The microwave atmosphere and common radar frequencies (compiled from Janza, 1976; Sabins, 1978).

.25 cm and then weakens asymptotically to an almost transparent level of less than .01 db/km at 10 cm (Janza, 1976).

In addition to the well-publicized ability of radar systems to penetrate cloud cover, radar remote sensing has several particular advantages over other sensing techniques:

1. Radar is not responsive to visible color or tone but is responsive to surface geometry, slope, roughness and orientation.
2. The low illumination angles typically employed in airborne radar highlights topographic features in a more pronounced manner than in most other imagery.
3. The appearance of vegetation in radar images is primarily due to physical vegetation canopy features (plant physiognomy). Plant communities which differ greatly in physical structure will have greatly differing tone and texture attributes on radar images.

SLAR Systems

In a side-looking airborne radar (SLAR) system, the antenna is usually a linear array resembling a cylinder cut lengthwise in half and mounted on the underbelly of the aircraft, parallel to its fuselage (Sabins, 1978). The antenna directs a radar pulse so that it sweeps obliquely across the ground surface in a fan-shaped beam. This configuration allows the radar to cover a much larger area than would conventional photography at similar altitudes.

In a typical SLAR system, a pulse generating device first sends

a burst of EM energy simultaneous to the transmitter and CRT (cathode ray tube) display device. The burst triggers a sweep of the CRT, and at the same time causes a pulse of energy with a specific wavelength, duration and pulse length to be transmitted from the transmitter to the ground. This microwave energy is directed from the antenna toward one side, the "look direction," in a narrow, fan-shaped beam (Figure 12). The beam interacts with the surface and is either reflected off into space or is returned to the antenna. Returns from near range are received before return from far range and the slant distance of any imaged surface is a function of the time it took for the pulse, travelling at the speed of light, to reach the surface and return to the antenna.

The return signal, usually received in the same antenna, first passes through an electronic switch or duplexer which prevents interference with energy from the transmitter. It is then sent to a receiver which amplifies the return signal and stimulates a brightness modulation of the moving spot (pulse) on the CRT. These modulations are recorded on a moving strip of photographic film so that with each sweep a strip of film is exposed. The speed of the film is proportional to the aircraft speed (Moore, 1976).

As illustrated in Figure 12, the resolved cell for a real aperture system (SLAR) is roughly a rectangle with the dimensions,

$$R_a \times R_t \quad (9)$$

where

R_a = the angular (azimuth) resolution

R_t = the radar ranging resolution

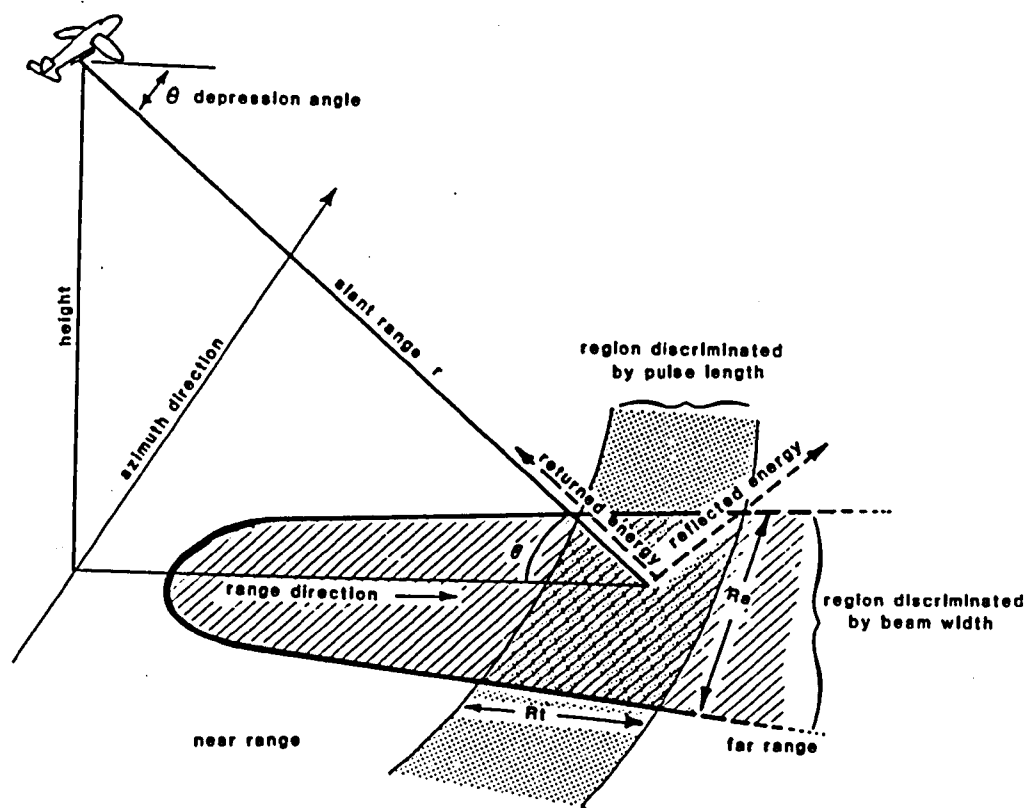


Figure 12. Basic geometry of a SLAR system (adapted from Moore, 1976).

R_a , the angular resolution discrimination by the beamwidth, when translated to ground resolution, has the dimension of:

$$R_a = r(A\lambda/D) \quad (10)$$

where

r = the slant range

A = a dimensionless design factor corresponding primarily to the beamwidth to sidelobe tradeoff

λ = the wavelength sensed

D = the antenna dimension

It is clearly seen that the angular ground resolution is proportional to A , r and λ and inversely proportional to D . In order to achieve superior ground resolution (R_a small), in a real aperture system the antenna must be made large in comparison to the wavelength sensed and any increase in slant range (distance from the receiver) will cause a proportional loss in resolution (Moore, 1976).

When A is made small, i.e., the main beam is made narrower, the sidelobe signal strength level increases (Sherman, 1970). Thus a trade-off exists between the increased resolution of a narrower main beam width, with its increase in sidelobe contribution which is a cause of ambiguity.

The radar ranging resolution, R_t , has the dimension of:

$$R_t = C\tau/2 \cos\theta \quad (11)$$

where

C = speed of light

τ = pulse duration

θ = radar depression angle or elevation angle

When targets are close to the aircraft, R_a and $\cos\theta$ are small so that the resolved cell will be narrow in the azimuth direction but wide in the range direction. As the distance to the target increases, the azimuth resolution becomes poorer while the range resolution becomes better. The resolution of conventional SLAR systems is inherently limited at long ranges by the width of its beam.

SAR Systems

Synthetic Aperture Radar (SAR) systems are a special class of SLAR in which both the amplitude and phase of the radar echo are recorded for enhanced resolution. In SAR systems a relatively short antenna is used to transmit and receive radar pulses. By utilizing the doppler effect, a long antenna is in effect synthesized by the forward motion of the platform. This is done in the following manner: A microwave pulse is generated, transmitted and received in a manner similar to the conventional SLAR system. As an object enters into the radar beam, the relative motion of the radar flux reflected from the object is against that of the antenna. Due to the doppler effect, the return signal has a higher frequency relative to the reference signal. As the object moves through the beam, the frequency of the radar return progressively lowers. When the object is in the midbeam position, the return frequency is equal to the reference signal. This is the zero

doppler shift position. Finally, as the object leaves the radar beam its return frequency is lower than the reference signal.

After reception and amplification, the frequency of the returned signal is compared to a reference signal sent from a coherent oscillator in a phase comparator (Figure 13).

Each feature on the ground within the radar swath produces its own phase and amplitude history. This history is recorded as interference patterns on a data film in the manner used to produce holograms. The data film is later decoded by a laser to produce an image film (Figure 13).

The resolution cell of a SAR system is illustrated in Figure 14. In a conventional SLAR system the azimuth resolution is directly related to the beamwidth so that a wider beam produces poorer resolution. However, since an object will produce a longer phase history if it stays in the beam longer, the azimuth resolution of SAR systems actually improves with a wider beam.

Theoretically, SAR systems can achieve an azimuth resolution of

$$R_a \approx D \quad (12)$$

where

R_a = azimuth resolution

D = antenna length

That is, the resolution of the system is independent of operating range, independent of operating wavelength and is improved when the physical antenna is reduced in size (Brown and Porcello, 1969; Moore, 1975).

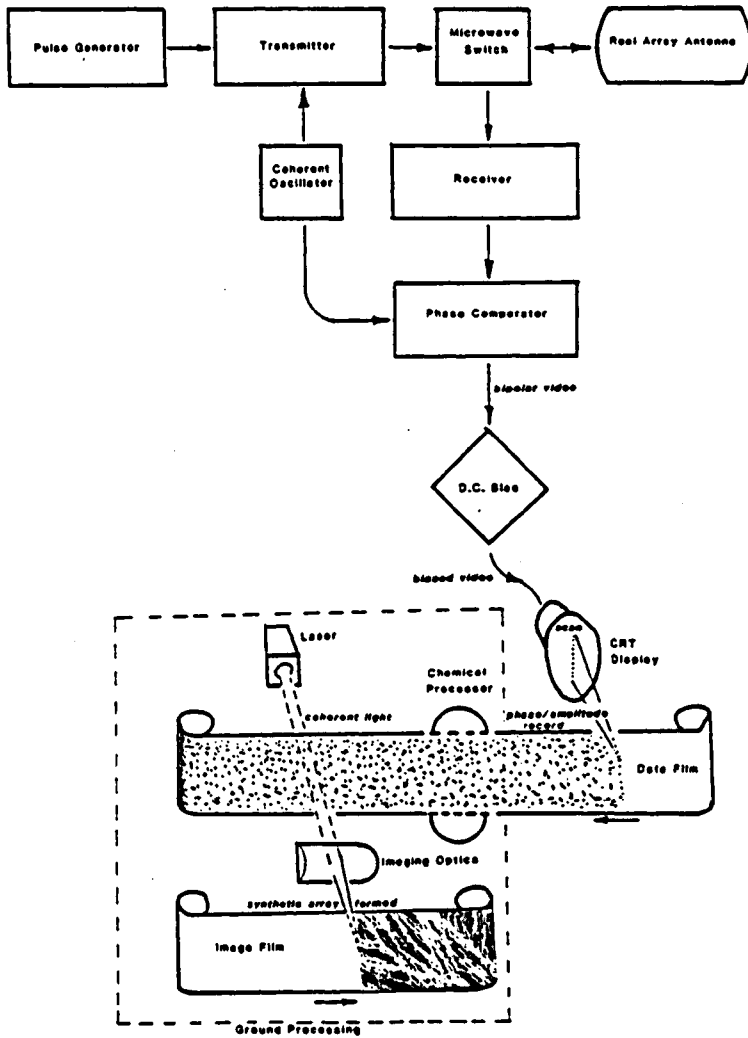


Figure 13. Block diagram of a SAR system (from Parry, 1977).

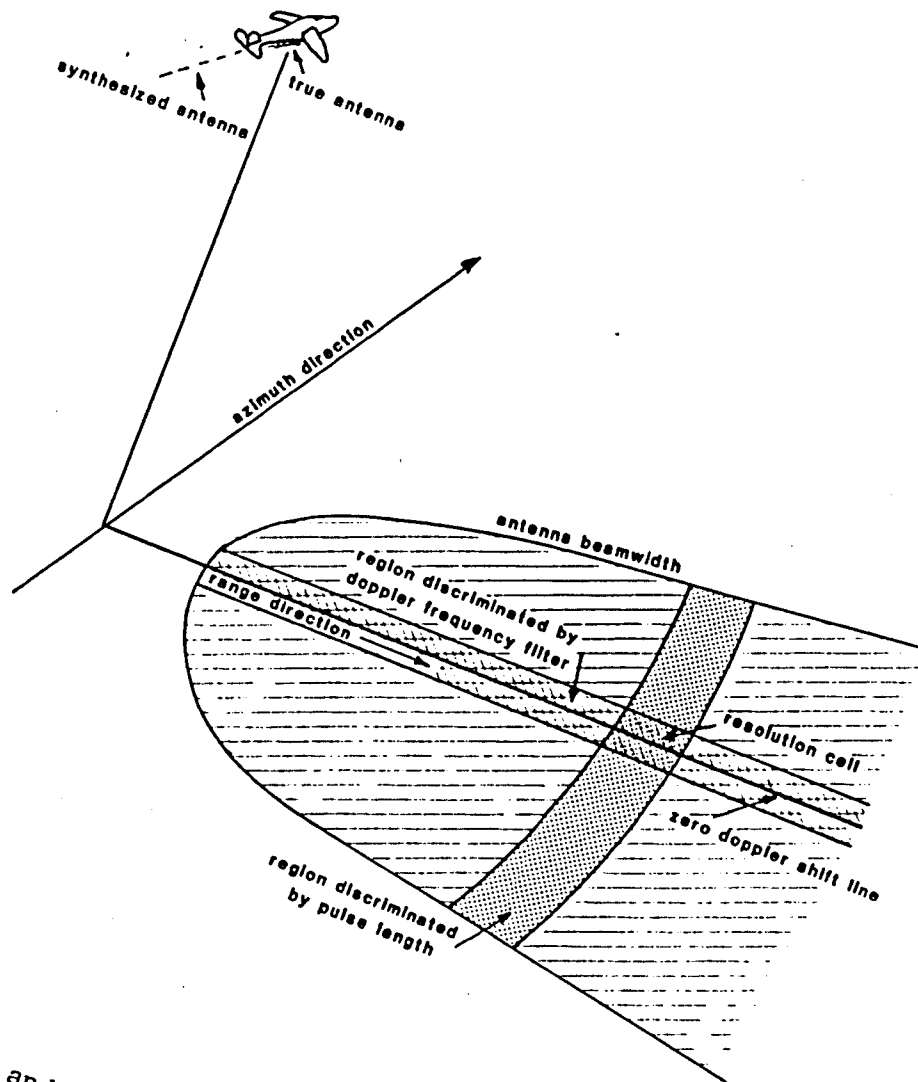


Figure 14. Azimuth and range discrimination in an unfocused SAR
(adapted from Moore, 1976).

An early limitation to the achievement of this phenomenal resolution was due to the curvature of the radiating radar wavefront. The advent of focusing SAR systems compensated for this curvature by inserting a phase shift, quadratic in distance along the aperture (Brown and Porcello, 1969). Other considerations, however, such as the necessity of maintaining true flight paths, power requirements, and processing and storage element requirements, place practical limitation on the achievable radar range resolution. Most modern public access radar imaging systems have resolution cells on the order of 10^1 meters.

Expanded discussion and detailed bibliographies on the physics and optics of SAR systems are available from Brown and Porcello (1969), Moore (1975) and Tomiyasu (1978).

Polarization

Microwave receiving and transmitting antennas of all types operate on the same principles as the Hertzian dipole. The dipole antenna radiates maximum intensity perpendicular to the direction of current flow and does not radiate along the current axis. In a dipole, the electric field at any given point is tangential to a circle centered on the dipole containing the dipole within its plane. The magnetic field at any given point is perpendicular to the electric field and is tangential to a circle through that point which is perpendicular to, and centered on, the current axis (Moore, 1975). A dipole transmitting antenna will therefore transmit an electric field which is plane-polarized. Conversely, a receiving antenna will only accept incident radiation which is polarized in the same direction as it is.

Common SLAR notation in reference to the polarization of the imaging system usually consisted of 2 upper-case letters, the first corresponding to the polarization of the transmitting antenna, and the second corresponding to the polarization of the receiving antenna. All SAR systems are polarized in one of four modes: (1) horizontally transmitted and received (HH); (2) horizontally transmitted and vertically received (HV); (3) vertically transmitted and received (VV); and vertically transmitted and horizontally received (VH).

Parameters of Radar Backscatter

The amount of radar energy returned to the antenna is known as the radar backscatter or radar return. Features with high returns are bright in the radar image while those with little or no return are dark.

Three major parameters of the radar systems itself influence the radar backscatter. These are: (1) the radar look angle (or depression angle); (2) radar frequency; and (3) radar polarization (Schaber et al., 1976; Sabins, 1978; McDonald and Waite, 1973). The look angle in combination with surface slope determines the angle of radar incidence (grazing angle). Radar frequency determines what surface features the radar will be most sensitive to. Generally radar is most sensitive to surface irregularities of a dimension near in size to its wavelength and longer wavelength microwave will penetrate surfaces to a greater extent than will shorter wavelength microwaves.

Cross-polarized imagery (HV, VH) is sensitive to the depolarizing effects of certain vegetative covers. The effect of depolarizing

vegetative cover on like-polarized imagery (HH, VV) is more difficult to assess. Cross-polarized imagery is a better indicator of average surface roughness than like-polarized imagery while like-polarized radar is more sensitive to roughness on a scale approximately equal to its wavelength. HV and VV radar are most sensitive to surface dielectric constant changes while HH appears to be the least sensitive (Daily et al., 1978).

Along with system constraints, radar backscatter from terrain surfaces are controlled by surface physical features. Numerous theories attempting to quantitatively model the scattering of microwave radiation from terrain surfaces have been developed over the years. (They are presented and reviewed in Beckmann and Spizzichino, 1963; Valenzuela, 1967 and 1968; Peake and Oliver, 1971; MacDonald and Waite, 1973; Schaber et al., 1976; Daily et al., 1978; and Blanchard, 1979.) However, due to the variety and complexity of natural terrains no one suitable model relating all the system and terrain parameters of scattering for all types of terrain configurations has been developed. Nevertheless, results from these studies and other more applied studies have given us a general idea of which terrain features most prominently influence the radar backscatter in any given situation. These are (in order of importance): (1) the surface slope and geometry; (2) surface roughness; (3) the complex dielectric constant of the surface material; and (4) Bragg condition resonance and cavity resonance effects (Daily et al., 1978; Parry, 1977).

Surface Slope and Geometry

The single most important terrain element influencing radar return is the surface geometry. Usually the brightest feature in the image will be due to steep mountain slopes that face the radar "look," thereby directly reflecting back radar energy. The darkest features are caused by slopes on the backside of mountains which are in the radar shadow. This characteristic of radar, coupled with the low illumination angles (depression angles) usually used in radar imaging is what makes topography so pronounced in radar images.

As in visible wavelengths, the angle of reflection for microwave energy is equal and opposite the angle of incidence. If a flat surface reflects specularly, that is, it is smooth relative to the radar wavelength, and if the depression angle is significantly less than 90° , it will reflect most of the radar energy forward with little or no radar backscatter. Surfaces fitting this description such as desert playas, flat sand fields, flat smooth desert pavements, will appear dark in the radar image. However, if the depression angle is high, which is the case for very near range imaging, and if the surface is sloped toward the radar look, then both the angle of incidence and the angle of reflection will be near 90° and a high backscatter will result.

Corner reflectors are produced when two or more planes are orthogonal to each other and perpendicular to the radar plane of incidence. When correctly oriented, corner reflectors produce a very bright return much like that from a specular reflector at a 90° incidence angle. Corner reflectors are usually associated with urban terrains

because intersecting planes of buildings and sidewalks produce numerous corners. While corner reflectors are not often associated with natural terrains, a properly oriented steep-walled arroyo (stream bank) along with its adjacent stream bed may create a corner reflector.

The importance of orientation of surface slope and geometries cannot be overstressed. In arid terrains this is especially apparent in the backscatter from ephemeral streams and wash channels which brighten when oriented perpendicular to the look direction then when oriented parallel to it.

Surface Roughness

The surface roughness is considered to be the next dominant factor in determining the amplitude of radar backscatter. As in visible wavelengths, a surface can be considered to reflect either in a specular or in a diffuse manner. Specular reflection occurs when the surface is smooth relative to the wavelength of light incident on that surface. In the case of specular reflection, the reradiated energy has a predictable phase relationship with the location and angle of incidence of the radar energy on that surface. In this case, maximum backscatter occurs at normal incidences and is near zero at all other angles.

In the case of a rough surface, the phase distribution of the reflected energy will no longer be linear or at angles related to the angle of incidence. Thus rough surfaces will scatter EM energy in different directions.

Clearly, the wavelength of incident radiation, the angle of

incidence and height differences between surface irregularities all play a part in determining whether a surface will behave as a specular or rough reflector. But at what point does the transition from smooth to rough occur? Rayleigh defined this point by analysis of the theoretical phase difference between two incident rays striking surface irregularities of height h and a grazing angle γ (derivation from Beckmann and Spizzichino, 1963). He determined that the phase difference, $\Delta\phi$, is:

$$\Delta\phi = \frac{4\pi h}{\lambda} \sin\gamma \quad (13)$$

where

h = height difference of surface irregularities

λ = wavelength

γ = grazing angle

If $\Delta\phi$ is very small then the two rays will be almost in phase and the surface is considered smooth. As $\Delta\phi$ increases the phase difference increases until the case of $\Delta\phi = \pi$ at which point the rays will be in phase opposite and cancel.

Rayleigh chose the midpoint $\Delta\phi = \pi/2$ as the arbitrary point between the two extremes. By substitution into Equation 13, and isolation of h on the left side of the equation, he stated that a surface is smooth if

$$h < \frac{\lambda}{8 \sin\gamma} \quad (14)$$

This is known as the Rayleigh criterion. The criterion is less stringent for longer wavelengths and lower grazing angles. That is, a surface

with height irregularities, h , may appear rough in X band (2-3 cm) images at a high grazing angle but could be smooth at either a lower grazing angle or at longer wavelengths such as the L band (25 cm). In the case of the X band imagery, used in this thesis, where $\lambda = 3$ cm and γ is 8° , the surface is smooth by the Rayleigh criterion if $h < 2.7$ cm.

Since Rayleigh's breakpoint between rough and smooth was both arbitrary and theoretical, others have quite naturally suggested other $\Delta\phi$ values, for example $\pi/4$ and $\pi/8$, as being more reasonable (Beckmann and Spizzichino, 1963). However, Schaber et al. (1976) found good agreement between the break predicted by the Rayleigh criterion and that from backscatter of gravelly alluvial fan surfaces in Death Valley.

Vegetation can behave as a rough surface, depending on the vegetation physiognomy, vegetation density and radar wavelength used. If the vegetation is dense arboreal or large scrub type, then it will not be penetrated by common radar frequencies and will reflect as an uneven rough scatterer. The return from a vegetation canopy of this type will appear as a region of light and medium light greys. Very sparse density but large physiognomy vegetation such as scattered oak trees will only occasionally influence the return, resulting in occasional light greys within the tone of the predominant scattering characteristics of the substrate.

The structure of vegetation can strongly depolarize the backscatter radiation in predominant directions. These effects have been reported by Sabins (1978) and by Schuchman and Lowry (1977); but the subtle effects of vegetation structure and depolarization have not been

completely understood. The effects of depolarization are most noticeable in dense homogeneous vegetation stands such as grasslands or field crops.

Dielectric Constant and Radar Penetration

When microwave energy is incident on a surface, part of that energy is reflected while the remainder penetrates a short distance into that surface. If that energy is reradiated, it creates a diffuse return known as volume scattering.

The degree of radar penetration is proportional to the radar wavelength and inversely proportional to the surface dielectric constant. The dielectric constant for most naturally occurring materials when dry, is on the order of 3 to 8. The dielectric constant for water is near 80 (MacDonald and Waite, 1973). Therefore the dielectric constant for most earth materials is primarily related to moisture content. The drier the soil, the lower its dielectric constant and therefore the greater surface penetration given the same radar frequency.

The texture of the soil does not greatly affect radar penetration. Lundien (1966) observed that under equal moisture conditions, laboratory samples of sand, loam and clay showed similar amounts of radar penetration. Hipp (1974) also found that under laboratory conditions, different clay loam soils showed similar increases in conductivity and dielectric constant values with increases in moisture. Limited data presented by Cosgriff, Peake and Taylor (1960) and Attema et al. (1974) also indicate that seasonal variations in radar backscatter

from relatively dense vegetation canopies were dominantly controlled by variations in the moisture content of the vegetation.

Differences in radar penetration due to radar frequency can produce dramatic differences in backscatter. In a study of near-shoreline vegetation using multispectral X (3 cm) and L (25 cm) band radar, Schuchman and Lowry (1977) reported a diffuse return in X-band and a specular return in L-band radar from a juncus-grass vegetation community with standing water. The shorter wavelength X-band radar did not penetrate the vegetation so that X-band backscatter was diffuse as if from a rough surface. The L-band radar was long enough to penetrate the vegetation and reflect specularly from the standing water.

Factoring the effects of radar penetration in the radar backscatter is usually more difficult than in the example above. While theoretical studies suggest a strong influence of volume scattering from radar penetration in the arid terrain, most practical studies tend to ignore this factor or fail to detect it. Laboratory data from Deane and Domville (1972) suggest that for very dry soils, X-band data will penetrate as much as 2 m. But Schaber et al. (1976) could find little evidence of volume scattering from surface penetration in L-band data of Death Valley.

Geometric and Cavity Resonance

Certain regular surface geometries and/or cavities, if they are near in dimension to the radar wavelength, will resonate with the incident radiation. When a certain spectral component of a rough surface

has a frequency equal to one-half the incident radar wavelength, a single Bragg scattering condition occurs. This leads to a resonance effect which is not unlike dihedral geometric reflectors. When the wavelength is equal to two surface spectral components, a double Bragg condition occurs. In either case, resonance to specific surface roughness frequencies leads to enhanced backscatter for certain rough surfaces (Dailey et al., 1978).

Cavities can also resonate if the cavity dimension is related to the incident frequency. The ideal situation for such resonance is when the cavity is bounded by good conduction such as metal plates. Thus many cavity resonators are found in manmade objects such as bridges, fences, etc. (Parry, 1974). This effect has been observed in Death Valley desert salt deposits, which have numerous solution cavities (Schaber et al., 1976).

Certain vegetation species also appear to resonate with incident radar frequencies on the same order of magnitude as the plant parts. Shuchman and Lowry (1977) found that returns from a forest of deciduous trees with twigs on the order of 20-25 cm long were extremely high on L-band wavelength radar in comparison to X-band radar. They attributed this to plant resonance.

CHAPTER 2

FIELD AND LABORATORY INVESTIGATIONS

Field and laboratory investigations were undertaken to obtain qualitative and quantitative descriptors of surface variables for the classification of geomorphic surfaces and the correlation of field data with image data. To this end, the first task in the field was the reconnaissance of the study area. This involved the location and identification of major rock types, observation of stratigraphic relationships, the identification of the suite of geomorphic vegetational surface types in the area, and the location of field sites for detailed investigations.

A mosaic of four orthophotoquads at a scale of 1:24,000 served as the base map for location and notational purposes (Figure 15). Although these black-and-white photographic products suffered from poor contrast and resolution, the advantages of being inexpensive, easily available, orthogonized and of relatively large scale made them the logical choice for a base map. Topographic maps were only available at the scale of 1:56,000. Since low-relief alluvial surfaces had to be located, these topographic maps had limited use and were only used as a source of place names and elevational data.

The second task involved the location of field sites for detailed investigations. Geomorphic data collected at these sites formed the basis

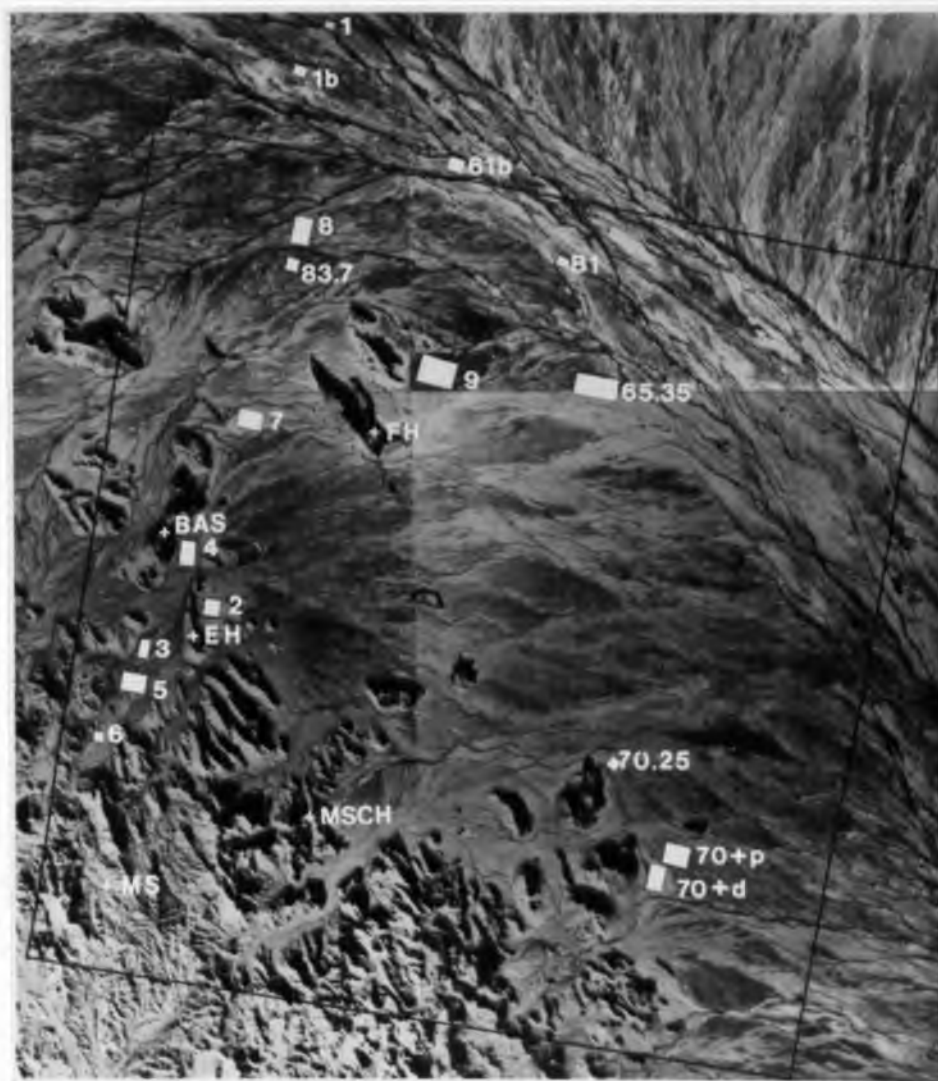


Figure 15. Orthophotoquad mosaic with outline of study area and location of field sites.

for a classification of the study area. Other more quantitative data were collected for the analysis of the relationship between various terrain features with the image data.

Radiometric investigations were undertaken in three steps: first in the analysis of the VNIR reflectance spectra of desert varnished rocks; then in a field reflectance study of desert pavement surfaces; and finally in the analysis of multispectral image data.

Geomorphic Reconnaissance

Geomorphic surfaces occurring in the study area range in age from oldest middle Pleistocene (Q2a) to latest Holocene (Q4) and consist of particles ranging in size from very coarse gravels (up to 30 cm) to fine silts and sands.

In the upland portions of the piedmont, a suite of gravelly alluvial surfaces from Q2a to Q4 age occurs as fill terraces along large mountain washes. The relationship of these stream terraces as observed in the field are illustrated in a generalized way in Figure 16.

Pleistocene Q2a and Q2b surfaces are found as remnants of a Pleistocene fan deposit which is elevated about 7 m above the modern wash. The oldest and highest surface is the Q2a. This surface is largely reduced to a series of knobby ridges separated by wide ravines. Only a few areas of flat pavement surface remain. These are, in most places, vertically degraded on the order of .5 m such that the surface is littered with pedogenic petracalcic clasts along with rocks whose surface coating ranged from dark to lightly varnished. Rocks on this surface show signs of salt-splitting, erosion of varnish, and are not well-mosaicked.

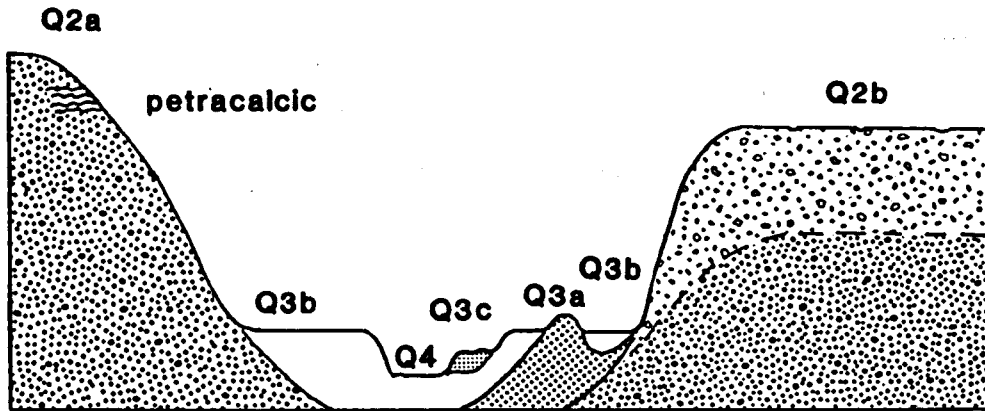


Figure 16. A generalized cross-section illustrating the terrace relationships in the mountain valleys (not to scale).

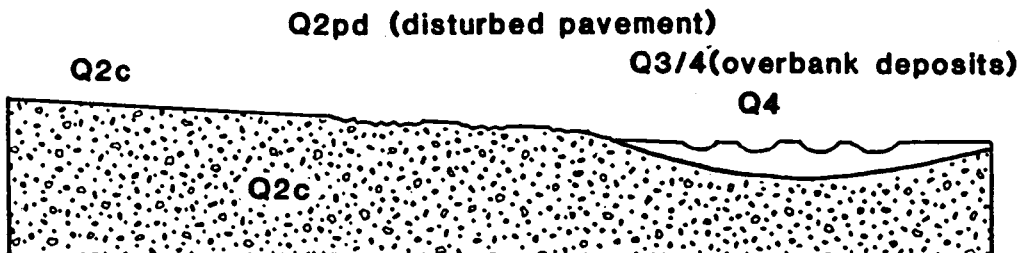


Figure 17. A generalized cross-section illustrating the alluvial geomorphic surfaces across the valley bottom (not to scale).

The Q2b pavement is about 2 m below the Q2a pavement and forms the surface of most of the old Pleistocene fan. This surface is flat with darkly varnished rocks and a tightly mosaicked pavement but is dissected by a regular series of valleys which are largely formed by streams which head on the surface. Its characteristic topography is that of a regular series of flat-top ridges alternating with small to large valleys.

The Q2c surface is a younger Pleistocene surface not found in the old Pleistocene fan. This is the most prevalent Quaternary surface in the middle parts of the study area valley and is found downstream from the older fan at an elevation of only 1 to 2 m above Q3 surfaces. Its absence in the upper part of the valley indicates that the upper reaches of streams were predominantly in an erosional mode during Q2c and early Q3 times.

Q3 surfaces are near the modern stream surface with the highest Q3 surface, the Q3a, being only about 2 m above the modern channel. The Q3a surface is the oldest and the least extensive. On this surface a thin patchy pavement has begun to form with rocks which have darkened somewhat with desert varnish. The surface morphology is a subdued bar and swale topography. A thin vesicular horizon has developed in this soil with slight carbonate coatings on pebbles in the C horizon.

The Q3b surface is the most extensive Q3 surface. This surface has a pronounced bar and swale surface morphology. There is no varnish but the rocks are weathered. A thin vesicular horizon and thin carbonate coatings on pebbles are present.

The youngest Q3 surface, the Q3c, shows only a slight alteration of the bar and channel surface morphology, no darkening of the surface, and only a trace of calcium coating on pebbles.

For the purposes of this thesis, the Q3 and Q4 surfaces have been grouped together since their individual areal extent is below the spatial resolution of sensors used in this study. Nevertheless, they have been described in relative detail for two sites, site 1 and site 3, which are modern stream channels with dense riparian vegetation and a wide modern drainage-way with evenly distributed riparian vegetation, respectively. The latter is an area of poorly channelized, wide floodplain Q4 and Q3 surfaces which act as an important ephemeral floodway.

Geomorphic surfaces found near and across the valley floor of the study area can be grouped into 5 basic types (Figure 17). The oldest type is the Q2c surface. These are described in great detail in subsequent sections and will only be briefly generalized here. The surface is characterized by a dark, flat pavement showing varying amounts of surface dissection. The pavement surface where it is not dissected is very flat, dark brown to black, and tightly mosaicked with a very low surface roughness. The surface roughness is much less than that suggested by the average particle size measurement since the flattest surface of the individual particles composing the pavement tends to align with the plane of the pavement. The vesicular horizon is thick (≈ 5 cm) and the calcic horizon is well developed. The B horizon is a bright reddish brown color and contains illuviated clay.

The Q2c pavement surface is devoid of vegetation except for a few ephemeral and hardy species, notably turks beard (Chorizanthe rigida) and skeleton weed (Eriogonum deflexum). Where dissection runnels occur or at circular sand mounds and cleared silty areas, the vegetation is more abundant and varied.

A second type of surface is informally named degraded or disturbed pavement (Q2pd). These are pavements which are, as a whole, undergoing active erosional transition to a modern alluvial surface but still retain much of the soil and morphologic characteristics of an older pavement surface. Mostly they are Q2c pavements which have been partially destroyed by sheetwash or surface runoff. These areas are transitional to Q3/Q4 poorly channelized active surfaces. The Q2pd surfaces often have small patches of preserved dark pavement occurring as isolated island remnants of the soil which has been truncated in most places. The truncation of Q2c soils and the removal of rock varnish results in a surface which is on the average bright, flat, and irregular (i.e., high roughness). Vegetation on these surfaces is thin but distributed evenly with ocotillo (Fouquieria splendens), creosote (Larrea tridentata), and brittlebush (Encelia farinosa) dominant.

The third type of surface is the Q3/Q4 poorly channelized floodway. This type of surface acts as surface runoff drainageways during ephemeral flood events and is characterized by rough, poorly sorted, poorly varnished particles; even and open distribution of riparian-type plants; and an irregular, undulating surface morphology created by numerous minor channels, bar and dune deposits.

The fourth type is the Q4 fine alluvium surface. These surfaces probably originate as stream overbank deposits and are found as slightly elevated (.5-2. m) flats of fine sand and silts along the axial stream complex. Often there is a surface crust which may include small pebbles. Invariably, these surfaces support pure stands of creosote bush (Larrea tridentata) which are distributed in an open even pattern but vary greatly in density from site to site. The Q4 fine alluvium surfaces are usually the brightest surfaces in the piedmont.

The fifth type of surface is the Q4 modern stream channel with associated dense riparian vegetation. These channels at the resolution level of Landsat data have a mixed reflectance which is an average of that for the vegetation and for the sand and gravel channel deposits.

Site Location and Field Descriptors

A group of field sites was chosen as representative of the range of alluvial geomorphic surfaces found in the study area. A total of 17 alluvial sites were investigated in detail. These are labeled by alphanumeric characters (Figure 15). Five bedrock sites labeled by alphabetic characters only were located for general lithologic and geologic control but were not sites of detailed investigation (Figure 15).

Field data collected at the alluvial field sites were as follows:

1. Surface Description: The general description of the site, its location, setting, geomorphology, vegetation and soil characteristics.
2. Soil Description: A description of the most developed or

characteristic soil pedon found in the site. Conventional soil terminology (Soil Taxonomy, USDA, 1975) is used except where conventional terminology is inadequate to describe the soil or soil horizon. For example, the desert pavement and vesicular silt horizons are informally designated P and V, respectively, since these horizons do not conform to the definitions for O, A, A1, or A2 horizon designations.¹ Another example is the classification of pedons at sites of fluvial activity as Torrifluvents, even though these soils may not meet the organic matter requirements for a Torrifluent in the Soil Taxonomy.²

3. Vegetation: Wherever possible the density, distribution, and type of vegetation found on a site is given. Density is given in percent cover based on 30-meter linear transects at the site. Due to the generally low densities and uneven distribution of vegetation encountered in these desert sites, density figures are often given in ranges. The dominance of plant types is given on a numerical scale where 1 = predominant, 2 = common, 3 = occasional, and 4 = rarely found.
4. Terrain descriptors: Only three terrain descriptors were used. These are:

1. This is not without precedent. Other authors (Peterson, 1980; McHargue, 1981) have used Av and V as informal designations for the vesicular horizon.

2. Naming soils Torrifluvents despite the organic matter requirement conforms to the usage of that term by Richardson, Clemmons and Walker (1979) in the soil survey of nearby Cochise and Pima counties.

- a. **Roughness:** The surface micro-relief is a subjective rating estimated from surface particle sizes, surface height differences (h) and the type and density of vegetation. Roughness is given on a scale of 1 to 5 where:
- 1 = h < 3 mm , < 5% veg
 - 2 = h > 3 mm - < 10 mm, < 5% veg
 - 3 = h > 10 mm - < 20 mm, and/or 5 - 15% veg
 - 4 = h > 20 mm - < 40 mm, and/or 15 - 30% veg
 - 5 = h > 40 mm and/or > 30% veg
- b. **Slope:** The most common direction and angle of slope. Given in compass quadrants and percent grade.
- c. **Variability:** The standard deviation of > 20 transit readings on a 30 m transect perpendicular to the slope.
5. **Surface particle sampling:** A 1 to 2 kilo sample of the surface clasts at the site. The samples were sieved and the larger clasts cut open for lithology identification. The methods of sieving and lithology identification are presented in Appendix B. Data are summarized as follows:
- a. Dominant lithology/ies.
 - b. Mean particle size, x, determined as:

$$x = \left(\sum_{i=j}^K w_i s_i \right) w_T^{-1} \quad (15)$$

where

i = ith sieve

j = first sieve (largest)

k = last sieve

w_i = net weight of particles which pass sieve $i-1$ but
not sieve i

s_i = size in mm of sieve i

w_t = total sample weight

- c. Range: The range of particle sizes given in the total number of phi size sieves with greater than 5% of the total weight.
6. Radiometer readings: The multispectral reflectance of the site surface obtained in 5 wavebands with a handheld radiometer. Raw radiometric data are included in Appendix C and are referenced in the individual site descriptions. Summary presentation of radiometric field data is given in a later section of this chapter.
7. Photography: Black-and-white photographs illustrating the site from ground level are included in the site descriptions.

Site Descriptions

Site 1. Q4 Stream Channel

1. Surface: The site is located in one of the major channels of the ephemeral, anastomosing King valley axial stream system. The channel is cut to 1 to 2 meters below the surrounding terrace and is composed of gravel-and-sand-size mixed volcanic rocks with some sedimentary and meta-sedimentary rocks. The volcanic rocks, for the most part, are light-colored rhyolitic tuffs and flowstones. The channel surface ranges from flat to irregularly planar with a low relief up to .5 m imparted by dune and riffle sequences. Areas of highest relief occur at channel confluences.

2. Soil: Typic Torrifuvent. The soil is undeveloped, A-C soil with no horizonation. Channel deposits are fresh, loose, and easily dug into by the hand.
3. Vegetation: The vegetation is dense riparian dominated by palo verde (Cercidium sp.) (2); jojoba (Simmondsia chinensis) (2); Acacia sp. (2); with common ironwood (Olneya tesota) (2); mesquite (Prosopis juliflora) (2); creosote bush (Larrea tridentata) (3); and Ambrosia ambrosioides (3); Brickellia coulteri (3); Bebbia juncea (3); Lycium sp. (3); and Beloperone californica (3). Distribution of vegetation is highly uneven and linear. In the channels the density is 0%; flanking the active channels density may exceed 90%.
4. Terrain: Roughness = 5, slope = 1.5% S50E; no variability data (ND).
5. Sample: No sample taken (ND).
6. Radiometric data: R35, R40, R42.
7. Photography: Figure 18.

Site 2. Q2pd Erosional Bedrock Basin

1. Surface: The site is located in a small bedrock basin whose surface is composed of exposed yellow tuff littered with thick white petrocalcic fragments and remnant varnished pavement rocks with occasional large boulders of darkly varnished tuff. The Q2 paved soils developed in situ on the tuff has been degraded in most places by at least one meter. The petrocalcic fragments are pedogenic and residual from Pleistocene soil.
2. Soil: Lithic Torriorthent. Erosional surface, not developed, no horizonation.



Figure 18. Site 1, Q4 stream channel.



Figure 19. View east overlooking site 2, erosional bedrock basin.

3. Vegetation: Very sparse, 0-3% density except at stream channels, where density may exceed 10%. Common plants are brittlebush (Encelia farinosa) (2); Ambrosia dumosa (2); skeleton seed (Erigonum deflexum) (2); Indian buckwheat (Plantago insularis) (2); with occasional ocotillo (Fouquieria splendens) (3); saguaro (Cereus giganteus) (3); and teddy-bear cholla (Opuntia bigelovii) (3).
4. Terrain: Roughness = 2, slope = 3%, N60E, variability = no data (ND).
5. Surface particle sample: ND.
6. Radiometer: R4.
7. Photography: Figure 19.

Site 3. Q3/Q4 Mountain Wash

1. Surface: A wide, relatively unincised wash system carrying gravel and coarse sand alluvium in the upland region. The surface consists of many poorly channelized streams and low terraces. Vegetation is common, riparian in character but spread evenly throughout rather than in a dense linear fashion as in channelized wash systems. In detail several of the Q3 terraces have more developed soils (Camborthids) than the soil described below.
2. Soil: Torrifuvent. Undeveloped A-C soil, no distinct pavement, no horizonation. Some soils on surface are more developed with signs of rock varnishing and formation of vesicular horizon. Surfaces in site range from Q3b to Q4.
3. Vegetation: A large variety of plants with densities from 12 to 20%. Common plants are ironwood (2); jojoba (2); creosote bush (2); saguaro

(2); Encelia (2); palo verde (2); desert smoketree (Dalea spinosa) (2); Erigonum sp. (2); Sphaeralcea sp. (2); Lycium sp. (2); Bebbia juncea (2); and greythorn (Kameria sp.) (2).

4. Terrain: Roughness = 4, slope = 3%, N60E, variability = .66

5. Sample: Lithology = mixed volcanic rocks, mostly rhyolites but some latites with sedimentary rocks. Mean = 19 mm. Range = 5 phi.

6. Radiometer: R32, R36, R37, R39, R41, R50, R51.

7. Photography: Figure 20.

Site 4. Q2c Pavement

1. Surface: Flat dark alluvial pavement.

2. Soil: Typic Haplargid.

cm

- | | | |
|-------|-----------------|--|
| 2-0 | P | Well-developed desert pavement, dark brownish red varnished gravel, tightly mosaicked but not perfectly fitted. Boundary very abrupt, irregular. |
| 0-2 | V | Vesicular horizon. 7.5YR6/4, dull brown pebbly, sandy, silt. Not indurated. Boundary clear, smooth. |
| 2-6 | V ₂ | Slightly redder, less pebbly sandy silt. Boundary abrupt, smooth. |
| 6-12 | B ₁ | 5YR5/6 bright reddish brown pebbly sandy silt with some clay. Clay is not sticky, not plastic. Boundary abrupt, wavy. |
| 12-30 | B _{2t} | Same color as above but more clays. Texture is silty clay loam. Clay is plastic and sticky. Common fine to |



Figure 20. View west overlooking site 3.



Figure 21. Site 4, Q2c pavement.

very fine. White to pinkish white (7.5 YR 8/1-8/2) mottles that effervesce violently when hydrochloric acid is applied. Boundary is clear and smooth.

30-55+ Cca Gravel with continuous thick calcium carbonate coating.

Stage II carbonate development.

3. Vegetation: Vegetation density ranges from 0 on the pavement to 20% where small channels or runoff runnels occur. Most of the site is desert pavement which is nearly barren of vegetation. Only Turks beard (Chorizanthe rigida) and Indian buckwheat exist on the pavement. On the surface runnels and fluves the common plants are palo verde, saguaro, brittlebush, and teddy bear cholla plus other Opuntia sp.
4. Terrain: Roughness = 2, slope = 1.7%, N30E, variability = .84.
5. Sample: Lithology = rhyolites with meta-sedimentary rocks, mean = 11.9 mm, range = 3 phi.
6. Radiometer: R12, R13, R14, R43, R45, R52, R54.
7. Photography: Figure 21.

Site 5. Q2b Dissected Desert Pavement

1. Surface: Dissected desert pavement developed on an elevated and truncated Pleistocene alluvial fan. Large channels which head on the surface as well as channels from upland bedrock sources have removed considerable amounts of material from the fan surface. Dark desert pavements form flat ridge tops between dissection valleys. Although rocks are tightly fitted and show dark varnish, pavement is not as continuous as in younger Q2c surfaces. Evidence of uniform surface degradation seen in calcium

rings around bedrock knobs but no greater than 50 cm and few pedogenic calcium clasts show on the surface. Surface shows slight hint of bar and swale macro-relief but the original depositional bar and channel morphology is primarily preserved in textural differentiation with coarser rocks at bars and finer rocks at swales. Larger clasts show signs of salt-splitting.

Due to dissection, overall relief is significant with height differences averaging 5 to 10 m from the largest stream levels to ridgetop. Valleys are wide, with ridges separated by approximately 100 m. Regularity of dissection channels alternating with paved ridgetops produce a ridge and valley topography.

2. Soil: Typic Haplargid.

cm

- | | | |
|-------|-----|--|
| 3-0 | P | Tightly fitted paved gravels. Dark reddish black varnish 2.5 YR 3/1. Varnish is blacker along pebble sides. Undersides of clasts are red although many appear red from being overturned. Clasts are mixed volcanic rocks, mostly rhyolites; average size from 1.5 - 3 cm, but many are much larger. Boundary very abrupt, irregular. |
| 0-4 | V | 7.5YR6/6, orange, cakey (partially indurated), calcareous, vesicular sandy silts. Bottom gradually more pebbly, redder. Boundary distinct, smooth. |
| 4-12 | B1 | 5YR6/4 dull orange sandy gravel. |
| 12-32 | B2t | 2.5YR4/8 reddish brown pebbly clay. Sticky, plastic to very plastic. At 15 cm abundant fine, distinct carbonate |

mottles. Boundary gradual, wavy.

32+ Cca Plugged calcic sandy gravel. Stage III carbonate development.

3. Vegetation: Less than 3% on pavement, up to 7% and higher in dissection channels. On pavement teddy bear cholla (2), creosote bush (2), brittlebush (2). In channels brittlebush (2), jojoba (2), saguaro (2), and ocotillo (2). In larger channels riparian bushes and small trees of large variety similar to site 3.
4. Terrain: Roughness = 2.5, slope = 3.9%, N30E, variability = 17 (very high due to large relief).
5. Sample: Lithology = mixed volcanics, mostly rhyolitic felsites, dacite-andesites; mean = 18.4 mm; range = 3 phi.
6. Radiometer: R7, R8, R9, R10, R11, R44, R53.
7. Photography: Figure 22.

Site 6. Q2a Dissected Pavement

1. Surface: Highest and oldest alluvial geomorphic surface approximately 2 m above Q2b on dissected and truncated Pleistocene fan. Most of site is sloped with only few flat pavement remnants. These pavement surfaces are not well sorted and poorly fitted, with particles ranging from 20 cm to fine sands and silts. Rocks are variously varnished, some dark and some light, pedogenic calcium clasts litter the surface, and the larger rocks show signs of salt-splitting. Relief is up to 12 m, slopes from 5 to 20% in all directions. Topography is hill and valley.
2. Soil: Paleargid.



Figure 22. View NW from site 5, Q2b pavement, to tuff hill



Figure 23. View NE from site 6, Q2a pavement.

cm

- 3-0 P Gravelly pavement, poorly sorted, not well fitted, darkly varnished to lightly varnished rocks and Cca clasts.
Boundary very abrupt, irregular.
- 0-3 V 5YR5/6, bright reddish brown, not indurated, pebbly fine sandy silt. Calcareous. Boundary abrupt, smooth.
- 3-15 C 5YR6/4, dull orange, calcareous, slightly indurated pebbly sandy silt. Boundary distinct, wavy.
- 15-40+ IIC 5YR6/4 dull orange clayey silty calcic gravel. Clay is not sticky, not plastic. Continuous carbonate coating stage III, plugged.

Soil is polygenetic in at least three cycles. Oldest cycle produced pedogenic calcium clasts found on surface. Second cycle is the truncated soil represented by the IIC horizon. The upper horizon's soil is a relatively young (Holocene) soil development.

3. Vegetation: Density on pavement is less than 5%, but in surface runnels density approaches 15%. Distribution is uneven, linear and dendritic. Common plants are creosote bush (2), ocotillo (2), Plantago insularis (2), teddy bear cholla and other Opuntia sp. (2). Large washes and stream valleys have other plants similar to lists in sites 3 and 4.

4. Terrain: Roughness = 3.5, slope = variable, variability = very high, not measured.

5. Sample: Lithology = metasedimentary rocks and rhyolites; mean = 29.9; range = 4.

6. Radiometry: R6.

7. Photography: Figure 23.

Site 7. Q2pd Degraded Desert Pavement

1. Surface: The surface is flat, near stream level, composed of gravels which have light to medium-light varnish along with scattered calcium carbonate clasts. Vegetation is sparse but common, occurring throughout the surface in an open, even distribution. The surface is bright compared to patches of dark pavement surrounding the site. Apparently surface runoff has degraded a uniformly dark pavement surface into a large area of interfingering pavement and degraded pavement soils.

2. Soil: Calciorthid.

cm

- | | | |
|-------|---|---|
| 2-0 | P | Brownish grey calcium-coated small volcanic gravels which have a light to medium-light varnish with pedogenic calcium clasts and sand and silts. Boundary very abrupt, irregular. |
| 0-3 | V | 5YR6/4 dull orange vesicular, calcareous, cakey silty sand. Boundary abrupt, smooth. |
| 3-20+ | C | 5YR6/4 dull orange calcareous pebbly sand. Stage 1 carbonate development, thick calcium coating around pebbles. |

3. Vegetation: Density is less than 5%. Common plants are ocotillo (2), creosote (2), brittlebush (2), teddy bear cholla (2), saguaro (2), Coldenia sp. (3), and various Opuntia (3).

4. Terrain: Roughness = 2, slope = 3%, N30E, variability = .58.

5. Sample: Lithology = rhyolitic volcanic rocks; mean = 15.7 mm; range = 3 phi

6. Radiometer: R23.

7. Photography: Figure 24.

Site 8. Q2pd Degraded Desert Pavement

1. Surface: A light-colored flat but irregular surface of pebbles, sand and silt. The pebbles are volcanic rocks, some of which are varnished but most are not. The site is located in the pediment region near the valley floor. Surface irregularities and features suggest eolian and fluvial deposition and reworking of surficial fines. However, bar and swale surface morphology of original Pleistocene surface and deposit is evident in larger-frequency surface undulations and in the distribution of fine and coarse gravels.

2. Soil: Haplargid.

cm

1.5-0 P Light-colored, little varnished to unvarnished, poorly interlocking, pebbly silty sand. Boundary very abrupt, irregular.

0-3 V 5YR7/3 dull orange, cakey, vesicular sandy silts. Boundary very abrupt, irregular.

3-7 B1 Same as above but texture is pebbly sandy silts. Less indurated. Boundary abrupt, smooth.

7-20 B2t 5YR6/4 dull orange pebbly, sandy clay. Clay is sticky and very plastic. Thin calcium coatings on bottom of pebbles. Boundary abrupt, irregular.

20-42+ C Dull white to orange sandy gravel. Thick continuous



Figure 24. Surface of site 7 (Q2pd), degraded pavement.



Figure 25. Surface of site 8 (Q2pd), degraded pavement.

calcium coatings on pebbles (stage II), calcium mottling in sand.

3. Vegetation: Density 2 to 7%. Almost all creosote bush with seasonal Turks beard.
4. Terrain: Roughness = 2, slope = 2.4%, N30E, variability = 1.6.
5. Sample: Lithology = rhyolitic volcanic rocks; mean = 12.7 mm; range = 3 phi.
6. Radiometer: R27, R28, R29, R30, R48.
7. Photography: Figure 25.

Site 9. Q2c Pavement

1. Surface: Extremely flat, dark, well-sorted and interlocked desert pavement. The surface is located downslope from a prominent inselberg and is well intact with only very moderate dissection.
2. Soil: Camborthid due to insufficient soil data, but probably Haplargid.

cm

- | | | |
|--------|-----|--|
| 2-0 | P | Dark brownish black varnished and paved pebbles, averaging 1-2 cm with maximum around 8 cm. Boundary very abrupt, irregular. |
| 0-10 | V | 7.5YR6/6 orange, vesicular, cakey, sandy silt. Boundary abrupt, smooth. |
| 10-25+ | B2t | 7.5YR6/8 orange pebbly fine sand and silts. Carbonate mottles in soil. |

3. Vegetation: Density = 0. Virtually barren pavement except for

ephemeral Indian buckwheat and Turks beard. Dissection channels have usual riparian-type vegetation.

4. Terrain: Roughness = 1.5, slope = ND (low slope), variability = ND (low).
5. Sample: Lithology = mixed volcanics, rhyolites to quartz latite; mean = 16.9 mm; range = 3 phi.
6. Radiometer: R15.
7. Photography: Figure 26.

Site 1B. Q2pd Fine-Grain Disturbed Pavement

1. Surface: A medium-dark flat pavement near the basin axis. The surface is composed of well-sorted pebbly gravels averaging 2 cm. In places the pavement is darkly varnished, but in other areas light-color silts of the vesicular horizon are brought to the surface by vehicular traffic. Encroaching vegetation disturbs pavement surface and also traps eolian deposits.

2. Soil: Typic Haplargid.

cm

- | | | |
|-------|-----|--|
| 2-0 | P | 2.5YR6/5-2.5YR5/3 dull orange to dull reddish brown fine gravel pavement. Pavement is discontinuous and patchy, alternating with silty in more vegetated areas. Boundary very abrupt, irregular. |
| 0-2 | V | 5YR5/8 bright reddish brown vesicular, cakey, silty loamy sand. Abrupt, smooth boundary. |
| 2-8.5 | B2t | 5YR5/8 bright reddish brown loamy sand. Clays plastic, |



Figure 26. Surface of site 9, Q2c pavement.

not sticky. Calcareous throughout, a few pebbles with thick Cca coatings. Boundary abrupt, wavy.

8.5-16+ Cca Sandy gravel. Gravels with continuous calcium coatings and plugged with Cca (stage III).

3. Vegetation: Density 0% on pavement except for usual Turks beard and Indian buckwheat. Between intact pavements, density approaches 23% with commonly: creosote bush (2), Ambrosia dumosa (2), ocotillo (2), ironwood (2), and palo verde (2).
4. Terrain: Roughness = 2, slope = ND, variability = ND.
5. Sample: Lithology = mostly flow-banded rhyolites with mixed acid volcanic rocks; mean = 12.9 mm; range = 3 phi.
6. Radiometer: R24, R25, R47.
7. Photography: ND.

Site B1. Q3/4 Sandy Alluvial Flat

1. Surface: Flat sandy valley floor with open stands of creosote bush. Mostly yellowish silts and fine sands with a litter of unvarnished volcanic pebbles. Average pebble sizes are 1-2 cm with none exceeding 5 cm. Site of active stream overbank and eolian deposition.
2. Soil: Typic Torriorthent.

cm

1-0 P Pebbly float of no greater than 2-5 cm-diameter rocks form an incipient pavement. Most of surface is yellowish sand and silt. Black organic surface crusts also occur in places. Abrupt and irregular boundary.

0-43+ C Loose unconsolidated 5YR7/3, dull orange pebbly sandy silt. Carbonate on pebbles are second cycle.

3. Vegetation: Density less than 6%, all creosote bush except for Turks beard and plantago.
4. Terrain: Roughness = 1, slope = 2.2% due east, variability = 1.02.
5. Sample: Lithology = rhyolitic tuffs and volcanic conglomerates; mean = estimated 2.4 mm; range = 4 phi +.
6. Radiometer: R33, R34.
7. Photography: Figure 27.

Site 61B. Q3a Lightly Varnished Flat Pavement

1. Surface: Light-colored, lightly varnished flat pavement composed of mixed volcanic clasts. Average pebble size is 1 cm, with the largest around 3 cm. In places, silts and sands with scrub vegetation.
2. Soil: Typic Calciorthid.

cm

- | | | |
|------|---|---|
| 1-0 | P | Unvarnished to lightly varnished volcanic pebbles with sand and silts. Abrupt, irregular boundary. |
| 0-1 | V | Thin, loose, vesicular sandy silts. Abrupt, wavy boundary. |
| 1-20 | B | 5YR6/6 orange gravelly sand. Clear, discontinuous boundary. |
| 20+ | C | Same color gravelly sand with discontinuous to continuous carbonate coatings on pebbles (stage II). |

3. Vegetation: Density from 0-10%. Common plants are creosote (1), Turks beard (2), Indian buckwheat (2).



Figure 27. Surface of site B1, sandy alluvial flat (Q3/Q4).



Figure 28. Site 65.35, Q2c dark pavement.

4. Terrain: Roughness = 1.5, slope = ND, variability = ND.
5. Sample: Lithology = rhyolites, mean = 5.9 mm, range = 5 phi.
6. Radiometer: R31, R49, R55.
7. Photography: ND.

Site 65.35. Q2c Dark Pavement with
Encroaching Vegetation.

1. Surface: Flat darkly varnished well-sorted gravel pavement surrounded by unpaved silty creosote flats.
2. Soil: Typic Haplargid.

cm

- | | | |
|--------|-----|--|
| 2-0 | P | Dark, well-interlocked but not completely mosaicked desert pavement. Some clasts are unvarnished, but majority darkly varnished with darkest band around edges intersecting surface plane. Average gravel diameter is 2 cm, with maximum at 7 cm. Boundary very abrupt, irregular. |
| 0-6 | V | 5YR8/3 pale orange, well indurated (cakey), vesicular, clayey silts. Free from pebbles. Abrupt, smooth boundary. |
| 6-12 | B1 | 5YR6/6, orange pebbly loam. Abrupt, wavy boundary. |
| 12-42+ | B2t | 5YR5/4 reddish brown, pebbly, sandy clay. Clay is sticky, very plastic. Pebbles are weathered with continuous calcium coatings. C horizon not found. |

3. Vegetation: Density is 0% on well-developed pavement. In silty pavement-free areas, density reaches 10%. Common plants are creosote (2), Turks beard (2), and Indian buckwheat (2).
4. Terrain: Roughness = 1.5, slope = 1.5%, S80E, variability = 1.4.

5. Sample: Lithology = mixed acidic to intermediate volcanic rocks from rhyolite to andesite; mean = 12.6 mm; range = 2 phi.
6. Radiometer: R16, R17, R20.
7. Photography: Figure 28.

Site 70.25. Q2c Dark Pavement with Intermediate Volcanic Composition

1. Surface: At base of dark basaltic andesite hill. Dark pavement barren of vegetation, moderately dissected with vegetation in dissection fluves.
2. Soil: Paleargid, similar to site 70+P.
3. Vegetation: Density 0% on pavement. In shallow surface dissection fluves, density reaches 5%. Plants are palo verde (2), creosote (2), brittlebush (2), and Indian buckwheat (2).
4. Terrain: Roughness = 1.5, slope = ND, variability = ND.
5. Sample: Lithology = intermediate volcanic rocks from quartz latite to trachyandesite, mean = 17.8, range = 4.
6. Radiometer: R18.
7. Photography: ND.

Site 70+P. Q2c Dark Pavement in Intermediate Volcanics

1. Surface: Moderately dissected flat dark well-developed pavement. Shallow dissection fluves and silty white circular areas break up continuous pavement and are the only surfaces with vegetation.
2. Soil: Paleargid.

cm

- 2-0 P Darkly varnished well-interlocked gravel pavement with most particles oriented with plane of pavement. Boundary very abrupt, irregular.
- 0-6 V 5YR6/4 dull orange, almost pebble-free, vesicular and cakey, calcareous, sandy silt. Reddening toward bottom to 5YR5/6 bright reddish brown, not indurated silty loam. Very abrupt, smooth boundary.
- 6-19 B2t 5YR5/6 bright reddish brown clayey gravel. Clay is sticky and plastic. Calcium coating on bottom of gravel up to 1 mm thick. Abrupt, wavy boundary.
- 19-39+ Cca Slightly duller gravels with continuous carbonate coatings on pebbles (stage III) but not plugged. Pebbles very weathered.

3. Vegetation: Density from 0 on well-developed pavement to 10% in dissection fluves. Common plants are creosote (2), brittlebush (2), ironwood (3), Ambrosia dumosa (3), pencil cholla (Opuntia arbuscula) (3), greythorn (Condalia sp.) (3).

4. Terrain: Roughness = 1.5, slope = 2%, S30E, variability = .59.

5. Sample: Lithology = mixed volcanics from rhyolite to andesite; mean = 14.7; range = 3.

6. Radiometer: R19.

7. Photography: Figure 29.

Site 70+D. Q3/4 Coarse Erosional Surface

1. Surface: Located close to the axial stream complex, the surface is



Figure 29. Site 70+P, dark Q2c pavement.



Figure 30. Site 70+D, Q3/4 coarse erosional surface.

a poorly sorted site of active fluvial erosion. Rocks are from large cobble size to gravels and sand. Clasts are unvarnished, some are rounded; strong bar and channel morphology creates surface undulations.

2. Soil: Torrifuvent.

cm

2-0 A Unpaved, mixed volcanic and sedimentary rock gravels and sand. Clasts are unoriented and unvarnished. Depositional sorting of coarse and fine in gravel bar and channel deposits.

0-30+ C 5YR6/3 dull orange loose, sandy gravel. Boundary gradual, irregular.

3. Vegetation: Density less than 15%, distribution is open and even. Common plants are creosote (2), ironwood (2), brittlebush (2), saguaro (3), and ocotillo (3).

4. Terrain: Roughness = 3, slope = 2.3%, S60E, variability = .59.

5. Sample: Lithology = sandstones with mixed volcanic rocks, mean = 12.2, range = 6 phi.

6. Radiometer: R38.

7. Photography: Figure 30.

Site 83.7. Q2c Dark Pavement

1. Surface: Fine grain, darkly varnished well-interlocked pavement of mostly rhyolitic gravels.

2. Soil: Camborthid.

cm

2-0 P Flat darkly varnished, well-interlocked gravels. Average

size 1 cm, with maximum size at 12 cm. Abrupt, irregular boundary.

0-4 V 5YR6/4 dull orange, vesicular, cakey, calcareous, sandy loam. Abrupt, smooth boundary.

4-10 B1 5YR6/6 orange, very gravelly loamy sand.

10+ B 5YR6/6 orange gravel with calcium coating on pebbles (stage I).

3. Vegetation: Density is 0% on pavement; in runnels >10%.
4. Terrain: Roughness = 1.5, slope = ND, variability = ND.
5. Sample: Lithology = rhyodacite to quartz latite volcanic rocks; mean = 11.1; range = 3.
6. Radiometer: R22, R26, R46.
7. Photography: ND.

Laboratory Reflectance of Desert Varnish

Laboratory spectral reflectance curves of desert varnish samples were obtained for the spectral range from .4 μm to 2.4 μm using the integrating sphere reflectometer (ISR) at the Optical Sciences Department, University of Arizona. A total of 5 varnished specimens of various lithologies were used in the study. Three of these were obtained from Carlton Allen and were the same samples used in his electron microprobe study (Allen, 1978). These are: (1) Colorado River terrace amphibole; (2) Colorado River terrace andesite; and (3) Pinecate basalt. The remaining two samples were collected from a Q2a remnant pavement surface at Sheep Mountain in the Gila mountain range, eastern Arizona.

These are (4) Sheep Mountain quartz monzonite and (5) Sheep Mountain amphibolite.

The Colorado River samples (numbers 7 and 2) are directly 20,000 to 60,000 years old (Bull, personal communication, 1981). The Pinacate basalt specimen (number 3) is heavily varnished and probably similar in age to the heavily varnished Malpais stage tools described by Hayden (1976). His chronology would place the age of this varnish as greater than 20,000 years old. Samples 4 and 5, being from a Q2a surface, are probably significantly older. The Q2a surface at Sheep Mountain has been dated by indirect geomorphic criteria as probably greater than 100,000 y.b.p. (Schenker, 1977).

The ISR is an optical instrument which measures the average bidirectional reflectance of a specimen by the indirect or hemispheric directional mode. A tungsten halogen light source is directed into the entrance port of a hemisphere which is internally coated with a white reflectant. The specimen is positioned within the hemisphere such that it is illuminated only by light reflected from the hemisphere. Two light beams, one reflected from the specimen, the other from the hemisphere wall (reference beam) are directed from the exit port of the hemisphere to a beam chopper and then dispersed by a prism. A computer-controlled servo-motor mechanically moves entrance and exit slits so that only a small spectral band pass from both the specimen-reflected beam, and the reference beam is directed to either a UV-enhanced silicon photovoltaic detector (visible) or a lead sulfide detector (IR).

Detailed specifications of the ISR is given in Jacobsen and Lamoreaux (1979), a part of which is included in Appendix C of this thesis.

Spectral measurements of aluminum and black glass standards of known reflectance are first taken to calibrate the instrument. These measurements are then stored on a micro-computer memory bank so that subsequent sample reflectance measurements are given directly in absolute spectral reflectance.

At least three spectral measurements were taken of each sample: one from the dark top varnish, one from the red bottom varnish, and one from the fresh rock within the sample. These are plotted in Figures 31 through 35 for each sample, respectively.

The plotted spectral curves show a range of reflectance values for desert varnish coatings, with the greatest range occurring in the infrared. However, the shape of the curve for both the top dark varnish and the bottom red varnish is distinctive so that each curve can be easily distinguished from the other and from the fresh rock curves for each specimen measured.

The top varnish coating has a gently sloping curve which increases from the visible to the infrared, generally peaking in the spectral region 2.1 to 2.2 μm . The lowest top varnish coating reflectance values were 6% and 6.5% in the .45 μm region for samples 3 (basalt) and 7 (andesite), respectively. Sample 5 had the highest top varnish reflectance of 10% for the same spectral region. The slope of the top varnish curve varied considerably from sample to sample, with the

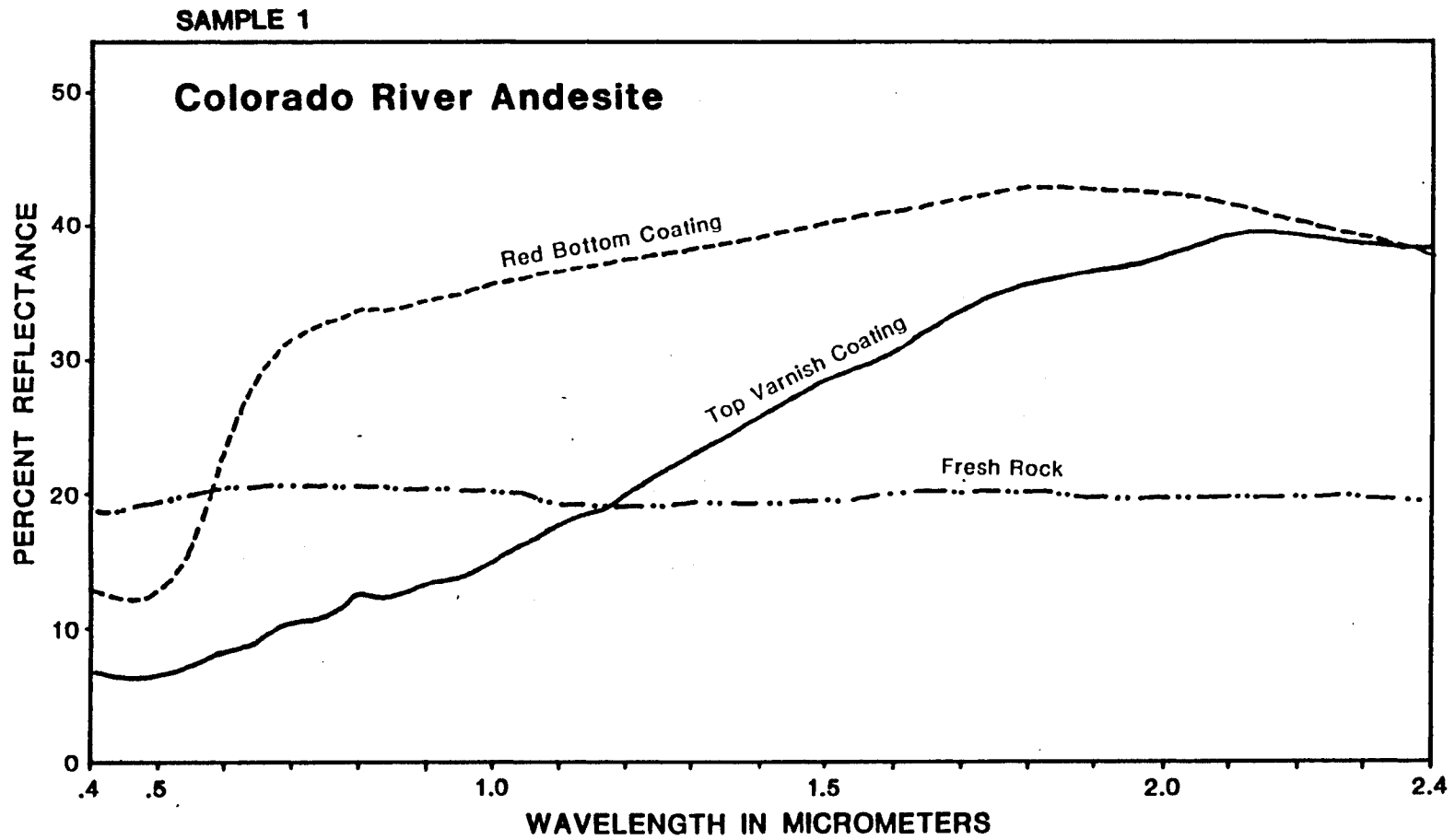


Figure 31. Spectral plot of Colorado River andesite (#1).

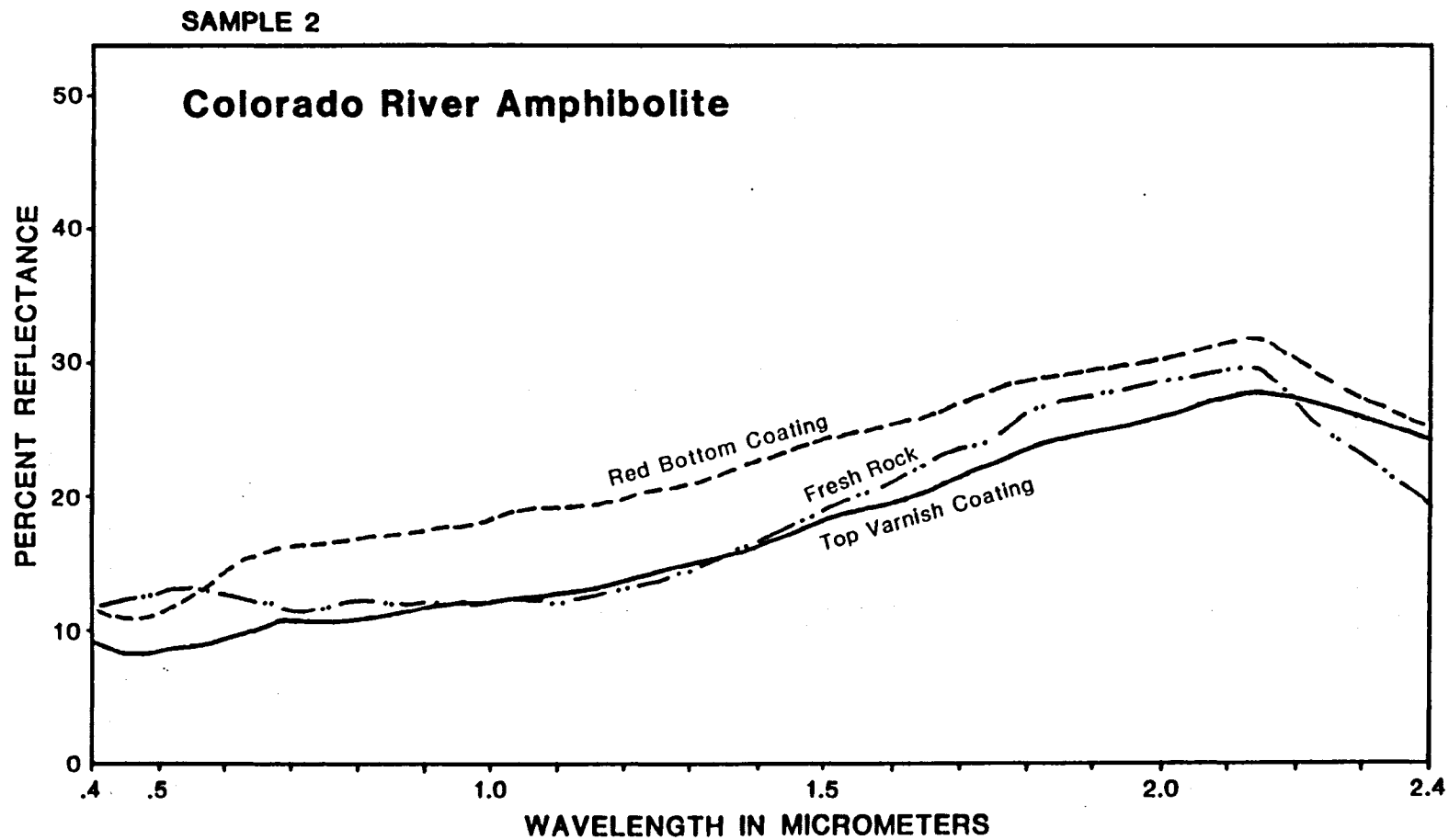


Figure 32. Spectral plot of Colorado River amphibolite (#2).

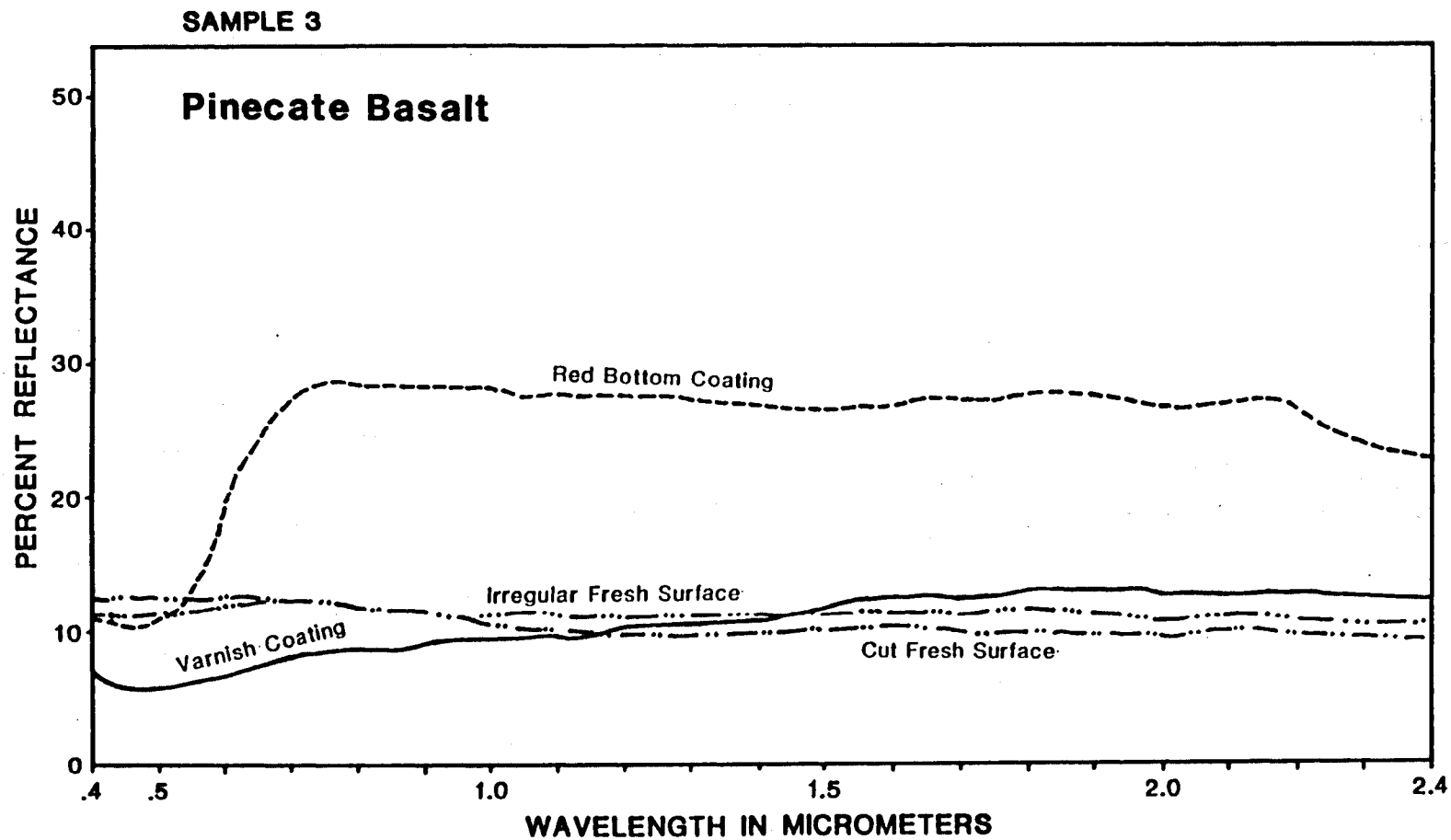


Figure 33. Spectral plot of Pinecate basalt (#3).

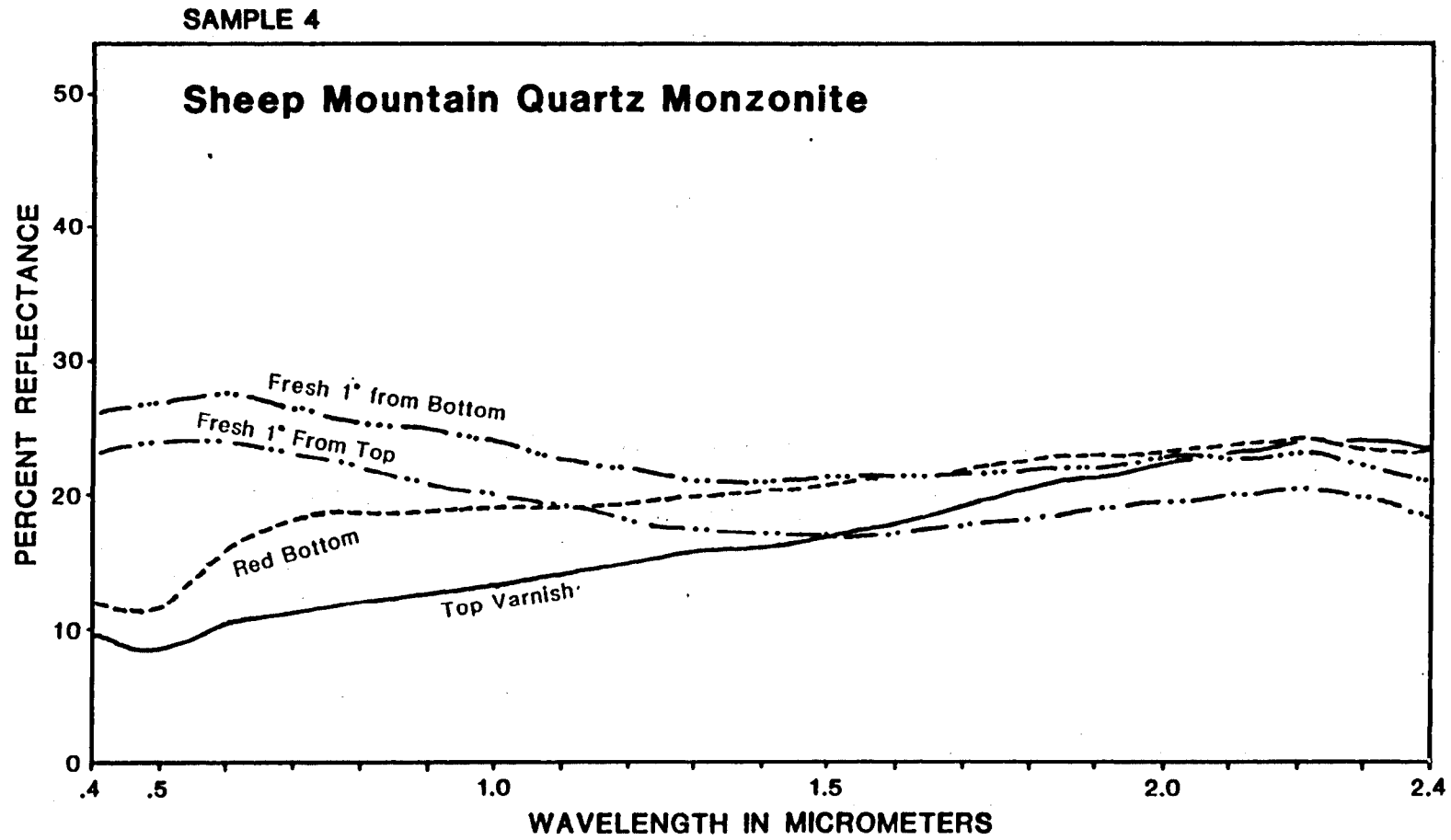


Figure 34. Spectral plot of Sheep Mountain quartz monzonite (#4).

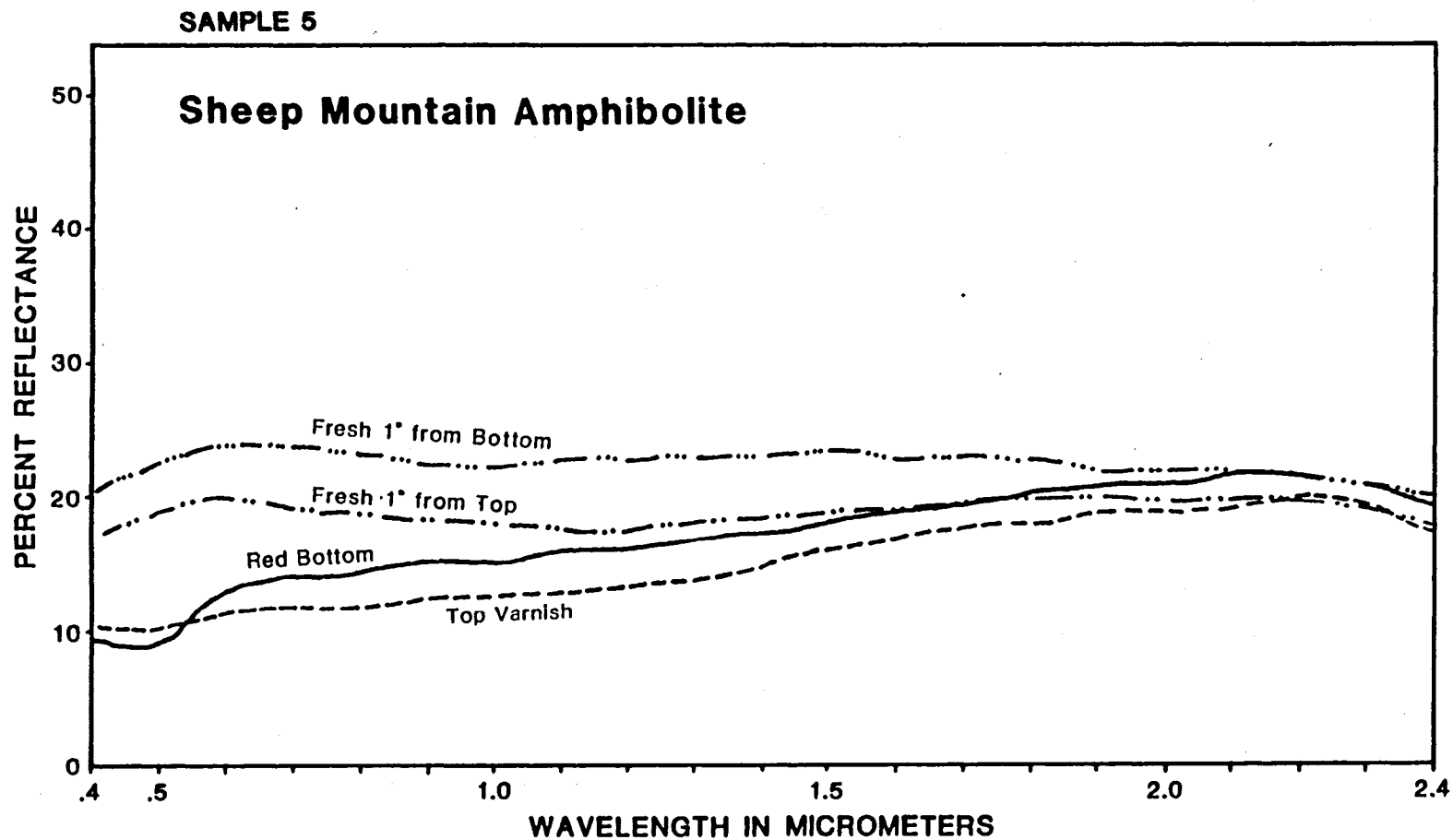


Figure 35. Spectral plot of Sheep Mountain amphibolite (#5).

steepest slopes found in the Colorado River terrace samples 1 and 2, and the flattest curve in Sample 3 (basalt).

In the best developed bottom coating curves (samples 1 and 3), the reflectance in the visible blue and green region is very low at approximately 10%. In the region from .5 to .7 μm , the reflectance rises very sharply from approximately 10% to 30%, thus giving the red color to the bottom coating. This is a characteristic of ferric oxide (Salisbury and Hunt, 1974), which may account for most of the iron in these coatings. From .8 μm on, the reflectance remains high with no specific features in the infrared.

The top varnish coating curves are similar to some published curves for altered rocks (oxidized and hydrated). The 2.1 peak may be due to water bands from alteration products near 1.9 and 2.2 μm (Salisbury and Hunt, 1974). Low values in the .4 to .5 μm range and the onset of a steeper slope in the .5 to .6 μm range suggest that the ferric oxide shoulder is also found in the top varnish coating but is masked by more opaque elements.

The darkest top varnish and steepest red bottom coating slopes were from curves of coatings on intermediate and basic composition (samples 1 and 3), raising the possibility that the availability of more mafic materials from the local vicinity may affect the reflectance of the desert varnish.

The weaker spectra were from amphibolite samples numbers 2 and 5 and from the quartz monzonite sample number 4. Amphibolite is known to be one of the less resistant rocks to the arid weathering environment.

This attribute may affect its ability to maintain dark distinctive varnish spectra. Samples number 5 and 4 are from a surface much older than that for the other three samples. The lack of distinction in the spectra may be due to this great probable age ($> 100,000$). Sample number 5, being both an amphibolite and from the oldest surface, has the least distinctive top and bottom varnish spectra.

The older Pleistocene surfaces are subject to stream dissections which destabilize the desert pavement. The rocks on these pavements have also been subject to physical and chemical weathering for a greater period of time. This raises two possible causes for the lack of distinctiveness in both varnish coatings for these older samples: (1) the varnish is physically abraded or weathered; (2) the rock has changed orientation when subjected to perturbation forces such that the same rock face has varnish coating from both top and bottom varnishing environments.

The two fresh surface curves for sample number 3 illustrate the difference in reflectance measurement for the same material with different surface characteristics and gives some indication of the repeatability of these measurements. Fresh sample curves for 5 and 4 were taken at 1" from the top and 1" from the bottom for each sample. Because of their probable great age, the difference of reflectance from the top to the bottom may also be related to rock weathering.

Varnish Reflectance and Oxide Abundance

Based on major element oxide abundances determined by Carlton

Allen with an electron microprobe (Allen, 1978), simple linear regressions were calculated between the average reflectance in spectral regions corresponding to Landsat MSS wavebands and the percent oxide of major varnish elements (Table 2). Correlations with varnish coatings are based on 4 microprobe analyses: 3 on top varnish coatings and 1 on bottom coating. Fresh rock correlations were based on only 3 microprobe analyses (Table 3).

Despite the small number of sample points, correlations between SiO and the 4 Landsat band reflectances of both fresh rock and varnish coatings and between FeO and varnish coatings are too strong to ignore. Interestingly, in all four bands fresh rock reflectances are highly positively correlated with SiO while varnish coatings are highly negatively correlated. The fresh rock positive correlations agree with the common observation that in igneous rocks reflectivity increases with silica content since high-silica-content minerals (felsitic minerals) tend to be both reflective and transparent. The negative correlation with SiO in varnish may be related to the fact that silicates in varnish are primarily sheet silicate clays (Potter and Rossman, 1977) which are hydrated and have more FeMag content than many other silicates.

High positive FeO correlation with varnish reflectance suggests that the FeO in the varnish is probably all ferric oxide. Conversely, the low correlation of FeO with fresh rock samples suggests a mixture of both ferric and ferrous iron species in the igneous rocks.

Surprisingly, no relationship was found between varnish reflectance and MgO or MnO content. In fact the darkest varnish reflectance

Table 2. Correlations between reflectance and oxide abundance for fresh rock surfaces (bnF), varnished surfaces (bnV), and fresh and varnished surfaces combined (bnV+F).

| | B4F | B5F | B6F | B7F | B4V | B5V | B6V | B7V | B4V+F | B5V+F | B6V+F | B7V+F |
|-----|------|------|------|------|------|------|------|------|-------|-------|-------|-------|
| SiO | .99 | .98 | .98 | .99 | -.91 | -.95 | -.96 | -.99 | .21 | -.29 | -.46 | -.55 |
| FeO | -.60 | -.47 | -.47 | -.60 | .98 | .99 | .99 | .99 | .20 | .66 | .80 | .83 |
| MgO | -.66 | -.54 | -.54 | -.66 | .06 | -.05 | .04 | .16 | -.36 | -.24 | -.10 | -.01 |
| MnO | .60 | .47 | .47 | .60 | -.42 | -.37 | -.34 | -.18 | -.50 | -.38 | -.28 | -.09 |

Table 3. Spectral and compositional data for correlation analysis. -- F = fresh; V = varnished; and B = bottom varnish.

| | | Data Table | | | | | | | | |
|---------------|----------------|------------|------|------|-------------|------|----------|------|---------------|--|
| | | BASALT | | | AMPHIBOLITE | | ANDESITE | | | |
| | | F | V | B | F | V | F | V | | |
| Constituent | SiO | 57.0 | 58.5 | 8.4 | 61.0 | 49.0 | 80.0 | 38.0 | % Abundance | |
| | FeO | 3.0 | .8 | 66.4 | 1.0 | 11.0 | 1.0 | 11.4 | | |
| | MgO | 2.0 | 0.0 | 1.3 | .4 | 2.0 | .3 | 2.5 | | |
| | MnO | .2 | .2 | .6 | .5 | 5.0 | .5 | 17.0 | | |
| Spectral Band | B4 (.5-.6) | 12.0 | 6.5 | 15.0 | 13.0 | 9.0 | 19.8 | 7.1 | % Reflectance | |
| | B5 (.6-.7) | 12.5 | 7.5 | 24.0 | 12.2 | 10.0 | 20.7 | 9.2 | | |
| | B6 (.7-.8) | 12.2 | 8.4 | 28.5 | 11.9 | 10.9 | 20.7 | 11.0 | | |
| | B7 (.8-1.1) | 11.0 | 9.0 | 28.0 | 12.2 | 11.6 | 20.0 | 14.5 | | |

values were obtained from sample 3, the Pinecate basalt, which had no measurable MgO and had the lowest value of MnO. While the darkness of desert varnish is commonly attributed to ferromanganese oxides in the varnish, the limited data obtained in this study suggests that among varnished rocks it is the clay minerals (SiO) which are associated with increased darkness and the ferric minerals (FeO) with an increase in brightness.

The difference in color, spectral signatures, and SiO and FeO content between top and bottom varnish is a strong indication that two quite different varnishing environments or even agents exist and operate on the same rock simultaneously. This raises the intriguing possibility that if these trends are verified, the analysis of either the rock varnish signatures or the Fe/Si ratios can be used to determine whether the rock has been varnishing in a fixed or varied orientation to ascertain the stability of surface orientation during the period of rock surface residency and perhaps the age of the surface. Intermediate and mafic rocks of younger Pleistocene age seem to obtain the darkest top varnish and most distinctive bottom varnish either due to more widely available FeMags or more resistance to physical weathering. Rocks from older Pleistocene surfaces and less resistant rocks such as amphibolites have brigher top varnish and less distinctive bottom varnish. Field observations of these older sites indicate that these surfaces have less stability such that the individual rocks may have turned over due to surface disturbances.

Field Spectral Radiometer Readings

A Radiometrics RMR-10 multispectral radiometer capable of measuring radiation in five wavebands was used to obtain multispectral readings. Each reading consisted of, on the average, 9 separate measurements in each of the five wavebands such that a total of approximately 45 separate measurements comprised the final spectral reading.

The radiometer senses in three visible and two infrared bands. These are: .4-.5 μm (B3), .5-.6 μm (B4), .6-.7 μm (B5), .7-.8 μm (B6), and 8-1.0 μm (B7). The three middle bands (B4, B5, B6) correspond to Landsat MSS bands 4, 5 and 6. The last band, B7, is half as wide as Landsat MSS band 7.

The instrument (Figure 36) is basically a sensitive light detector with a filter wheel and aperture wheel mounted between the lens and the detecting element. The electronics converts an analog signal to a digital signal, insures a linearity of response, and allows for operation in either photometer or reflectance mode. When operated in a reflectance mode the signal is processed through a potentiometer feedback loop so that reflectance readings may be calibrated for variations in solar irradiation. Output for the radiometer is a LCD display but there is also an outlet for an external recording device. Specifications and laboratory calibration test results for the RMR-10 are included in Appendix C.

The method of obtaining spectral reflectance was first to note the surface of interest: its location; the time and date; the instrumental field of view (FOV); and the angle of the solar zenith, measured



Figure 36. Radiometrics RMR-10 multispectral radiometer shown in field operation.

with the inclinometer of a brunton compass. Each reading was given a number n and referred to as R_n . All recorded data for spectral readings are presented in Appendix C.

A Kodak standard card rated as 90% white on one side and 18% grey on the other was used to calibrate the instrument in reflected mode. By placing the Kodak standard over the surface of interest and turning the potentiometer knob so that the LCD read the appropriate reflectance value for the card surface, the instrument would then be calibrated to read values directly. This calibration was repeated for each spectral band. After calibration, for each band, the instrument was read over several different locations of the same geomorphic surface type within the general vicinity. All measurements were made normal to the surface and at the same altitude above the surface as that for the calibration measurement. The reflectance of each location was recorded by an assistant. The group of measurements thus recorded constituted the distribution of sampled reflectances over that geomorphic surface type for that spectral band. After the last sample measurement was made for a particular band, the radiometer was returned to the white card standard and recalibrated.

Tests measuring the white surface against the grey surface of the Kodak card indicated an error of 2-3% between the stated reflectances and measured values. Measurements of the card surface as it was rotated were not perceptibly different--indicating that the card was fairly uniformly diffuse with no significant bidirectionality in reflectance. Measurements of the standard after obtaining several

values indicated that errors most likely due to tilts and altitude changes introduced by the operator were on the order of 2-3%. Total errors for field measurements were on the order of 5% for flat planar surfaces. For surfaces which depart from this ideal, i.e., coarse gravel bars and especially plants--these errors will be greater. The measurements of plant reflectances which have no large smooth surface, such as creosote (Larrea tridentata) or teddy bear cholla (Opuntia bigelovii) will have unreliable means and very high variances. These spectral signatures can only be used to indicate general trends. The use of a soft standard such as fibrefax instead of a rigid card would alleviate this problem somewhat since a soft standard can conform to non-planar surfaces.

Reflectance measurements were made with the instrumental FOV at 2 and 20 degrees. At an operating height of 50 cm above the surface the diameter of coverage subtended by a 2° FOV was 1.8 cm, the diameter for a 20° FOV was 17.6 cm. Measurements of the same surface at both FOV settings (R10, R11) indicated that with a sample size of 9, the difference between mean reflectances was, on the average 2%, but the variance of the measurements at 2 FOV was always higher for a gravelly pavement surface.

No clear effects were detected from differences in solar zenith angles. This was to be expected, since the cosine square effect due to the angle of illumination was eliminated by the standard reflectance calibration; the only effect due to varying the angle of illumination

would be in the percent area covered by shadow. It was expected that for a fairly rough surface the percent shadow would be greater at lower angles of illumination than at high illumination angles and the average reflectance reading would therefore be darker. The data was not sufficient to show this trend. However, radiometer reading R15, taken at site 9 when the solar zenith angle was at 70° (20° elevation), was rejected as anomalous due to too low of a sun angle.

The difference between a sunny versus a cloudy day reading was not significant as long as the solar irradiation remained constant throughout the reading. Once again at low illumination angles, a rough surface texture should theoretically cause a difference in values between a sunny-day reading with dark shadows and a cloudy-day reading with little or no shadow component. This was not evident in the data.

Field Spectral Reflectances

Fifty-five separate field reflectance readings were taken during the period from December 8, 1979 to April 1, 1980. These readings were taken of soil, rock and plant reflectances found in the individual field sites. Data from these readings were plotted on nine individual computer plots which depict the mean and standard deviation for each reading (Appendix C). Commonly, several different reflectance readings characterizing different geomorphic surface types on the same alluvial study site were taken in order to encompass the range of particle size, color or materials found for that geomorphic class. The most representative curves were used to summarize the field spectral signatures of geomorphic classes in Figures 37 through 41.

Bedrock spectra fall into two distinct classes: those which are light-colored and do not have a varnish, and those which do have a varnish coating (Figure 37). Readings R4 and R3 are representative of these two types, respectively. A third type of rock which does not acquire a dark coating but weathers to a greenish-gray color (Mesozoic sedimentary and metamorphic rocks) probably has a different spectral signature, but unfortunately, was not sampled.

Curves for the varnished welded tuff rock (R3) are quite similar to the laboratory top varnish coating for andesite (No. 1T). These were the darkest and flattest field spectra obtained. The reflectance ranged from 8% in B3 to 16% in B7.

The curve representing light-colored bedrock is the reflectance of the erosional surface of yellow welded tuff with some petracalcic surface litter at site 2 (R4, Figure 37). It has a nearly straightline slope from about 16% in B3 to 37% in B7.

Older Pleistocene pavements are represented by reflectance readings R6 and R11 (Figure 38). These curves were obtained from dark pavements on a remnant alluvial fan composed of acidic volcanic rocks with some sedimentary and metasedimentary rocks intermixed. The oldest Pleistocene pavement, the Q2a (R6), is the coarsest and also the brightest of the dark desert pavements. Although the average particle size for this pavement is rather large (29.9 mm), the effects of erosion and turning over of the varnish rocks and the presence of large amounts of petracalcic clasts at the surface tend to make the reflectance of this pavement bright. The R6 curve is a dark 12% reflectance in B3.

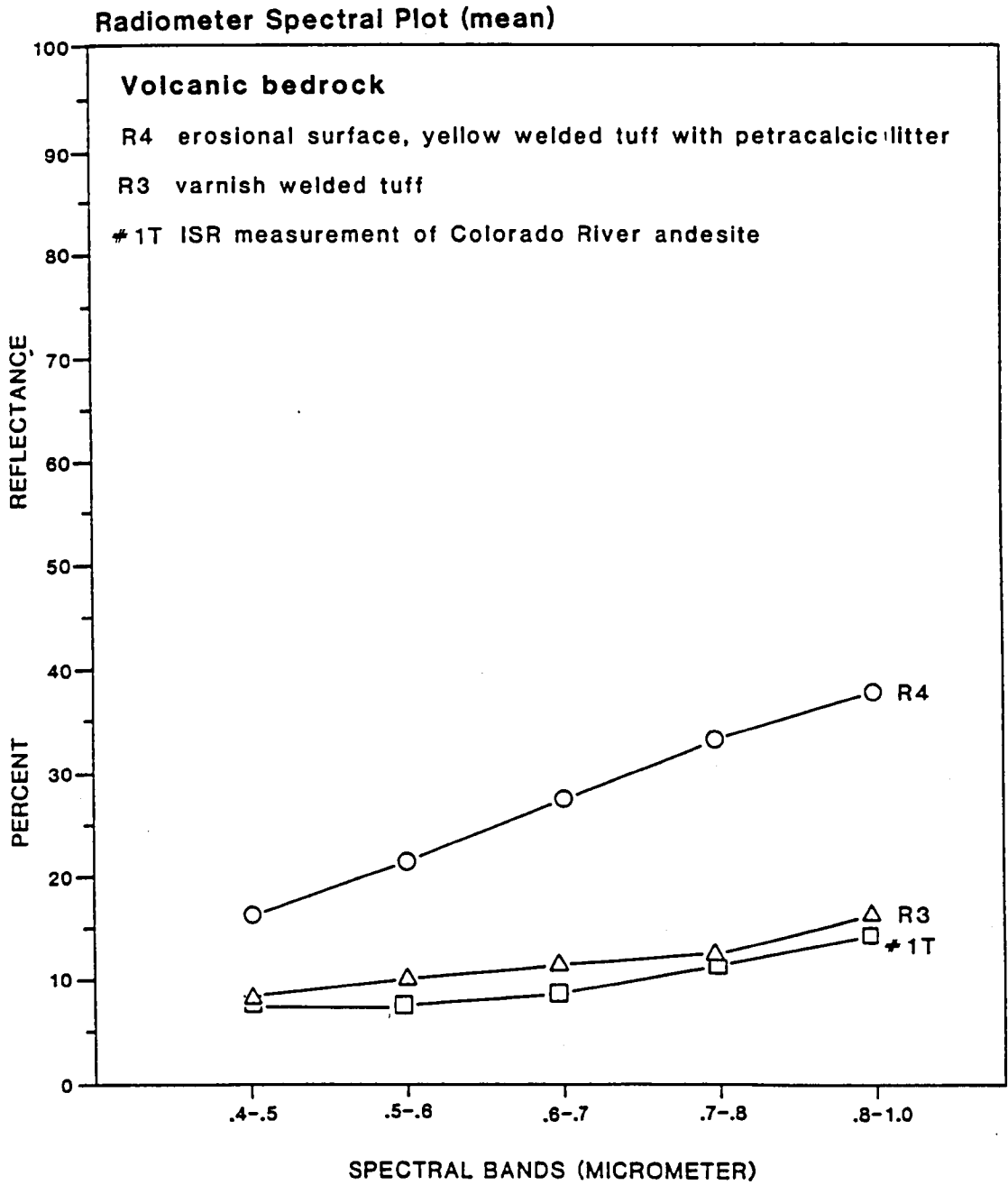


Figure 37. Field spectral signature of volcanic bedrock.

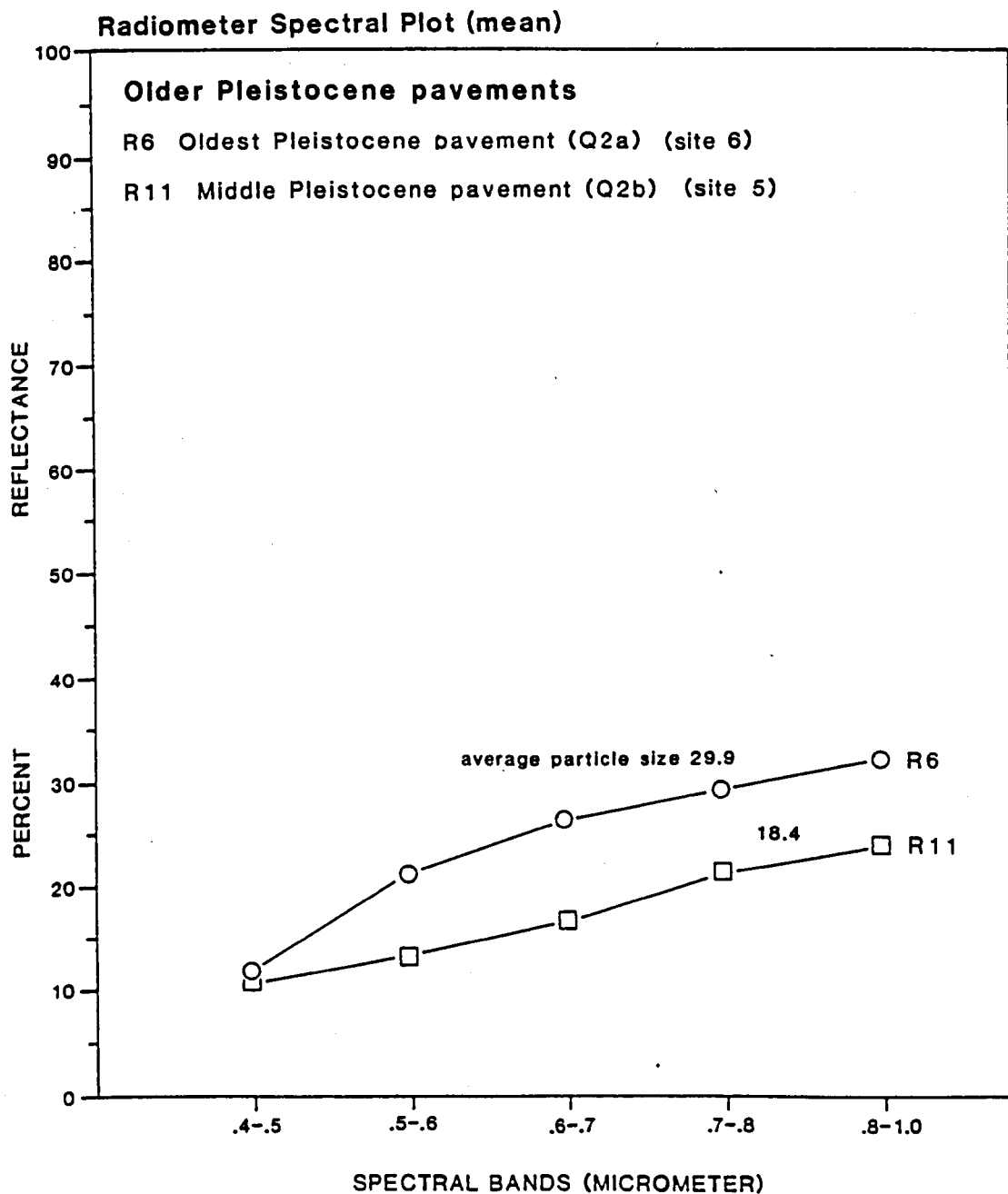


Figure 38. Field spectral signature of older Pleistocene pavements.

Its slight reddishness is represented by large increases in reflectance in B4 (22%) and B5 (26%) whereupon the curve begins to flatten out to a 32% reflectance in B7.

The curve for the Q2b pavement (R11, Figure 38) is darker and less convex than that for the Q2a. The reflectance ranges from 11% in B3 to 24% in B7 for this pavement. Although it is difficult to distinguish the Q2b pavement from the Q2a pavement by the eye using only color and darkness, their different reflectance signatures suggest that most of the difference in the visible is due to the reflectance in the green and red spectral region.

Differences in the reflectance between Q2c young Pleistocene dark pavements seem to be primarily attributable to variations in composition and particle size distribution. Pavements composed of acid volcanic rocks, represented by R14 (Figure 39), are brighter, given the same age than those composed of intermediate or basic volcanic rocks (R20, R18; Figure 39). Pavements which have similar composition such as those represented by curves R18, and R20 (Figure 39), which are both of intermediate volcanic composition, have different reflectances due to a difference in particle size distribution.

Spectral signatures of the disturbed pavements (Q2pd) can be grouped into two types of curves (Figure 40): they are the convex curve type and the steep-sloped, broken-line type. The steep-sloped, broken-line type is represented by R27 and R28 in Figure 40. Both these reflectances are from site 8 but are of lighter and darker surface types, respectively. It is not known from which of these surfaces in site 8 the

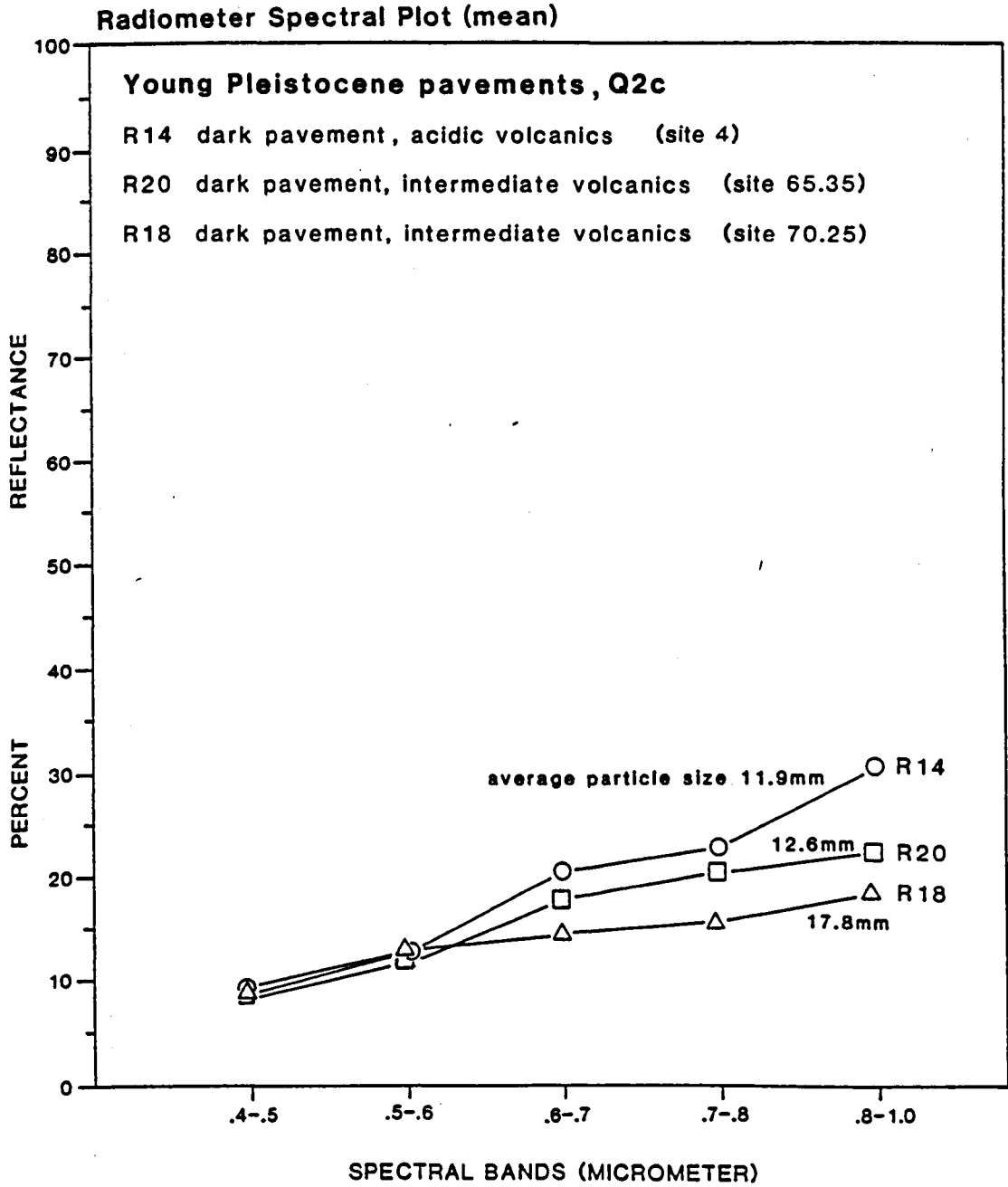


Figure 39. Field spectral signature of young Pleistocene pavements.

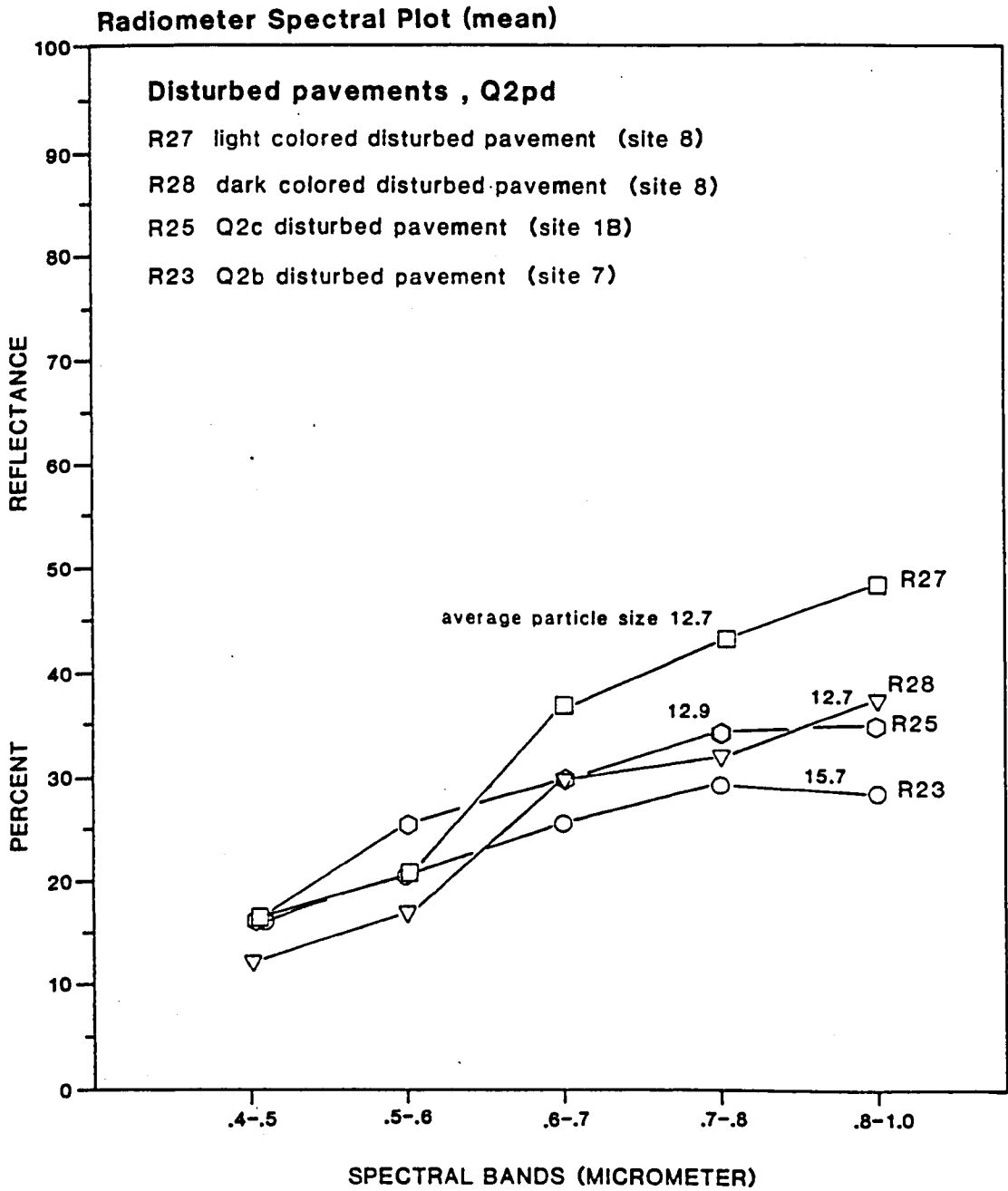


Figure 40. Field spectral signature of disturbed pavements.

12.7 mm mean particle size was sampled. Curves R25 and R23 (Figure 40) represent the convex curve type. The average particle size of R23 is coarser than that for R25 and accounts for the lower reflectance of R23 with respect to R25.

Qualitative comparison of the soil and surface descriptions for sites 6, 7 and 1B, all of which have convex spectral curves, suggest the speculation that the presence of much calcium carbonate on the surface may contribute to a convexly curved spectral signature. On the other hand, the broken line, steep-sloped curves of site 8 (R27, R28) are very similar but darker than those for modern alluvial stream deposits (Figure 41) and may be related to weathering of rock surfaces on freshly deposited material. The steepest line segment for curves R27 and R28 (Figure 40) and for the fine-grain modern alluvium occur in the .5 to .7 μm range. This is also similar to the laboratory curves for red bottom varnish coatings.

Spectral reflectance signatures of modern alluvial surfaces (Figure 41) are generally steep-sloped, broken-line curves with reflectances most directly related to particle size distribution. The four curves in Figure 41 range from fresh sand and silt channel deposits to Q3 age coarse gravel deposits. The steepest and brightest reflectance signature is that for an overbank sand and silt deposit (R34). The darkest and flattest is from a coarse gravel bar (R36).

Comparison of these curves with those for fresh rocks (Figures 8, Figures 31 through 35) suggests that the increase in red and infrared reflectance, due probably to iron oxide, occurs quite rapidly; and

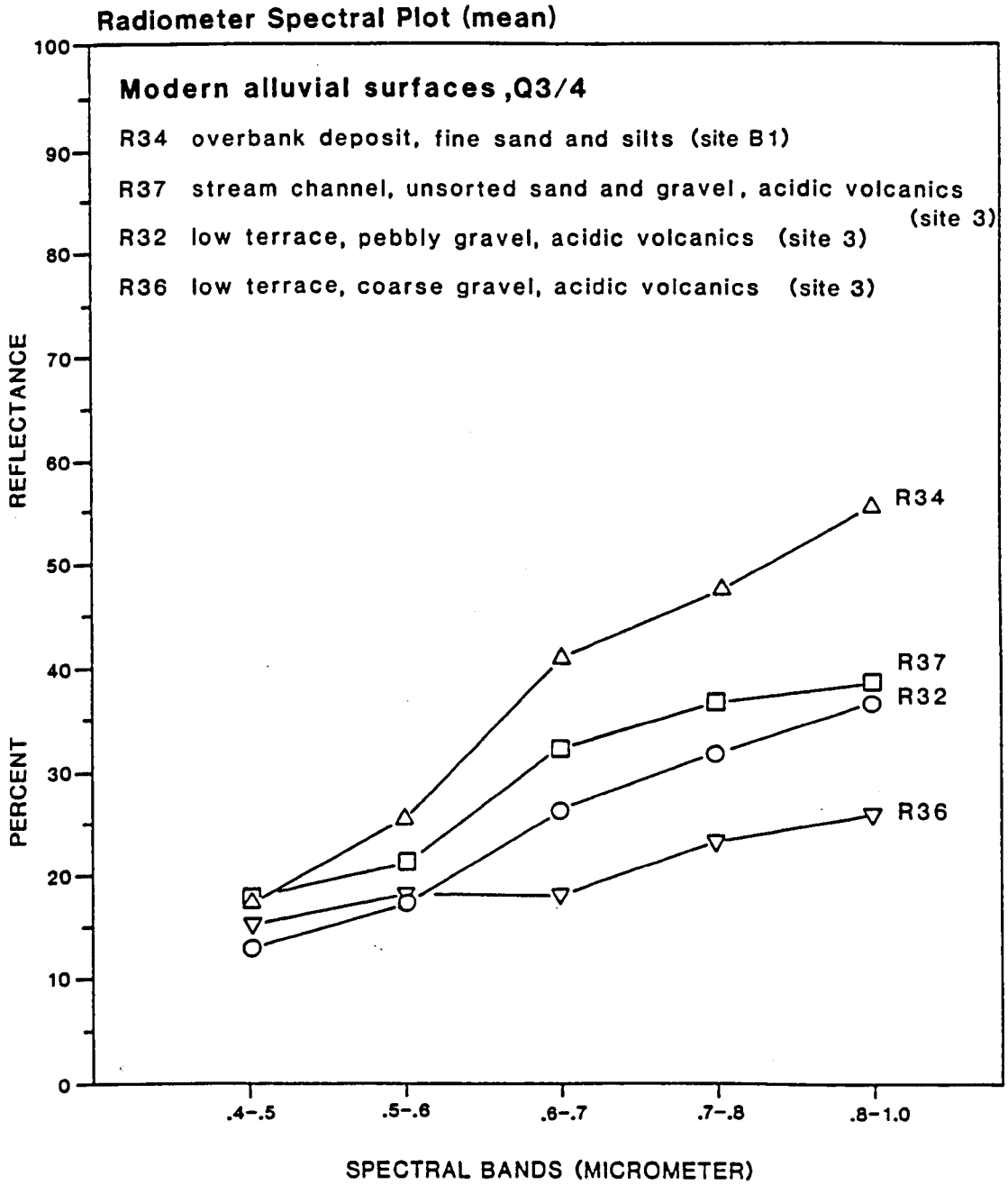


Figure 41. Field spectral signature of modern alluvial surfaces.

since diminishing particle size increases weathering surfaces, the brightest red and infrared reflectances are in the fine-grained modern deposits.

Reflectance readings of plants in the field were characterized by such high variances that no definitive spectral signature plots could be produced. However, some general conclusions can be drawn from the data presented in Appendix C. The reflectance of small riparian trees such as jojoba, acacia and palo verde are quite similar to each other and to published curves for typical arboreal vegetation. The reflectance signatures of shrubs and bushes such as brittlebush and creosote bush are highly variable between specimens and seasons. Most cacti, especially teddy bear cholla, have very high reflectance (probably due to spine sheaths).

The reflectance of surfaces in plant shadows (R55) tend to be very dark and flat on a clear sunny day. If plant shadows are very long, their relative low reflectances can average out the bright reflectances of the plant canopy itself.

Summary and Correlation of Field Data

Field descriptors for the 17 alluvial sites are summarized in Table 4 under the four major headings of geology, vegetation, terrain and radiometric descriptors. The first two major headings are qualitative and synoptic. Vegetation density figures are particularly difficult to use because of the highly heterogeneous distribution of vegetation in most of the pavement sites. Terrain descriptors range

Table 4.. Summary of field descriptors.

| Site | Geology | | Vegetation | | Terrain | | | | | Radiometric (mean/std) | | | | | Source |
|-------|---|---------------------------------------|---|----------|-----------|--------------|-------------|----------------|---------------|------------------------|------------|------------|------------|-------------|----------------|
| | Surface Soil | Lithology | Type | Density | Roughness | Slope | Variability | Mean (mm) Size | Range Phi (φ) | B3 .4 - .5 | B4 .5 - .6 | B5 .6 - .7 | B6 .7 - .8 | B7 .8 - 1.0 | |
| 1 | Q4 wash Typic Torrifluent | Acidic volcanic | Woody riparian | 0 - 90% | 5 | S50E 1.5% | ND | ND | ND | 18/ | 27.5/ | 32.5/ | 39./ | 37 | R35 |
| 2 | Q2pd bedrock erosional, Lithic Torriorthent | Volcanic tuff | Scrub | 0 - 3% | 2 | N60E 3% | ND | ND | ND | 15.8/3.1 | 21.5/2.5 | 27.5/5. | 33.2/7.6 | 37.3/4.3 | R4 |
| 3 | Q3/4 mtn wash torrifluent | Rhyolites, latites, sedimentary | Woody open riparian | 12 - 20% | 4 | N60E 3% | .66 | 19. | 5 | 14.9/3.2 | 18.6/2.6 | 26.2/6.3 | 31.3/5.8 | 34.5/6.0 | R36,32 37 |
| 4 | Q2c dark pavement Typic haplargid | Acidic volcanics meta-sed. | Mostly barren, scrub, succulents on runnels | 0 - 20% | 3 | N30E 1.7% | .7 | 11.9 | 3 | 10.1/2.8 | 14.2/3.5 | 20/2.5 | 22.6/2.1 | 30.3/2.6 | R12, R14 |
| 5 | Q2b dark pavement Typic haplargid | Mixed volcanics, mostly acidic | Scrub, succulents in dissection runnels | 3 - 7% | 3 | N30E 3.9% | 17 | 18.4 | 3 | 11/2.5 | 13.6/3.3 | 18.4/3.7 | 21.5/3.8 | 24.4/3.2 | 27,8, 11,10 |
| 6 | Q2a dissected pavement, Paleargid | Acidic and meta/sed. | Scrub, succulents in dissection | 0 - 15% | 4 | ND | ND | 29.9 | 4 | 12.5/3.2 | 21.8/4.3 | 26.5/6.4 | 29.4/5.6 | 32.2/5.6 | R6 |
| 7 | Q2pd, degraded pavement, Calciorthid | Acidic volcanic | Scattered scrub | 2 - 5% | 3 | N30E 3% | .58 | 15.7 | 3 | 16.5/3.1 | 20.4/1.5 | 25.5/7.2 | 29.3/4.9 | 28.2/3.8 | R23 |
| 8 | Q2pd, degraded pavement, Haplargid | Acidic volcanic | Scattered creosote | 2 - 7% | 3 | N30E 2.4% | 1.6 | 12.7 | 3 | 14.3/2.3 | 19.7/3.1 | 30/7.2 | 35.2/6.9 | 40.4/6.9 | R27,28, 29 |
| 9 | Q2c, dark pavement Camborthisd | Acid to intermediate volcanic | Barren except for runnels | 0 - 2% | 3 | ND | ND | 16.9 | 3 | 3/.8 | 12.1/1.5 | 12.5/2.4 | 14/1.6 | 13.7/1.4 | R15* |
| 1B | Q2pd, fine grain disturbed pavement Typic Haplargid | Acidic volcanics | Barren except for dissection runnels | 0 - 23% | 2 | ND | ND | 12.9 | 3 | 15.5/2.4 | 25.5/3.0 | 30.5/4.3 | 35.6/4.3 | 36.3/6.5 | R24 R25 |
| B1 | Q3/4, sandy flat Typic Torriorthent | Acidic volcanic | Scattered creosote | 2 - 6% | 2 | E 2.2% | 1.0 | 2.4 | 4+ | 16.3/1.6 | 23.3/2.8 | 37/4.3 | 43.8/4.0 | 50.2/5.6 | R33,34 |
| 61B | Q3a pavement typic Calciorthisd | Acidic volcanic | Creosote and ephemerals | 0 - 10% | 2 | ND | ND | 5.9 | 5 | 13.3/1.3 | 20.6/2.2 | 26.1/3.5 | 28.9/2.6 | 33.3/4.0 | R31 |
| 65.35 | Q2c pavement Typic Haplargid | Acidic and intermediate | Barren, except scrub in runnels | 0 - 10% | 3 | S80E 1.5% | 1.4 | 12.6 | 2 | 10.8/3.6 | 14.7/4.5 | 20.5/6.3 | 23.3/5.5 | 25/8. | R16,20 17 |
| 70.25 | Q2c pavement Paleargid | Intermediate | Barren, except scrub in runnels | 0 - 5% | 2 | ND | ND | 17.8 | 4 | 8.8/1. | 12.9/1.8 | 14.4/2.2 | 15.6/2.7 | 18.5/2.3 | R18 |
| 70+P | Q2c pavement Paleargid | Intermediate | Barren, except scrub in runnels | 0 - 10% | 3 | S30E 2% | .59 | 14.7 | 3 | 8/.5 | 10.9/.8 | 15.2/1.2 | 16.8/1.2 | 19.2/1.6 | R19 |
| 70+D | Q3/Q4 coarse erosional, Torrifluent | Mixed volc. & meta sed. | Even open riparian | 10 - 15% | 3 | S60E 2.3% | .59 | 12.2 | 6 | 12/.8 | 16.6/1.4 | 20.5/1.8 | 26.1/2.2 | 28.3/2.2 | R38 |
| 83.7 | Q2c pavement Camborthisd | Acidic volcanics | Barren except for runnels | 0 - 10% | 3 | ND | ND | 11.1 | 3 | 12.2/3.5 | 16.9/3.2 | 22.5/7.8 | 26.7/6.7 | 26.2/6.6 | R26,22 |

* Unreliable due to low sun angle.

from semi-qualitative as in the roughness estimates to quantitative as in the mean particle size descriptors.

Precise measurements of surface roughness such as the method outlined by Brennan and Quade (1967) have limited usefulness because they fail to take into consideration the variability of surface slope or the distribution and physical canopy characteristics of the vegetation. Precision in the mean particle size is also misleading because it is based on only one sample for each surface and because there is no standard method to the calculation of a mean particle size for gravel-size materials.

The radiometric reflectance values in Table 3 are mean values from unweighted pooled radiometric readings taken from all representative geomorphic surface types sampled within the geomorphic class at the site. Large standard deviations are due to the pooling of data from different surface types.

The field data indicates a strong relationship between the mean particle size and reflectance. However, the relationship is only revealed when the data is grouped into the Q2c pavement and the non-Q2c-pavement classes. The first regression line (solid line, Figure 42) was based on all the Q2c pavements with the exception of the site 9 radiometer reading which was rejected as anomalously low due to too low a sun angle. A correlation coefficient value of $r = -.91$ was found for these pavement classes. The older pavements at site 6 (Q2a) and to a lesser extent at site 5 (Q2b) deviate substantially from this regression line and would be too bright even if a curvilinear fit was applied to the data.

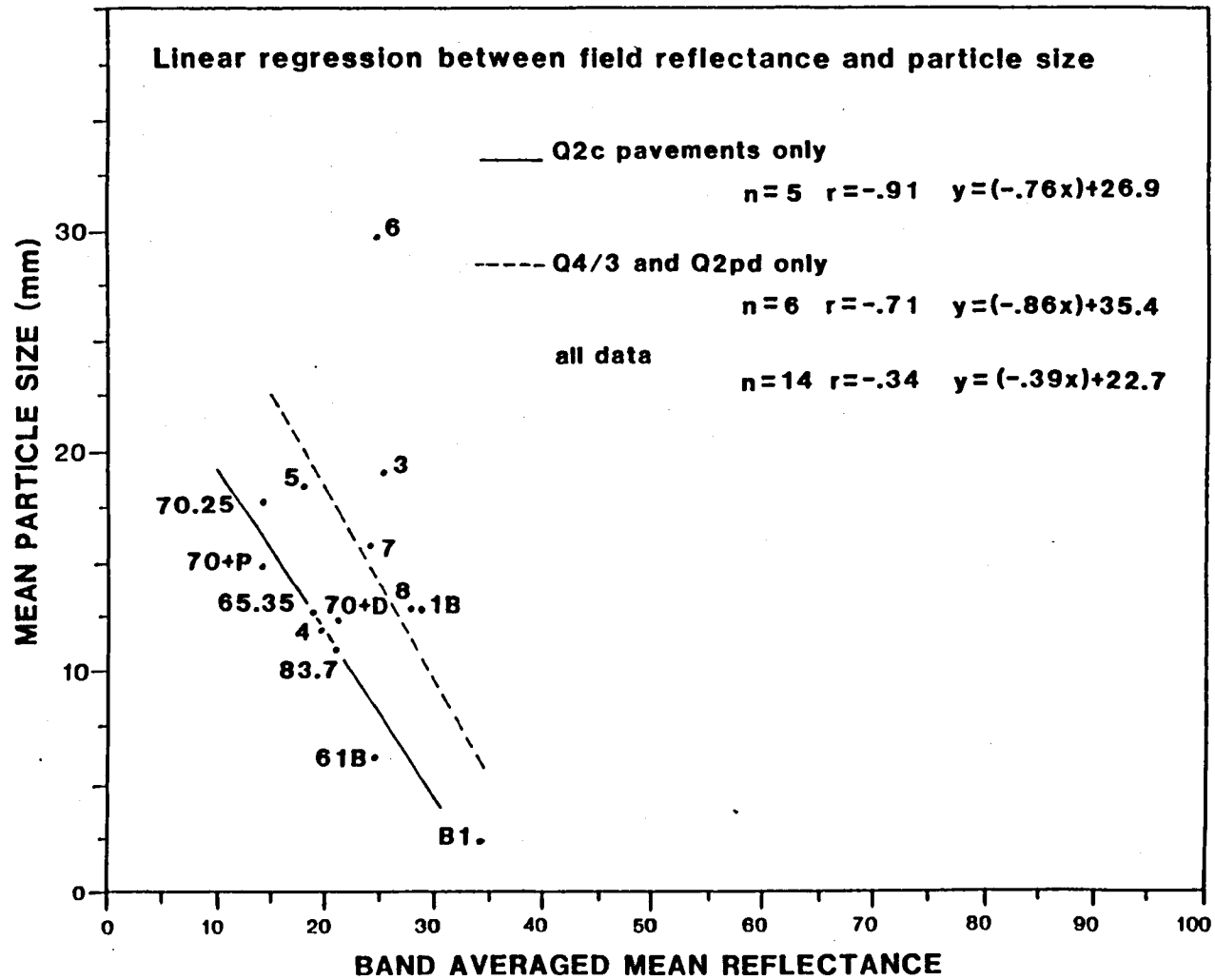


Figure 42. The relationship between field reflectance and average particle size.

Clearly the effects of age on well-developed pavements is to brighten up the average reflectance of that pavement surface.

The linear regression line of non-pavement surfaces is brighter than that for the Q2c pavements but has a similar slope (broken line, Figure 42). The greater scatter of data points is reflected by a correlation coefficient of $r = -.71$. A greater scatter is expected because non-varnished surfaces have reflectances more sensitive to rock composition than varnish surfaces.

The linear regression lines probably do not hold true for surfaces with an average particle size greater than 20 mm and of course do not hold true for points at the line intersects. The best fit set of lines for both sets of data is probably curved and asymptotic, with a segment in the middle particle size ranges which can be approximated by the regression lines in Figure 42.

An analysis of the relationship between the averaged standard deviations of spectral radiometer data with the mean particle size showed no strong relationship between the two sets of data. Here again there seems to be several factors at work. There is an overall tendency of increased standard deviations in ground reflectance with increasing particle size, but well-formed pavements have much lower variances than that predicted by the particle size trend. On the other hand, highly disturbed surfaces show a tendency toward higher standard deviations than predicted.

Although small sample sizes and somewhat inconsistent data collection preclude any definitive statement about this relationship,

it seems clear that sites classified as disturbed, and sites of Q2a, Q2b older pavements tend to have a higher degree of spectral heterogeneity at the ground sampling level than the best formed flat desert pavements (Q2c).

CHAPTER 3

IMAGE INVESTIGATIONS

Digital image investigations were conducted in three major areas: the extraction of image data and correlation with field data; image texture analysis and texture feature extraction; and supervised Bayesian maximum-likelihood classification.

Facilities used in data analysis and manipulation were the Cyber 175 at the University Computing Center, University of Arizona, and the I2S 11/70 system at DIAL (Digital Image Analysis Laboratory), University of Arizona. SADIE 2.4 (System at Arizona for Digital Image Experimentation) (University of Arizona, 1981a) programs were used for many of the routine processing functions. The program CALSCAN (Schowengerdt, 1979) was used for image classification. At DIAL, System 511, DIPP and MIPP packages (University of Arizona, 1981b) were used as well as many routines written by the author. Program TRAINS (Shih, 1982) was written and used for detail site investigation. Program KOUNT (Shih, 1982) was developed for texture feature extraction. Other programs used in the investigation are mentioned where appropriate. All software facilities are listed in Appendix D.

Preprocessing

Landsat

Landsat MSS data was preprocessed to remove detector striping

and geometric distortions. Program PREPROC (Schowengerdt, 1978) was used on the CYBER 175 to perform these functions on "raw" CCT data. The area of interest was then extracted using program EXTRACT (Schowengerdt, 1978). This extract was written as 240 pixel (p) by 252 line (ℓ) DIAL compatible image files.

Radar

The radar image was acquired as a film positive transparency. It was necessary to digitize the data for image processing. The Perkin Elmer PDS microdensitometer-Data General Eclipse system at Optical Sciences, University of Arizona, was used to digitize and write the data to tape. Digitization was set at a 25 μm aperture and sampling distance in order to approximate the .31 μm resolution of the original data. A scan direction was chosen parallel to the Landsat scan direction in order to minimize rotation requirements during data registration. Digitization produced an image file of a size of 1820 (p) by 1282 (ℓ) and a dynamic range of 297 grey levels.

Registration

An intermediate scale was chosen to work with both the radar and Landsat data in register. To accomplish this the Landsat file was doubled by pixel replication to a 480 (p) by 504 (ℓ) file. The radar data was reduced by a factor of four using bilinear interpolation to a file size of 512 (p) by 456 (ℓ).

The Landsat data was chosen as the base for registration. Registration was by polynomial warping using the SADIE program GEOM

(University of Arizona, 1981a). Eight tie-points for warping control were chosen interactively at DIAL. Both Landsat band 5 and radar images were loaded into separate video channels. Individual tie-points were chosen by cursor at easily identified low-relief features such as stream bifurcations. Mountain peaks were avoided to minimize the effects of radar layover.

The point coordinates were obtained from program TRAINS. These coordinates served as input into SADIE program SCOEf, which produced a four-term polynomial least squares fit to the data. The polynomial expression was then used by SADIE program GEOM to warp the radar data into registration.

Image Site Investigations

Data was extracted from fourteen sites in the registered four-band Landsat image and single-band radar image using program TRAINS. These sites correspond to field sites within the extracted study area. Sites 1 and 61B were not within the extracted images, and could not be compared with field data.

Each of the fourteen sites are outlined in green on the band 4, 5, 6 standard false color composite (FCC) image (Figure 43), and the registered radar image (Figure 44). The sites ranged in size from 9 to 81 samples. Because the original Landsat images were doubled, each original Landsat pixel is represented by four pixels in the 2x image. The number of original Landsat pixels sampled in each site ranged from 4 to 28 samples. On the other hand, the radar data was reduced in

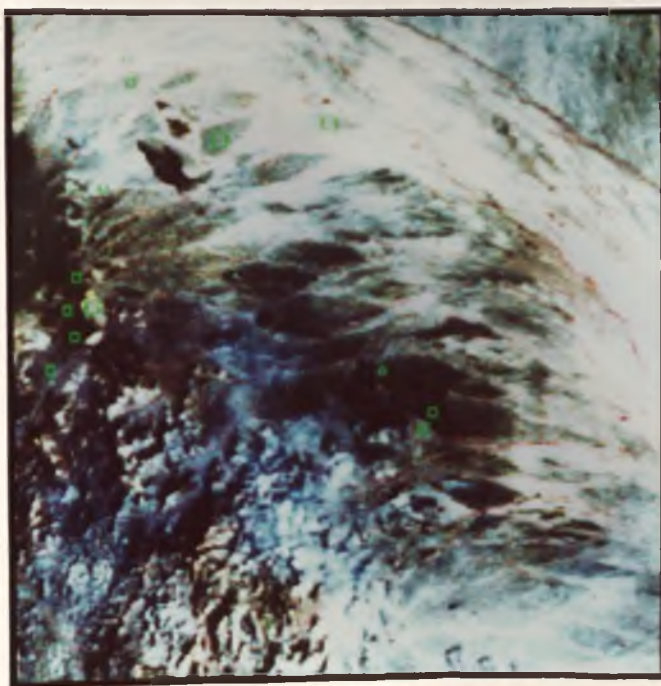


Figure 43. Band 4, 5, 6 false color composite with field sites outlined. -- Refer to Figure 15 for site names.

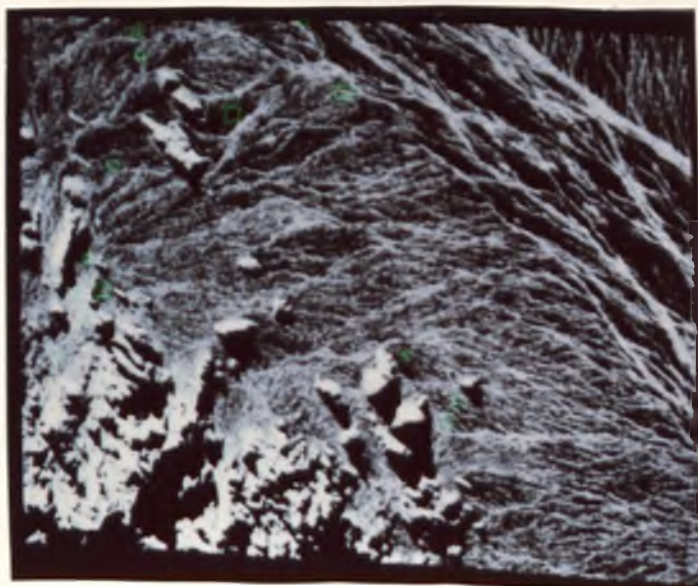


Figure 44. Registered radar with field sites outlined. -- Refer to Figure 15 for site names.

resolution to bilinear interpolation so that each pixel is an average of approximately 4 original radar pixels.

The program TRAINS produced a data dump, first-order statistics, and image histogram for each site for each image band. Only the mean and standard deviation is presented in Table 5. A full TRAINS data set is included in Appendix D.

Landsat, Field Corrections

In order to compare the two sets of data (field and image), Landsat images were corrected for band gain and atmospheric path radiance (haze) using scene light and dark (L/D) calibration sites. This method was first developed by Honey, Prelat and Lyon (1974), used by Ballew (1975), and Marsh and Lyon (1980). The procedure is to choose two calibration sites, one light and one dark, each with a known ground reflectance and a high degree of homogeneity. By fitting the Landsat digital numbers (DN) to these two values, a linear transformation of the form $y = ax + b$ is found, where a is the band gain and b the atmospheric haze factor. The function is then used to transform all the Landsat DN's to corrected DN (CDN).

The method is highly sensitive to the choice of the L/D standards. Site B1 was chosen as the light standard, and site 70+P the dark. Reasons for choosing these two sites were their extreme in reflectance, relatively flat surface topography, homogeneity, and representative sets of field reflectance measurements.

Transformations were performed on mean values, using mean ground reflectances and mean image site DN's. The transformation for each band

Table 5. Image data from field sites.

| Site | (DN/STD) | | | | | N Size |
|-------|----------|----------|----------|----------|------------|-----------|
| | B4 | B5 | B6 | B7 | Radar | |
| 2 | 33.3/1.4 | 34.5/2.0 | 35.3/1.6 | 31.9/1.4 | 58.8/24.2 | 81 |
| 3 | 28.4/2.0 | 27.0/0.7 | 27.5/0.9 | 24.5/2.2 | 103.3/21.9 | 25 |
| 4 | 27.8/3.8 | 24.6/1.4 | 24.0/1.9 | 21.5/2.9 | 67.4/25.8 | 25 |
| 5 | 28.3/2.3 | 25.0/1.2 | 24.4/1.0 | 20.6/1.3 | 83.2/28.6 | 25 |
| 6 | 30.5/0.7 | 30.5/1.4 | 28.7/1.6 | 25.2/1.0 | 95.2/24.4 | 25 |
| 7 | 35.8/1.6 | 39.0/2.0 | 37.5/1.7 | 33.4/1.1 | 44.4/29.8 | 25 |
| 8 | 37.4/0.5 | 41.8/2.2 | 42.2/1.7 | 37.5/0.9 | 54.5/15.7 | 25 |
| 9 | 33.4/1.4 | 34.5/0.9 | 33.2/1.2 | 30.0/1.3 | 32.3/17.6 | 81 |
| B1 | 40.9/2.5 | 46.3/4.1 | 46.5/2.9 | 39.9/3.1 | 19.9/17.0 | 15 |
| 65.35 | 34.9/1.3 | 37.6/1.6 | 37.3/1.7 | 32.4/1.0 | 67.3/23.1 | 81 |
| 70.25 | 28.3/0.7 | 26.8/1.3 | 24.8/2.0 | 22.0/1.4 | 58.3/21.8 | 9 |
| 70+P | 27.2/0.4 | 24.3/0.9 | 23.6/1.5 | 20.2/1.3 | 68.2/30.3 | 25 |
| 70+D | 31.8/1.8 | 32.4/1.2 | 31.0/1.1 | 27.4/0.9 | 70.8/21.7 | 25 |
| 83.7 | 34.5/1.1 | 36.6/2.2 | 36.4/0.5 | 31.8/1.1 | 55.8/16.6 | 25 |

is presented in Appendix D. The CDN (B_n) and corresponding averaged field radiometer reflectances (aR_n) for each site except sites 2 and 9 are listed in Table 6. Sites 2 and 9 were omitted due to non-representative field reflectances.

Correlation coefficients for the relationship between these 2 sets of data are also listed on Table 6. The correlation between CDN and field reflectance for 10 sites (excluding L/D standards) ranged from $r = .43$ to $r = .61$. The probability with 10 sites for all bands except band 7 was greater than 80% in a two-tailed t test. (The probability for band 7 was just under 80%.) Band 6 showed the strongest relationship with $r = .61$, which has a probability of greater than 90%. A difference in bandwidth from $.2 \mu\text{m}$ for the field data and $.3 \mu\text{m}$ for the Landsat data may have contributed to the poor performance of band 7.

Regressions which included all 12 sites were calculated and plotted in Figures 45, 46, 47, and 48 for bands 5, 6, 7, and 8, respectively. These regressions have, of course, much higher r values since they include two perfectly correlated sites by definition. The dashed lines in each of these plots represent the expected line, $y = x$.

The examination of the consistent pattern of scatter for each band reveals some factors which may account for the lack of a stronger relationship. Sites 65.35, 8, 7 and 83.7 are consistently above the expected line; that is, the mean radiant flux detected by Landsat for each of these sites is higher than expected from ground sampling. The sites are all sites of either discontinuous desert pavement or vertically degraded desert pavement. The Landsat CDN is an average over the

Table 6. Landsat corrected DN (Bn), radiometer reflectance (aRn), and linear regression for 12 sites.

| Site | B4 | aR4 | B5 | aR5 | B6 | aR6 | B7 | aR7 |
|---|---|------|------------|------|------------|------|-------------|------|
| 3 | 12.0 | 18.6 | 17.9 | 26.2 | 21.4 | 31.3 | 26.0 | 34.5 |
| 4 | 11.4 | 14.2 | 15.5 | 20.0 | 17.3 | 22.6 | 21.2 | 30.3 |
| 5 | 11.9 | 13.6 | 15.9 | 18.4 | 17.7 | 21.5 | 19.8 | 24.4 |
| 6 | 13.9 | 21.8 | 21.4 | 26.5 | 22.8 | 29.4 | 27.1 | 32.2 |
| 7 | 18.7 | 20.7 | 29.8 | 25.5 | 33.2 | 29.3 | 40.0 | 28.2 |
| 8 | 20.1 | 19.7 | 32.5 | 30.0 | 38.7 | 35.2 | 46.4 | 40.4 |
| B1* | 23.3 | 23.3 | 37.0 | 37.0 | 43.8 | 43.8 | 50.2 | 50.2 |
| 65.35 | 17.9 | 14.7 | 28.4 | 20.5 | 33.0 | 23.3 | 38.4 | 25.0 |
| 70.25 | 11.9 | 12.9 | 17.7 | 14.4 | 18.2 | 15.6 | 22.0 | 18.5 |
| 70+P* | 10.9 | 10.9 | 15.2 | 15.2 | 16.8 | 16.8 | 19.2 | 19.2 |
| 70+D | 15.1 | 16.6 | 23.2 | 20.5 | 25.5 | 26.1 | 30.5 | 28.3 |
| 83.7 | 17.5 | 16.9 | 27.4 | 22.5 | 32.0 | 26.7 | 37.5 | 26.2 |
| For N = 12, | r = .70 | | .77 | | .80 | | .70 | |
| | y = .74x + 2.9 | | .89x + 2.9 | | .94x + 1.6 | | .84x + 6.4 | |
| For N = 10, (without L/D standards) | r = .47 | | .56 | | .61 | | .43 | |
| | y = .50x + 6.6 | | .76x + 5.9 | | .84x + 4.0 | | .65x + 12.1 | |
| At N = 10, | r = .61 is greater than 90% probability | | | | | | | |
| | r = .47 is greater than 80% probability | | | | | | | |
| At N = 12, | r = .70 is greater than 95% probability | | | | | | | |

* Denotes light/dark standards.

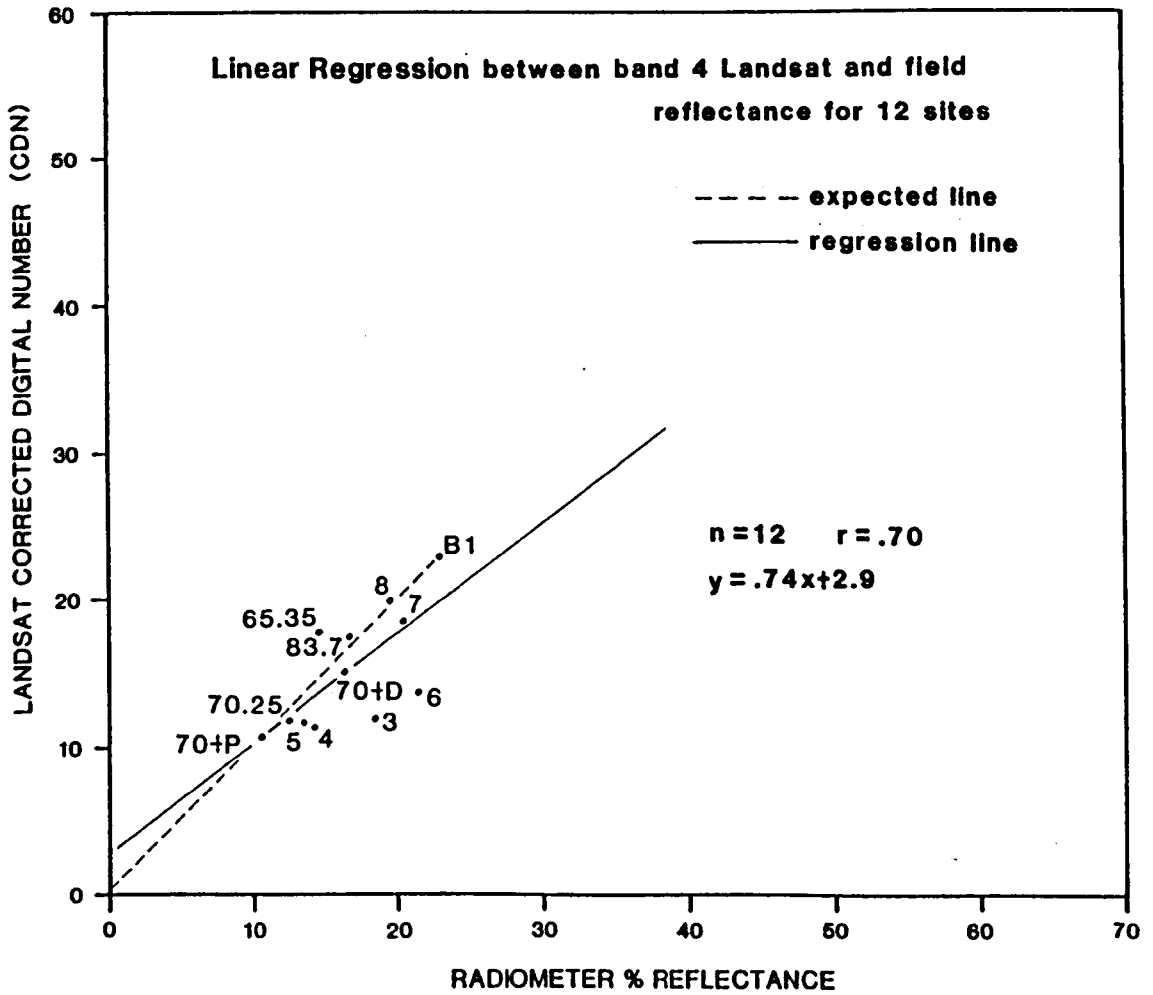


Figure 45. Linear regression between band 4 field and Landsat data.

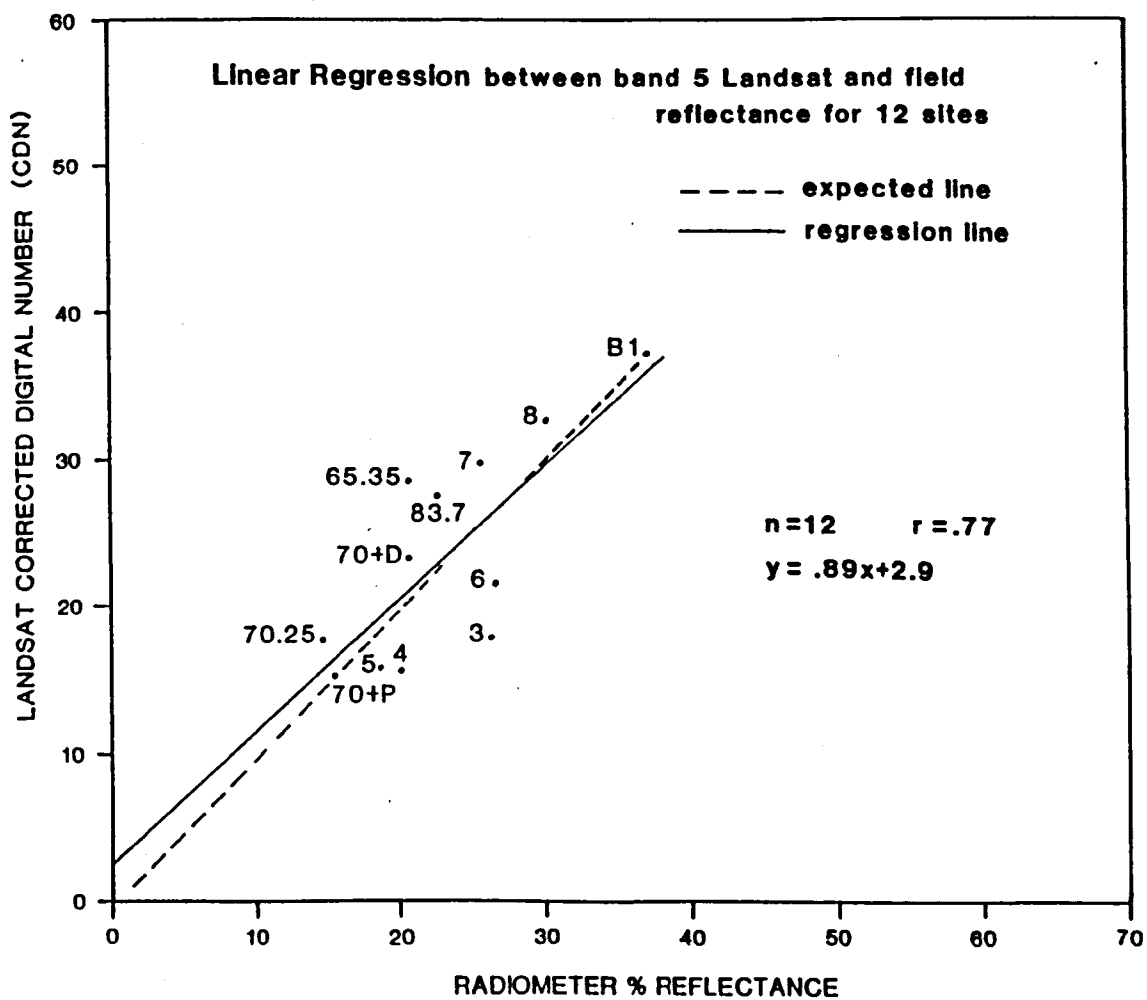


Figure 46. Linear regression between Band 5 field and Landsat data.

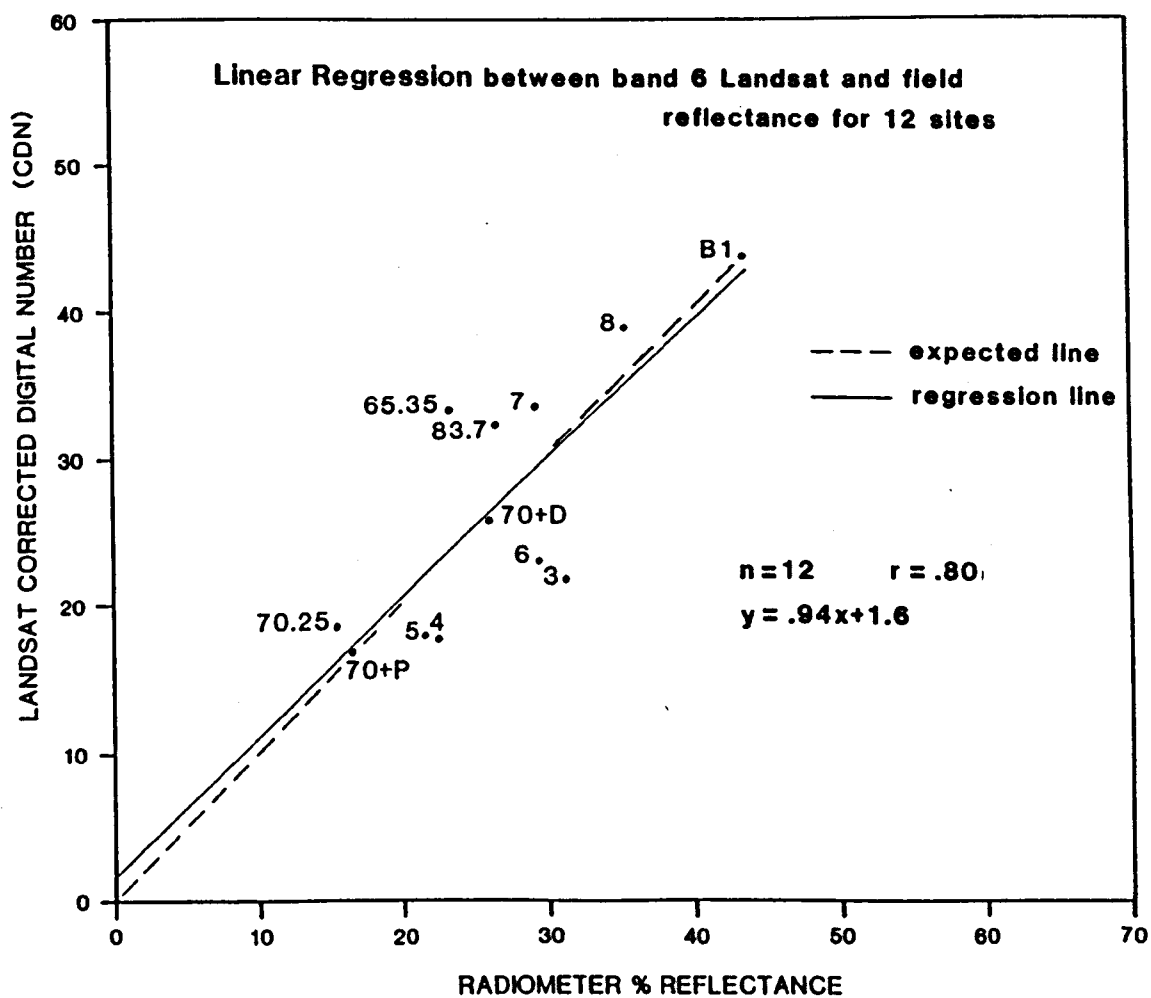


Figure 47. Linear regression between Band 6 field and Landsat data.

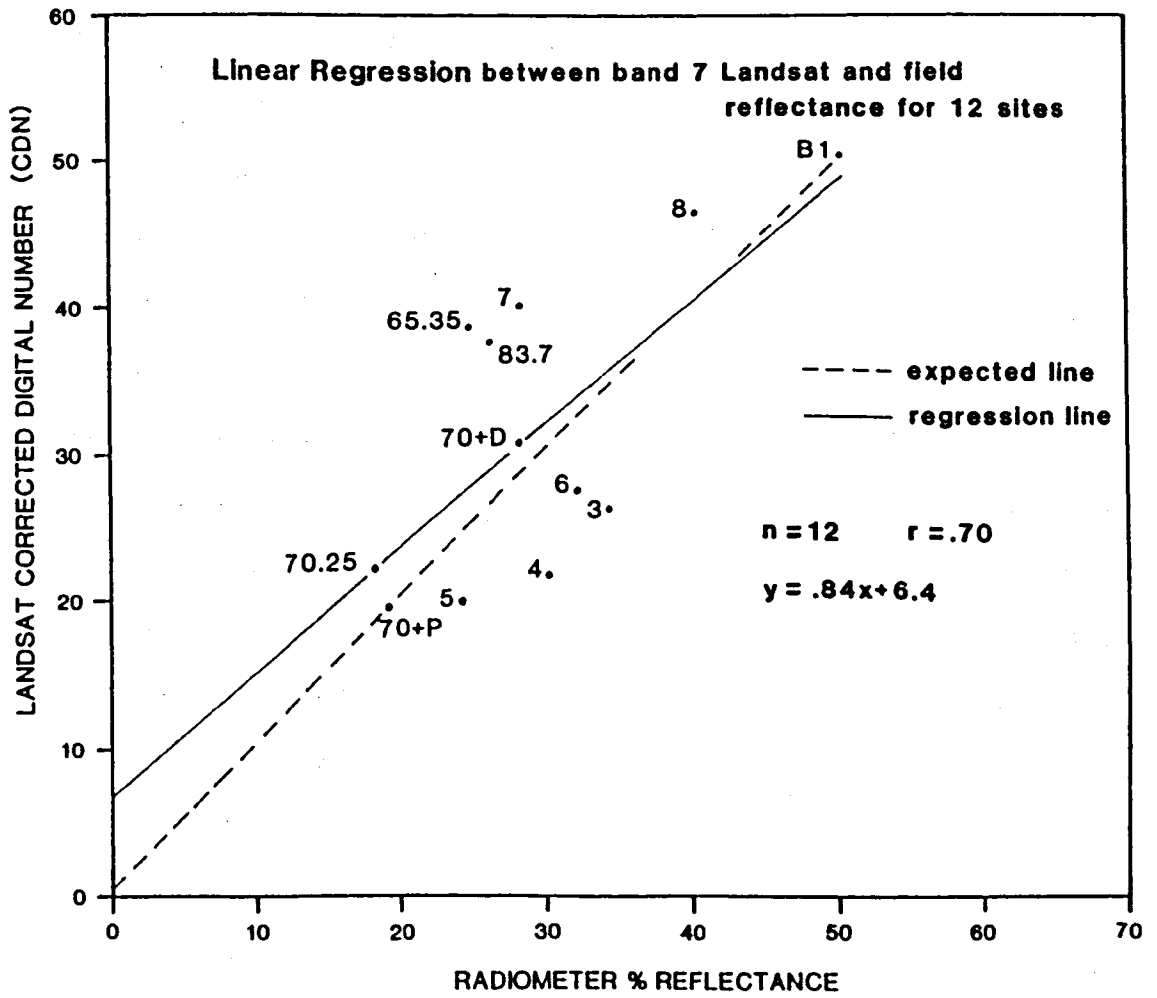


Figure 48. Linear regression between Band 7 field and Landsat data.

entire outlined site (Figure 43), whereas the ground reflectance is an average over only surfaces sampled. These were never larger than 20 x 20 m. Lower ground reflectance values suggest that ground sampling was biased toward the darker desert pavement areas within a site such that sites which were composed of large areas of desert pavement but also had significant areas of non-pavement were misrepresented by field sampling.

Shadowing is another cause of the data scatter. The Landsat data contains a large shadowing component because it was acquired at 9:00 a.m. on February 2, 1973, when the sun angle was only 31° . In contrast, most of the field reflectance data was obtained in the late morning and early afternoon when sun angles were from 45° to 65° . Sites most strongly affected by shadowing are sites which have large relief, coarse particles (micro-shadowing), or large scattered vegetation. The effects of shadowing from each of these factors, when averaged into a Landsat pixel, is illustrated in Figure 49.

Sites which appear to be most affected by shadowing (consistently plot below expected line) are sites 3, 4, 5, and 6--all of which are located in the upland region. This is not surprising because sites in the upland region tend to have greater dissection, coarser surface particles, and a greater amount of vegetation.

Sites 5 and 6 are dissected desert pavements on older alluvium. Shadowing in these sites is probably caused by coarse particles and large relief. Most of the relief is due to dissection valleys which run nearly perpendicular to the solar azimuth in the Landsat scene (143°).

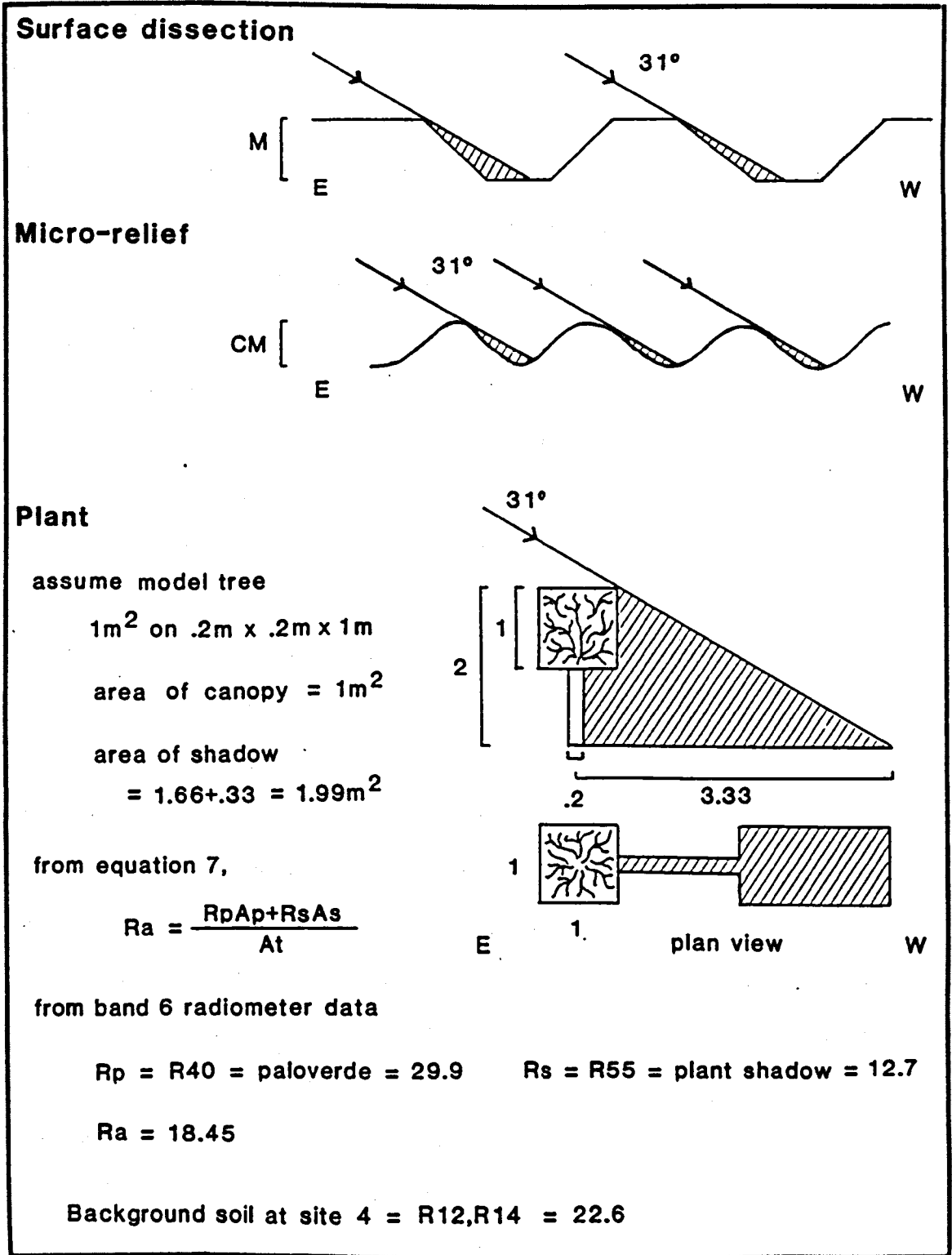


Figure 49. Influence of shadowing on reflectance with a 31° solar elevation.

This orientation maximizes the amount of shadowing in the valley. The highest reflectance components in these sites are in the dissection valleys which contain channel sands, unvarnished rocks, and exposed caliche--but they are cast in shadow by the low sun angle. The ridge-tops, which are in full sunlight, are composed largely of desert pavement, the lowest reflectance components in these sites. A large amount of shadowing will therefore lower the average reflectance values of a dissected pavement class.

Site 3 is more likely influenced by plant shadowing. As seen in the photos of these sites (Figure 20), site 3 has a relatively high density of small tree and large shrub vegetation (16%). However, the site shows no influence of an increase in infrared reflectance, which is characteristic of plant reflectance signatures. Because of the low sun angle and relatively open spacing of plants, the reflectance due to the plant canopy is canceled by that, due to the canopy shadow. For a theoretical tree 2 meters high (as illustrated in Figure 49), and a sun angle of 31° , the average reflectance of both plant canopy and shadow can be below background soil reflectance.

An interesting conclusion from the analysis presented in Figure 49 is that as long as the full shadow from the plant is cast on the ground, a higher biomass, or greater plant density will only contribute to a lowering of average reflectance.

Site 4 has relatively dense corridors of vegetation localized in surface runoff channels between nearly barren desert pavements.

Shadowing from these plants could be a contributing factor in the low Landsat CDN values of this site.

A better correlation between field and satellite reflectance data could be obtained if the contributing amount of reflectance forming each major reflectance component (including shadow) is measured in the field. For most sites, ground reflectance measurements did not sufficiently represent many components of the site surface. Low-level aerial photography would have been necessary to determine what the major components were and what the areal percentage of each component is within the site.

Other field data collected at the site (vegetation, density, particle size, variability) could only provide a qualitative explanation of the data scatter. Future field work would require more careful attention to the reflectance and area of each reflectance component.

Radar, Field Correlations

The radar data was used in its raw form without any attempts at calibration or smoothing. The radar DN is assumed to be a monotonic function, proportional to the radar backscatter, although some non-linear errors are present in the data. These are mostly from a slight degree of side-lobe banding or shading (see Chavez, 1979), and from the characteristic transfer curve of the film transparency.

The mean radar DN (RADN) for each site was used to compare the radar backscatter with field parameters. There is a degree of uncertainty associated with the RADN value because radar data is characterized

by high local variances (Table 5). This is typical for radar data (Jensen, 1979), and is a function of random facet orientations of local surface irregularities.

In the correlation analysis, RADN values were compared to mean particle sizes (P) and average vegetation density (V) for thirteen sites. These are presented in Table 7, ranked from highest to lowest RADN.

It was apparent that both average particle size (P) and vegetation density (V) contributed to the RADN value for each site. Because these were not known to be definitely additive or multiplicative factors, three combinations of the two field parameters were calculated (Table 7). These were P multiplied by V ($P \times V$), P added to V ($P + V$), and a two to three weighting of P added to V ($2P + 3V$).

Two tests were performed on the total of five field descriptors and combination of descriptors. The first was a non-parametric sum rank difference ($\Sigma\Delta$ rank) between the RADN and individual descriptor variable, and the second was a simple linear regression analysis (Table 7).

The poorest performances in both tests were the individual particle size and vegetation density descriptors. These had correlation coefficients of $r = .51$ and $.69$, respectively, and a $\Sigma\Delta$ rank of 38 and 20, respectively. The multiplicative ($P \times V$) and unweighted additive ($P + V$) descriptors scored much better with $r = .87$ and $.89$, and $\Sigma\Delta$ rank = 17 and 23, respectively.

The multiplicative combination ($P \times V$) scored better in the $\Sigma\Delta$ rank test while the additive ($P + V$) scored better in the regression

Table 7. Ranked mean radar DN (RADN), particle size (P), and vegetation density (V) correlations.

| Site | RADN | P | V | PxV | P+V | 2P+3V |
|---------------------|--------------|----------|---------|------------------|----------|----------|
| 3 | 103.3(1) | 19.0(2) | 16.0(1) | 304.0(1) | 35.0(2) | 36.0(1) |
| 6 | 95.2(2) | 29.9(1) | 7.5(4) | 224.3(2) | 37.4(1) | 82.3(2) |
| 5 | 83.2(3) | 18.4(3) | 5.0(5) | 92.5(5) | 23.4(4) | 51.8(5) |
| 70+D | 70.8(4) | 12.2(10) | 12.5(2) | 152.5(3) | 24.7(3) | 61.9(3) |
| 70+P | 68.2(5) | 14.7(7) | 5.0(6) | 73.5(7) | 19.7(7) | 44.4(6) |
| 4 | 67.4(6) | 11.9(11) | 10.0(3) | 119.0(4) | 21.9(5) | 53.8(4) |
| 65.35 | 67.3(7) | 12.6(9) | 5.0(7) | 63.0(8) | 17.6(10) | 40.2(9) |
| 70.25 | 58.3(8) | 17.8(4) | 2.5(12) | 44.5(11) | 20.3(6) | 43.1(7) |
| 83.7 | 55.8(9) | 11.1(12) | 5.0(8) | 83.0(6) | 16.1(12) | 37.2(11) |
| 8 | 54.5(10) | 12.7(8) | 4.5(9) | 57.2(9) | 17.2(11) | 38.9(10) |
| 7 | 44.4(11) | 15.7(6) | 3.5(11) | 55.0(10) | 19.2(8) | 41.9(8) |
| 9 | 32.3(12) | 16.9(5) | 1.0(13) | 16.8(12) | 17.9(9) | 36.8(12) |
| B1 | 19.9(13) | 2.4(13) | 4.0(10) | 9.6(13) | 6.4(13) | 16.8(13) |
| $\Sigma\Delta$ rank | | 38 | 20 | 17 | 23 | 14 |
| Correlations: | RADN W/P | n = 13, | r = .51 | y = .13x - 7.44 | | |
| | RADN W/V | n = 13, | r = .69 | y = .13x - 1.63 | | |
| | RADN W/PxV | n = 13, | r = .87 | y = 3.01x - 83.2 | | |
| | RADN W/P+V | n = 13, | r = .89 | y = .31x + 2.02 | | |
| | RADN W/2P+3V | n = 13, | r = .91 | y = .74x + 2.41 | | |

analysis. This may be due to the high sensitivity of (P x V) to vegetation differences, which tends to increase the mean square error for many sites, thereby lowering the correlation coefficient (r).

A 2 to 3 weighted combination of P and V (2P + 3V) produced the best results of any simple additive combination calculated. (A closer fit could be obtained by the least squares method, but would not be significantly better.). The $\Sigma\Delta$ rank value for 2P + 3V was 14, while the correlation coefficient was $r = .91$. This regression is plotted in Figure 50.

Although the strength of this association has yet to be demonstrated in the general case, it seems fairly safe to conclude that for relatively low relief, low regional slope natural arid terrains such as those in the thesis site, a good estimate of any one of the three variables (RADN, P, V) can be predicted from any of the other two once these variables are calibrated.

Although surface geometry and orientation (slope, aspect) are the most important factors determining the radar backscatter, this data suggests that for generally low relief, low regional slope sites such as these, the effects of local slopes and aspects on the mean radar return over a sufficiently large area must average out.

One possible application of this relationship is the use of a registered Landsat and radar scene to produce a particle size map of the surface. This could be accomplished with any good estimate of the vegetation density such as a multispectral vegetation ratio (7/5) or other

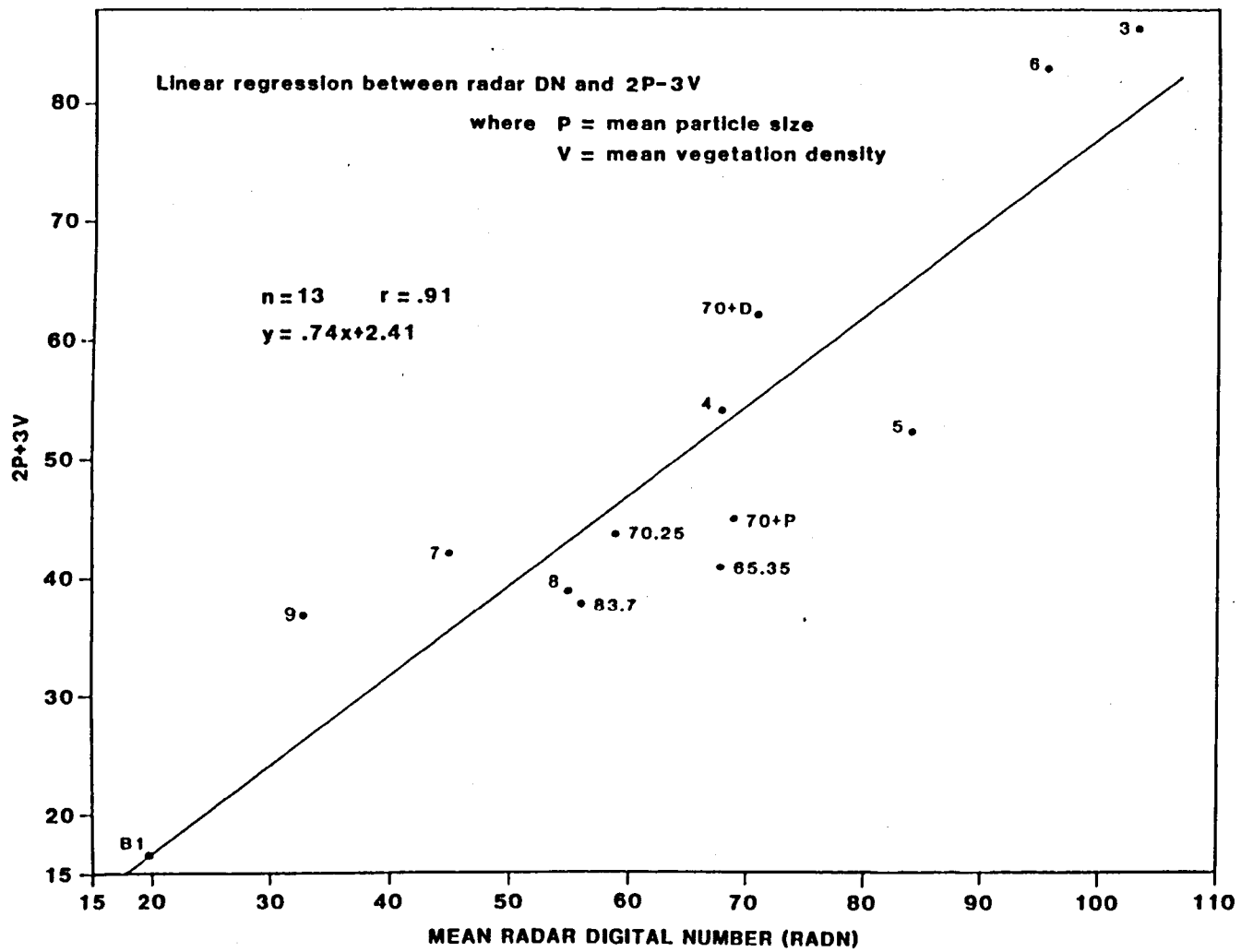


Figure 50. Linear regression between RADN and 2P+3V.

vegetation transforms (e.g., greenness: Richardson and Wiegand, 1977). However, the Landsat image must have a high enough solar elevation in order to reduce the effects of shadowing. If the assumption is made that the vegetation transform is a good approximation of that part of the radar backscatter due to vegetation and if the radar DN, vegetation transform value and particles sizes were calibrated for several sites. Then the two knowns, radar DN and vegetation index, could be used to predict and map the unknown particle size.

Radar-Roughness Map

A radar-roughness map was produced by smoothing the radar image with a 5x5 averaging spatial filter. The result was color coded with an eight-step density slice (Figure 51). Smoothing removes the local high-frequency component which is the cause of high variances in RADN numbers. By reducing the high-frequency component, image speckle is averaged out. Pixel values in the smoothed image are mean values which can be used to map surface-roughness classes.

The smoothed image is referred to as a radar-roughness map, although the image is technically a mean backscatter image. Radar backscatter is a function of surface geometry, roughness and orientation. In the image, the mean backscatter is divided into eight classes (Table 8). When geometry (slope) is extreme, it becomes the dominant control on backscatter. The high-backscatter Classes 6, 7, and 8 are dominantly slope controlled. The highest radar-return, Class 8, occurs when slopes are relatively smooth and are normal to radar incidence. Another class

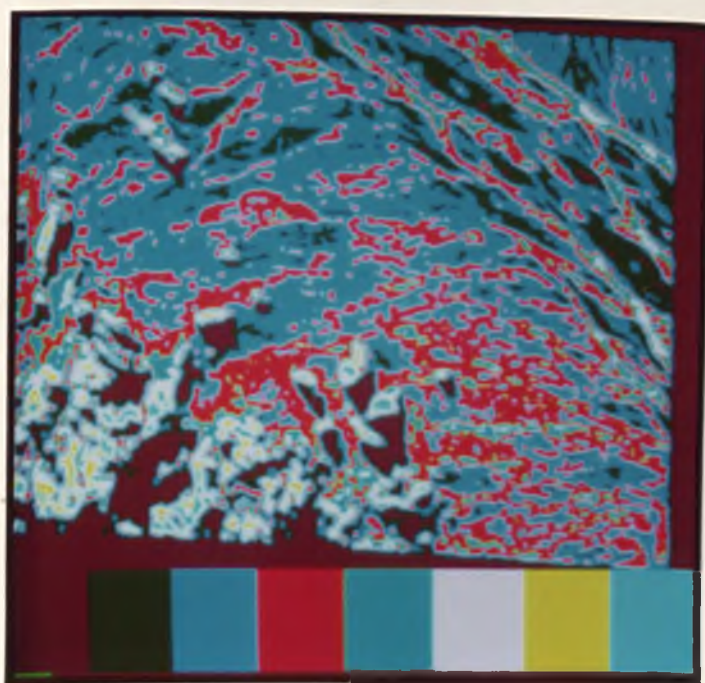


Figure 51. Radar roughness map. -- Refer to Table 8 for class descriptions.

Table 8. Classes of radar-roughness map.

| Class | Color | RADN | Description |
|-------|------------|---------|---|
| 1 | dk brown | 0 | Radar shadow or flat "Rayleigh smooth" sand and silt overbank deposits. No vegetation. |
| 2 | dk green | 1-36 | Flat sand and silt deposits and fine desert pavement or vertically degraded pavements. |
| 3 | dk blue | 37-73 | Flat but slightly irregular surface of desert pavement or vertically degraded desert pavement with little dissection or vegetation. Also coarser or more irregular overbank deposits. |
| 4 | red | 74-109 | Dissection valleys or coarse erosional surfaces with low relief, some vegetation and/or preferential orientation. |
| 5 | blue-green | 110-146 | Valleys with dense riparian vegetation or surfaces with large relief. |
| 6 | pink | 147-148 | Densest community of the largest vegetation types, or rough slopes near normal to incident radar. |
| 7 | yellow | 183-219 | Smooth slopes near normal to incident radar or rough slopes normal to incident radar. |
| 8 | lt. blue | 220→MAX | Smooth slopes normal to incident radar. |

dominantly controlled by geometry is Class 1, which has a mean backscatter of zero. Only two surface types fall into this class: those which are in radar shadow and those which are flat "Rayleigh smooth" surfaces. The former surfaces have no return because there is no incident microwave energy. The latter are flat smooth sand and silt deposits with a maximum particle size less than 2.7 cm (refer to surface-roughness section, Equation 14) and no vegetation. These surfaces specularly reflect all the incident radar energy away from the antenna.

Most of the sand and silt overbank deposits, along with some particularly undisturbed and fine (particle size) pavements, fall into Class 2. These surfaces range from 1 to 36 RADN's and are characterized by fine-grain particles (< 17 mm), flat surface morphology and very sparse vegetation.

The majority of desert pavements along with overbank deposits which have somewhat irregular surfaces fall into Class 3. This class encompasses the RADN range from 37 to 73, which includes almost all the desert pavement sites samples. These surfaces have minor surface irregularities or undulations but remain flat with sparse vegetation.

Alluvial surfaces which have rough topography, coarse particles or a large vegetation component fall into Class 4. This class also includes ephemeral channels without very dense riparian vegetation. Some of the field sites which fall into this class are Sites 5 and 6, which are Older Pleistocene surfaces with significant relief, and Site 3, which is a wide riparian floodway.

Class 4 appears to be affected by the orientation of stream drainage with the radar look. Channels which run perpendicular to the radar look have enhanced backscatter due to the geometric corner-reflector effect. This explains, in part, the reason for more pixels of Class 4 in the southwest portion of the map, where drainage is perpendicular to the radar look.

Class 5 covers the RADN range from 129 to 159. The class includes dense riparian vegetation and very irregular, coarse and sloping alluvial and bedrock surfaces.

The densest vegetation community composed of the largest vegetative types falls into Class 6, which is dominantly composed of look-facing slopes. These slopes are neither not exactly normal to the incident radar energy or they are coarse and therefore scatter much of that energy away.

Slopes with either smoother surfaces or more incident normal orientations fall into the highest backscatter Classes 7 and 8.

Image Texture

One of the more subjective--and yet valuable--interpretive elements in image analysis is image texture. The experienced image analyst may use the clumpy texture of scrublands to distinguish it from a more velvety textured grassland, or use the dendritic texture of finely dissected alluvium to separate it from a smooth, evenly fractured appearance of granitic outcrops with similar tone.

As suggested by the vocabulary used above, the element of

texture is particularly difficult to objectify or quantify. As a consequence of this situation, texture has been little used in applications of image processing and only recently has there emerged a quantitative vocabulary and data-processing techniques to analyze this image element.

In digital images, texture can be defined as patterns of spatial relationships, often quite complex, among the grey levels of neighboring pixels. The concept of texture involves a magnitude of tonal changes associated with a spatial arrangement of tones in a regular, repetitious manner. It follows that the textural signature for any object is dependent on the size of that object in relation to the scale and resolution of the imagery under consideration. The importance of image texture in geologic terrain classification has been demonstrated in experiments by Haralick, Shanmugam and Dinstein (1973) and by Weszka, Dyer and Rosenfeld (1976). For example, Weszka et al. (1976) were able to distinguish three rock types from 180 samples with accuracies of up to 95 percent based on textural measures alone.

Although textural features have been increasingly incorporated into multispectral classification (Wiersma and Landgrebe, 1976; Hsu, 1978; Jensen, 1979; Fasler, 1980; Irons and Petersen, 1981; Jensen and Toll, 1982), no single algorithm combining both efficiency and effectiveness has been widely accepted. Numerous textural measures have been developed. Surveys and algorithm comparisons of the various textural measures are given in Weszka et al. (1976), Haralick (1979), and Connors and Harlow (1980).

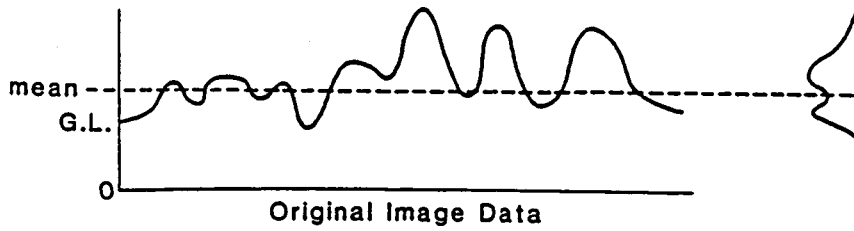
Hsu (1979) divided textural measures into two broad categories: Fourier-based features and statistical features. Weszka et al. (1976) demonstrated the superiority of statistical features over Fourier-based features. The most commonly used set of statistical textural features is the second-order textural measures based on Haralick's grey-tone spatial dependency matrix (Haralick, 1979). However, these textural measures incur large computational cost when used on a pixel-by-pixel basis.

Mitchell's max-min textural measure has been shown to perform equally well or slightly better than second-order statistical measures but with less computational effort (Mitchell, Myers and Boyne, 1977). The max-min method uses the relative frequency of local extrema (extremes) in grey level as the principal measure. Local extreme are divided into extrema of a specific threshold range (Carlton and Mitchell, 1977). In the one-dimensional case, a pixel is assigned to be a local extremum of threshold T if it is the largest (or smallest) value occurring in that vicinity on the line before the values drop (or rise) to an amount T .

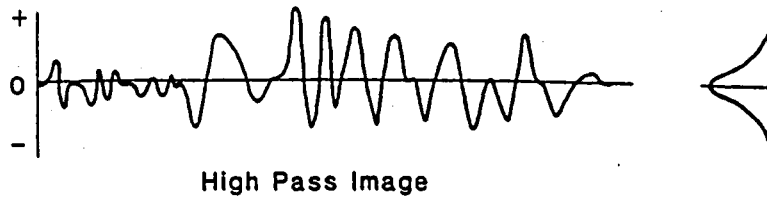
LEAD Texture Extraction

The LEAD extractor (Local Edge Amplitude and Density) is similar to Mitchell's max-min measure except that the algorithm does not look for extrema only. Textural feature extraction by the LEAD measure was done in three steps (Figure 52). The first step was the convolution of the image with a 3×3 high-pass spatial filter. As illustrated in

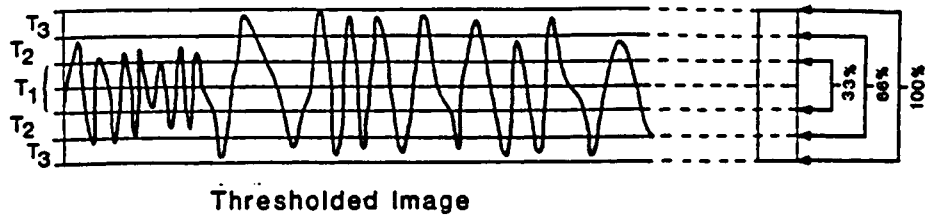
OPERATION GREY LEVEL TRANSECT HISTOGRAM



STEP 1. SPATIAL CONVOLUTION WITH HIGH PASS WINDOW



STEP 2. HISTOGRAM EQUALIZATION AND THRESHOLDING



STEP 3. COUNT WINDOWS WITH CONVOLUTION

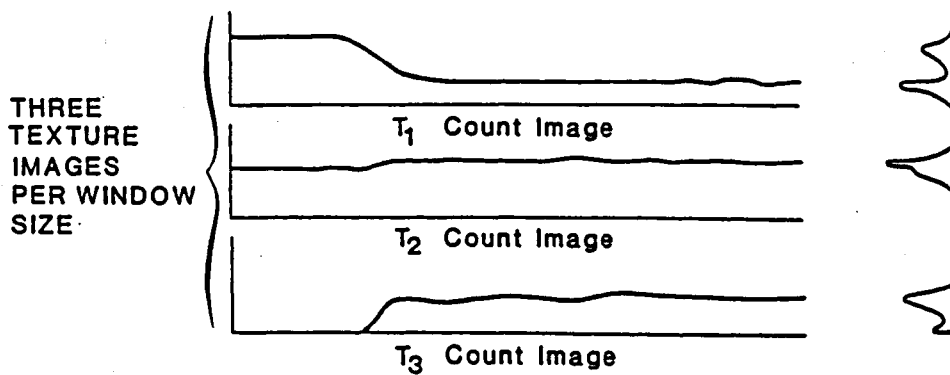


Figure 52. LEAD texture extraction.

Figure 52, Step 1, this produces a high-pass image with an approximately normal grey level distribution about a mean of zero. High-pass filtering removes the low-frequency background variations and only allows the high-frequency image information to remain. The rationale for using a high-pass filter follows from the intuition that textural information is primarily found in local contrast variations; that is, the human eye recognizes similar textures regardless of average background tone. Sharp transitions in radiance levels (edges) in the original image become spikes dependent on the width and contrast of the transitions in the original image.

In the second step (Figure 52, Step 2), absolute value thresholds were applied to the high-pass image so that each pixel was classified into one of three mutually exclusive threshold ranges. These threshold ranges are analogous to the T_1 , T_2 , T_3 grey level distances of Carlton and Mitchell (1977). Because no a priori arguments exist for the placement of threshold boundaries, it was decided that these thresholds would be set by an equal probability rule that could be implemented automatically. The procedure was simply to perform a contrast stretch which equalized grey level probabilities (histogram equalization) in the high-pass image. Thresholds were chosen at points that divided the resulting uniform histogram into three equal areas.

In Step 3 (Figure 52, Step 3), a count image was produced by convolving the thresholded high-pass image with a pixel window that counts the number of pixels in each threshold range within the window neighborhood. The number of pixels within each range is a measure of a

specific amplitude and density of image activity; that is, edges, lines, points and other elements of texture within the neighborhood defined by the window. Each combination of window size and threshold range produced one image textural feature.

Textural Features. Using program KOUNT, LEAD type textural features were extracted from both Radar and Landsat Band 5 images. For each window size used, three separate images were produced: the high threshold, medium threshold, and low threshold image. Windows of 5 x 5, 7 x 7, and 11 x 11 pixels were used to extract texture from radar. Landsat Band 5 texture was extracted with 5 x 5, 9 x 9, and 11 x 11 windows.

Window sizes were chosen empirically. The window sizes of 5 x 5, 9 x 9, and 11 x 11 pixels were used for the Landsat image, because the most significant textural variations were of this scale. For example, the texture of shadowed and illuminated slopes of bedrock has a spatial frequency of one cycle per 5 to 11 pixels, with a cycle consisting of one shadowed and one illuminated slope. The texture of a moderately dissected desert pavement, consisting of dark grainy flat areas with fine filaments and mottles, has several cycles per 5 to 11 pixels.

Two example textural color composite (TCC) images (Figures 53, 54) are shown to illustrate LEAD textural features. The TCC image is one in which all three textural features (high, medium, low thresholds) for a given window size are loaded into the red, green, and blue (RGB) video channels. This display system has the advantage of showing all three

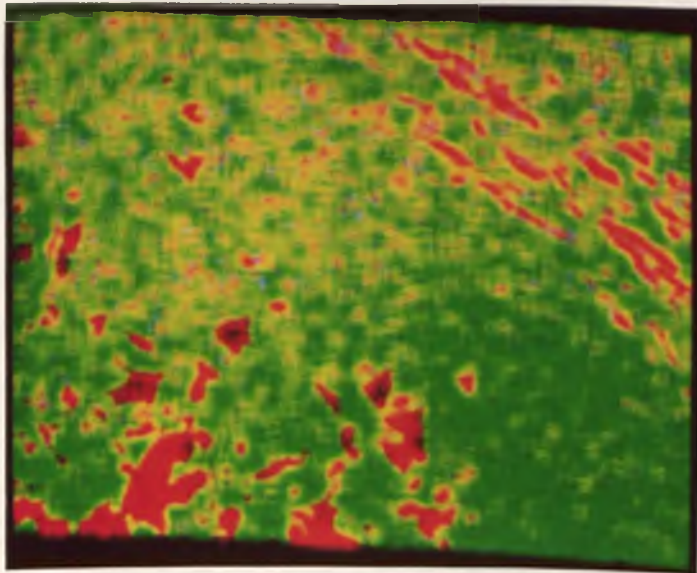


Figure 53. TCC display of 7 x 7 radar textural feature.
-- Low = red; medium = blue; high = green.

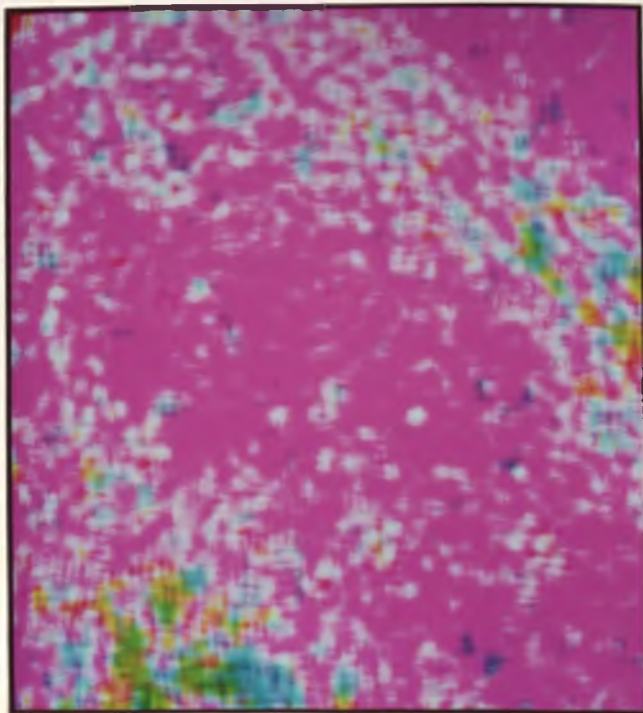


Figure 54. TCC display of 9 x 9 Landsat textural feature.
-- Low = blue; medium = green; high = red.

threshold levels at one time but does not highlight the full range of possible LEAD values in the image.

The first figure (53) is the TCC of radar textural features from a 7 x 7 pixel window count. In this image pixels which have a high count of low thresholded pixels are red, those with high counts of medium threshold are blue, and those with high counts of high threshold are green. Where there are large values of two or more threshold levels, the color code is a combination of colors for each individual threshold level. For example, pixels with high counts of both low (red) and high (green) thresholds are colored yellow. High counts of all three thresholds produce a white color.

The most prominent features in this image (Figure 53) are the pure red and pure green areas which correspond to the highest counts of low and high thresholded pixels, respectively. The highest count of low threshold (pure red) occurs in radar shadow and flat overbank deposit regions. These are also areas of lowest mean radar backscatter. Non-shadowed mountain range surfaces and the alluvial surfaces of Class 4 (red) in the roughness map are dominantly the high count of high threshold areas (green) in the radar TCC image. According to this textural measure, these regions have similar LEAD characteristics. The LEAD textural extractor is based only on statistical parameters. The fact that in a 7 x 7 radar TCC image the regions of bedrock and alluvium along the southern margin of the area are not differentiated indicates that the perceived textural differences between these areas in the radar image are due to structural rather than statistical textural differences.

Colors in the Landsat TCC images (Figure 54) are different from the radar TCC image. In this image of LEAD features produced by a 9 x 9 window count, the high threshold is red, medium is green, and low is blue. The Landsat Band 5 TCC image, unlike the radar TCC image, enhances the difference between mountain, pediment and basin regions. Most of the image is magenta, indicating that a combination of high (red) and low (blue) threshold pixels dominate the TCC image. The white-colored areas are where there are high pixel counts of all three threshold levels. These generally occur at transitional areas such as around bedrock hillslopes or at the boundaries between overbank deposits and channels of the axial stream complex.

Areas with large counts of high (red) thresholded pixels and low counts of other pixels occur in the mountainous region and in the densest riparian channels. Desert pavements are mostly magenta, although in some areas they are nearly all blue. Other combinations of medium threshold only (green), medium and high thresholds (yellow) and medium and low thresholds (cyan) differentiate the Mesozoic (sedimentary and metamorphic) rocks from Tertiary volcanic rocks and also differentiate a variety of alluvial and fluvial deposits in the basin area.

Image Classification

Image classifications were produced using program CALSCAN (Schowengerdt, 1979), a supervised Bayesian maximum-likelihood classifier. The version of CALSCAN at the University of Arizona was adapted from CALSCAN at the University of California, Berkeley. The Berkeley

version was in turn based on an earlier LARSYS classifier at Purdue University.

Four classifications were produced with CALSCAN: a simple 4-band Landsat spectral classification (S4); a four-feature classification with the best Landsat and radar textural features (STR4); a four-feature classification with the best Landsat and Landsat textural features (STL4); and a seven-feature classification with four Landsat bands and three textural features (STL7).

Supervised Bayesian Classification. In a supervised Bayesian classification, the classifier is "trained" by statistics calculated for each class, from each feature considered. At least one "training site" is defined for each class by the analyst. Class statistics constitute a (multivariate) probability density function, $p(x/w_i)$. A Bayesian classifier makes the assumption that the probability density function, $p(x/w_i)$, is multivariate normal or Gaussian (Tou and Gonzales, 1974; Swain, 1978).

The decision function, $d_i(x)$, for Class w_i is:

$$d_i(x) = p(x/w_i) p(w_i) \quad (16)$$

Where $p(x/w_i)$ is the probability that x belongs to Class w_i

$p(w_i)$ the a priori probability of Class w_i

In the multivariate case, the decision function expressed in natural logarithms is:

$$d_i(x) = \ln p(w_i) - \frac{1}{2} \ln |c_i| - \frac{1}{2} [(x-m_i)' c_i^{-1} (x-m_i)] \quad \text{Equation (17)}$$

where

m_i = the mean vector for Class i

c_i = the covariance matrix for Class i

In CALSCAN the working assumption is made that the a priori probability of each class is equal. In that case the first term of Equation (17) is dropped.

The decision function used in CALSCAN is therefore:

$$d_i(x) = -1/2[\ln|C_i| + \{(x - m_i)' C_i^{-1} (x - m_i)\}] \quad (18)$$

x' belongs to Class i if:

$$p(x/w_i) > p(x/w_j), p(x/w_k) \dots p(x/w_m).$$

Spectral/Geomorphic Classes. Twelve spectral/geomorphic classes (Table 9) were defined for three of the image classifications. The fourth classification, the four best Landsat and radar texture features, (STR) had only eleven classes. The difference was that Classes 4 and 5 (Q2a and Q2b) were lumped into one class (older alluvium).

The classes are called spectral/geomorphic classes because class definitions are based on reflectance data as well as geomorphic data. For example, bedrock classes, which are differentiated lithologically in the geologic/geomorphic system (Table 1) are grouped by reflectance in the spectral/geomorphic classes (Table 9).

Alluvial classes are more refined in the spectral/geomorphic system. They are classified on the basis of reflectance, age, and relative

Table 9. Spectral/geomorphic class descriptions used in classification.

| No. | Name | Description | Equivalent Geologic-Geomorphic Classes |
|------------------------|-------|---|--|
| <u>Bedrock</u> | | | |
| 1 | ROCKL | Rock hills and hillsides with no desert varnish, light-colored irregularly weathered surface. Mostly tuffs and flow-banded rhyolites. | Trt |
| 2 | ROCKD | Dark rock hills and hillslopes, with composition ranging from rhyolitic to basaltic andesitic volcanic rocks--all heavily coated with desert varnish. | Trt, Ta, Tvf |
| 3 | ROCKB | Rock hills, hillslopes, and associated alluvium of Mesozoic sedimentary and metamorphic rock, generally weathered to a grey green color and having a blue color in the Landsat standard false-color composite images. | Ms, Msch |
| <u>Desert Pavement</u> | | | |
| 4 | Q2a | Highly dissected alluvial surface of Older middle Pleistocene age. Limited in extent, rounded hill and valley morphology (forming smooth concave and convex surfaces), a few remnant dark desert pavement surfaces, and exposed caliche clasts. | Q2a |
| 5 | Q2b | Dissected alluvial surface of Middle Pleistocene age; flat-top ridges and concave valley morphology. Dark desert pavements on ridge. | Q2b |
| 6 | Q2cd | Darkest desert pavement of latest Pleistocene age, very flat with darkly varnished rock armor; moderate dissection. Darker due to enhanced varnish on more basic volcanic rocks (quartz latite, basaltic andesite, etc.). | Q2c |

Table 9. -- Continued

| No. | Name | Description | Equivalent Geologic-Geomorphic Classes |
|---|--------------|---|--|
| 7 | Q2c <u>1</u> | Dark desert pavement of latest Pleistocene age but lighter than Class 6. Surface is flat, with limited dissection. Varnish dark but lighter than Q2c <u>d</u> , in part due to more acidic rock composition. | Q2c |
| <u>Eroded Desert Pavement</u> | | | |
| 8 | PAV DIS | Desert pavement vertically degraded by sheetwash erosion; a very flat planar surface which is light in color due to exposed sand, silts, and clays, with caliche clasts on surface. In areas, alternating with patches of Q2c <u>d</u> , Q2c <u>1</u> , and C EROS. | Q2pd, Q4/Q3 |
| 9 | C EROS | Coarse erosional surface, a gravelly modern surface mostly composed of coarse unvarnished rocks of mixed lithology and reflectances, with no soil development and sparse vegetation; low relief and undulating surface morphology. | Q4/Q3 |
| <u>Modern Fluvial Deposits and Vegetation</u> | | | |
| 10 | SAND | Overbank deposits of fine sand and silt with varying amounts of creosote bush in pure stands. | Q4/Q3 |
| 11 | WRP | Relatively unchannelized wide ephemeral floodway composed of sand and gravels with open clustered riparian vegetation. | Q4/Q3 |
| 12 | DRP | Major incised ephemeral stream channels with dense riparian vegetation. | Q4/Q3 |

erosional activity or stability on the surfaces. The complex of surfaces in the pediment and basin regions, which are generalized in the sketch map (Figure 5), are divided into two pavement classes, two erosional classes, and three vegetation and fluvial classes.

Classification Training and Feature Selection. At least one training site was chosen for each of the twelve classes. A total of twenty-five training sites were selected for classification. Pixel locations of all the training sites are included in Appendix C. Because of the limited spatial extent of many classes, some of the training sites were by necessity very small. The smallest class was defined by nine samples (on the unduplicated file). Larger sites usually consisted of twenty-five samples, with the largest having fifty-four samples.

Using STATS, a CALSCAN program overlay, probability density functions were generated for each class ($p(x/w_i)$), for each feature. Due to the large number of textural features (9 radar textural features and 9 Landsat textural features), the number of features to be incorporated into a Bayesian classification had to be reduced.

The "best" feature was defined as that which produced the largest average pair-wise class divergences (Swain and Davis, 1978). Using the CALSCAN overlay SELECT, divergences were calculated for all textural features and for the Landsat spectral bands. The best four combination of Landsat and radar textural features were Landsat Bands 4 and 7, and the medium threshold, 11 x 11 window (RTM(11 x 11)), and the high threshold, 11 x 11 window (RTH(11 x 11)) textural features. These features were used in the STR4 classification.

The best four combination of Landsat and Landsat Band 5 derived textural features was found to be Landsat Bands 5 and 6 and the high threshold, 5 x 5 window (LTH(5 x 5)) and the low threshold, 11 x 11 window (LTL(11 x 11)) textural features. These were the features used in the STL4 classification.

In the seven-feature Landsat and Landsat textural classification, STL7, all four Landsat bands were used along with the three "best" Landsat textural features. The three "best" textural features were LTH(5 x 5), LTL(11 x 11), and the high threshold, 9 x 9 window (LTH(9 x 9)) textural feature.

Classification Results. Of the four classifications, the seven-feature classifications with Landsat spectral and textural features combined (STL7) produced the best map in terms of training site accuracies and map interpretation. Training site accuracies (Table 10) ranged from a low of 73% for the Landsat spectral classification (S4) to 96% for the Landsat spectral and textural (STL7) classification. The best four Landsat spectral and Landsat textural feature combination (STL4) outperformed the best four Landsat spectral and radar textural feature combination (STR4). Accuracies for these classification were 86.2% and 81.9%, respectively.

Significant improvements in classification STL7 over S4 are illustrated in the grey-level plots of spectral and textural features (Figures 55, 56). In the grey-level plots of darkly varnished Classes 2, 4, 5, 6, and 7 (Figure 55), many classes which are not separable by spectral features are separable by textural features.

Table 10. Performance based on training site statistics.

| Class | S4 | STL4 | STL7 | STR4 |
|-----------|-------|-------|-------|-------|
| 1 ROCKL | 55.6 | 100.0 | 100.0 | 100.0 |
| 2 ROCKD | 44.0 | 91.0 | 93.0 | 58.6 |
| 3 ROCKB | 96.0 | 68.0 | 100.0 | 100.0 |
| 4 Q2A | 88.9 | 100.0 | 100.0 | 80.0 |
| 5 Q2B | 100.0 | 100.0 | 100.0 | |
| 6 Q2cd | 71.0 | 93.5 | 100.0 | 64.3 |
| 7 Q2c1 | 70.0 | 94.0 | 94.0 | 78.4 |
| 8 PAV DIS | 73.5 | 79.4 | 94.1 | 86.8 |
| 9 C EROS | 44.1 | 55.9 | 88.2 | 60.4 |
| 10 SAND | 75.8 | 89.5 | 97.9 | 96.6 |
| 11 WRP | 88.9 | 100.0 | 100.0 | 92.0 |
| 12 DRP | 68.4 | 63.2 | 84.2 | 83.7 |
| Average | 63.0 | 86.2 | 96.0 | 81.9 |

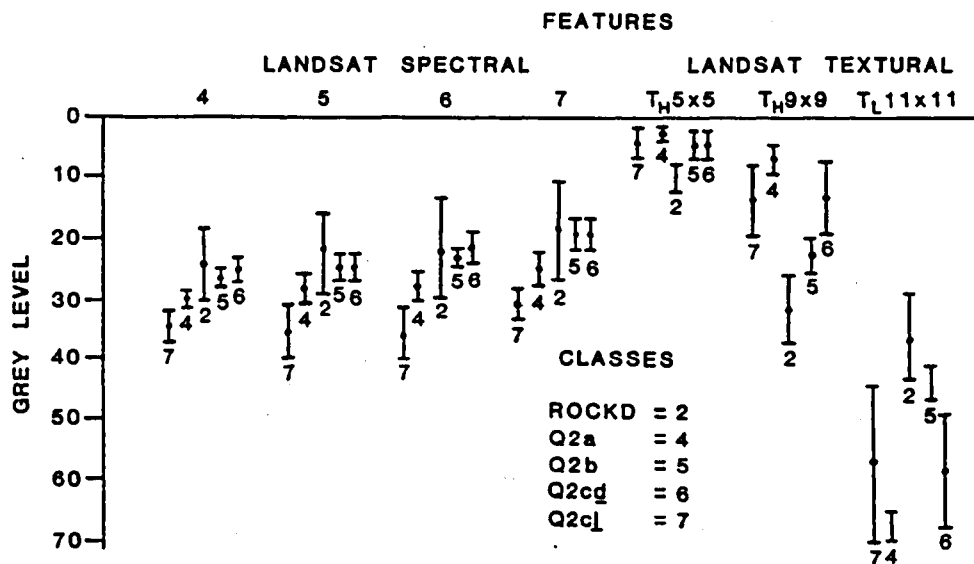


Figure 55. Grey-level plots for classes 2, 4, 5, 6, and 7. -- Bars represent ± 1 standard deviation.

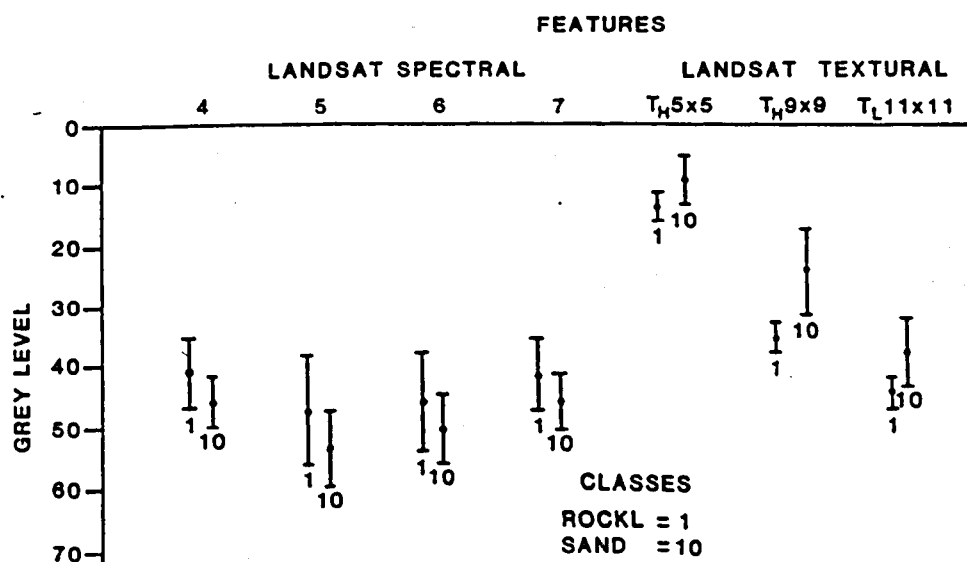


Figure 56. Grey-level plots for classes 1 and 10. -- Bars represent ± 1 standard deviation.

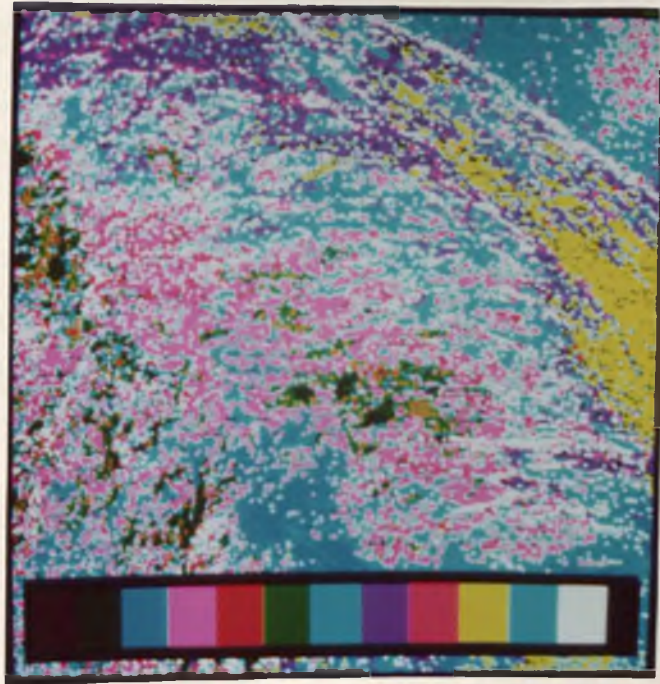
Because Class 2 is composed of hillslopes, the radiance range of this class is large in each of the Landsat bands. This is shown by the grey-level standard deviation of the spectral bands. But textural features separate Class 2 from the pavement classes because of its larger number of high-threshold pixels (LTH 5 x 5, LTH 9 x 9) and smaller number of low-threshold pixels (LTL 11 x 11). Textural features also separate Classes 5 and 6, which are not separable in the original spectral bands (Figure 55). Class 5 (Q2b) has dark pavement but is characterized by greater relief than Class 6 (Q2cd), which is equally dark. The textural features produced with larger window sizes (LTH 9 x 9, LTL 11 x 11) respond to this with a higher count of high-threshold pixels (LTH 9 x 9) in Class 5 than Class 6 and a lower count of low-threshold pixels (LTL 11 x 11) in Class 5 than Class 6. It is interesting to note that Classes 6 and 7, which are lighter and darker desert pavement classes of the same age, cannot be separated by textural features (Figure 55) because of their similar topographic and drainage characteristics. They are separated, however, by spectral differences.

Significant improvements were also found in the separation of Class 1, light bedrock, from the light-colored sands and silts of Class 10 (Figure 56). Class 1, light rock, and Class 10, sand--both high-reflectance classes--are inseparable in the Landsat bands but once again are differentiated by Landsat texture (Figure 57). Thus, it appears that the inclusion of landsat textural features improves the separation of spectrally similar but texturally dissimilar bedrock and alluvial classes.

A comparison of classification maps produced by all four classifications (Figures 57, 58, 59, 60) to each other and to the geologic/geomorphic sketch map shows marked improvement of Map STL7 over Map S4 and the other two four-band combination maps, STL4 and STR4. Due to significant spectral overlap between classes, random single-pixel misclassifications created a "noisy" appearing map in the S4 classification (Figure 57). The three other maps which incorporated either Landsat-derived or radar-derived textural features had significantly reduced "pixel noise."

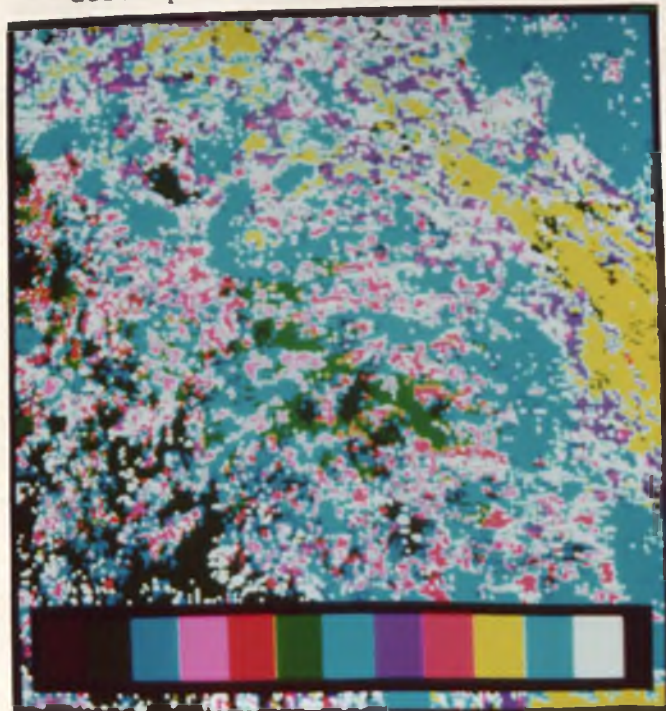
One of the major deficiencies in the S4 map (Figure 57) is the confusion of bedrock and pavement classes. The inclusion of two textural features in STL4 (Figure 58) and three textural features in STL7 (Figure 59) progressively improves the separation of bedrock and pavement classes. This is most dramatic in the pediment region where isolated inselbergs are exposed above the surrounding alluvium. The inselbergs are almost completely lost in the alluvium due to misclassifications in S4, but in STL4 and to a greater extent in STL7 these inselbergs are classified correctly and stand out in contrast to the surrounding alluvial classes.

The replacement of two spectral features with textural features in STL4 gives the resultant classified map (Figure 58) some interesting characteristics. Classes which are defined primarily by spectral characteristics such as Class 3 "blue rock" (dark blue in Figure 58) are poorly mapped because of the deletion of two spectral bands. Also map classes have an overall "blocky" appearance due to the square windows



Class 1 2 3 4 5 6 7 8 9 10 11 12

Figure 57. S4 map. -- Refer to Table 9 for class descriptions.



Class 1 2 3 4 5 6 7 8 9 10 11 12

Figure 58. STL4 map. -- Refer to Table 9 for class descriptions.

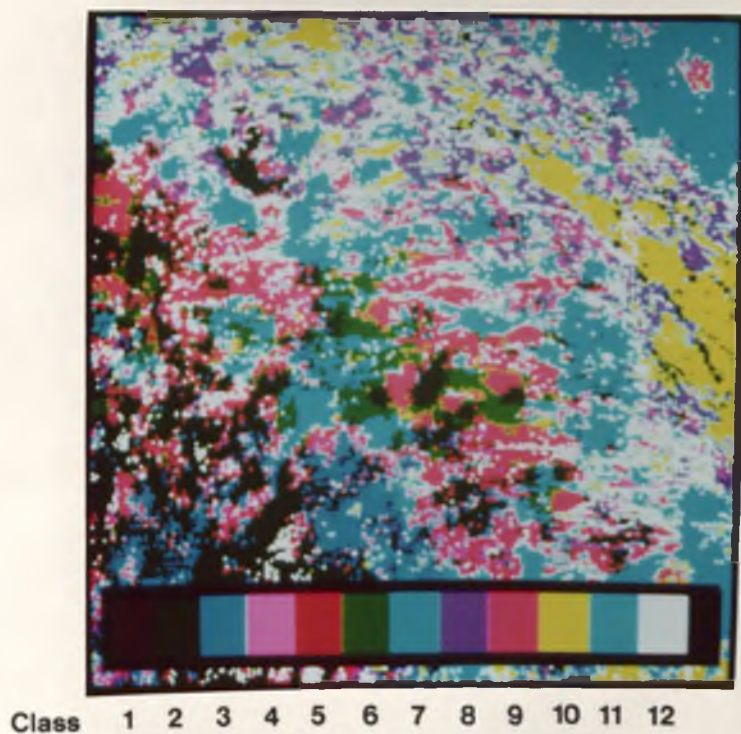


Figure 59. STL7 map. -- Refer to Table 9 for class descriptions.

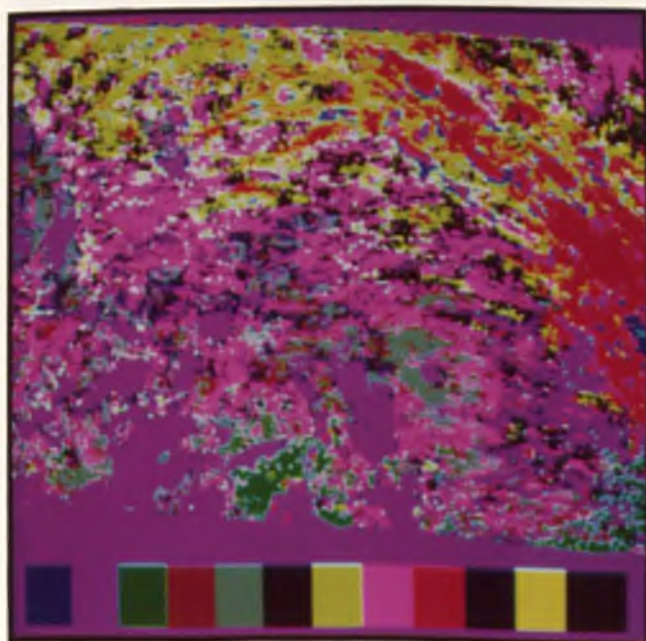


Figure 60. STR4 map. -- Refer to Table 9 for class descriptions.

used in the production of textural features. The map of classification STL7 overcomes these drawbacks by retaining all the spectral bands.

The map of classification STR4 (Figure 60), which combines two Landsat bands and two radar textural features, was the poorest as judged by photo interpretation. This was due to three factors: lack of information in radar shadows; radar geometric-orientation problems; and lack of significant differences in LEAD texture. The first two factors are inherent in the radar-terrain combination. Orientation problems are probably more apparent in an extremely arid terrain such as in this study site than in other terrain types. In this type of terrain drainage channels are usually aligned in parallel rather than dendritic, and channel morphologies are usually steep-walled and flat rather than concave. These drainages when aligned perpendicular to the incident radar radiation will have a much higher backscatter than in other orientations.

Radar speckle is to a large degree responsible for the lack of LEAD textural discrimination between high-backscatter oriented alluvial surfaces and bedrock surfaces. A smoothing procedure before texture extraction would probably improve radar textural features.

CHAPTER 4

SUMMARY AND CONCLUSIONS

Arid geomorphic surfaces can be differentiated and mapped into spectral/geomorphic units (classes) by computer, using Landsat band 5 derived LEAD textural features to augment a Landsat multispectral classification.

In a fashion similar to the morphostratigraphic units proposed by Frye and Willman (1962), which used morphologic and stratigraphic criteria to map glacial deposits, spectral/geomorphic classes are proposed as appropriate to the nature of the data source and the geomorphic importance of both surface reflectance and morphology in the arid terrain.

Spectral/geomorphic classes, as mapped by classification STL7, are morphogenetically significant because they are based on the VNIR spectral reflectance and the statistical spatial distribution of spectral reflectance (image texture) of arid geomorphic surfaces. In the arid terrain spectral reflectance is largely a function of rock weathering, desert varnish coating, lithology and particle size. Image texture as measured by the Landsat-derived LEAD textural features used in this study are surface topography, morphology, and dissection related.

One of the major determinants of spectral reflectance in the desert is rock weathering and desert varnish coating. The VNIR reflectance of desert varnish is characterized by a dark top varnish coating

curve and a bright red bottom varnish curve. Rocks with the darkest top varnish coating usually have the brightest red bottom coating. The darkness of top varnish is correlated with SiO content whereas the brightness of the bottom varnish is correlated with FeO content. Because of this relationship, rocks which have varnish coating with a SiO/FeO ratio approaching one are speculated to have been overturned several times such that all rock surfaces have experienced both top and bottom varnishing environments.

Alluvial surfaces ranging from recent lightly weathered deposits to dark desert pavements are best differentiated in the red and infrared regions of the VNIR spectrum. They are most similar in the blue regions (.4 - .5 μm) of the spectrum.

The reflectance of fine-grain alluvial surfaces are determined by particle size and lithologic composition. When exposed to weathering, fine-grain alluvial deposits of acid volcanic composition generally attain a high infrared reflectance rather quickly. The VNIR curves for these surfaces can be described as straight-line segments sloped upward toward the infrared. The VNIR reflectance curve flattens as the particle size increases such that given the same composition, modern surfaces with coarser particle sizes have a lower overall reflectance than those composed of finer particle sizes.

The reflectance of undisturbed Q2c age (Late Pleistocene) desert pavements appears to be purely a function of average particle size. The lowest and flattest reflectance curves of any alluvial surface are those of undisturbed, coarse-grain Q2c-age desert pavements composed of inter-

mediate to basic volcanic rocks. Because the large Q2c-age particle size distributions are also, in this case, compositionally the most basic, it is unclear what influence the composition plays in the reflectance of these stable Q2c surfaces.

With age, desert alluvial surfaces become brighter as the varnish coating is eroded, desert pavement rocks are overturned and either surface degradation or dissection exposes pedogenic silts, clays and calcium carbonate clasts. The desert pavements of Q2b and Q2a age (Middle and older Middle Pleistocene) are much brighter than predicted by their particle size distribution. The highest-reflectance desert pavement is the Q2a pavement. The VNIR curve for this surface is slightly convex in shape due to the influence of exposed red bottom varnish coating and pedogenic calcium clasts.

Desert pavements which have been disturbed by surface erosional degradation tend to have VNIR reflectance curves which can be described as either straight-line segments sloped upward toward the infrared or a convex-shaped curve sloped upward toward the infrared. The straight-line-segment curves are similar to curves for modern alluvium (stream channel sand and silt deposits), whereas the convex reflectance curves are similar to those of dissected older alluvium (Q2a). The former is probably due to fresh oxidation of newly deposited material and the latter due to exposure of soil vesicular horizon and calcic horizon material (calcium carbonate, silt, and clay).

The topography and vegetation attributes of geomorphic surfaces tends to obscure spectral differences between geomorphic surfaces--but

these attributes are geomorphically significant and related to image texture. The use of textural and spectral features tailors a supervised computer classification to significant geomorphic parameters.

The collection of on-ground field data proved useful in establishing a link between image data and map classes. However, on-ground collection of field radiometer and surface terrain data did not adequately represent Landsat MSS spectral response in heterogeneous sites. This is primarily due to field-sampling biases and scale differences between field and satellite sampling. Differences in scene shadowing also contributed to a poor correlation between field radiometer and Landsat MSS data.

An intermediate scale data such as obtainable from large-scale aerial photography would have been useful in establishing a better fit between field and image data. From large-scale aerial photography, more useful terrain parameters such as drainage density orientation, and average relief could have been established on a statistical basis. By assigning an average percent area for each surface reflectance component (pavement, wash, etc.) in a given geomorphic class, the effect of heterogeneity can be modelled to produce a tighter fit between surface reflectance data and satellite data.

Of field data collected, the average particle size measurement had the greatest significance in both Landsat MSS and X-Band HH radar images. The relationship of the averaged radar DN to a weighted addition of average particle size and vegetation density field parameters

produced a strong correlation for alluvial sites. This correlation can be usefully exploited if two of the three variables are known.

The LEAD textural measure is a statistical rather than structural statistical textural measure. It is significantly better than a simple variance-type textural descriptor because it looks only at high-frequency information and classifies pixels according to the density of a particular amplitude of image "activity." While it has performed well in this application, a textural measure which incorporates structural attributes should be superior. One possibility is to use second-order statistics based on a Haralick co-occurrence matrix quantized to four threshold levels using a LEAD-type thresholded image as the data source.

The utility of textural features in numerous remote sensing applications is apparent from this study. Many geologic resource problems can be addressed more successfully by incorporating textural features into the analysis. Another obvious application is in the field of forestry, because the interpretation of forest composition is usually based on texture-tone photoanalysis.

The overall benefit of image textural analysis is in the separation of classes which have significant spectral overlap but are texturally distinct. Other classification improvement techniques, such as stratification, require the input of additional data, usually terrain or geographical map-base-type data. The advantage (and elegance) of using derived textural data is that more useful information is obtained from the original image data set without the requirement of other additional data sets.

APPENDIX A

IMAGE SOURCES AND SPECIFICATIONS

Type: LANDSAT MSS

Specifications: Scene ID ERTS-E-1194-17391-501
 Path/Row 40/37
 Date 2 February 1973
 Sun Elevation 31°
 Azimuth 143°

Source: Obtained as CCT from- USGS
 Eros Data Center
 Sioux Falls, South Dakota 57198

MSS System Specifications- See Figure A1, Table A1

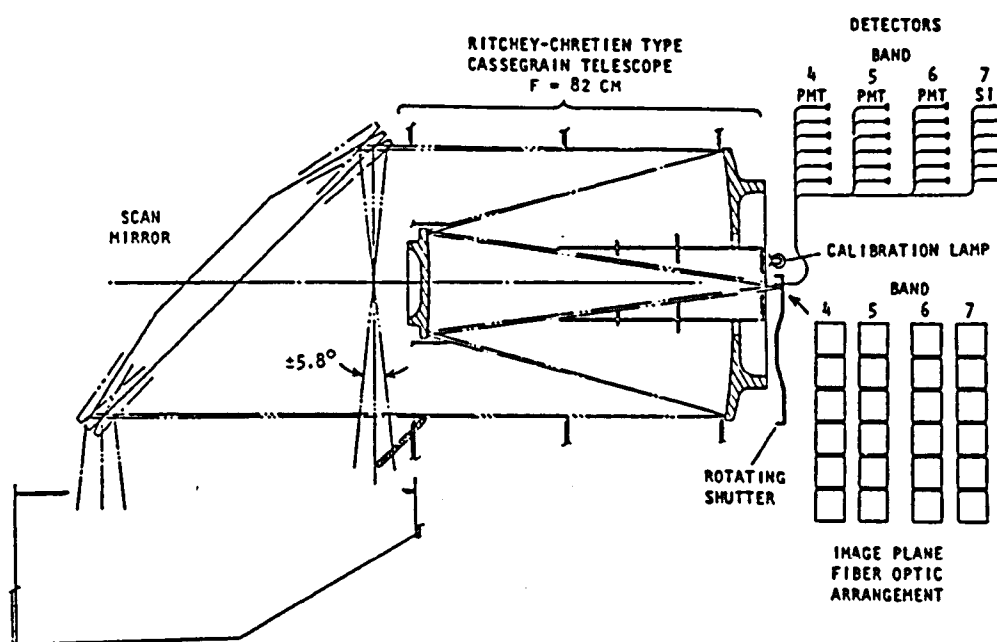


Figure A.1. Layout of four-band Landsat MSS (source: NASA, 1972).

Table A.1. Landsat multispectral scanner system^a
(source: NASA, 1972).

| | |
|--|--|
| <i>Scanner</i> | |
| Telescope optics | 22.9-cm-aperture Ritchey-Chretien with 8.9-cm-aperture secondary mirror |
| Focal length | 82.3 cm |
| <i>f</i> number | 3.6 |
| Scanning method | Oscillating flat mirror $\pm 2.9^\circ$ at 13.62 Hz |
| Cross-track field of view | 11.6° |
| Scan duty cycle (active scan) | Approximately 33 ms of 73.42-ms cycle min (45% active scan time) |
| Optical fiber core | 68.3- μm side of square |
| Diameter of blur circle | 27 μm |
| Instantaneous field of view | 0.083 mrad |
| Spectral bands and detectors | Band 4: 0.5–0.6- μm photomultiplier tubes Band 5: 0.6–0.7- μm photomultiplier tubes Band 6: 0.7–0.8- μm photomultiplier tubes Band 7: 0.8–1.1- μm silicon photodiodes |
| Number of lines scanned/scan/band | 6 |
| Area of fiber optics array | (396 μm along track) \times (432 μm across track) |
| Geometrical projection of square side of fiber core onto ground | 76 m |
| Gap between scan lines | 5.5 m |
| Sampling distance: across track in track | 56m to 58m 81.5 m |
| Video bandwidth (–3 dB) | 42.3 kHz per channel |
| <i>Radiometric quantities</i> | |
| Optical transmittance including secondary mirror obscuration | 0.26 |
| Radiance ($\text{W m}^{-2} \text{sr}^{-1}$) at entrance pupil to produce full-scale output; signal-to-noise ratio ^b | 24.8 (Band 4); 112:1 20.0 (Band 5); 86:1 17.6 (Band 6); 72:1 46.0 (Band 7); 122:1 |
| <i>Multiplexer</i> | |
| Number of channels | 24 |
| Quantization | 6 bits (64 shades of gray); 7 bits in bands 4, 5, and 6 after processing |
| Quantization accuracy | Within ± 30 mV at any quantum level |

Table A.1. -- Continued

| | |
|-----------------------------|------------------------------------|
| Processing modes | Linear and signal compression |
| Clock stability | ± 1 part in 10^4 over a year |
| Output bit rate | 15.06×10^6 bit/s |
| Sampling rate each channel | 100,418 samples/s |
| Crosstalk | > 40-dB rejection |
| <i>Interface parameters</i> | |
| Scanner weight | 47.6 kg |
| Multiplexer weight | 2.7 kg |
| Scanner size | $\sim 36 \times 38 \times 90$ cm |
| Multiplexer size | $10 \times 15 \times 17$ cm |
| Regulated power, -24.5 V | 20-W scanner, 19.6-W multiplexer |
| Unregulated power, -39 V | 22 W |
| Command Capability | 72 (55 assigned) |
| Telemetry channels | 97 |

*Nominal altitude 918.6 km.

^bValues are for Landsat 1 (they are different for Landsats 2 and 3).

Type: X-HH SAR Radar

Specification: USAF AN/APS-73(XH-4) (experimental)
Flight 655-079, Pass 11
5 November 1964

Unfocused synthetic aperture
X-band 2.4 - 3.8 cm
HH polarized
Ground range sweep corrected
Depression angle 8 deg. to 4 deg.
Film scale 1:480,000
Resolution 50 ft. or 15 meter

AN/APS-73 (XH-4) System Specifications:

Manufacturer: Goodyear Aerospace Corporation. The AN/APS-73 (XH-4) system was an experimental predecessor to the AN/APQ-102 system. Both were X-band HH SAR installed in the RF4C aircraft. It relies upon a CRT-film-type photographic recorder in the aircraft and employs a coherent optical processor to convert photographically stored radar signals into an output image recorded on a second photographic film (Moore, 1975).

Digitization: On Perkin Elmer PDS Microdensimeter
Aperture 25 μ m
Sampling distance 25 μ m

Source: C. A. Anderson
Dept. 408A, Building 13-2S
Goodyear Aerospace
Litchfield Park, Arizona 85340

APPENDIX B

FIELD DATA

Lithology Determination

Bedrock samples were taken from the field, cut open, and identified by their mineralogy, texture, and color as observed in hand sample. The larger clasts from sieved alluvial soil samples were also identified by the same method in order to characterize the predominant lithologies of alluvial sediments in the study field sites.

Volcanic rocks were identified by texture and phenocryst content whenever possible. Assignment of compositional names to these rocks was given according to Table B-1, the volcanic rock phenocryst guide, kindly furnished by Bob Scarborough of the Arizona Bureau of Geology and Mineral Technology.

The amount of varnish and calcium carbonate coating on each rock sample was also described, since these are indicative of the rock sample's previous history. The varnish is given in terms of a seven-value arbitrary scale: no v., light v., light-medium v., medium v., medium-dark v., dark v., and heavy v. The amount of calcium carbonate is given in millimeter thicknesses. Calcium carbonate is simply referred to as Ca in the following descriptions.

Rock identification by hand sample is not the preferred method for positive identification but is used here for practical reasons. Only detailed petrographic studies can yield positive rock identifications, especially in volcanic and other fine-grain rocks. The scope of such an undertaking for representative samples in this study area would be so large as to warrant another thesis. Similarly, the use of only the larger clasts to represent alluvial deposits and the limited number

Table B-1. The volcanic rocks phenocryst guide.

| | Quartz | Potassic Feldspar | Plagioclase | Feldspathoid |
|----------------|--------|----------------------|-------------|--------------|
| Rhyolite | X | X | | |
| Rhyodacite | X | | X | |
| Dacite | X | | X | |
| Quartz Latite | X | X | X | |
| Latite | | X | X | |
| Trachyte | | X | | |
| Trachyandesite | | | X | |
| Andesite | | | X | |
| Basalt | | | X | |
| Phonolite | | X | | X |

of clasts used inevitably introduces a bias to the identification.

This is also due to pragmatic concerns because only the larger rocks can be cut open and identified, and only so many samples can be taken from the field. Consequently, these rock identification must be viewed as tentative, not definitive.

Bedrock Samples

| <u>Name</u> | <u>Description</u> |
|----------------------|---|
| EH #1 | Rhyolitic welded tuff. Heavy v. Purple, vesicular in appearance, dense lithic welded ash-flow tuff. Quartz, potassic feldspar, and hornblende phenocrysts, moderately flattened pumice fragments, white felsite, maroon to brown aphanitic sometimes auto-brecciated, rhyolitic to trachytic lithic fragments. Irregular rough alignment of flattened vesicles and pumice fragments. No Ca coating. |
| Site 2 #1 | Rhyolitic welded tuff. No v. Weathered pinkish yellow, fresh mustard yellow, dense, lithic welded ash-flow tuff. Dominant phenocrysts are hornblende lathes, quartz irregular sub-hedral equigranular grains. Pumice fragments are flattened and hard due to silicification. Flow banded rhyolite and felsite lithic fragments. Remnant Ca coating maximum 4 mm probably from petracalcic. |
| Site 2 #2 | Flow banded rhyolite. Light v. Maroon, pink and white flow bands. Few quartz, K-spar, and hornblende phenocrysts. Milky white quartz exsolution mottles. Ca very thick up to 10 mm. |
| Bas (near site 7) #1 | Basaltic-andesite. Medium v. Black, vesicular, aphanitic, idinsite and olivine bearing with rare white plagioclase laths. Looks like basalt but probably andesitic in composition (S. Reynolds, B. Scarborough, D. Lynch, personal communication, 1980). Slight Ca coating less than 1 mm. |
| Bas (near site 7) #2 | Vitrophyre. No v. Dark blue-purple volcanic vitrophyre, subhedral quartz phenocryst, calcium fracture fillings. No Ca coating. |

| <u>Name</u> | <u>Description</u> |
|----------------|--|
| Near site 6 #1 | Epidotized volcanic rock, probably rhyolitic. Light v. Dark green, aphanitic, epidotized volcanic with thin fractures containing calcite. No Ca. |
| Ms #1 | Rhyolitic porphry. Medium-dark v. Grey, red and pink hypabyssal or rhyolitic porphry. Almost completely equigranular K-spar and quartz phenocryst in dark red groundmass. No Ca. |
| Ms #2 | Lithic felsite flow rock. Light v. Blue-green gray lithic felsic flow rock, large quartz and felsitic lithic fragments, probably rhyolitic. No Ca. |
| Ms #3 | Slate. No v. Red-brown slate. No Ca. |
| Ms #4 | Slate. No v. Red-brown slate. No Ca. |

Alluvium Samples

| | |
|---------------------|--|
| <u>Site 3</u> #1 | Flow banded rhyolite. No v. Milky white, orange and pink flow banded rhyolite. No Ca. |
| #2 | Latite-andesite. No v. Melanocratic purple-red volcanic rock, possibly from latite to andesite in composition. Plagioclase and amphibole phenocrysts with red auto-oxidation mottles. No Ca. |
| #3 | Rhyolitic tuff. No v. Light green and pink tuff with K-spar, quartz phenocrysts. No Ca. |
| #4 | Rhyolite. No v. Pink, maroon and white auto-brecciated rhyolite. No Ca. |
| #5 | Latite-trachyte. No v. Dark green-brown latitic to trachytic, possibly altered volcanic. Anhedral feldspar and amphibole phenocrysts. No Ca. |
| #6 | Latite-trachyte. Sample as #5. |
| #7 | Quartz sandstone. No v. Light grey coarse-grain quartz sandstond. No Ca. |

Summary: Mixed volcanics, mostly rhyolites and latites, some sedimentary rocks.

| <u>Name</u> | <u>Description</u> |
|---------------------|---|
| <u>Site 4</u> #1 | Rhyolite. Heavy v. Rose pink rhyolite with felsite lithic fragments. No Ca. |
| #2 | Rhyolite. Medium-light v. Pink-white rhyolite. No Ca. |
| #3 | Rhyolite. Medium v. Maroon, green rhyolite. No Ca. |
| #4 | Slate. Light v. Green gray slate. No Ca. |
| #5 | Felsite. Medium dark v. White felsite with few hornblende phenocrysts, probably rhyolitic. No Ca. |
| #6 | Quartzite. Medium dark v. Pink grey quartzite. No Ca. |

Summary: Rhyolitic volcanic and metasedimentary rocks.

| | |
|---------------------|---|
| <u>Site 5</u> #1 | Felsite. Light-medium v. Weathered pink, white pink when fresh, much quartz exsolution, probably rhyolitic. No Ca. |
| #2 | Felsite. Medium-dark v. Olive green felsite, no phenocrysts, probably rhyolitic. No Ca. |
| #3 | Felsite. Dark v. Green felsite. No Ca. |
| #4 | Felsite. Heavy v. Green with pink mottles. Biotite and hornblende phenocrysts. No Ca. |
| #5 | Dacite-andesite. Heavy v. Dark green to grey, very fine unidentified orange white phenocrysts in aphanitic groundmass--probably plagioclase. Also black anhedral indistinct lithic fragment or mafic inclusion. Rock is probably dacite to andesite slightly altered volcanic. No Ca. |
| #6 | Felsite. Dark v. Dark red, auto-oxidized felsitic flow rock. Some biotite grains, small areas of quartz exsolution. No Ca. |

Summary: Mostly rhyolitic felsites. Mixed volcanic rocks, some dacite-andesite.

| <u>Name</u> | <u>Description</u> |
|---------------------|--|
| <u>Site 6</u> #1 | Quartzite. Dark v. Pinkish grey "dirty quartzite" containing amphibole and lots of white plagioclase grains. No Ca. |
| #2 | Rhyolite. Medium-dark v. Maroon to pinkish white auto-brecciated flow banded rhyolite. No Ca. |
| #3 | Quartzite. Medium-dark v. Similar to #1. |
| #4 | Quartzite. Medium-light v. Brown to maroonish-white very dirty quartzite with large anhedral grains of quartz. Thick Ca coating, 5 mm. |
| #5 | Rhyolite. Medium v. Green-white to pink brecciated rhyolite flow stone. Felsite lithic fragments with amphibole phenocrysts and quartz exsolution mottles. Thick Ca coatings, 10 mm. |

Summary: Metamorphic rocks and rhyolites.

| | |
|---------------------|---|
| <u>Site 7</u> #1 | Rhyolite. Light v. Purple rhyolite to possibly quartz latite with quartz phenocrysts and numerous quartz exsolution mottles. Thick Ca coating up to 8 mm. |
| #2 | Rhyolite. Medium-light v. Purplish-pink flow banded rhyolite. Extremely thick Ca coating up to 15 mm. |
| #3 | Dacite. Heavy v. Reddish maroon, auto-brecciated dacite. No Ca. |
| #4 | Rhyolite. Medium v. Pink flow banded rhyolite. Extremely thick Ca coating up to 15 mm. |
| #5 | Felsite. Medium-light v. Maroonish white with quartz and amphibole phenocrysts. Very thick Ca coating up to 15 mm. |

Summary: Rhyolitic volcanic rocks.

| | |
|---------------------|--|
| <u>Site 8</u> #1 | Rhyolite. No v. Whitish-lavender lithic ash-flow tuff with biotite phenocrysts. Thin Ca coating up to .5 mm. |
| #2 | Dacite. No v. Whitish-lavender lithic ash-flow tuff with quartz, biotite and plagioclase phenocrysts. Thin Ca coating less than .5 mm. |

| <u>Name</u> | <u>Description</u> |
|-------------|---|
| #3 | Rhyolite. Light v. Brownish-red and white auto-oxidized flow banded rhyolite. Slight Ca coating. |
| #4 | Felsite. Medium-dark v. Lavender white, lithic felsite, probably rhyolitic. Slight Ca coating. |
| #5 | Rhyolite. Medium-light v. Dark lavender-red auto-oxidized rhyolite to dacite with lots of quartz phenocrysts. No Ca. |
| #6 | Rhyolite-dacite. Dark v. Dark maroon-red, auto-brecciated oxidized rhyolite to dacite flow stone with felsitic lithic fragments. No Ca. |

Summary: Rhyolitic volcanic rocks.

| <u>Site 9</u> | |
|---------------|--|
| #1 | Quartz latite. Medium-dark v. Dark red, with quartz, orthoclase, and plagioclase phenocrysts and quartz exsolution mottles. Slight Ca coating. |
| #2 | Rhyolite to rhyodacite. Heavy varnish. Pinkish-white felsitic with red auto-oxidation and small black unidentified mafic phenocrysts. No Ca. |
| #3 | Rhyolite to quartz latite. Medium v. Dark brown with aligned mottles of quartz exsolution and quartz phenocrysts. No Ca. |
| #4 | Rhyolite to quartz latite. Medium v. Dark brown with large areas of quartz exsolution and white felsite breccia fragments. No Ca. |
| #5 | Rhyolite to dacite. Light-medium v. Light brown with quartz phenocrysts and felsite breccia fragments. |

Summary: Rhyolite to quartz-latite volcanic rocks.

| <u>Site 1b</u> | |
|----------------|---|
| #1 | Rhyolite. No v. Greyish white and pink flow banded rhyolite. No Ca. |
| #2 | Rhyolite. Medium v. Same as #1. No Ca. |
| #3 | Rhyolite. Dark v. Same as #1. No Ca. |
| #4 | Rhyolite. Medium-dark v. Same as #1. No Ca. |

| <u>Name</u> | <u>Description</u> |
|-------------|--|
| #5 | Quartz latite. Light-medium v. Maroon and grey aphanitic groundmass with white plagioclase, quartz and orthoclase phenocrysts and large irregular areas of quartz exsolution. No Ca. |

Summary: Mostly flow-banded rhyolite with mixed acidic volcanic rocks.

Site B1

| | |
|----|--|
| #1 | Rhyolitic tuff. Light v. Pink tuff with quartz and amphibole phenocrysts. No Ca. |
| #2 | Rhyolitic volcanic conglomerate. Light v. Pink and white conglomerate, subrounded corase (1-3 mm) grains of feldspars and quartz. No Ca coating. |
| #3 | Rhyolitic tuff. Light v. Brown welded ash flow tuff. Thin Ca coating less than .5 mm. |
| #4 | Rhyolitic tuff. No v. Light brown welded ash-flow tuff with amphibole phenocrysts. Thin Ca coating less than .5 mm. |

Summary: Rhyolitic tuffs and volcanic conglomerates.

Site 61b

| | |
|----|--|
| #1 | Rhyolite to rhyodacite. Light v. Pink, grey auto-brecciated rhyolitic to rhyodacitic flowstone. No Ca. |
| #2 | Rhyolite. Light v. Pink, maroon and grey flow banded rhyolite. Thin Ca coating 1 mm. |
| #3 | Rhyolite to rhyodacite. Light v. Dark red auto-oxidized rhyolite to rhyodacite. Ca coating 1.5 mm. |
| #4 | Rhyolite. Medium light v. Grey pink flow banded rhyolite. No Ca. |
| #5 | Felsite. No v. Greyish white felsite, probably rhyolitic. No Ca. |

Summary: Rhyolites.

| <u>Name</u> | <u>Description</u> |
|-------------------------|--|
| <u>Site 65.35</u> #1 | Latite to trachyte. Medium v. Red brecciated, mostly aphanitic with amphibole phenocrysts and large white felsitic breccia fragments (1 cm). No Ca. |
| #2 | Felsite. Heavy v. Pink felsite with amphibole phenocrysts. No Ca. |
| #3 | Trachyandesite to andesite. Medium-dark v. Maroon brown with plentiful white plagioclase phenocrysts. No Ca. |
| #4 | Rhyolite. Dark v. Red to pink flow banded rhyolite. No Ca. |
| #5 | Rhyolitic welded tuff. Heavy v. Black welded ash-flow tuff with small (.1 mm) quartz grains and numerous smaller unidentified lithic fragments. No Ca. |
| #6 | Rhyodacite to dacite. Heavy v. Black flowstone with numerous quartz and dark plagioclase phenocrysts. No Ca. |
| #7 | Felsite. Heavy v. Brown felsite with orthoclase phenocrysts, probably rhyolite to rhyodacite. No Ca. |

Summary: Mixed acidic to intermediate volcanic rocks (from rhyolite to andesite).

| | |
|-------------------------|--|
| <u>Site 70.25</u> #1 | Quartz latite. Heavy v. Brown groundmass with large (1 mm) quartz, small (less than .1 mm) orthoclase and plagioclase phenocrysts, and quartz exsolution areas. No Ca. |
| #2 | Rhyolite to quartz latite. Dark v. Brown, brecciated flowstone with quartz phenocrysts. No Ca. |
| #3 | Latite to trachyandesite. Heavy v. Dark maroon aphanitic groundmass with plagioclase, orthoclase and amphibole phenocrysts. No Ca. |

Summary: Intermediate volcanic rocks, from quartz latite to trachyandesite.

| <u>Name</u> | <u>Description</u> |
|------------------------|--|
| <u>Site 70+p</u> #1 | Latite to trachyte. Heavy v. Dark maroon groundmass with large (1 mm) white orthoclase and plagioclase phenocrysts. No Ca. |
| #2 | Quartz latite. Dark v. Lavender grey groundmass with large (1 mm) quartz phenocrysts and smaller white orthoclase and plagioclase phenocrysts. No Ca. |
| #3 | Felsite. Dark v. Orange felsite with very large (2 mm) white quartz grains. No Ca. |
| #4 | Rhyolite. Medium-dark v. Lavender and grey flow banded rhyolite. No Ca. |
| #5 | Rhyolite. Heavy v. Dark red auto-oxidized flow banded rhyolite. No Ca. |
| #6 | Quartz monzonite. Medium v. Grey medium grain (1-2 mm) plutonic rock with quartz, white plagioclase, orthoclase biotite and hornblende crystals. No Ca. |
| #7 | Andesite. Heavy v. Reddish brown groundmass with large (1 mm) dark plagioclase phenocrysts. No Ca. |
| #8 | Quartz latite. Dark v. Reddish grey groundmass with quartz, plagioclase and orthoclase phenocrysts. No Ca. |
| #9 | Quartz latite. Dark v. Brown groundmass with small (.5 mm) quartz and plagioclase phenocrysts. No Ca. |
| #10 | Dacite. Medium v. Lavender grey groundmass with large white plagioclase (1 mm) and smaller hornblende and quartz phenocrysts. Thick weathering rind but no Ca. |

Summary: Mixed volcanic rocks from rhyolite to andesite.

| | |
|------------------------|---|
| <u>Site 70+d</u> #1 | Rhyolitic tuff. No v. Light pink grey lithic ash-flow tuff with quartz and orthoclase phenocrysts. No Ca. |
| #2 | Quartz sandstone. No v. Grey well-sorted medium-grain cemented sandstone. No Ca. |

| <u>Name</u> | <u>Description</u> |
|-------------|--|
| #3 | Quartz sandstone. No v. Grey poorly sorted coarse-grain quartz sandstone. No Ca. |
| #4 | Quartz sandstone. No v. Grey poorly sorted medium-grain sandstone. No Ca. |
| #5 | Sandstone. No v. Lavender poorly sorted medium-grain feldspar and quartz sandstone. No Ca. |
| #6 | Trachyte. Light v. Maroon and grey mottled groundmass with orthoclase and hornblende phenocrysts and quartz exsolution. No Ca. |

Summary: Primarily sandstones with mixed volcanic rocks.

| <u>Site 83.7</u> | |
|------------------|---|
| #1 | Quartz latite. Medium-light v. Orange and grey mottled groundmass with quartz, plagioclase and orthoclase phenocrysts. No Ca. |
| #2 | Rhyodacite to dacite. Heavy v. Red auto-oxidized felsite with one large white plagioclase phenocryst. No Ca. |
| #3 | Rhyodacite to dacite. No v. Pink, fine-grain volcanic rock with small quartz, plagioclase and hornblende phenocrysts. Thin patchy Ca. |
| #4 | Rhyodacite to dacite. Heavy v. Red auto-oxidized groundmass with small quartz, hornblende and plagioclase phenocrysts. No Ca. |

Summary: Rhyodacite to quartz latite volcanic rocks.

Particle Size Distribution Determination

Determination of particle size distribution was done with sieve analysis. Six sieves ranging from -6 to -1 phi size sieves in increments of 1 phi were used.

Percentages were calculated in two ways: percent is a straight weight percentage which includes the weight of particles smaller than -1 phi (pan). N percent was calculated for most gravelly alluvial

samples because it was assumed that samples smaller than -1 phi were from the vesicular horizon--not the pavement surface. N percent does not include the pan. Because of small particle sizes in Site 1b, a special procedure was used to calculate the mean for that site; otherwise calculation of the mean was according to the formula given in Equation (15), Chapter 2. Range is also defined in Chapter 2.

Particle Size

Site 3; Total = 1668.4 gm.

| Size phi (mm) | Wt. | % | N% |
|---|--------------|--------------|------|
| -6 (64) | - | | |
| -5 (32) | 566.6 | 33.96 | 38.6 |
| -4 (16) | 464.8 | 27.86 | 31.6 |
| -3 (8) | 210.7 | 12.63 | 14.3 |
| -2 (4) | 136.5 | 8.18 | 9.3 |
| -1 (2) | 75.5 | 4.53 | 5.1 |
| PAN | <u>214.3</u> | <u>12.85</u> | 1.0 |
| Totals | 1668.4 | 100.00 | |
| Mean = 19.04 mm Mode = 32 mm Range = 5φ | | | |

Site 4; Total = 2827.1 gm.

| Size phi (mm) | Wt. | % | N% |
|---|--------------|------------|-------|
| -6 (64) | | | |
| -5 (32) | 42.8 | 1.51 | 1.9 |
| -4 (16) | 1089.8 | 38.6 | 47.7 |
| -3 (8) | 969.4 | 34.3 | 42.4 |
| -2 (4) | 127.8 | 4.5 | 5.6 |
| -1 (2) | 56.3 | 2.0 | 2.5 |
| PAN | <u>541.0</u> | <u>0.0</u> | |
| Totals | 2827.1 | 100.0 | 100.0 |
| Mean = 11.9 mm Mode = 16mm Range = 3φ | | | |

Site 5; Total = 2170.4 gm.

| Size phi (mm) | Wt. | % | N% |
|------------------|--------------|------------|-------|
| -6 (64) | - | | |
| -5 (32) | 497.3 | 22.9 | 24.4 |
| -4 (16) | 916.6 | 42.2 | 44.9 |
| -3 (8) | 584.3 | 26.9 | 28.6 |
| -2 (4) | 27.4 | 1.3 | 1.4 |
| -1 (2) | 15.4 | .7 | .7 |
| PAN | <u>129.4</u> | <u>6.0</u> | |
| Totals | 2170.4 | 100.0 | 100.0 |

Mean = 18.4mm Mode = 16 mm Range = 3 ϕ

Site 6; Total = 2859.8 gm.

| Size phi (mm) | Wt. | % | N% |
|------------------|-------------|------------|-------|
| -6 (64) | 679.5 | 23.8 | 24.0 |
| -5 (32) | 667.1 | 23.3 | 23.5 |
| -4 (16) | 1094.3 | 38.3 | 38.7 |
| -3 (8) | 370.0 | 12.9 | 13.0 |
| -2 (4) | 16.1 | .6 | .6 |
| -1 (2) | 5.6 | .2 | .2 |
| PAN | <u>27.2</u> | <u>1.0</u> | |
| Totals | 2859.8 | 100.1 | 100.0 |

Mean = 29.9 mm Mode = 16 mm Range = 4 ϕ

Site 7; Total = 1584.2 gm.

| Size ph (mm) | Wt. | % | N% |
|-----------------|----------|----------|----|
| -6 (64) | - | | |
| -5 (32) | 285.1 | 18.0 | |
| -4 (16) | 698.6 | 44.1 | |
| -3 (8) | 538.9 | 34.0 | |
| -2 (4) | 61.6 | 3.9 | |
| -1 (2) | - | | |
| PAN | <u>-</u> | <u>-</u> | |
| Totals | 1584.2 | 100.0 | |

Mean = 15.7 mm Mode = 16 mm Range = 3 ϕ

Site 8; Total = 1134.4 gm.

| Size phi (mm) | Wt. | % | N% |
|------------------|--------|-------|------|
| -6 (64) | - | - | |
| -5 (32) | 57.8 | 5.1 | 5.1 |
| -4 (16) | 513.9 | 45.3 | 45.5 |
| -3 (8) | 531.0 | 46.8 | 47.0 |
| -2 (4) | 24.4 | 2.2 | 2.2 |
| -1 (2) | .9 | .1 | .1 |
| PAN | 6.4 | .6 | |
| Totals | 1134.4 | 100.1 | 99.9 |

Mean = 12.72 mm Mode = 8 mm Range = 3 ϕ

Site 9; Total = 1473.4 gm.

| Size phi (mm) | Wt. | % | N% |
|------------------|--------|-------|-------|
| -6 (64) | - | | |
| -5 (32) | 352.9 | 24.0 | 25.1 |
| -4 (16) | 527.4 | 35.8 | 37.4 |
| -3 (8) | 474.3 | 32.2 | 33.7 |
| -2 (4) | 47.8 | 3.2 | 3.3 |
| -1 (2) | 7.5 | .5 | .5 |
| PAN | 63.5 | 4.3 | |
| Totals | 1473.4 | 100.0 | 100.0 |

Mean = 16.9 mm Mode = 16 mm Range = 3 ϕ

Site 1B; Total = 2950.2 gm.

| Size phi (mm) | Wt. | % | N% |
|------------------|--------|-------|-------|
| -6 (64) | - | | |
| -5 (32) | 178.9 | 6.1 | 6.2 |
| -4 (16) | 1294.5 | 43.9 | 44.8 |
| -3 (8) | 1318.3 | 44.7 | 45.6 |
| -2 (4) | 93.4 | 3.2 | 3.3 |
| -1 (2) | 6.4 | .2 | .2 |
| PAN | 58.7 | 2.0 | |
| Totals | 2950.2 | 100.1 | 100.0 |

Mean = 12.9 mm Mode = 8 mm Range = 3 ϕ

Site B1; Total = 1759.9 gm.

| Size phi (mm) | Wt. | % | N% |
|------------------|---------------|-------------|----|
| -6 (64) | - | | |
| -5 (32) | - | | |
| -4 (16) | 65.0 | 3.7 | |
| -3 (8) | 253.5 | 14.4 | |
| -2 (4) | 132.3 | 7.5 | |
| -1 (2) | 88.0 | 5.0 | |
| PAN | <u>1221.1</u> | <u>69.4</u> | |
| Totals | 1759.9 | 100.0 | |

Est. Mean (assume PAN = .5) = 2.4 mm
 Mode = less than 2 mm
 Range = 4 ϕ

Site 61B; Total = 425.3 gm.

| Size phi (mm) | Wt. | % | N% |
|------------------|--------------|-------------|----|
| -6 (64) | - | | |
| -5 (32) | - | | |
| -4 (16) | 53.6 | 12.6 | |
| -3 (8) | 155.4 | 36.5 | |
| -2 (4) | 66.4 | 15.6 | |
| -1 (2) | 31.3 | 7.4 | |
| PAN | <u>118.6</u> | <u>27.9</u> | |
| Totals | 425.3 | 100.0 | |

Mean = 5.9 mm (assume PAN = 1); Mode = 8 mm; Range = 5 ϕ

Site 65.35; Total = 1275 gm.

| Size phi (mm) | Wt. | % | N% |
|------------------|-------------|------------|------|
| -6 (64) | - | | |
| -5 (32) | - | | |
| -4 (16) | 730.1 | 57.3 | 58.2 |
| -3 (8) | 484.7 | 38.0 | 38.6 |
| -2 (4) | 34.8 | 2.7 | 2.7 |
| -1 (2) | 5.1 | .4 | .4 |
| PAN | <u>20.3</u> | <u>1.6</u> | |
| Totals | 1275.0 | 100.0 | 99.9 |

Mean = 12.6 mm Mode = 16 mm; Range = 2 ϕ

Site 70.25; Total = 1977.6 gm.

| Size phi (mm) | Wt. | % | N% |
|------------------|-------------|------------|-------|
| -6 (64) | - | | |
| -5 (32) | 571.7 | 28.9 | 29.8 |
| -4 (16) | 715.3 | 36.2 | 37.4 |
| -3 (8) | 470.1 | 23.8 | 24.6 |
| -2 (4) | 145.2 | 7.3 | 7.5 |
| -1 (2) | 13.4 | .7 | .7 |
| PAN | <u>61.9</u> | <u>3.1</u> | |
| Total | 1977.6 | 100.0 | 100.0 |

Mean = 17.8 mm Mode = 16 mm Range = 4 ϕ

Site 70+P; Total = 1976.8 gm.

| Size phi (mm) | Wt. | % | N% |
|------------------|-------------|------------|-------|
| -6 (64) | - | | |
| -5 (32) | 260.2 | 13.2 | 13.5 |
| -4 (16) | 877.9 | 44.4 | 45.5 |
| -3 (8) | 731.3 | 37.0 | 37.9 |
| -2 (4) | 54.0 | 2.7 | 2.8 |
| -1 (2) | 6.5 | .3 | .3 |
| PAN | <u>46.9</u> | <u>2.4</u> | |
| Totals | 1976.8 | 100.0 | 100.0 |

Mean = 14.75 mm Mode = 16 mm Range = 3 ϕ

Site 70+D; Total = 1860.5 gm.

| Size phi (mm) | Wt. | % | N% |
|------------------|--------------|-------------|------|
| -6 (64) | | | |
| -5 (32) | 387.1 | 20.8 | 26.0 |
| -4 (16) | 317.3 | 17.1 | 21.4 |
| -3 (8) | 475.3 | 25.5 | 31.9 |
| -2 (4) | 208.8 | 11.2 | 14.0 |
| -1 (2) | 97.7 | 5.3 | 6.6 |
| PAN | <u>374.3</u> | <u>20.1</u> | |
| Totals | 1860.5 | 100.0 | 99.9 |

Mean = 12.2 mm Mode = 8 mm Range = 6 ϕ
Mean without PAN = 15.0 mm

Site 83.7; Total = 2303.5 gm.

| Size phi (mm) | Wt. | % | N% |
|---|-------------|------------|-------|
| -6 (64) | - | | |
| -5 (32) | - | | |
| -4 (16) | 963.1 | 41.8 | 42.3 |
| -3 (8) | 1160.8 | 50.4 | 51.0 |
| -2 (4) | 143.8 | 6.3 | 6.4 |
| -1 (2) | 8.4 | .4 | .4 |
| PAN | <u>27.4</u> | <u>1.2</u> | |
| Totals | 2303.5 | 100.1 | 100.1 |
| Mean = 11.1 mm Mode = 8 mm Range = 3ϕ | | | |

APPENDIX C

RADIOMETRIC INSTRUMENTATION AND DATA

Integrating Sphere Reflectometer (from Jacobsen and Lamoreaux, 1979)

The ISR provides critical reflectance data on non-specular selective surfaces. Scattering from rough surfaces can cause spectrophotometers measuring reflectance at near-normal incidence to err by neglecting the diffuse component of the reflectance. A hemispherical measurement not only takes scattering into account, but allows the non-specular component to be estimated by comparison with the specular component. Our ISR operates in the indirect, or hemispherical-directional mode. As shown in Figure 1, a tungsten-halogen source is mounted at a side port of the integrating sphere; the sample is placed in the center of the sphere and is illuminated hemispherically. The sample is baffled to prevent its direct illumination by the source. The sphere is coated with Eastman White Reflectance Coating, a material which maintains a diffuse reflectance of above 70% up to around 3 μm . In order to observe the directional reflection at various angles, the sampleholder is supported by a shaft which can be rotated by a knob outside of a second sphere port. The radiation reflected from the sample at the chosen angle emerges from the sphere through a third sphere port and encounters a relay mirror and a collimating mirror before entering the dual beam monochromator as the sample beam. A reference arc on the sphere wall is reflected onto a second collimating mirror by a cylindrical mirror mounted in the exit port; the collimating mirror then directs the reference beam into the other arm of the monochromator.

The monochromator, part of a heavily modified Perkin-Elmer 21 Spectrophotometer, is shown in Figure 2. The beam-combining optics employ a three-phase chopper: One 120° sector is cut-away and passes the reference beam, a second 120° sector is reflective and directs the sample beam into the same path, and a third 120° sector is coated with Nextel black paint and serves as an indicator of the background level. Figure 3 schematically presents this chopping arrangement. After the beams are combined, a Littrow-mounted prism disperses the radiation. The entrance and exit slits are mechanically linked and are servo-controlled by the electronics to keep the reference beam constant. The radiation is then focussed on the detector, a two-color device consisting of a UV-enhanced silicon photovoltaic detector and a lead sulfide detector. The former absorbs and detects radiation from 0.4 to about 1.0 μm and transmits longer wavelengths, which are detected by the underlying lead sulfide. The detector, made by Infrared Industries, covers 96% of the Air Mass 2, $\alpha=1.3$, $\beta=0.04$ insolation computed by Thomas and Richmond[1].

Figure 4 reproduces the optical components and shows in flow chart form the overall sample-and-hold scheme for measuring signal levels. The actual electronics in the dashed rectangle are shown in Figure 5. The monochromator is stepped to a specific wavelength, and synchronizing pulses from LED-phototransistor pairs at the chopper trigger a gate which sequentially selects one of three lines for each of the three phases. The signal is integrated by an RC network utilizing the sample-

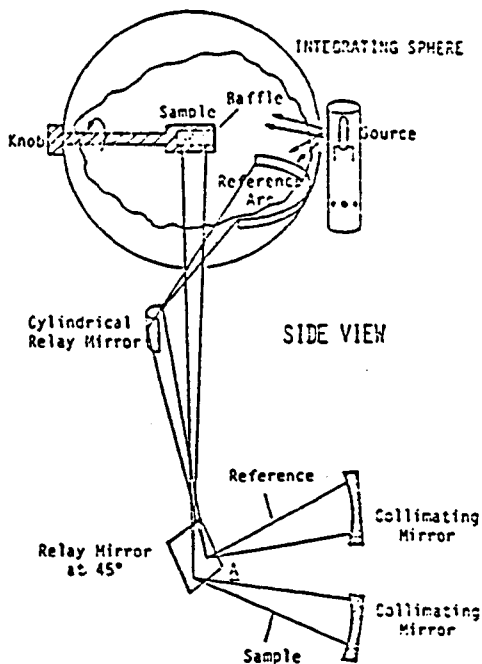


FIGURE 1. INTEGRATING SPHERE AND RELAY OPTICS OF ISR.

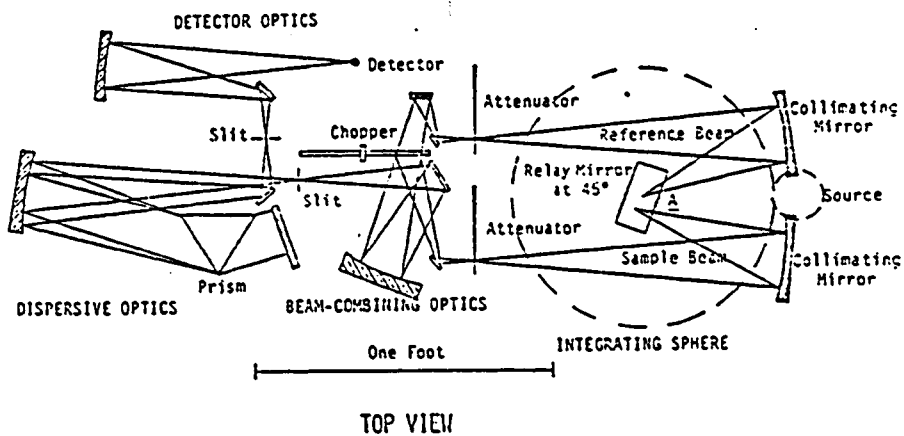


FIGURE 2. MONOCHROMATOR OPTICS OF ISR. DASHED CIRCLE IS PROJECTION OF INTEGRATING SPHERE.

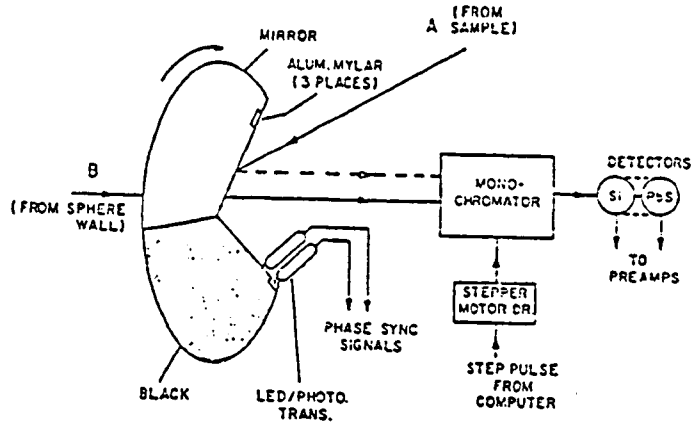


FIGURE 3. THREE-PHASE CHOPPER AND PHASE-SYNCHRONIZATION SYSTEM IN THE ISR.

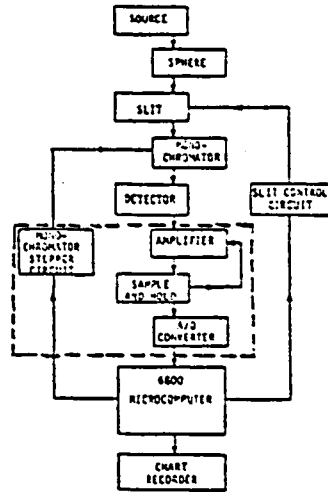


FIGURE 4. GENERAL FLOW CHART OF ISR COMPONENTS.

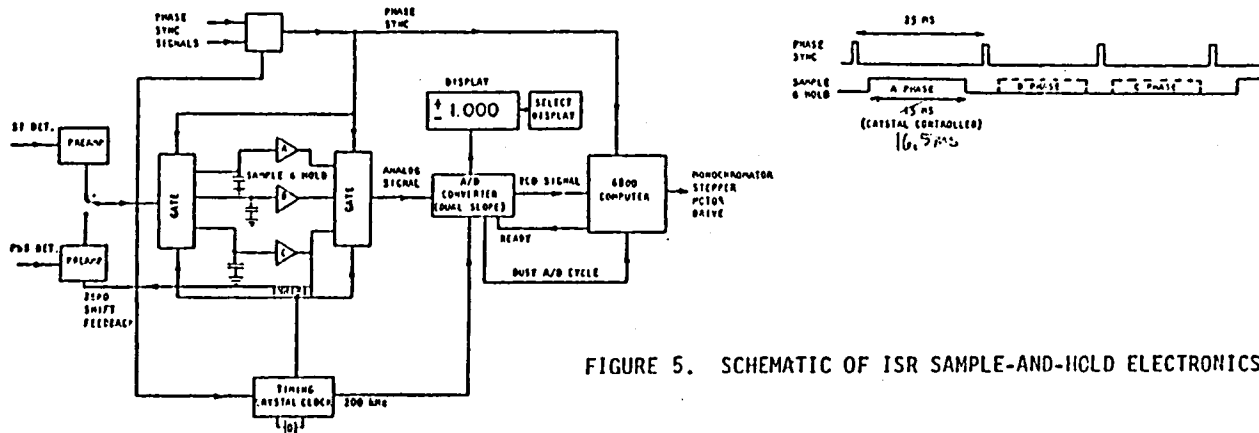


FIGURE 5. SCHEMATIC OF ISR SAMPLE-AND-HOLD ELECTRONICS.

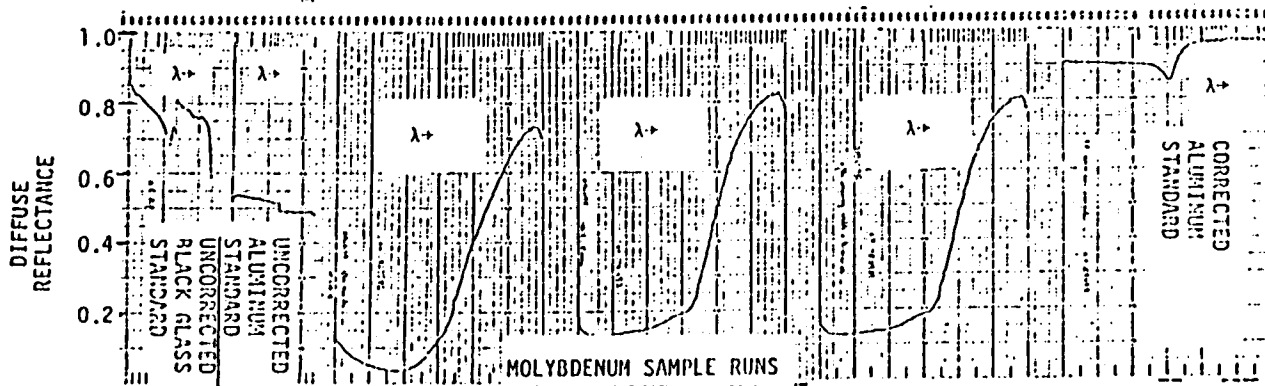


FIGURE 6. EXAMPLE OF STRIP CHART RECORD FOR INTEGRATING SPHERE REFLECTOMETER. THE CALIBRATION AND SAMPLE RUNS ARE INDICATED ON THE FIGURE. WAVELENGTH RANGE FOR EACH RUN IS 0.4 TO 2.7 μm .

and-hold capacitor, and the resulting analog level is transferred by a second gate to a dual-slope A/D converter. The BCD output moves to a Southwest Technical Products 5800 microcomputer and to a front panel LED display. After data at this wavelength are analysed, the monochromator is stepped to the next wavelength, and the process is repeated until the entire spectrum is scanned.

Data analysis proceeds in the following fashion. Before the sample series is run, black glass and evaporated aluminum standards are measured and the results are stored in the computer's memory. It should be noted that all measurements are made with respect to the reference arc on the sphere wall, the reflectance of which is carried by the reference beam of the ISR. Background is removed by first removing the stray radiation due to the monochromator, indicated by the blackened chopper sector, from the aluminum's reflectance factor. Then, by comparing the known and measured reflectances of the black glass standard, the remaining background is calculated and subtracted. At this point, a background-corrected aluminum reflectance factor has been compiled. The sample is then run, and both the background indicated by the blackened chopper sector and the residual background revealed by the black glass standard are subtracted, leaving a background-corrected sample reflectance factor.

This procedure provides corrected reflectance factors for both the sample and for the aluminum standard; the former is divided by the latter, causing the sphere wall's reflectance to cancel. The last step is the multiplication of this ratio by the absolute reflectance of aluminum, which is presently presumed to be equal to the published data on the absolute reflectance of laboratory aged aluminum films. This dependence on external data sources will end shortly when a double reflection Bennett absolute reflectometer, described below, is made operational in the summer of 1979. The spectral reflectances are sampled at 240 points; reflectances at wavelengths corresponding to the selected ordinates of Thomas and Richmond [1] are summed and divided by the total number of ordinates to yield the solar absorptance "a". Figure 6 shows a strip chart output for a series of molybdenum films made in our chemical vapor deposition laboratory. It is followed by a trace of the aluminum standard, which tests the system's accuracy. If the true absolute reflectance of aluminum is reproduced, we can be reasonably sure that the optical and computer components are acting properly.

RMR-10 (from Palmer, 1979)

SECTION 1.
GENERAL DESCRIPTION

1.1 Description

The Radiometrics Model RMR-10 Multispectral Radiometer is a general purpose radiometric instrument for measurements of radiance, irradiance and reflectance in several fields of view over the visible and near-infrared spectrum. It is a portable, self-contained instrument powered by rechargeable batteries and features a digital readout. Three fixed ranges for radiance and irradiance measurements and one variable range for reflectance measurements are included. Figure 1-1 shows the operating controls of the Model RMR-10. The spectral channels are nominally the same as those found on the ERTS and LANDSAT satellite mapper systems. The readout is directly in W/m^2 sr for radiance and in $W/m^2 \times 10$ for irradiance measurements. These values apply over the stated wavelength band.

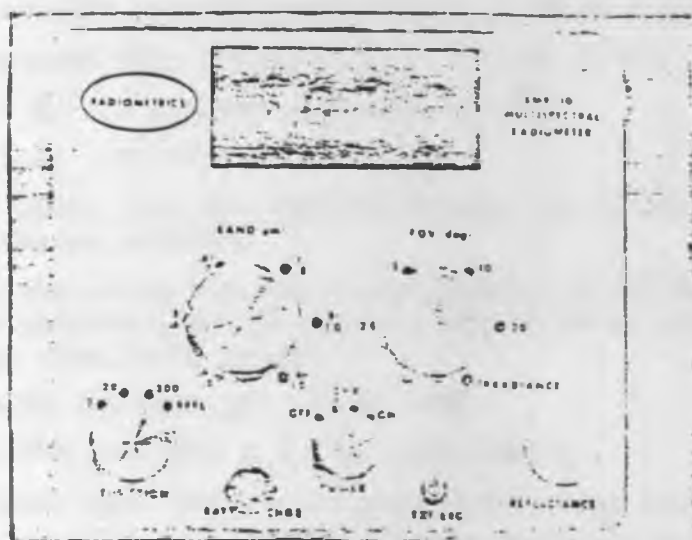


Fig. 1-1 Front Panel, RMR-10 Multispectral Radiometer

1.2 Applications

The Model RMR-10 has many applications; it is useful when multispectral ground-truth measurements are needed to calibrate ERTS and LANDSAT data; it can be used to measure reflectances of environmental surfaces; it will measure irradiance with nominal cosine weighting, etc.

RADIOMETRICS MODEL RMR-10 MULTISPECTRAL RADIOMETER

SPECIFICATIONS

SPECTRAL CHANNELS (standard):

| <u>Channel</u> | <u>Wavelength Range (μm)</u> |
|----------------|--|
| 1 | .4-.5 |
| 2 | .5-.6 |
| 3 | .6-.7 |
| 4 | .7-.8 |
| 5 | .8-1.0 |
| 6 | .4-1.0 |

RADIANCE RANGES: 0-2, 0-20, 0-200 $\text{W}/\text{m}^2 \text{ sr}$

FIELDS OF VIEW (full-angle): 1, 2, 5, 10, 20 deg; 2 π sr

DETECTOR: Blue-enhanced silicon photovoltaic, 400-1000 nm response

REFLECTANCE: Variable scaling, reflectance standard supplied.

IRRADIANCE (measured with cosine adapter): 0-20, 0-200, 0-2000 W/m^2

ACCURACY: $\pm 6\%$ F.S. all ranges; traceable to NBS

STABILITY: $\pm 2\%$ per year FS

CONNECTORS: $\frac{1}{4}$ " phone jack for battery charger; $\frac{3}{16}$ " phone jack for external recorder

POWER: 8 hours operating time on 2 rechargeable Ni-Cd batteries; charger included, may be used in lab to power instrument, recharge time 14-16 hours.

TEMPERATURE RANGE (operating): -20 to 40°C.

DIMENSIONS: 5.75"H x 6.25"W x 7.0"D, less handle

WEIGHT: less than 4lbs. net; 20lbs gross (including case)

MOUNTING: $\frac{1}{4}$ "x20 tripod mount, removeable pistol grip

READOUT: Digital, 0-1.999 with analog output jack

ACCESSORIES SUPPLIED: Cosine adapter, reflectance standard, battery charger, carrying case, lens cap

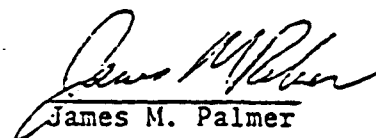
CALIBRATION DATA FOR
 RADIOMETRICS RMR-10 MULTISPECTRAL RADIOMETER
 Ser. No. 1001

ANGULAR CALIBRATION

| <u>INDICATED FOV (deg)</u> | <u>MEASURED FOV 50% HW</u> |
|--------------------------------|--------------------------------|
| 1 | 1.2 |
| 2 | 2.05 |
| 5 | 5.3 |
| 10 | 10.9 |
| 20 | 16.7 |

SPECTRAL BANDWIDTH (um)

| <u>INDICATED</u> | <u>MEASURED</u> |
|------------------|-----------------|
| .4-.5 | .418-.489 |
| .5-.6 | .507-.580 |
| .6-.7 | .597-.690 |
| .7-.8 | .686-.790 |
| .8-1.0 | .752-1.027 |
| .4-1.0 | .399-.980 |


 James M. Palmer

Spectral Radiometer Data

| <u>READING</u> | <u>.4-.5</u> | <u>.5-.6</u> | <u>.6-.7</u> | <u>.7-.8</u> | <u>.8-1.0</u> |
|---|---|---|---|------------------------------------|---|
| R1 Site 70.25 basaltic-andesite boulder slope with Encelia Feb.3,1980 11:15 Z52 2FOV | | | | | |
| | 9,15,8,18, 11,18,8 | 18,15,17, 15,21 | 18,20,17, 18,10,18 | 17,9,16,7, 8,9 | 27,20,13 12,10,11 9,8,7 |
| n | 7 | 5 | 6 | 6 | 9 |
| m | 12.4 | 17.2 | 16.8 | 11. | 13. |
| std | 4.5 | 2.5 | 3.5 | 4.3 | 6.5 |
| R2 Enigma hill yellow welded tuff, single specimen Feb.3,1980 15:20 Z62 2FOV | | | | | |
| | 20,21,19, 16,19 | 31,32,32, 28,34,28, 36 | 36,30,36, 31,32,34 | 42,41,41, 35,42,41, 38 | 43,41,38, 39,38,41, 43,38,45, 44 |
| n | 5 | 7 | 6 | 7 | 10 |
| m | 19. | 31.6 | 33.2 | 40. | 41. |
| std | 1.9 | 2.9 | 2.6 | 2.6 | 2.7 |
| R3 Enigma hill varnished purple welded tuff, single specimen Feb.3,1980 15:20 Z62 2FOV | | | | | |
| | 7,8,8,8, 9 | 8,11,11,9, 10,9,10,10 | 11,12,10, 10,9,12, 13,11,12 | 13,14,13, 12,13,12 14,14,11 | 17,16,16, 14,20,16 16,17,16, 18 |
| n | 5 | 8 | 9 | 9 | 10 |
| m | 8. | 9.8 | 11.1 | 12.9 | 16.6 |
| std | .7 | 1. | 1.3 | 1.1 | 1.6 |
| R4 Site 2 erosional surface on yellow tuff with calcium clasts Feb.3,1980 15:45 Z61 2FOV | | | | | |
| | 20,16,14 13,17,16 13,14,16, 22 | 22,18,20, 18,25,24, 23,24,20, 21 | 37,34,29, 25,25,29, 18,24,24, 26,30,29 | 41,37,40, 31,24,44, 32,24,26 | 42,35,33, 38,44,42, 34,35,33 |
| n | 10. | 10. | 12. | 9. | 9. |
| m | 15.8 | 21.5 | 27.5 | 33.2 | 37.3 |
| std | 3.1 | 2.5 | 5. | 7.6 | 4.3 |

| <u>READING</u> | <u>.4-.5</u> | <u>.5-.6</u> | <u>.6-.7</u> | <u>.7-.8</u> | <u>.8-1.0</u> |
|---|---|--|---|--|--|
| R5 hill at site 70+p varnished basaltic-andesite April 1 1980 11:00 cloudy 20FOV | | | | | |
| | 8 | 10 | 11 | 10 | 13 |
| R6 Site 6 Q2a pavement Feb.2 1980 15:45 Z66 2FOV | | | | | |
| | 10,11,10, 11,13,18, 12,12,19, 15,10,8, 13 | 27,21,28, 23,19,26, 22,17,16, 26,16,21 | 28,20,21, 25,37,35, 24,22 | 30,28,25, 38,21,26, 32,24,37, 33 | 31,28,32, 24,32,35, 32,34,34, 37,35 |
| n | 13 | 12 | 8 | 10 | 11 |
| m | 12.5 | 21.8 | 26.5 | 29.4 | 32.2 |
| std | 3.2 | 4.3 | 6.4 | 5.6 | 3.6 |
| R7 Site 5 Q2b pavement Dec.9 1979 10:15 Z60 2FOV | | | | | |
| | 12,19,19, 11,10,11, 11,12,10, 11,10,17 | 18,14,15, 12,14,13, 25,16,16 | 18,15,18, 19,14,20, 20,17,22, 19 | 18,16,28, 19,19,20 17,16,18 | 20,22,24, 24,28,21, 23,24 |
| n | 12 | 9 | 10 | 9 | 8 |
| m | 12.8 | 15.9 | 17.2 | 19. | 23.3 |
| std | 3.5 | 3.9 | 4.8 | 3.6 | 2.4 |
| R8 Site 5 Q2b pavement Feb. 2 1980 15:05 Z61 2FOV | | | | | |
| | 10,11,12, 11,9,8,9, 8,9,8,12, 13 | 14,16,14, 14,19,10, 12,6,7,9, 8,11,15, 14,20 | 25,15,9, 18,16,23, 17,12,15, 14,20,18, 16 | 19,20,20, 25,27,18, 19,18,16, 27,20,24, 20,20,24 | 25,20,32, 22,24,27, 20,20,20, 18,25,23, 21 |
| n | 12 | 15 | 13 | 15 | 13 |
| m | 10. | 12.6 | 16.8 | 21.1 | 22.9 |
| std | 1.8 | 4.1 | 4.3 | 3.4 | 3.8 |
| R9 Site 5 Q2b pavement Feb.23 1980 10:14 Z59 2FOV moist ground | | | | | |
| | 29,18,15, 16,15,16, 18,16,16, 11,14,17 | 22,23,25, 23,24,25, 28,28,23, 23,25 | 21,22,21, 27,21,20, 20,19,20, 21 | 30,31,29, 25,28,20, 26,24,27, 29,28,25 | 28,33,28, 25,28,31, 30,29,26, 30,30,25 |
| n | 12 | 11 | 10 | 12 | 12 |
| m | 16.8 | 24.5 | 21.2 | 26.8 | 28.6 |
| std | 4.3 | 2.0 | 2.2 | 3.0 | 2.4 |

READING .4-.5 .5-.6 .6-.7 .7-.8 .8-1.0 223

R10 Site 5 Q2b pavement March 30 1980 10:07 Z44 20FOV

| | | | | |
|-----------|-----------|-----------|-----------|-----------|
| 10,9,10, | 13,12,15 | 22,22,21, | 23,26,24, | 27,29,27, |
| 10,11,11, | 14,13,11, | 22,22,20, | 23,22,28, | 27,28,26, |
| 10,9 | 13,12 | 24,23,22 | 21,24,23, | 28,28,27 |
| | | | 25 | |

| | | | | | |
|-----|-----|------|-----|------|------|
| n | 8 | 8 | 9 | 10 | 9 |
| m | 10. | 12.9 | 22. | 23.9 | 27.4 |
| std | .8 | 1.3 | 1.1 | 2.0 | .9 |

R11 Site 5 Q2b pavement Mar.30,1980 10:07 Z44 2FOV

| | | | | |
|-----------|-----------|-----------|-----------|-----------|
| 10,11,14, | 12,13,15, | 15,21,16, | 24,13,21, | 27,25,23, |
| 12,10,11, | 13,12,16, | 14,20,20, | 24,20,16, | 20,25,28, |
| 9,8,12, | 12,16,13, | 19,11 | 23,24,29, | 25,21,26 |
| 10,10,13 | 14 | | 25 | |

| | | | | | |
|-----|------|------|-----|------|------|
| n | 12 | 10 | 8 | 10 | 9 |
| m | 10.8 | 13.6 | 17. | 21.9 | 24.4 |
| std | 1.7 | 1.6 | 3.6 | 4.6 | 2.7 |

R12 Site 4 Q2c pavement Dec.8 1979 15:50 Z65 2FOV

| | | | | |
|----------|-----------|----------|----------|----------|
| 12,14,18 | 17,20,22, | 15,19,24 | 21,25,19 | 28,25,31 |
| 9 | 18 | | | |

| | | | | | |
|-----|------|------|------|------|-----|
| n | 4 | 4 | 3 | 3 | 3 |
| m | 13.3 | 19.3 | 19.3 | 21.7 | 28. |
| std | 3.8 | 2.2 | 4.5 | 3.1 | 3. |

R13 Site 4 Q2c pavement with sand,silt and Plantago Dec.8 1979 15:50 Z65 2FOV

| | | | | |
|-----------|-----------|-----------|-----------|-----------|
| 14,18,13, | 29,31,30, | 27,36,18, | 43,46,28, | 41,35,38, |
| 17,18,17, | 20,24,21 | 12,8,28, | 38,43,26, | 43 |
| 16,17 | | 28,35 | 37,43,37 | |

| | | | | | |
|-----|------|------|------|------|------|
| n | 8 | 6 | 8 | 9 | 4 |
| m | 16.3 | 25.8 | 24. | 37.9 | 39.3 |
| std | 1.8 | 4.8 | 10.3 | 6.9 | 3.5 |

R14 Site 4 Q2c pavement March 30 1980 14:40 Z43 20FOV

| | | | | |
|----------|-----------|-----------|-----------|-----------|
| 9,9,8,9, | 12,12,11, | 19,20,19, | 22,25,23, | 26,31,29, |
| 8,9,9,9, | 12,14,12, | 20,19,24, | 21,25,23, | 31,31,34, |
| 9,9 | 12,13,12, | 22,20,19 | 22,24,26, | 31,32,33, |
| | 12 | | 22,21,20 | 32 |

| | | | | | |
|-----|-----|------|------|------|------|
| n | 10 | 10 | 9 | 12 | 10 |
| m | 8.8 | 12.2 | 20.2 | 22.8 | 31.0 |
| std | .4 | .8 | 1.7 | 1.9 | 2.2 |

| <u>READING</u> | <u>.4-.5</u> | <u>.5-.6</u> | <u>.6-.7</u> | <u>.7-.8</u> | <u>.8-1.0</u> |
|--|-----------------------------------|------------------------------------|---|---|---|
| R15 Site 9 Q2c pavement Dec.9 1979 15:40 Z70 2FOV | | | | | |
| | 8,8,7,9 | 14,12,10 11,13,14, 12,11 | 14,15,11, 10 | 14,16,12, 15,13 | 15,14,13, 12,15,12, 15 |
| n | 4 | 8 | 4 | 5 | 7 |
| m | 8 | 12.1 | 12.5 | 14. | 13.7 |
| std | .8 | 1.5 | 2.4 | 1.6 | 1.4 |
| R16 Site 65.35 Q2c pavement dark Feb.3 1980 10:15 Z62 2FOV | | | | | |
| | 9,9,8,8, 10,8 | 15,14,13, 12,13,13, 13 | 15,19,16, 18,18;18 | 17,19,20, 19,18,24, 21 | 18,17,19, 22,21,21, 20 |
| n | 6 | 7 | 6 | 7 | 7 |
| m | 8.7 | 13.3 | 17.3 | 19.7 | 19.7 |
| std | .8 | 1.0 | 1.5 | 2.3 | 1.8 |
| R17 Site 65.35 Q2c pavement with mudcracks Feb.3 1980 10:15 Z62 2FOV | | | | | |
| | 13,15,17, 8,20,12, 18,14,13 | 27,16,14, 24,13,24, 20 | 27,24,28, 37,35,22, | 32,28,33, 36,27,30, 29 | 34,32,24, 33,31,46, 46,17 |
| n | 9 | 7 | 6 | 7 | 8 |
| m | 14.4 | 19.7 | 28.8 | 30.7 | 32.9 |
| std | 3.6 | 5.5 | 6.0 | 3.2 | 9.9 |
| R18 Site 70.25 Q2c pavement dark Feb.3 1980 11:15 Z52 2FOV | | | | | |
| | 7,9,9,9, 10,9 | 12,11,15, 11,12,16, 13,13 | 14,14,15, 15,19,15, 14,14,14, 10 | 20,16,12, 19,14,18, 13,14,14, 16 | 18,18,17, 21,20,15, 23,17,18, 18 |
| n | 6 | 8 | 10 | 10 | 10 |
| m | 8.8 | 12.9 | 14.4 | 15.6 | 18.5 |
| std | 1. | 1.8 | 2.2 | 2.7 | 2.3 |
| R19 Site 70+p Q2c pavement April 1 1980 10:20 cloudy 20FOV | | | | | |
| | 8,8,9,8, 8,7,8,8, 8 | 10,11,11, 10,12,12, 11,11,10 | 14,15,14, 17,17,15, 16,14,15 | 16,16,17, 17,18,19, 17,16,15 | 19,20,22, 21,18,18, 17,20,18 |
| n | 9 | 9 | 9 | 9 | 9 |
| m | 8. | 10.9 | 15.2 | 16.8 | 19.2 |
| std | .5 | .8 | 1.2 | 1.2 | 1.6 |

| <u>READING</u> | <u>.4-.5</u> | <u>.5-.6</u> | <u>.6-.7</u> | <u>.7-.8</u> | <u>.8-1.0</u> |
|--|--|--|---|---|---|
| R20 Site 65.35 Q2c pavement April 1 1980 9:30 cloudy 20FOV | | | | | |
| | 9,8,8,8, 9,9,9,8, 8 | 12,11,12, 12,12,13, 12,12,11 | 17,15,18, 19,18,16, 18,17,16 | 18,18,22, 21,23,21, 20,21,20 | 19,21,24, 23,24,24, 21,22,22 |
| n | 9 | 9 | 9 | 9 | 9 |
| m | 8.4 | 11.9 | 17.1 | 20.4 | 22.2 |
| std | .5 | .6 | 1.3 | 1.7 | 1.7 |
| R21 Shrimp site near site 65.35 Q2c pavement April 1 1980 11:30 cloudy 20FOV | | | | | |
| | 10,10,11, 11,11,10, 10,10,11 | 14,14,13, 14,15,16, 16,14,15, 16 | 23,22,20, 23,26,23, 24,25,23, | 20,23,27, 30,29,30, 22,25,24 | 24,26,27, 29,26,28, 32,29,27 |
| n | 9 | 10 | 9 | 9 | 9 |
| m | 10.4 | 14.7 | 23.2 | 25.6 | 27.6 |
| std | .5 | 1.1 | 1.7 | 3.6 | 2.3 |
| R22 Site 83.7 Q2c pavement Feb. 3 1980 12:45 Z46 2FOV | | | | | |
| | 9,9,9,10 9,9 | 14,17,15, 15,15,12, 17,13,15, 16,14 | 12,20,17, 14,18,18, 18,16,18, 19 | 23,16,23, 22,20,21, 25,22,27, 20 | 30,24,18, 25,21,27, 18,23,25, 21,21,19, 23,17 |
| n | 6 | 11 | 10 | 10 | 14 |
| m | 9.2 | 14.8 | 17. | 21.9 | 22.3 |
| std | .4 | 1.5 | 2.4 | 3.0 | 3.7 |
| R23 Site 7 Q2b/disturbed pavement Dec.9 1979 12:45 Z55 2FOV | | | | | |
| | 19,14,12, 13,19,15, 14,16,18, 21,20 | 21,22,21, 18,20 19,22 | 25,24,27, 29,26,30, 20,23 | 35,30,29, 36,33,24, 21,23,34, 26,29,32 | 26,33,30, 23,24,32, 26,31,32, 25 |
| n | 11 | 7 | 8 | 12 | 10 |
| m | 16.5 | 20.4 | 25.5 | 29.3 | 28.2 |
| std | 3.1 | 1.5 | 3.3 | 4.9 | 3.8 |

| <u>READING</u> | <u>.4-.5</u> | <u>.5-.6</u> | <u>.6-.7</u> | <u>.7-.8</u> | <u>.8-1.0</u> |
|---|--|--|--|--|---|
| R24 Site 1B Q2c sandy fluve on pavement Feb.2 1980 10:02 Z65 2FOV | | | | | |
| | 18,13,15, 14,15,16, 17,16,17, 18 | 25,27,29, 25,26,24, 28,25,29, 26,23,25 | 33,32,35, 34,31,30, 30,31,37, 35 | 37,40,31, 43,33,43, 36,41,33, 35 | 43,41,32, 33,53,42, 39,34,46 |
| n | 10 | 12 | 10 | 10 | 9 |
| m | 15.9 | 26 | 32.8 | 37.2 | 40.3 |
| std | 1.7 | 1.9 | 2.4 | 4.3 | 6.8 |
| R25 Site 1B Q2c pavement Feb.2 1980 10:02 Z65 2FOV | | | | | |
| | 14,18,14, 13,19,12, 12,15,15, 13,15,16, 16,16,12, 18,18,19, 13,18,16 | 29,30,22, 28,23,29, 25,22,30, 24,19,21, 23,27, | 28,30,35, 41,32,26, 25,24,21, 26,28,29, 30,26,30, 25,35,33, 32,29,33 | 36,32,34, 29,33,26, 32,38,40, 35,36,32, 39 | 43,33,41, 32,33,33, 41,41,40, 35,29,37, 32,28,25, 33,36,23, 32,38,35, 32,35,49 |
| n | 21 | 14 | 21 | 13 | 24 |
| m | 15.3 | 25.1 | 29.4 | 34. | 34.8 |
| std | 2.4 | 3.7 | 4.6 | 4.0 | 5.9 |
| R26 Site 83.7 Q2c disturbed pavement Feb.3 1980 12:45 Z46 2FOV | | | | | |
| | 16,17,15, 16,15 | 23,19,18, 21,19,23, 18 | 41,34,30, 25,23,30, 27 | 41,41,28, 28,31,29, 28,29,34 | 41,38,34, 31,35,27, 33,26,31, 21 |
| n | 5 | 7 | 7 | 9 | 10 |
| m | 15.8 | 20.1 | 30. | 32.1 | 31.7 |
| std | .84 | 2.2 | 6.1 | 5.4 | 5.9 |
| R27 Site 8 Q2c disturbed light pavement March 31 1980 12:30 Z24 20FOV | | | | | |
| | 16,16,12, 17,18,17, 16,17,15 | 22,20,21, 21,22,23, 18,20,16 | 35,38,37, 40,39,28, 43,38,33 | 43,39,43, 47,45,43, 44,44,39 | 45,44,45, 52,47,51, 53,45,51 |
| n | 9 | 9 | 9 | 9 | 9 |
| m | 16. | 20.3 | 36.8 | 43. | 48.1 |
| std | 1.7 | 2.2 | 4.4 | 2.6 | 3.6 |

| <u>READING</u> | <u>.4-.5</u> | <u>.5-.6</u> | <u>.6-.7</u> | <u>.7-.8</u> | <u>.8-1.0</u> |
|----------------|--------------|--------------|--------------|--------------|---------------|
|----------------|--------------|--------------|--------------|--------------|---------------|

R28 Site 8 Q2c disturbed dark pavement March 31 1980 12:30 Z24 20FOV

| | | | | | |
|-----|-----------|-----------|-----------|-----------|-----------|
| | 11,14,11 | 18,14,16, | 29,34,27, | 34,31,28, | 36,40,33, |
| | 11,11,15, | 15,16,18, | 27,28,29, | 30,29,32, | 36,42,34, |
| | 13,13,13 | 17,20,19 | 28,31,37 | 33,32,39 | 36,42,38 |
| n | 9 | 9 | 9 | 9 | 9 |
| m | 12.4 | 17. | 30. | 32. | 37.4 |
| std | 1.5 | 1.9 | 3.4 | 3.2 | 3.3 |

R29 Site 8 Q2c disturbed pavement Dec.9 1979 14:00 Z54 2FOV

| | | | | | |
|-----|-----------|-----------|-----------|-----------|-----------|
| | 17,15,13, | 23,24,26, | 19,18,16, | 23,24,39, | 35,30,38, |
| | 12,15 | 19,22,23, | 25,26,25, | 33,37,25, | 37,32,35, |
| | | 19 | 23 | 32,34,29 | 32 |
| n | 5 | 7 | 7 | 9 | 7 |
| m | 14.4 | 22.3 | 21.7 | 30.7 | 34.1 |
| std | 1.6 | 2.6 | 4.0 | 5.8 | 2.9 |

R30 Site 8 Q2c disturbed pavement with Eriogonum Dec.9 1979 14:00 Z54 2FOV

| | | | | | |
|-----|-----------|-----------|-----------|-----------|-----------|
| | 13,12,13, | 17,13,20, | 19,18,20, | 24,27,32, | 40,31,37, |
| | 12,13,11, | 19,18,16, | 19,21,18, | 34,29,30 | 38,42 |
| | 10,8,9 | 17,22,14 | 22,17,15 | | |
| n | 9 | 9 | 9 | 6 | 5 |
| m | 11.2 | 17.3 | 18.8 | 29.3 | 37.6 |
| std | 1.9 | 2.8 | 2.1 | 3.6 | 4.2 |

R31 Site 61b Q3a soil Feb.3 1980 9:28 Z67 2FOV

| | | | | | |
|-----|-----------|-----------|-----------|-----------|-----------|
| | 12,14,12, | 20,20,20, | 29,27,25, | 31,29,32, | 33,30,37, |
| | 12,14,15, | 24,21,18, | 23,28,26, | 29,32,28, | 38,38,28, |
| | 14, | 24,18,20 | 20,31 | 29,25,25 | 28,34,34 |
| n | 7 | 9 | 8 | 9 | 9 |
| m | 13.3 | 20.6 | 26.1 | 28.9 | 33.3 |
| std | 1.3 | 2.2 | 3.5 | 2.6 | 4.0 |

R32 Site 3 Q3 soil in coarse gravel March 30 1980 14:00 Z35 20FOV

| | | | | | |
|-----|-----------|-----------|-----------|-----------|-----------|
| | 15,13,11, | 18,19,17, | 26,32,19, | 29,25,33, | 37,37,36, |
| | 11,14,13, | 19,18,15, | 21,30,29, | 36,31,30, | 35,41,36, |
| | 12,15,12, | 13,16,16, | 29,22,27, | 36,32,29, | 34,39,36, |
| | 15,12,13, | 18,18,17 | 23,29,29 | 33,33,30 | 36,37,35 |
| | 11 | | | | |
| n | 13 | 12 | 12 | 12 | 12 |
| m | 12.9 | 17.0 | 26.3 | 31.4 | 36.6 |
| std | 1.5 | 1.7 | 4.1 | 3.1 | 1.9 |

| <u>READING</u> | <u>.4-.5</u> | <u>.5-.6</u> | <u>.6-.7</u> | <u>.7-.8</u> | <u>.8-1.0</u> |
|---|---|---|--|---|--|
| R33 Site B1 Q3 soil dark March 31 1980 15:00 Z44 20FOV | | | | | |
| | 16,15,16, 16,15,16, 15,14,14, | 22,21,21, 20,22,22, 21,20,20 | 34,35,36, 34,34,34, 35,33,29 | 40,43,38, 40,42,40, 39,40,41 | 44,45,45, 44,48,43, 45,46,44 |
| n | 9 | 9 | 9 | 9 | 9 |
| m | 15.2 | 21.0 | 33.8 | 40.3 | 44.9 |
| std | .8 | .9 | 2.0 | 1.5 | 1.5 |
| R34 Site B1 Q3 soil light March 31 1980 15:00 Z44 20FOV | | | | | |
| | 16,18,20, 18,18,18, 17,17,15, 17 | 27,28,23, 25,25,24, 28,27,24 | 44,41,37, 42,43,42, 36,41 | 50,49,43, 46,48,49, 45,48,47 | 57,54,53, 56,55,56, 55,55,58 |
| n | 10 | 9 | 8 | 9 | 9 |
| m | 17.4 | 25.7 | 40.8 | 47.2 | 55.4 |
| std | 1.4 | 1.9 | 2.8 | 2.2 | 1.5 |
| R35 Site 1 Q4 channel Dec.8 1979 11:05 Z61 2FOV | | | | | |
| | 19,17 | 30,25 | 35,30 | 43,35 | 40,34 |
| n | 2 | 2 | 2 | 2 | 2 |
| m | 18 | 27.5 | 32.5 | 39. | 37. |
| std | - | - | - | - | - |
| R36 Site 3 Q4/3 wash and gravel bar Feb.3 1980 15:00 Z60 2FOV | | | | | |
| | 12,11,12, 14,26,15 | 14,18,13, 20,19,22 | 25,20,12, 13,21,18, 16,18 | 26,26,21, 19,26,18, 24 | 27,33,25, 24,21,25, 25,23 |
| n | 6 | 6 | 8 | 7 | 8 |
| m | 15 | 17.7 | 17.9 | 22.8 | 25.4 |
| std | 5.6 | 3.5 | 4.3 | 3.5 | 3.5 |
| R37 Site 3 Q4 stream channel March 30 1980 14:00 Z35 20FOV | | | | | |
| | 17,16,17, 18,18,16, 16,17,17, 18,17,18 | 20,23,20, 21,21,20, 21,22,21, 18,20,21 | 31,32,33, 32,36,30, 29,32,34, 31,33 | 35,37,39, 38,36,33, 38,32,35, 36,37,38 | 39,40,38, 42,35,39, 39,40,40, 37,38 |
| n | 12 | 12 | 11 | 12 | 11 |
| m | 17.1 | 20.7 | 32.1 | 36.2 | 38.8 |
| std | .8 | 1.2 | 1.9 | 2.1 | 1.8 |

| <u>READING</u> | <u>.4-.5</u> | <u>.5-.6</u> | <u>.6-.7</u> | <u>.7-.8</u> | <u>.8-1.0</u> |
|--|--|--|---|--|--|
| R38 site 70+d Q4/3 April 1 1980 10:30 cloudy 20FOV | | | | | |
| | 12,12,11 11,13,13, 11,12,12, 13 | 16,19,16, 15,15,16, 16,18,18 | 20,22,21, 19,19,18, 19,21,22, 24 | 25,24,25, 24,25,27, 26,29,30 | 26,27,29, 27,28,32, 27,32,27 |
| n | 10 | 9 | 10 | 9 | 9 |
| m | 12 | 16.6 | 20.5 | 26.1 | 28.3 |
| std | .8 | 1.4 | 1.8 | 2.2 | 2.2 |
| R39 Site 3 <u>Simmondsia chinensis</u> Feb.4 1980 9:35 Z61 2FOV | | | | | |
| | 7,6,8, 7,5,6, 5,6,8, 6,5,7 | 16,15,9, 10,12,13, 15,9,7, 15,13,16 | 6,5,10, 12,9,8, 7,7,8, 10,9,12, 11,12,9 | 29,35,40, 38,23,21, 22,26 27,40, 37,39,35, 28 | 35,36,30, 29,25, 26,23, 35,29, 25,32,37, 39 |
| n | 12 | 12 | 15 | 14 | 13 |
| m | 6.3 | 12.5 | 9.0 | 31.4 | 30.8 |
| std | 1.1 | 3.1 | 2.2 | 7.0 | 5.2 |
| R40 Site 1 <u>Simmondsia chinensis</u> Dec.8 1979 11:05 Z61 2FOV | | | | | |
| | 7,8 | 11,10,14 | 9,8,10 | 33,45 | 40,41 |
| n | 2 | 3 | 3 | 2 | 2 |
| m | 7.5 | 11.6 | 9. | 39. | 40.5 |
| std | - | - | - | - | - |
| R41 Site 3 <u>Cercidium sp.</u> Feb.4 1980 9:35 Z61 2 | | | | | |
| | 8,9,7, 7,6,7, 8,7 | 11,12,10, 11,11,10, 10,11,12, 11 | 10,9,11, 10,12,11, 13,12 | 30,30,31, 33,27,30, 29,29,30 | 38,41,42, 33,43,43, 41,38,39, 39 |
| n | 8 | 10 | 8 | 9 | 13 |
| m | 7.4 | 10.9 | 11.0 | 29.9 | 39.2 |
| std | .9 | .7 | 1.3 | 1.6 | 2.9 |
| R42 Site 1 <u>Cercidium sp.</u> dry Dec.8 1979 11:05 Z61 2FOV | | | | | |
| | 6 | 8 | 12 | 26 | 34 |
| n | 1 | 1 | 1 | 1 | 1 |
| m | 6 | 8 | 12 | 26 | 34 |
| std | - | - | - | - | - |

| <u>READING</u> | <u>.4-.5</u> | <u>.5-.6</u> | <u>.6-.7</u> | <u>.7-.8</u> | <u>.8-1.0</u> |
|---|------------------------------|---------------------------------|------------------------------------|---------------------------------|------------------------------------|
| R43 Site 4 <u>Encelia farinosa</u> Dec. 8 1979 15:50 Z65 2FOV | | | | | |
| | 18,17,15, 14,15 | 21,23,23, 22 | 23,38,29, 28 | 37,34,38, 47 | 29,30,28, 27,24,33 |
| n | 5 | 4 | 4 | 4 | 6 |
| m | 15.8 | 22.3 | 29.5 | 39.0 | 28.5 |
| std | 1.6 | 1.0 | 6.3 | 5.6 | 3.0 |
| R44 Site 5 <u>Encelia farinosa</u> Feb.2 1980 15:05 Z61 2FOV | | | | | |
| | - | 15,19,24, 41,17,20, 38 | 30,23,45, 35,34,24, 53,45 | 16,15,36, 28,25,26, 36,35 | 35,34,35, 37 |
| n | | 7 | 8 | 8 | 4 |
| m | | 24.9 | 36.1 | 27.1 | 35.3 |
| std | | 10.4 | 10.7 | 8.4 | 1.3 |
| R45 Site 4 <u>Encelia farinosa</u> March 30 1980 14:40 Z43 20FOV | | | | | |
| | 11,12,10, 11 | 16,17,15, 14,17 | 16,15,16, 16,18,15 | 32,30,37, 35,42,36 | 45,53,48, 54,45,54, 48 |
| n | 4 | 5 | 6 | 6 | 7 |
| m | 11.0 | 15.8 | 16.0 | 35.3 | 49.6 |
| std | .8 | 1.3 | 1.1 | 4.2 | 4.0 |
| R46 Site 83.7 <u>Ambrosia dumosa</u> (dry) Feb. 3 1980 12:45 Z46 2FOV | | | | | |
| | 11,14,9, 16,16,12, 15 | 19,21,19, 15,18,21 | 22,27,25, 20,20,19, 14,33,23 | 18,36,18, 17,21,17, 40,27 | 25,23,23, 11,26,31, 31,17,36 |
| n | 7 | 6 | 9 | 8 | 9 |
| m | 13.3 | 18.8 | 22.6 | 24.3 | 24.8 |
| std | 2.7 | 2.2 | 5.4 | 9.2 | 7.6 |
| R47 Site 1b <u>Ambrosia dumosa</u> Feb.2 1980 10:02 Z65 2FOV | | | | | |
| | 22,21,18, 17,18,19, 13 | 39,27,25, 24,34,24, 32,33 | 38,27,29, 41,23,35, 28,34 | 46,48,36, 47,48 | 53,64,56, 55,57,36 |
| n | 7 | 8 | 8 | 5 | 6 |
| m | 18.3 | 29.8 | 31.9 | 45.0 | 53.5 |
| std | 2.9 | 5.6 | 6.1 | 5.1 | 9.4 |

| <u>READING</u> | <u>.4-.5</u> | <u>.5-.6</u> | <u>.6-.7</u> | <u>.7-.8</u> | <u>.8-1.0</u> |
|--|--|--|--|--|---|
| R48 Site 8 <u>Larrea diveracata</u> Dec. 9 1979 14:00 Z54 2FOV | | | | | |
| | 7,6,7, 5,8,7, 10,11,15, 7,6,7 | 9,8,12, 10,8,14, 15,15,14, 11 | 18,7,13, 9,8,18, 20,19,12, 13,12,15 | 20,28,25, 24,32,17, 19,20,29, 38,25,24, 18,32,37 | 38,28,29, 25,39,25, 44,19,36, 34 |
| n | 12 | 10 | 12 | 15 | 10 |
| m | 8.0 | 11.6 | 13.6 | 25.9 | 31.7 |
| std | 2.8 | 2.8 | 4.4 | 6.7 | 7.8 |
| R49 Site 61.b <u>Larrea diveracata</u> Feb. 3 1980 9:28 Z67 2FOV | | | | | |
| | 8,10,7 10 | 11,18,20, 13,16,15 | 14,19,25 7,20,15 | 31,28,41, 36 | 35,44,56, 58,48,48 |
| n | 4 | 6 | 6 | 4 | 6 |
| m | 8.8 | 15.5 | 16.7 | 34.0 | 48.2 |
| std | 1.5 | 3.3 | 6.2 | 5.7 | 8.4 |
| R50 Site 3 <u>Carnegiea gigantea</u> Feb.4 1980 9:35 Z61 2FOV | | | | | |
| | 14,15,6, 8,13,6, 14 | 9,11,12, 13,15,16, 15,11 | 6,9,13, 24,9,7, 11,13 | 23,29,27, 45,42,23, 37,43 | 30,34,76, 77,62,86, 46,43,42 |
| n | 7 | 8 | 8 | 8 | 9 |
| m | 10.9 | 12.8 | 11.5 | 33.6 | 55.1 |
| std | 4.0 | 2.4 | 5.7 | 9.2 | 20.6 |
| R51 Site 3 <u>Opuntia acanthocarpa</u> Feb.4 1980 9:35 Z61 2FOV | | | | | |
| | 8,9,10, 11,11,8, 8,9,12, 9,10 | 10,14,7, 8,20,13, 15,19,8, 10 | 21,11,16, 17,11,19, 21,18 | 21,22,19, 32,26,11, 22,28,31, 26,23,31, 32,29,30 | 22,25,26, 35,23,40, 36,33,23, 21,26,34 |
| n | 11 | 10 | 8 | 15 | 12 |
| m | 9.6 | 12.4 | 16.8 | 25.5 | 28.7 |
| std | 1.4 | 4.6 | 4.0 | 5.9 | 6.5 |

| <u>READING</u> | <u>.4-.5</u> | <u>.5-.6</u> | <u>.6-.7</u> | <u>.7-.8</u> | <u>.8-1.0</u> |
|---|------------------------------|---------------------------------|-----------------------|---------------------------------|---|
| R52 Site 4 <u>Opuntia bigelovii</u> Dec.8 1979 15:50 Z65 2FOV | | | | | |
| | 50,32,29, 28,35,36, 37 | 48,52,88, 68,48,57, 54,61 | 79,89,55, 48,97,60 | 67,99,82, 95,45,67, 50,47 | 97,65,63, 63,70,78, 74,69,71, 75,80, |
| n | 7 | 8 | 6 | 8 | 11 |
| m | 35.3 | 59.5 | 71.3 | 69.0 | 73.2 |
| std | 7.3 | 13.3 | 19.8 | 21.3 | 9.7 |
| R53 Site 5 <u>Opuntia bigelovii</u> Dec.9 1979 10:15 Z60 2FOV | | | | | |
| | 18,17,23, 14,19 | 30,26,29, 25,54 | 46,45,77, 16,68 | 79,67,58 | 86,95 |
| n | 5 | 5 | 5 | 3 | 2 |
| m | 18.2 | 32.8 | 50.4 | 68.0 | 96.7 |
| std | - | - | - | - | - |
| R54 Site 4 <u>Opuntia bigelovii</u> March 30 1980 14:40 Z43 20FOV | | | | | |
| | 9,11,10, 7,11 | 13,11,12, 14,12,15 | 21,18,27, 23,18,25 | 31,45,37, 40,41,42, 31 | 54,42,50, 49,42,38 48 |
| n | 5 | 6 | 6 | 7 | 7 |
| m | 9.6 | 12.8 | 22.0 | 38.1 | 46.1 |
| std | 1.7 | 1.4 | 3.7 | 5.4 | 5.6 |
| R55 Site 6lb plant shadow on soil Feb.3 1980 9:28 Z67 2FOV | | | | | |
| | 8,10,11 | 10,14,14 10 | 11,18,14 | 12,11,15 | 13,14,12 |
| n | 3 | 4 | 3 | 3 | 3 |
| m | 9.7 | 12.0 | 14.3 | 12.7 | 13.0 |
| std | - | - | - | - | - |

Spectral Plots Output from Program PLOTS

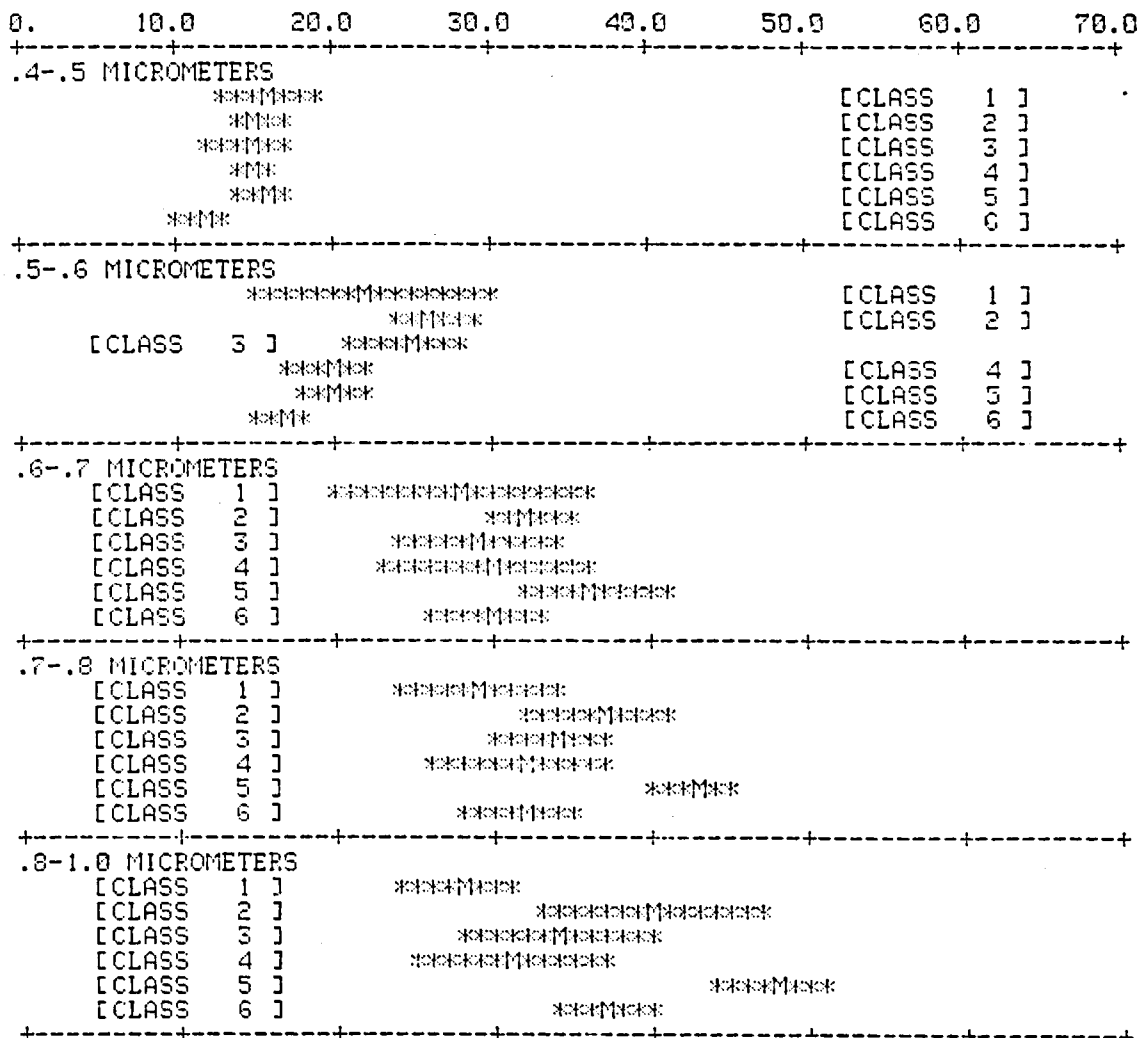
VOLCANIC BEDROCK, RADIOMETER
SPECTRAL PLOT [MEAN +/- ONE STD]
UNITS IN PERCENT ABSOLUTE REFLECTANCE

| 0. | 10.0 | 20.0 | 30.0 | 40.0 | 50.0 | 60.0 | 70.0 |
|---|------------|-------|------|------|------|------------|------|
| +-----+-----+-----+-----+-----+-----+-----+ | | | | | | | |
| .4-.5 MICROMETERS | | | | | | | |
| | ***** | | | | | [CLASS 1] | |
| | | **** | | | | [CLASS 2] | |
| | ** | | | | | [CLASS 3] | |
| | | ***** | | | | [CLASS 4] | |
| | ?***? | | | | | [CLASS 5] | |
| +-----+-----+-----+-----+-----+-----+-----+ | | | | | | | |
| .5-.6 MICROMETERS | | | | | | | |
| | | **** | | | | [CLASS 1] | |
| | [CLASS 2] | | **** | | | [CLASS 3] | |
| | ** | | | | | [CLASS 4] | |
| | | **** | | | | [CLASS 5] | |
| | ?***? | | | | | | |
| +-----+-----+-----+-----+-----+-----+-----+ | | | | | | | |
| .6-.7 MICROMETERS | | | | | | | |
| | | ***** | | | | [CLASS 1] | |
| | [CLASS 2] | | **** | | | [CLASS 3] | |
| | ** | | | | | [CLASS 4] | |
| | [CLASS 4] | ***** | | | | [CLASS 5] | |
| | ?***? | | | | | | |
| +-----+-----+-----+-----+-----+-----+-----+ | | | | | | | |
| .7-.8 MICROMETERS | | | | | | | |
| | | ***** | | | | [CLASS 1] | |
| | [CLASS 2] | | **** | | | [CLASS 3] | |
| | ** | | | | | [CLASS 4] | |
| | [CLASS 4] | ***** | | | | [CLASS 5] | |
| | ?***? | | | | | | |
| +-----+-----+-----+-----+-----+-----+-----+ | | | | | | | |
| .8-1.0 MICROMETERS | | | | | | | |
| | | ***** | | | | [CLASS 1] | |
| | [CLASS 2] | | **** | | | [CLASS 3] | |
| | ** | | | | | [CLASS 4] | |
| | [CLASS 4] | ***** | | | | [CLASS 5] | |
| | ?***? | | | | | | |
| +-----+-----+-----+-----+-----+-----+-----+ | | | | | | | |

KEY TO CLASSES

| | |
|---------------------|--|
| 1= R1, SITE70.25 | HEAVILY VARNISHED INTERMEDIATE VOLCANIC BOULDER SLOPE WITH ENCELIA FARINOSA |
| 2= R2, ENIGMA HILL | LIGHTLY VARNISHED, YELLOW ASH-FLOW TUFF. SINGLE ROCK |
| 3= R3, ENIGMA HILL | HEAVILY VARNISHED LITHIC ASH-FLOW TUFF. SINGLE ROCK. |
| 4= R4, SITE2 | YELLOW TUFF EROSIONAL SURFACE WITH PETRACALCIC CLASTS. |
| 5= R5, HILL AT 70+P | VARNISHED INTERMEDIATE VOLCANIC ROCK |
| | ? INDICATES UNSURE STD DUE TO LOW # SAMPLES |

Q2B AND Q2C DISTURBED PAVEMENT, RADIOMETER
SPECTRAL PLOT [MEAN +/- ONE STD]
UNITS IN PERCENT ABSOLUTE REFLECTANCE



KEY TO CLASSES

1=R23.SITE7

2=R24.SITE1B

3=R25.SITE1B

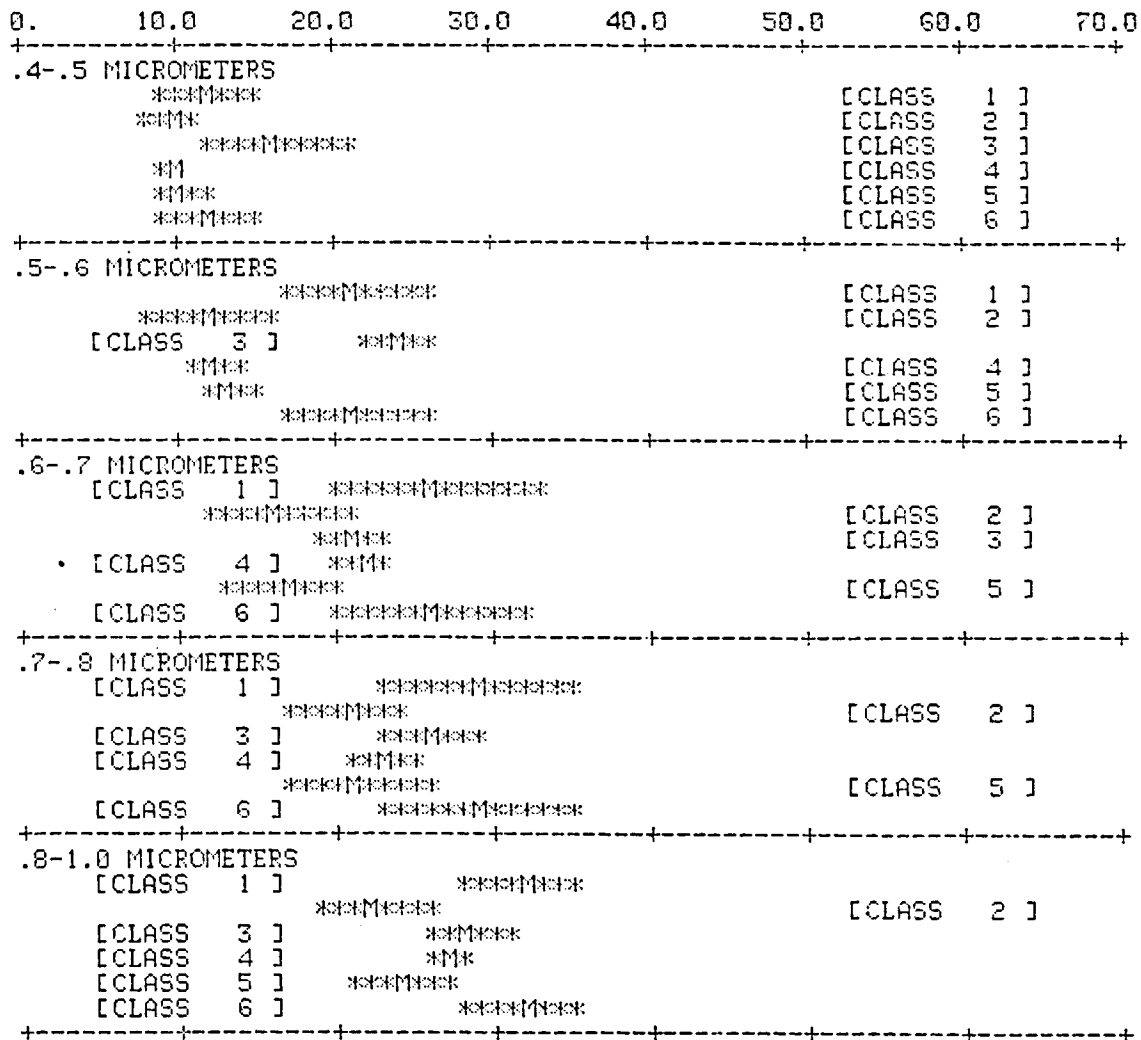
4=R26.SITE83.7

5=R27.SITE8

6=R27.SITE8

Q2B DENUDED PAVEMENT ACIDIC VOLCANICS AND
PETRACLACIC CLASTSQ2C PAVEMENT ACIDIC VOLCANICS, SCATTERED
VARNISHED GRAVEL IN GRAVELLY SANDY SOIL
SAME AS ABOVE BUT IN LESS SANDY PARTQ2C PAVEMENT IN INTERMEDIATE VOLCANICS
WITH SAND, SILTS AND SANDBLASTED VARNISHQ2C PAVEMENT IN ACIDIC VOLCANICS WITH
SAND SILTS AND SANDBLASTED VOLCANICS.Q2C PAVEMENT SAME AS ABOVE BUT IN DARKER
PORTION OF SURFACE.

OLDER PLEISTOCENE SURFACES Q2A AND Q2B, RADIOMETER
SPECTRAL PLOT [MEAN +/- ONE STD]
UNITS IN PERCENT ABSOLUTE REFLECTANCE



KEY TO CLASSES

| | |
|---------------|---|
| 1= R7, SITES | Q2B PAVEMENT VARNISHED ACIDIC VOLCANICS |
| 2= R8, SITES | " " " " |
| 3= R9, SITES | " " " " |
| 4= R10, SITES | " " " " |
| 5= R11, SITES | " " " " |
| 6= R6, SITE6 | Q2A PAVEMENT VARNISHED ACIDIC VOLCANICS |

Q2C PAVEMENT RADIOMETER
SPECTRAL PLOT (MEAN +/- ONE STD)
UNITS IN PERCENT ABSOLUTE REFLECTANCE



KEY TO CLASSES

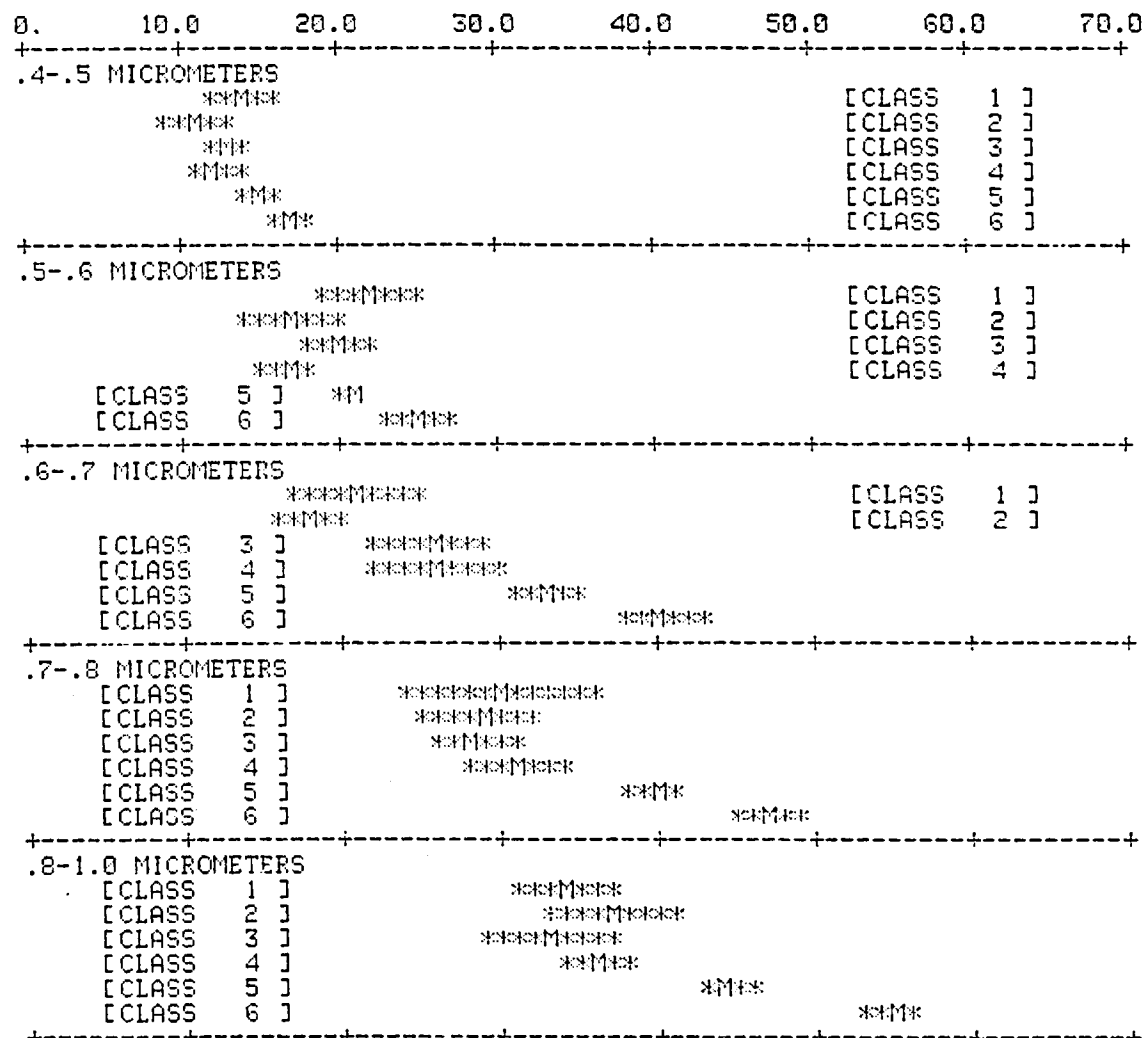
- 1= P12. SITE 4.0
- 2= P14. SITE 4.0
- 3= P13. SITE 4.0
- 4= P15. SITE 9.0
- 5= P16. SITE 65.35
- 6= P18. SITE 70.25
- 7= P19. SITE 70+P
- 8= P20. SITE 65.35
- 9= P17. SITE 65.35

Q2C PAVEMENT WORNISHED ACIDIC VOLCANICS

Q2C PAVEMENT WORNISHED ACIDIC VOLCANICS WITH LIGHT COLOR SILTS AND PLANTAGO INSULARIS. Q2C PAVEMENT HEAVILY WORNISHED INTERMEDIATE VOLCANICS.

Q2C PAVEMENT HEAVILY WORNISHED INTERMEDIATE VOLCANIC WITH LIGHT COLOR SILTS AND SILTS.

Q3 SOILS RADIOMETER
SPECTRAL PLOT [MEAN +/- ONE STD]
UNITS IN PERCENT ABSOLUTE REFLECTANCE



KEY TO CLASSES

1=R29, SITE8
2=R30, SITE8
3=R31, SITE61.B
4=R32, SITE3
5=R33, SITEB1
6=R34, SITEB1

Q3 SOIL PEBBLY GRAVEL ACIDIC VOLCANICS
SAME WITH ERIOGONUM SP.
Q3 SOIL IN PEBBLY ACIDIC VOLCANIC
Q3 COARSE GRAVELS ACIDIC VOLCANICS
Q3 IN FINE SANDS, SILTS AND PEBBLES
SAME BUT IN LIGHTER SILTER PORTION

RIPARIAN TREES RADIOMETER
SPECTRAL PLOT [MEAN +/- ONE STD]
UNITS IN PERCENT ABSOLUTE REFLECTANCE

| 0. | 10.0 | 20.0 | 30.0 | 40.0 | 50.0 | 60.0 | 70.0 |
|---|------------|-------|-------|--------|------|------------|------|
| +-----+-----+-----+-----+-----+-----+-----+ | | | | | | | |
| .4-.5 MICROMETERS | | | | | | | |
| | *** | | | | | [CLASS 1] | |
| | ?***? | | | | | [CLASS 2] | |
| | *** | | | | | [CLASS 3] | |
| | ?***? | | | | | [CLASS 4] | |
| +-----+-----+-----+-----+-----+-----+-----+ | | | | | | | |
| .5-.6 MICROMETERS | | | | | | | |
| | ***** | | | | | [CLASS 1] | |
| | ?*****? | | | | | [CLASS 2] | |
| | *** | | | | | [CLASS 3] | |
| | ?*****? | | | | | [CLASS 4] | |
| +-----+-----+-----+-----+-----+-----+-----+ | | | | | | | |
| .6-.7 MICROMETERS | | | | | | | |
| | ***** | | | | | [CLASS 1] | |
| | ?***? | | | | | [CLASS 2] | |
| | *** | | | | | [CLASS 3] | |
| | ?*****? | | | | | [CLASS 4] | |
| +-----+-----+-----+-----+-----+-----+-----+ | | | | | | | |
| .7-.8 MICROMETERS | | | | | | | |
| | [CLASS 1] | ***** | | | | | |
| | [CLASS 2] | ***** | | | | | |
| | [CLASS 3] | | *** | | | | |
| | [CLASS 4] | | ?***? | | | | |
| +-----+-----+-----+-----+-----+-----+-----+ | | | | | | | |
| .8-1.0 MICROMETERS | | | | | | | |
| | [CLASS 1] | ***** | | | | | |
| | [CLASS 2] | ***** | | | | | |
| | [CLASS 3] | | | ***? | | | |
| | [CLASS 4] | | | *****? | | | |
| +-----+-----+-----+-----+-----+-----+-----+ | | | | | | | |

KEY TO CLASSES

1=R39, SITE3

2=R40, SITE1

3=R41, SITE3

4=R42, SITE1

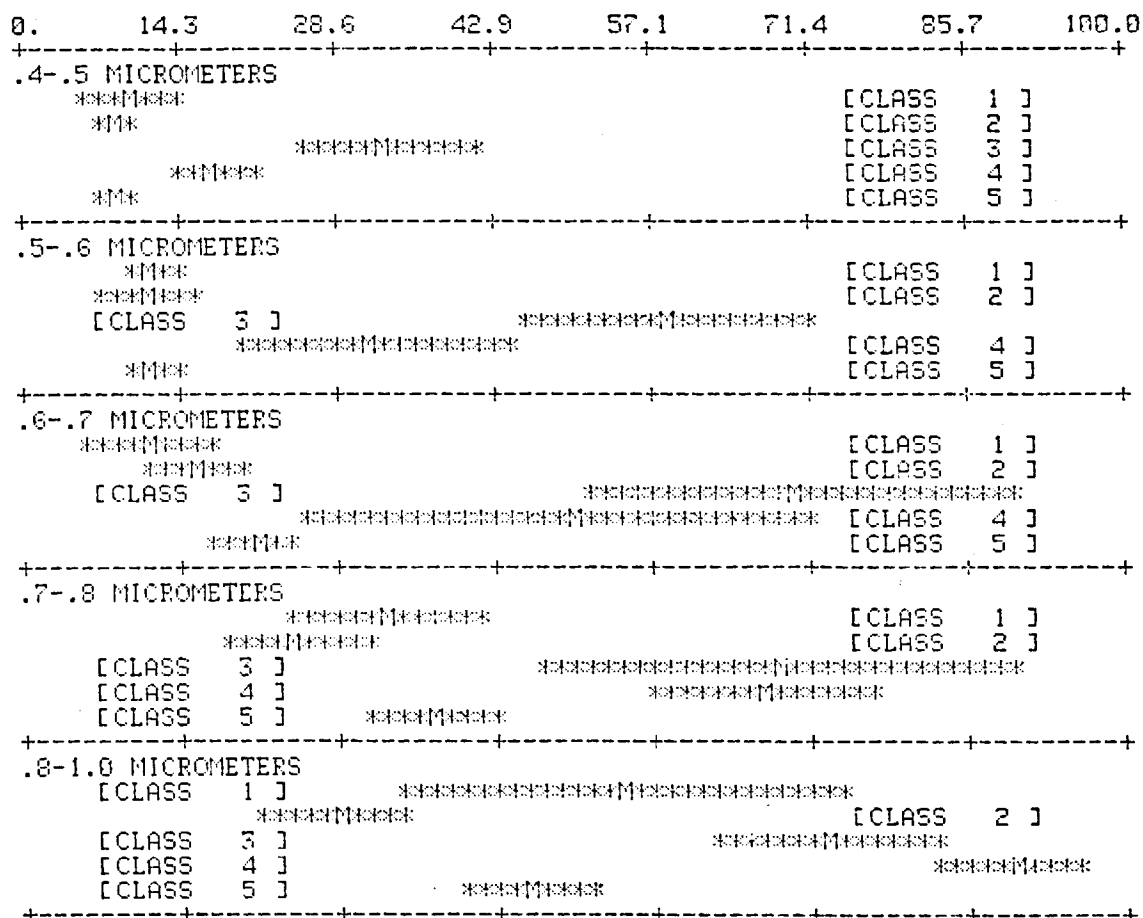
JOJOBA (SIMMONDSIA CHINENSIS)

JOJOBA

PALO VERDE (CERCIDIUM SP.)

PALO VERDE , DRY YELLOWING LEAVES

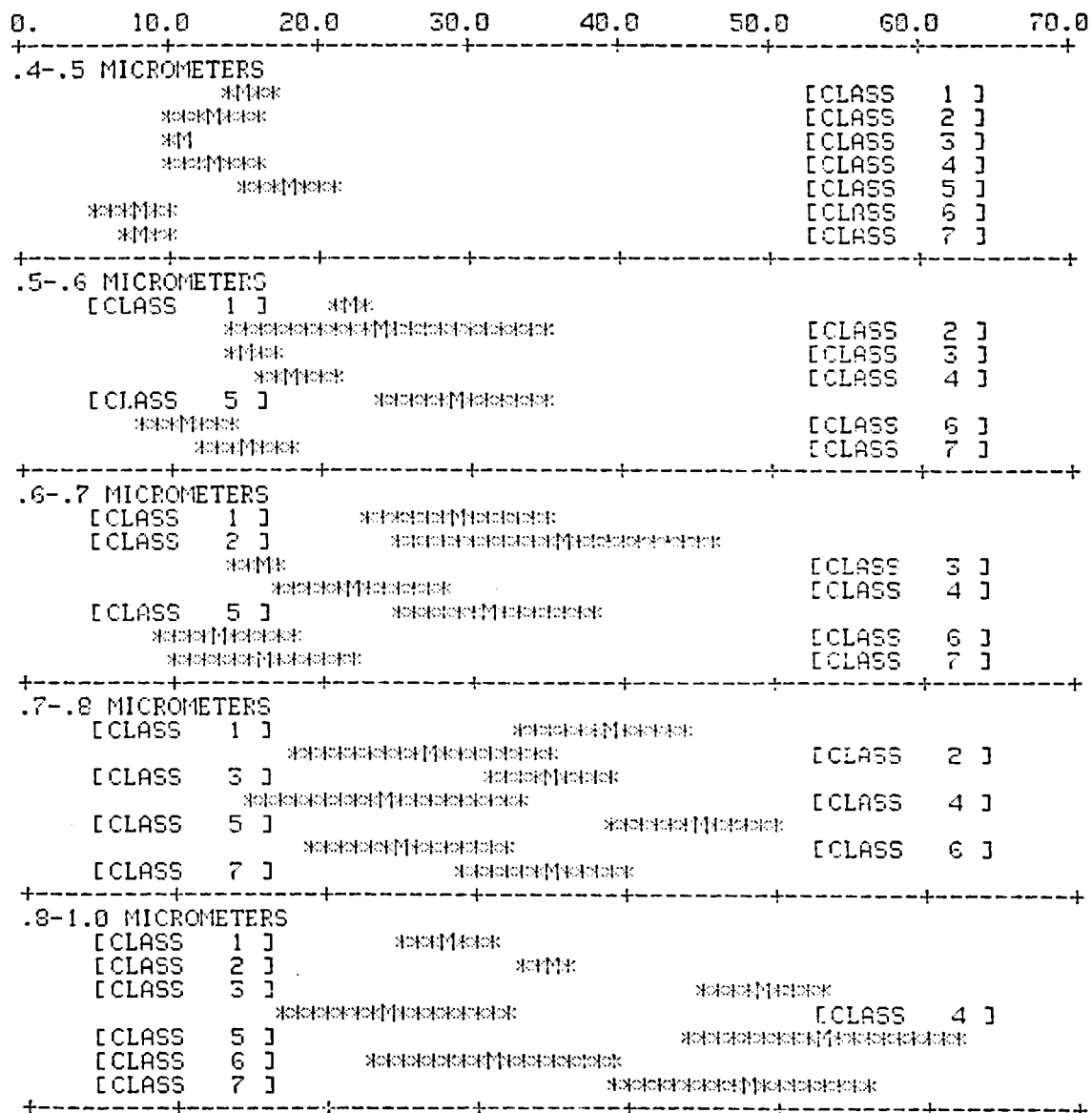
DESERT CACTUS RADIOMETER
SPECTRAL PLOT [MEAN +/- ONE STD]
UNITS IN PERCENT ABSOLUTE REFLECTANCE



KEY TO CLASSES

| | |
|--------------|--|
| 1=R50, SITE3 | CARNEGIEA GIGANTEA (SAGUARO) FEB.3, 1980 |
| 2=R51, SITE3 | OPUNTIA ACANTHACAEPA FEB.4, 1980 |
| 3=R52, SITE4 | OPUNTIA BIGELOV'II DEC.8, 1979 |
| 4=R53, SITE5 | OPUNTIA BIGELOV'II DEC.9, 1979 |
| 5=R54, SITE4 | OPUNTIA BIGELOV'II MAR.30, 1980 |

DESERT SCRUB RADIOMETER
SPECTRAL PLOT [MEAN +/- ONE STD]
UNITS IN PERCENT ABSOLUTE REFLECTANCE



KEY TO CLASSES

| | |
|-----------------|--|
| 1=R43, SITE4 | ENCELIA FARINOSA DEC.8, 1979 |
| 2=R44, SITE5 | ENCELIA FARINOSA FEB.2, 1980 |
| 3=R45, SITE4 | ENCELIA FARINOSA MAR.30, 1980 |
| 4=R46, SITE83.7 | AMBROSIA DUMOSA (VERY DRY) FEB.3, 1980 |
| 5=R47, SITE1B | AMBROSIA DUMOSA FEB.2, 1980 |
| 6=R48, SITE8 | LARREA TRIDENTATA DEC.9, 1979 |
| 7=R49, SITE61B | LARREA TRIDENTATA FEB.3, 1980 |

APPENDIX D

SOFTWARE AND IMAGE DATA

Software Summary

| <u>Name</u> | <u>Function</u> | <u>Documentation</u> |
|-------------|---|------------------------------|
| CALSCAN | Multifeature supervised Bayesian maximum likelihood classifier. Used in batch mode. Four overlays: 1. STATS: Calculate statistics from training sites. 2. SELECT: Calculates pair-wise divergences to determine best features. 3. CLASSIFY: Classifies image data. 4. DISPLAY: Displays classified map and obtains site performance statistics. | Schowengerdt, 1979 |
| CCODE | Writes bar scale on video refresh memories by cursor input. Used to display classification color code. Interactive mode. | Shih, 1982 |
| DIPP | A package of interactive programs used in DIAL most commonly used routine was: HISTOGRAM: Samples image histogram from video screen feedback and displays the histogram in the graphics channel. | University of Arizona, 1981b |
| EXTRACT | Extracts subscene from Landsat scene using pixel coordinates and Landsat data as input. Batch mode. | Schowengerdt, 1978 |
| KOUNT | Uses two identical high-pass filtered images, performs histogram equalization, thresholding and window count to produce LEAD texture features. Interactive and batch mode. | Shih, 1982 |
| PLOTS | Plots spectral plots from field radiometer data. Interactive mode. | Shih, 1982 |

| <u>Name</u> | <u>Function</u> | <u>Documentation</u> |
|-------------|--|-------------------------------|
| PREPROC | Performs geometric correction, reformatting, and destriping on "raw" Landsat CCTs. Batch mode. | Schowengerdt, 1978 |
| PSEUDO | Does a pseudo color density slice of any black and white image. Interactive mode. | Shih, 1982 |
| SADIE | A Fortran subroutine package for image experimentation. Most important routines used are: I2SOUT: Reformats SADIE work-files for DIAL lab. MDIN: Reads microdensitometer scanned data and translates it to raster scan. SCONVL: Spatial convolution routine used to generate high-pass images. SCOEF: Calculates least squares fit polynomial expression for geometric warp. GEOM: Performs geometric warp. | University of Arizona, 1981a. |
| TRAINS | Interactively locates sites, obtains site data and calculates first-order statistics. Stores all information on disc. Interactive mode. | Shih, 1982 |

Output from TRAINS: Site Information

Band 4= 2x Landsat MSS band 4

Band 5= 2x Landsat MSS band 5

Band 6= 2x Landsat MSS band 6

Band 7= 2x Landsat MSS band 7

Band 8= X-HH Radar

| <u>Site Name</u> | <u>Class no.</u> | <u>N</u> |
|------------------|------------------|----------|
| 2 | 1 | 81 |
| 3 | 2 | 25 |
| 4 | 3 | 25 |
| 5 | 4 | 25 |
| 6 | 5 | 25 |
| 7 | 6 | 25 |
| 8 | 7 | 25 |
| 9 | 8 | 81 |
| B1 | 10 | 15 |
| 65.35 | 11 | 81 |
| 70.25 | 12 | 9 |
| 70+p | 13 | 25 |
| 70+d | 14 | 25 |
| 83.7 | 15 | 25 |

CLASS SITE 2

CLASS NO. 1 SITE NO. 1 BAND NO.04

SITE 15 9 BY 9 CENTERED ON: X 78 Y 230

| | 74 | 75 | 76 | 77 | 78 | 79 | 80 | 81 | 82 |
|-----|----|----|----|----|----|----|----|----|----|
| 226 | 34 | 32 | 32 | 32 | 35 | 35 | 32 | 32 | 32 |
| 227 | 34 | 32 | 32 | 32 | 35 | 35 | 32 | 32 | 32 |
| 228 | 34 | 31 | 34 | 34 | 34 | 34 | 34 | 34 | 34 |
| 229 | 34 | 31 | 34 | 34 | 34 | 34 | 34 | 34 | 34 |
| 230 | 33 | 30 | 34 | 34 | 34 | 34 | 34 | 34 | 31 |
| 231 | 30 | 30 | 34 | 34 | 34 | 34 | 34 | 34 | 31 |
| 232 | 37 | 33 | 33 | 33 | 34 | 34 | 33 | 33 | 33 |
| 233 | 37 | 33 | 33 | 33 | 34 | 34 | 33 | 33 | 33 |
| 234 | 35 | 31 | 33 | 33 | 33 | 33 | 31 | 31 | 33 |

MEAN: 33.3 VARIANCE: 2.0 STD: 1.4
 MIN: 30.0 MAX: 37.0 RANGE: 7.0

HISTOGRAM

| LOW | HIGH | FTS | % |
|-------|-------|-----|-------------|
| 30.00 | 32.00 | 25 | 22.12 ***** |
| 32.00 | 34.00 | 50 | 61.74 ***** |
| 34.00 | 36.00 | 7 | 8.64 *** |
| 36.00 | 38.00 | 2 | 2.48 * |

CLASS SITE 2

CLASS NO. 1 SITE NO. 1 BAND NO.06

SITE 15 9 BY 9 CENTERED ON: X 78 Y 230

| | 74 | 75 | 76 | 77 | 78 | 79 | 80 | 81 | 82 |
|-----|----|----|----|----|----|----|----|----|----|
| 226 | 35 | 35 | 34 | 34 | 34 | 34 | 34 | 34 | 35 |
| 227 | 35 | 35 | 34 | 34 | 34 | 34 | 34 | 34 | 35 |
| 228 | 34 | 34 | 36 | 36 | 34 | 34 | 36 | 36 | 39 |
| 229 | 34 | 34 | 36 | 36 | 34 | 34 | 36 | 36 | 39 |
| 230 | 29 | 29 | 38 | 38 | 36 | 36 | 34 | 34 | 36 |
| 231 | 29 | 29 | 38 | 38 | 36 | 36 | 34 | 34 | 36 |
| 232 | 35 | 35 | 35 | 35 | 35 | 35 | 35 | 35 | 34 |
| 233 | 35 | 35 | 35 | 35 | 35 | 35 | 35 | 35 | 34 |
| 234 | 30 | 30 | 33 | 33 | 34 | 34 | 33 | 33 | 33 |

MEAN: 34.5 VARIANCE: 3.9 STD: 2.0
 MIN: 29.0 MAX: 39.0 RANGE: 10.0

HISTOGRAM

| LOW | HIGH | FTS | % |
|-------|-------|-----|-------------|
| 29.00 | 31.00 | 6 | 7.41 *** |
| 31.00 | 33.00 | 7 | 8.64 *** |
| 33.00 | 35.00 | 48 | 59.26 ***** |
| 35.00 | 37.00 | 14 | 17.28 ***** |
| 37.00 | 39.00 | 6 | 7.41 *** |

CLASS SITE 2

CLASS NO. 1 SITE NO. 1 BAND NO.06

SITE 15 9 BY 9 CENTERED ON: X 78 Y 230

| | 74 | 75 | 76 | 77 | 78 | 79 | 80 | 81 | 82 |
|-----|----|----|----|----|----|----|----|----|----|
| 226 | 35 | 35 | 35 | 35 | 35 | 35 | 32 | 32 | 32 |
| 227 | 35 | 35 | 35 | 35 | 35 | 35 | 32 | 32 | 32 |
| 228 | 33 | 33 | 36 | 36 | 33 | 33 | 36 | 36 | 40 |
| 229 | 33 | 33 | 36 | 36 | 33 | 33 | 36 | 36 | 40 |
| 230 | 32 | 32 | 36 | 36 | 36 | 36 | 36 | 36 | 36 |
| 231 | 32 | 32 | 36 | 36 | 36 | 36 | 36 | 36 | 36 |
| 232 | 36 | 36 | 36 | 36 | 36 | 36 | 36 | 36 | 36 |
| 233 | 36 | 36 | 36 | 36 | 36 | 36 | 36 | 36 | 36 |
| 234 | 34 | 34 | 32 | 32 | 34 | 34 | 34 | 34 | 34 |

MEAN: 35.2 VARIANCE: 2.45 STD: 1.56
 MIN: 32.0 MAX: 40.0 RANGE: 8.0

HISTOGRAM

| LOW | HIGH | FTS | % |
|-------|-------|-----|-------------|
| 32.00 | 34.00 | 21 | 21.93 ***** |
| 34.00 | 36.00 | 50 | 64.20 ***** |
| 36.00 | 38.00 | 8 | 10.41 *** |
| 38.00 | 40.00 | 1 | 1.46 * |

CLASS

CLASS NO. 1 SITE NO. 1 BAND NO.07

SITE 15 9 BY 9 CENTERED ON: X 78 Y 230

| | 74 | 75 | 76 | 77 | 78 | 79 | 80 | 81 | 82 |
|-----|----|----|----|----|----|----|----|----|----|
| 226 | 32 | 32 | 32 | 32 | 32 | 32 | 32 | 32 | 32 |
| 227 | 32 | 32 | 32 | 32 | 32 | 32 | 32 | 32 | 32 |
| 228 | 32 | 32 | 32 | 32 | 32 | 32 | 32 | 32 | 32 |
| 229 | 32 | 32 | 32 | 32 | 32 | 32 | 32 | 32 | 32 |
| 230 | 28 | 28 | 32 | 32 | 32 | 32 | 32 | 32 | 32 |
| 231 | 28 | 28 | 32 | 32 | 32 | 32 | 32 | 32 | 32 |
| 232 | 32 | 32 | 32 | 32 | 32 | 32 | 32 | 32 | 32 |
| 233 | 32 | 32 | 32 | 32 | 32 | 32 | 32 | 32 | 32 |
| 234 | 30 | 30 | 30 | 30 | 32 | 32 | 32 | 32 | 32 |

MEAN: 31.9 VARIANCE: 2.1 STD: 1.4
 MIN: 28.0 MAX: 34.0 RANGE: 6.0

HISTOGRAM

| LOW | HIGH | FTS | % |
|-------|-------|-----|-------------|
| 28.00 | 30.00 | 14 | 19.75 ***** |
| 30.00 | 32.00 | 41 | 62.96 ***** |
| 32.00 | 34.00 | 14 | 19.28 ***** |

CLASS
 CLASS NO. 1 SITE NO. 1 BANK NO. 06

| SITE IS | 9 BY | | 9 CENTERED ON: X 2R Y 230 | | | | | | | | |
|---------|------|----|---------------------------|----|----|----|-----|-----|----|----|--|
| | 74 | 75 | 76 | 77 | 78 | 79 | 80 | 81 | 82 | 83 | |
| 274 | 18 | 10 | 20 | 37 | 52 | 53 | 55 | 61 | 61 | | |
| 277 | 5 | 9 | 36 | 41 | 97 | 76 | 41 | 92 | 49 | | |
| 228 | 50 | 22 | 50 | 50 | 34 | 55 | 66 | 74 | 56 | | |
| 9 | 75 | 16 | 53 | 71 | 66 | 90 | 104 | 97 | 44 | | |
| 140 | 27 | 48 | 85 | 77 | 65 | 79 | 65 | 56 | 59 | | |
| 271 | 8 | 54 | 45 | 51 | 87 | 80 | 88 | 64 | 85 | | |
| 137 | 26 | 17 | 34 | 50 | 59 | 66 | 79 | 77 | 41 | | |
| 158 | 5 | 20 | 73 | 62 | 75 | 50 | 68 | 53 | 20 | | |
| 258 | 94 | 51 | 96 | 63 | 86 | 85 | 94 | 109 | 50 | | |

MEAN: 58.8 VARIANCE: 584.1 SD: 24.16
 MIN: 5.0 MAX: 109.0 RANGE: 104.0

HISTOGRAM

| LOW | HIGH | FREQ | % |
|--------|--------|------|------|
| 1.00 | 2.00 | 1 | 1.23 |
| 2.00 | 3.00 | 2 | 2.47 |
| 3.00 | 4.00 | 1 | 1.23 |
| 4.00 | 5.00 | 0 | 0.00 |
| 5.00 | 6.00 | 0 | 0.00 |
| 6.00 | 7.00 | 2 | 2.47 |
| 7.00 | 8.00 | 1 | 1.23 |
| 8.00 | 9.00 | 2 | 2.47 |
| 9.00 | 10.00 | 1 | 1.23 |
| 10.00 | 11.00 | 0 | 0.00 |
| 11.00 | 12.00 | 0 | 0.00 |
| 12.00 | 13.00 | 0 | 0.00 |
| 13.00 | 14.00 | 0 | 0.00 |
| 14.00 | 15.00 | 0 | 0.00 |
| 15.00 | 16.00 | 1 | 1.23 |
| 16.00 | 17.00 | 2 | 2.47 |
| 17.00 | 18.00 | 1 | 1.23 |
| 18.00 | 19.00 | 0 | 0.00 |
| 19.00 | 20.00 | 0 | 0.00 |
| 20.00 | 21.00 | 0 | 0.00 |
| 21.00 | 22.00 | 1 | 1.23 |
| 22.00 | 23.00 | 0 | 0.00 |
| 23.00 | 24.00 | 0 | 0.00 |
| 24.00 | 25.00 | 0 | 0.00 |
| 25.00 | 26.00 | 0 | 0.00 |
| 26.00 | 27.00 | 1 | 1.23 |
| 27.00 | 28.00 | 2 | 2.47 |
| 28.00 | 29.00 | 1 | 1.23 |
| 29.00 | 30.00 | 0 | 0.00 |
| 30.00 | 31.00 | 0 | 0.00 |
| 31.00 | 32.00 | 0 | 0.00 |
| 32.00 | 33.00 | 1 | 1.23 |
| 33.00 | 34.00 | 1 | 1.23 |
| 34.00 | 35.00 | 1 | 1.23 |
| 35.00 | 36.00 | 1 | 1.23 |
| 36.00 | 37.00 | 2 | 2.47 |
| 37.00 | 38.00 | 2 | 2.47 |
| 38.00 | 39.00 | 2 | 2.47 |
| 39.00 | 40.00 | 2 | 2.47 |
| 40.00 | 41.00 | 1 | 1.23 |
| 41.00 | 42.00 | 1 | 1.23 |
| 42.00 | 43.00 | 2 | 2.47 |
| 43.00 | 44.00 | 2 | 2.47 |
| 44.00 | 45.00 | 0 | 0.00 |
| 45.00 | 46.00 | 0 | 0.00 |
| 46.00 | 47.00 | 0 | 0.00 |
| 47.00 | 48.00 | 0 | 0.00 |
| 48.00 | 49.00 | 0 | 0.00 |
| 49.00 | 50.00 | 3 | 3.70 |
| 50.00 | 51.00 | 4 | 4.94 |
| 51.00 | 52.00 | 4 | 4.94 |
| 52.00 | 53.00 | 4 | 4.94 |
| 53.00 | 54.00 | 2 | 2.47 |
| 54.00 | 55.00 | 2 | 2.47 |
| 55.00 | 56.00 | 4 | 4.94 |
| 56.00 | 57.00 | 4 | 4.94 |
| 57.00 | 58.00 | 3 | 3.70 |
| 58.00 | 59.00 | 3 | 3.70 |
| 59.00 | 60.00 | 3 | 3.70 |
| 60.00 | 61.00 | 2 | 2.47 |
| 61.00 | 62.00 | 2 | 2.47 |
| 62.00 | 63.00 | 3 | 3.70 |
| 63.00 | 64.00 | 3 | 3.70 |
| 64.00 | 65.00 | 2 | 2.47 |
| 65.00 | 66.00 | 2 | 2.47 |
| 66.00 | 67.00 | 2 | 2.47 |
| 67.00 | 68.00 | 2 | 2.47 |
| 68.00 | 69.00 | 2 | 2.47 |
| 69.00 | 70.00 | 1 | 1.23 |
| 70.00 | 71.00 | 2 | 2.47 |
| 71.00 | 72.00 | 2 | 2.47 |
| 72.00 | 73.00 | 2 | 2.47 |
| 73.00 | 74.00 | 3 | 3.70 |
| 74.00 | 75.00 | 3 | 3.70 |
| 75.00 | 76.00 | 3 | 3.70 |
| 76.00 | 77.00 | 2 | 2.47 |
| 77.00 | 78.00 | 2 | 2.47 |
| 78.00 | 79.00 | 1 | 1.23 |
| 79.00 | 80.00 | 1 | 1.23 |
| 80.00 | 81.00 | 1 | 1.23 |
| 81.00 | 82.00 | 1 | 1.23 |
| 82.00 | 83.00 | 3 | 3.70 |
| 83.00 | 84.00 | 3 | 3.70 |
| 84.00 | 85.00 | 1 | 1.23 |
| 85.00 | 86.00 | 1 | 1.23 |
| 86.00 | 87.00 | 1 | 1.23 |
| 87.00 | 88.00 | 1 | 1.23 |
| 88.00 | 89.00 | 1 | 1.23 |
| 89.00 | 90.00 | 1 | 1.23 |
| 90.00 | 91.00 | 1 | 1.23 |
| 91.00 | 92.00 | 1 | 1.23 |
| 92.00 | 93.00 | 1 | 1.23 |
| 93.00 | 94.00 | 2 | 2.47 |
| 94.00 | 95.00 | 2 | 2.47 |
| 95.00 | 96.00 | 3 | 3.70 |
| 96.00 | 97.00 | 3 | 3.70 |
| 97.00 | 98.00 | 0 | 0.00 |
| 98.00 | 99.00 | 0 | 0.00 |
| 99.00 | 100.00 | 0 | 0.00 |
| 100.00 | 101.00 | 0 | 0.00 |
| 101.00 | 102.00 | 0 | 0.00 |
| 102.00 | 103.00 | 0 | 0.00 |
| 103.00 | 104.00 | 1 | 1.23 |
| 104.00 | 105.00 | 1 | 1.23 |
| 105.00 | 106.00 | 0 | 0.00 |
| 106.00 | 107.00 | 0 | 0.00 |
| 107.00 | 108.00 | 1 | 1.23 |
| 108.00 | 109.00 | 1 | 1.23 |

CLASS SITE 3

CLASS NO. 2 SITE NO. 1 BAND NO.04

SITE IS 5 BY 5 CENTERED ON: X 59 Y 232

57 58 59 60 61

230 28 28 28 28 28
231 33 28 28 28 28
232 33 27 27 27 27
233 33 27 27 27 27
234 32 26 28 28 28

MEAN: 28.4 VARIANCE: 3.9 STD: 2.0
MIN: 25.0 MAX: 33.0 RANGE: 8.0

HISTOGRAM

LOW HIGH FTS Z
27.00 29.00 21 84.00 *****
29.00 31.00 0 0.00
31.00 33.00 4 16.00 *****

CLASS SITE 3

CLASS NO. 2 SITE NO. 1 BAND NO.05

SITE IS 5 BY 5 CENTERED ON: X 59 Y 232

57 58 59 60 61

230 27 27 27 28 28
231 27 27 27 28 28
232 27 26 26 27 27
233 27 26 26 27 27
234 26 26 28 26 26

MEAN: 27.0 VARIANCE: 0.5 STD: 0.7
MIN: 26.0 MAX: 28.0 RANGE: 2.0

HISTOGRAM

LOW HIGH FTS Z
26.00 28.00 25100.00 *****

CLASS SITE 3

CLASS NO. 2 SITE NO. 1 BAND NO.06

SITE IS 5 BY 5 CENTERED ON: X 59 Y 232

57 58 59 60 61

230 28 28 28 28 28
231 28 28 28 28 28
232 27 28 28 27 27
233 27 28 28 27 27
234 27 25 25 28 28

MEAN: 27.5 VARIANCE: 0.8 STD: 0.9
MIN: 25.0 MAX: 28.0 RANGE: 3.0

HISTOGRAM

LOW HIGH FTS Z
25.00 27.00 5 16.00 *****
27.00 29.00 16 64.00 *****

CLASS

CLASS NO. 2 SITE NO. 1 BAND NO.07

SITE IS 5 BY 5 CENTERED ON: X 59 Y 232

57 58 59 60 61

230 26 26 28 26 26
231 26 26 28 26 26
232 26 26 27 27 27
233 26 26 26 27 27
234 26 26 28 24 24

MEAN: 26.5 VARIANCE: 4.8 STD: 2.2
MIN: 25.0 MAX: 28.0 RANGE: 3.0

HISTOGRAM

LOW HIGH FTS Z
25.00 26.00 15 60.00 *****
26.00 26.00 6 24.00 *****
26.00 28.00 4 16.00 *****

CLASS
 CLASS NO. 2 SITE NO. 1 BAND NO. 08
 SITE IS 5 PY 5 CENTERED ON: X 59 Y 237
 57 58 59 60 61
 230 103 116 93 94 96
 231 115 101 92 93 113
 232 127 128 83 107 117
 233 109 120 89 110 121
 234 19 121 117 97 117

MEAN: 102.3 VARIANCE: 481.6 STD: 21.9
 MIN: 19.0 MAX: 128.0 RANGE: 109.0

HISTOGRAM

| LOW | HIGH | FIS | % |
|--------|--------|-----|-------------|
| 19.00 | 21.00 | 1 | 4.00 ** |
| 21.00 | 23.00 | 0 | 0.00 |
| 23.00 | 25.00 | 0 | 0.00 |
| 25.00 | 27.00 | 0 | 0.00 |
| 27.00 | 29.00 | 0 | 0.00 |
| 29.00 | 31.00 | 0 | 0.00 |
| 31.00 | 33.00 | 0 | 0.00 |
| 33.00 | 35.00 | 0 | 0.00 |
| 35.00 | 37.00 | 0 | 0.00 |
| 37.00 | 39.00 | 0 | 0.00 |
| 39.00 | 41.00 | 0 | 0.00 |
| 41.00 | 43.00 | 0 | 0.00 |
| 43.00 | 45.00 | 0 | 0.00 |
| 45.00 | 47.00 | 0 | 0.00 |
| 47.00 | 49.00 | 0 | 0.00 |
| 49.00 | 51.00 | 0 | 0.00 |
| 51.00 | 53.00 | 0 | 0.00 |
| 53.00 | 55.00 | 0 | 0.00 |
| 55.00 | 57.00 | 0 | 0.00 |
| 57.00 | 59.00 | 0 | 0.00 |
| 59.00 | 61.00 | 0 | 0.00 |
| 61.00 | 63.00 | 0 | 0.00 |
| 63.00 | 65.00 | 0 | 0.00 |
| 65.00 | 67.00 | 0 | 0.00 |
| 67.00 | 69.00 | 0 | 0.00 |
| 69.00 | 71.00 | 0 | 0.00 |
| 71.00 | 73.00 | 0 | 0.00 |
| 73.00 | 75.00 | 0 | 0.00 |
| 75.00 | 77.00 | 0 | 0.00 |
| 77.00 | 79.00 | 0 | 0.00 |
| 79.00 | 81.00 | 0 | 0.00 |
| 81.00 | 83.00 | 2 | 8.00 **** |
| 83.00 | 85.00 | 0 | 0.00 |
| 85.00 | 87.00 | 0 | 0.00 |
| 87.00 | 89.00 | 1 | 4.00 ** |
| 89.00 | 91.00 | 0 | 0.00 |
| 91.00 | 93.00 | 2 | 8.00 **** |
| 93.00 | 95.00 | 1 | 4.00 ** |
| 95.00 | 97.00 | 2 | 8.00 **** |
| 97.00 | 99.00 | 0 | 0.00 |
| 99.00 | 101.00 | 1 | 4.00 ** |
| 101.00 | 103.00 | 1 | 4.00 ** |
| 103.00 | 105.00 | 0 | 0.00 |
| 105.00 | 107.00 | 1 | 4.00 ** |
| 107.00 | 109.00 | 1 | 4.00 ** |
| 109.00 | 111.00 | 1 | 4.00 ** |
| 111.00 | 113.00 | 2 | 8.00 **** |
| 113.00 | 115.00 | 0 | 0.00 |
| 115.00 | 117.00 | 4 | 16.00 ***** |
| 117.00 | 119.00 | 0 | 0.00 |
| 119.00 | 121.00 | 3 | 12.00 ***** |
| 121.00 | 123.00 | 0 | 0.00 |
| 123.00 | 125.00 | 0 | 0.00 |
| 125.00 | 127.00 | 1 | 4.00 ** |
| 127.00 | 129.00 | 1 | 4.00 ** |

CLASS SITE 4
CLASS NO. 3 SITE NO. 1 BAND NO.04

SITE IS 5 BY 5 CENTERED ON: X 66 Y 207

| | | | | | |
|-----|----|----|----|----|----|
| | 64 | 65 | 66 | 67 | 68 |
| 205 | 34 | 24 | 27 | 27 | 28 |
| 206 | 35 | 27 | 27 | 27 | 28 |
| 207 | 35 | 27 | 27 | 27 | 28 |
| 208 | 35 | 24 | 24 | 24 | 27 |
| 209 | 35 | 24 | 24 | 24 | 27 |

MEAN: 27.8 VARIANCE: 14.7 STD: 3.8
MIN: 24.0 MAX: 35.0 RANGE: 11.0

HISTOGRAM

| LOW | HIGH | PTS | % |
|-------|-------|-----|-------------|
| 24.00 | 26.00 | 7 | 28.00 ***** |
| 26.00 | 28.00 | 13 | 52.00 ***** |
| 28.00 | 30.00 | 0 | 0.00 |
| 30.00 | 32.00 | 0 | 0.00 |
| 32.00 | 34.00 | 1 | 4.00 ** |
| 34.00 | 36.00 | 4 | 16.00 ***** |

CLASS SITE 4
CLASS NO. 3 SITE NO. 1 BAND NO.05

SITE IS 5 BY 5 CENTERED ON: X 66 Y 207

| | | | | | |
|-----|----|----|----|----|----|
| | 64 | 65 | 66 | 67 | 68 |
| 205 | 25 | 25 | 25 | 25 | 28 |
| 206 | 24 | 24 | 24 | 24 | 27 |
| 207 | 24 | 24 | 24 | 24 | 27 |
| 208 | 23 | 23 | 24 | 24 | 27 |
| 209 | 23 | 23 | 24 | 24 | 27 |

MEAN: 24.6 VARIANCE: 2.1 STD: 1.4
MIN: 23.0 MAX: 28.0 RANGE: 5.0

HISTOGRAM

| LOW | HIGH | PTS | % |
|-------|-------|-----|-------------|
| 23.00 | 25.00 | 20 | 80.00 ***** |
| 25.00 | 27.00 | 4 | 16.00 ***** |
| 27.00 | 29.00 | 1 | 4.00 ** |

CLASS SITE 4
CLASS NO. 3 SITE NO. 1 BAND NO.06

SITE IS 5 BY 5 CENTERED ON: X 66 Y 207

| | | | | | |
|-----|----|----|----|----|----|
| | 64 | 65 | 66 | 67 | 68 |
| 205 | 23 | 23 | 24 | 24 | 28 |
| 206 | 23 | 23 | 23 | 23 | 29 |
| 207 | 23 | 23 | 23 | 23 | 29 |
| 208 | 23 | 23 | 23 | 23 | 27 |
| 209 | 23 | 23 | 23 | 23 | 27 |

MEAN: 24.0 VARIANCE: 3.5 STD: 1.9
MIN: 23.0 MAX: 28.0 RANGE: 5.0

HISTOGRAM

| LOW | HIGH | PTS | % |
|-------|-------|-----|-------------|
| 23.00 | 24.00 | 20 | 80.00 ***** |
| 24.00 | 27.00 | 2 | 8.00 **** |
| 27.00 | 28.00 | 3 | 12.00 ***** |

CLASS SITE 4
CLASS NO. 3 SITE NO. 1 BAND NO.07

SITE IS 5 BY 5 CENTERED ON: X 66 Y 207

| | | | | | |
|-----|----|----|----|----|----|
| | 64 | 65 | 66 | 67 | 68 |
| 205 | 20 | 20 | 21 | 22 | 26 |
| 206 | 20 | 20 | 24 | 24 | 26 |
| 207 | 20 | 20 | 24 | 24 | 26 |
| 208 | 19 | 19 | 18 | 18 | 24 |
| 209 | 19 | 18 | 18 | 18 | 24 |

MEAN: 21.5 VARIANCE: 8.4 STD: 2.9
MIN: 18.0 MAX: 26.0 RANGE: 8.0

HISTOGRAM

| LOW | HIGH | PTS | % |
|-------|-------|-----|-------------|
| 18.00 | 20.00 | 10 | 40.00 ***** |
| 20.00 | 22.00 | 6 | 24.00 ***** |
| 22.00 | 24.00 | 6 | 24.00 ***** |
| 24.00 | 26.00 | 3 | 12.00 ***** |

CLASS
 CLASS NO. 3 SITE NO. 1 RAMP NO. 05

SITE IS 5 BY 5 CENTERED ON: X 65 Y 207

| | 64 | 65 | 66 | 67 | 68 |
|-----|-----|----|----|-----|----|
| 205 | 50 | 63 | 64 | 33 | 84 |
| 206 | 114 | 46 | 34 | 75 | 96 |
| 207 | 7 | 21 | 21 | 35 | 91 |
| 208 | 63 | 50 | 80 | 106 | 71 |
| 209 | 70 | 97 | 91 | 54 | 79 |

MEAN: 67.4 VARIANCE: 665.3 STD: 25.8
 MIN: 21.0 MAX: 114.0 RANGE: 93.0

HISTOGRAM

| Lower | Upper | FTS | % |
|--------|--------|-----|-----------|
| 23.00 | 24.00 | 2 | 8.00 **** |
| 24.00 | 25.00 | 0 | 0.00 |
| 25.00 | 26.00 | 0 | 0.00 |
| 26.00 | 27.00 | 0 | 0.00 |
| 27.00 | 28.00 | 0 | 0.00 |
| 28.00 | 29.00 | 0 | 0.00 |
| 29.00 | 30.00 | 0 | 0.00 |
| 30.00 | 31.00 | 0 | 0.00 |
| 31.00 | 32.00 | 1 | 4.00 ** |
| 32.00 | 33.00 | 2 | 8.00 **** |
| 33.00 | 34.00 | 0 | 0.00 |
| 34.00 | 35.00 | 0 | 0.00 |
| 35.00 | 36.00 | 0 | 0.00 |
| 36.00 | 37.00 | 0 | 0.00 |
| 37.00 | 38.00 | 0 | 0.00 |
| 38.00 | 39.00 | 0 | 0.00 |
| 39.00 | 40.00 | 0 | 0.00 |
| 40.00 | 41.00 | 0 | 0.00 |
| 41.00 | 42.00 | 0 | 0.00 |
| 42.00 | 43.00 | 0 | 0.00 |
| 43.00 | 44.00 | 0 | 0.00 |
| 44.00 | 45.00 | 0 | 0.00 |
| 45.00 | 46.00 | 0 | 0.00 |
| 46.00 | 47.00 | 0 | 0.00 |
| 47.00 | 48.00 | 1 | 4.00 ** |
| 48.00 | 49.00 | 1 | 4.00 ** |
| 49.00 | 50.00 | 0 | 0.00 |
| 50.00 | 51.00 | 2 | 8.00 **** |
| 51.00 | 52.00 | 0 | 0.00 |
| 52.00 | 53.00 | 0 | 0.00 |
| 53.00 | 54.00 | 0 | 0.00 |
| 54.00 | 55.00 | 0 | 0.00 |
| 55.00 | 56.00 | 0 | 0.00 |
| 56.00 | 57.00 | 2 | 8.00 **** |
| 57.00 | 58.00 | 0 | 0.00 |
| 58.00 | 59.00 | 0 | 0.00 |
| 59.00 | 60.00 | 0 | 0.00 |
| 60.00 | 61.00 | 0 | 0.00 |
| 61.00 | 62.00 | 2 | 8.00 **** |
| 62.00 | 63.00 | 0 | 0.00 |
| 63.00 | 64.00 | 0 | 0.00 |
| 64.00 | 65.00 | 0 | 0.00 |
| 65.00 | 66.00 | 0 | 0.00 |
| 66.00 | 67.00 | 1 | 4.00 ** |
| 67.00 | 68.00 | 1 | 4.00 ** |
| 68.00 | 69.00 | 1 | 4.00 ** |
| 69.00 | 70.00 | 1 | 4.00 ** |
| 70.00 | 71.00 | 1 | 4.00 ** |
| 71.00 | 72.00 | 1 | 4.00 ** |
| 72.00 | 73.00 | 1 | 4.00 ** |
| 73.00 | 74.00 | 1 | 4.00 ** |
| 74.00 | 75.00 | 1 | 4.00 ** |
| 75.00 | 76.00 | 1 | 4.00 ** |
| 76.00 | 77.00 | 1 | 4.00 ** |
| 77.00 | 78.00 | 1 | 4.00 ** |
| 78.00 | 79.00 | 1 | 4.00 ** |
| 79.00 | 80.00 | 0 | 0.00 |
| 80.00 | 81.00 | 0 | 0.00 |
| 81.00 | 82.00 | 0 | 0.00 |
| 82.00 | 83.00 | 0 | 0.00 |
| 83.00 | 84.00 | 2 | 8.00 **** |
| 84.00 | 85.00 | 0 | 0.00 |
| 85.00 | 86.00 | 0 | 0.00 |
| 86.00 | 87.00 | 0 | 0.00 |
| 87.00 | 88.00 | 0 | 0.00 |
| 88.00 | 89.00 | 2 | 8.00 **** |
| 89.00 | 90.00 | 2 | 8.00 **** |
| 90.00 | 91.00 | 2 | 8.00 **** |
| 91.00 | 92.00 | 0 | 0.00 |
| 92.00 | 93.00 | 0 | 0.00 |
| 93.00 | 94.00 | 0 | 0.00 |
| 94.00 | 95.00 | 0 | 0.00 |
| 95.00 | 96.00 | 2 | 8.00 **** |
| 96.00 | 97.00 | 2 | 8.00 **** |
| 97.00 | 98.00 | 0 | 0.00 |
| 98.00 | 99.00 | 0 | 0.00 |
| 99.00 | 100.00 | 0 | 0.00 |
| 100.00 | 101.00 | 0 | 0.00 |
| 101.00 | 102.00 | 0 | 0.00 |
| 102.00 | 103.00 | 0 | 0.00 |
| 103.00 | 104.00 | 0 | 0.00 |
| 104.00 | 105.00 | 0 | 0.00 |
| 105.00 | 106.00 | 1 | 4.00 ** |
| 106.00 | 107.00 | 1 | 4.00 ** |
| 107.00 | 108.00 | 0 | 0.00 |
| 108.00 | 109.00 | 0 | 0.00 |
| 109.00 | 110.00 | 0 | 0.00 |
| 110.00 | 111.00 | 0 | 0.00 |
| 111.00 | 112.00 | 0 | 0.00 |
| 112.00 | 113.00 | 0 | 0.00 |
| 113.00 | 114.00 | 1 | 4.00 ** |

CLASS SITE 5
CLASS NO. 4 SITE NO. 1 BAND NO.04

SITE IS 5 BY 5 CENTERED ON: X 65 Y 252

| | 63 | 64 | 65 | 66 | 67 |
|-----|----|----|----|----|----|
| 250 | 31 | 27 | 27 | 27 | 27 |
| 251 | 31 | 27 | 27 | 27 | 27 |
| 252 | 33 | 27 | 27 | 27 | 27 |
| 253 | 33 | 27 | 27 | 27 | 27 |
| 254 | 35 | 28 | 28 | 26 | 28 |

MEAN: 28.2 VARIANCE: 5.3 STD: 2.3
MIN: 27.0 MAX: 35.0 RANGE: 8.0

HISTOGRAM

| LOW | HIGH | PTS | % |
|-------|-------|-----|-------------|
| 27.00 | 29.00 | 20 | 80.00 ***** |
| 29.00 | 31.00 | 2 | 8.00 **** |
| 31.00 | 33.00 | 2 | 8.00 **** |
| 33.00 | 35.00 | 1 | 4.00 ** |

CLASS SITE 5
CLASS NO. 4 SITE NO. 1 BAND NO.04

SITE IS 5 BY 5 CENTERED ON: X 65 Y 252

| | 63 | 64 | 65 | 66 | 67 |
|-----|----|----|----|----|----|
| 250 | 24 | 24 | 24 | 26 | 26 |
| 251 | 24 | 24 | 24 | 26 | 26 |
| 252 | 23 | 25 | 25 | 26 | 26 |
| 253 | 24 | 25 | 25 | 26 | 26 |
| 254 | 24 | 27 | 27 | 24 | 24 |

MEAN: 25.0 VARIANCE: 1.4 STD: 1.2
MIN: 23.0 MAX: 27.0 RANGE: 4.0

HISTOGRAM

| LOW | HIGH | PTS | % |
|-------|-------|-----|-------------|
| 23.00 | 25.00 | 15 | 60.00 ***** |
| 25.00 | 27.00 | 10 | 40.00 ***** |

CLASS SITE 5
CLASS NO. 4 SITE NO. 1 BAND NO.06

SITE IS 5 BY 5 CENTERED ON: X 65 Y 252

| | 63 | 64 | 65 | 66 | 67 |
|-----|----|----|----|----|----|
| 250 | 25 | 25 | 25 | 25 | 25 |
| 251 | 25 | 25 | 25 | 25 | 25 |
| 252 | 23 | 23 | 23 | 25 | 25 |
| 253 | 23 | 23 | 23 | 25 | 25 |
| 254 | 25 | 25 | 25 | 25 | 25 |

MEAN: 24.4 VARIANCE: 1.0 STD: 1.0
MIN: 23.0 MAX: 25.0 RANGE: 2.0

HISTOGRAM

| LOW | HIGH | PTS | % |
|-------|-------|-----|-------------|
| 23.00 | 24.00 | 8 | 20.00 ***** |
| 24.00 | 25.00 | 18 | 45.00 ***** |

CLASS SITE 5
CLASS NO. 4 SITE NO. 1 BAND NO.06

SITE IS 5 BY 5 CENTERED ON: X 65 Y 252

| | 63 | 64 | 65 | 66 | 67 |
|-----|----|----|----|----|----|
| 250 | 18 | 20 | 20 | 22 | 22 |
| 251 | 18 | 20 | 20 | 22 | 22 |
| 252 | 20 | 20 | 20 | 22 | 22 |
| 253 | 20 | 20 | 20 | 22 | 22 |
| 254 | 20 | 26 | 26 | 22 | 22 |

MEAN: 20.6 VARIANCE: 1.6 STD: 1.3
MIN: 18.0 MAX: 26.0 RANGE: 4.0

HISTOGRAM

| LOW | HIGH | PTS | % |
|-------|-------|-----|-------------|
| 18.00 | 20.00 | 15 | 60.00 ***** |
| 20.00 | 22.00 | 10 | 40.00 ***** |

CLASS

1 1000 NO. 4 SITE NO. 1 HAMP NULOP

SITE IS 5 FT 5 CENTERED UNIT X 60 Y 200

| | 63 | 64 | 65 | 66 | 67 |
|-----|----|-----|-----|----|----|
| 100 | 0 | 70 | 93 | 97 | 75 |
| 105 | 48 | 58 | 102 | 78 | 58 |
| 110 | 10 | 10 | 125 | 90 | 90 |
| 115 | 4 | 10 | 108 | 60 | 90 |
| 124 | 70 | 100 | 85 | 98 | 60 |

MEAN: 87.0 VARIANCE: 819.0 STD: 28.4
 MIN: 20.0 MAX: 115.0 RANGE: 100%

HISTOGRAM

| BIN | START | END | FREQ | REL |
|--------|--------|--------|------|-------------|
| 20.00 | 20.00 | 24.00 | 1 | 4.00 ** |
| 24.00 | 24.00 | 28.00 | 0 | 0.00 |
| 28.00 | 28.00 | 32.00 | 0 | 0.00 |
| 32.00 | 32.00 | 36.00 | 0 | 0.00 |
| 36.00 | 36.00 | 40.00 | 0 | 0.00 |
| 40.00 | 40.00 | 44.00 | 1 | 4.00 ** |
| 44.00 | 44.00 | 48.00 | 0 | 0.00 |
| 48.00 | 48.00 | 52.00 | 0 | 0.00 |
| 52.00 | 52.00 | 56.00 | 1 | 4.00 ** |
| 56.00 | 56.00 | 60.00 | 1 | 4.00 ** |
| 60.00 | 60.00 | 64.00 | 0 | 0.00 |
| 64.00 | 64.00 | 68.00 | 0 | 0.00 |
| 68.00 | 68.00 | 72.00 | 1 | 4.00 ** |
| 72.00 | 72.00 | 76.00 | 2 | 8.00 **** |
| 76.00 | 76.00 | 80.00 | 0 | 0.00 |
| 80.00 | 80.00 | 84.00 | 0 | 0.00 |
| 84.00 | 84.00 | 88.00 | 1 | 4.00 ** |
| 88.00 | 88.00 | 92.00 | 0 | 0.00 |
| 92.00 | 92.00 | 96.00 | 1 | 4.00 ** |
| 96.00 | 96.00 | 100.00 | 1 | 4.00 ** |
| 100.00 | 100.00 | 104.00 | 3 | 12.00 ***** |
| 104.00 | 104.00 | 108.00 | 0 | 0.00 |
| 108.00 | 108.00 | 112.00 | 0 | 0.00 |
| 112.00 | 112.00 | 116.00 | 0 | 0.00 |
| 116.00 | 116.00 | 120.00 | 0 | 0.00 |
| 120.00 | 120.00 | 124.00 | 1 | 4.00 ** |
| 124.00 | 124.00 | 128.00 | 1 | 4.00 ** |
| 128.00 | 128.00 | 130.00 | 0 | 0.00 |
| 130.00 | 130.00 | 134.00 | 1 | 4.00 ** |

CLASS SITE 6
 CLASS NO. 5 SITE NO. 1 BAND NO.04
 SITE IS 5 Pr 5 CENTERED ON: X 46 Y 277

44 45 46 47 48

275 32 32 31 31 31
 276 30 30 30 30 30
 277 30 30 30 30 30
 278 30 30 31 31 31
 279 30 30 31 31 31

MEAN: 30.5 VARIANCE: 0.4 STD: 0.7
 MIN: 30.0 MAX: 32.0 RANGE: 2.0

HISTOGRAM
 LOW HIGH FTS %
 30.00 32.00 2500.00 *****

CLASS SITE 6
 CLASS NO. 5 SITE NO. 1 BAND NO.05
 SITE IS 5 Pr 5 CENTERED ON: X 46 Y 277

44 45 46 47 48

275 29 29 28 28 28
 276 30 30 30 30 30
 277 30 30 30 30 30
 278 31 31 31 31 31
 279 32 32 32 32 32

MEAN: 30.5 VARIANCE: 2.0 STD: 1.4
 MIN: 28.0 MAX: 32.0 RANGE: 4.0

HISTOGRAM
 LOW HIGH FTS %
 28.00 32.00 1500.00 *****
 30.00 32.00 1000.00 *****

CLASS SITE 6
 CLASS NO. 5 SITE NO. 1 BAND NO.06
 SITE IS 5 Pr 5 CENTERED ON: X 46 Y 277

44 45 46 47 48

275 30 30 26 26 26
 276 30 30 28 28 28
 277 30 30 28 28 28
 278 31 31 28 28 28
 279 31 31 29 29 28

MEAN: 28.2 VARIANCE: 2.5 STD: 1.6
 MIN: 26.0 MAX: 31.0 RANGE: 5.0

HISTOGRAM
 LOW HIGH FTS %
 26.00 28.00 1500.00 *****
 28.00 30.00 600.00 *****
 30.00 32.00 400.00 *****

CLASS SITE 6
 CLASS NO. 5 SITE NO. 1 BAND NO.07
 SITE IS 5 Pr 5 CENTERED ON: X 46 Y 277

44 45 46 47 48

275 26 26 26 26 26
 276 26 26 26 26 26
 277 26 26 26 26 26
 278 26 26 26 26 26
 279 26 26 26 26 26

MEAN: 26.0 VARIANCE: 1.0 STD: 1.0
 MIN: 24.0 MAX: 26.0 RANGE: 2.0

HISTOGRAM
 LOW HIGH FTS %
 24.00 26.00 2500.00 *****

CLASS
 CLASS NO. 5 SITE NO. 1 BAND NO. 08
 SITE IS 5 BY 5 CENTERED ON: X 46 Y 27
 44 45 46 47 48

| | | | | | |
|-----|-----|-----|-----|-----|-----|
| 27 | 90 | 118 | 132 | 32 | 83 |
| 276 | 123 | 112 | 83 | 77 | 118 |
| 277 | 98 | 120 | 85 | 118 | 86 |
| 278 | 87 | 118 | 90 | 112 | 86 |
| 279 | 81 | 98 | 101 | 110 | 44 |

MEAN: 91.2 VARIANCE: 544.0 STD. DEV: 23.3
 MIN: 81.0 MAX: 123.0 RANGE: 42.0

HISTOGRAM

| Bin | RTN | FTR | S |
|--------|--------|-----|-----------|
| 32.00 | 34.00 | 1 | 4.00 ** |
| 34.00 | 36.00 | 0 | 0.00 |
| 36.00 | 38.00 | 0 | 0.00 |
| 38.00 | 40.00 | 0 | 0.00 |
| 40.00 | 42.00 | 0 | 0.00 |
| 42.00 | 44.00 | 1 | 4.00 ** |
| 44.00 | 46.00 | 0 | 0.00 |
| 46.00 | 48.00 | 0 | 0.00 |
| 48.00 | 50.00 | 0 | 0.00 |
| 50.00 | 52.00 | 0 | 0.00 |
| 52.00 | 54.00 | 0 | 0.00 |
| 54.00 | 56.00 | 0 | 0.00 |
| 56.00 | 58.00 | 0 | 0.00 |
| 58.00 | 60.00 | 0 | 0.00 |
| 60.00 | 62.00 | 0 | 0.00 |
| 62.00 | 64.00 | 0 | 0.00 |
| 64.00 | 66.00 | 0 | 0.00 |
| 66.00 | 68.00 | 0 | 0.00 |
| 68.00 | 70.00 | 1 | 4.00 ** |
| 70.00 | 72.00 | 1 | 4.00 ** |
| 72.00 | 74.00 | 0 | 0.00 |
| 74.00 | 76.00 | 0 | 0.00 |
| 76.00 | 78.00 | 0 | 0.00 |
| 78.00 | 80.00 | 0 | 0.00 |
| 80.00 | 82.00 | 1 | 4.00 ** |
| 82.00 | 84.00 | 2 | 8.00 **** |
| 84.00 | 86.00 | 2 | 8.00 **** |
| 86.00 | 88.00 | 1 | 4.00 ** |
| 88.00 | 90.00 | 2 | 8.00 **** |
| 90.00 | 92.00 | 0 | 0.00 |
| 92.00 | 94.00 | 0 | 0.00 |
| 94.00 | 96.00 | 1 | 4.00 ** |
| 96.00 | 98.00 | 1 | 4.00 ** |
| 98.00 | 100.00 | 0 | 0.00 |
| 100.00 | 102.00 | 1 | 4.00 ** |
| 102.00 | 104.00 | 0 | 0.00 |
| 104.00 | 106.00 | 0 | 0.00 |
| 106.00 | 108.00 | 0 | 0.00 |
| 108.00 | 110.00 | 1 | 4.00 ** |
| 110.00 | 112.00 | 2 | 8.00 **** |
| 112.00 | 114.00 | 0 | 0.00 |
| 114.00 | 116.00 | 1 | 4.00 ** |
| 116.00 | 118.00 | 2 | 8.00 **** |
| 118.00 | 120.00 | 2 | 8.00 **** |
| 120.00 | 122.00 | 0 | 0.00 |
| 122.00 | 124.00 | 1 | 4.00 ** |
| 124.00 | 126.00 | 0 | 0.00 |
| 126.00 | 128.00 | 0 | 0.00 |
| 128.00 | 130.00 | 0 | 0.00 |
| 130.00 | 132.00 | 0 | 0.00 |
| 132.00 | 134.00 | 1 | 4.00 ** |

CLASS SITE 7

CLASS NO. 6 SITE NO. 1 BAND NO.04

SITE IS 5 BY 5 CENTERED ON: X 86 Y 139

R4 R5 R6 R7 R8

137 35 35 37 37 37
 138 35 35 36 38 35
 139 36 35 38 38 35
 140 34 33 35 35 35
 141 34 33 35 35 35

MEAN: 35.8 VARIANCE: 2.7 STD: 1.6
 MIN: 33.0 MAX: 39.0 RANGE: 6.0

HISTOGRAM

| LOW | HIGH | PTS | % |
|-------|-------|-----|-------------|
| 33.00 | 35.00 | 14 | 56.00 ***** |
| 35.00 | 37.00 | 8 | 24.00 ***** |
| 37.00 | 39.00 | 5 | 20.00 ***** |

CLASS SITE 7

CLASS NO. 6 SITE NO. 1 BAND NO.05

SITE IS 5 BY 5 CENTERED ON: X 86 Y 139

R4 R5 R6 R7 R8

137 40 40 41 41 42
 138 36 36 41 41 36
 139 36 36 41 41 36
 140 37 39 39 39 39
 141 39 39 39 39 39

MEAN: 39.0 VARIANCE: 4.1 STD: 2.0
 MIN: 36.0 MAX: 42.0 RANGE: 6.0

HISTOGRAM

| LOW | HIGH | PTS | % |
|-------|-------|-----|-------------|
| 36.00 | 38.00 | 6 | 24.00 ***** |
| 38.00 | 40.00 | 12 | 48.00 ***** |
| 40.00 | 42.00 | 7 | 28.00 ***** |

CLASS SITE 7

CLASS NO. 6 SITE NO. 1 BAND NO.06

SITE IS 5 BY 5 CENTERED ON: X 86 Y 139

R4 R5 R6 R7 R8

137 38 38 40 40 48
 138 37 37 35 39 37
 139 37 37 39 39 37
 140 35 35 37 39 35
 141 35 35 39 39 35

MEAN: 37.5 VARIANCE: 2.9 STD: 1.7
 MIN: 35.0 MAX: 40.0 RANGE: 5.0

HISTOGRAM

| LOW | HIGH | PTS | % |
|-------|-------|-----|-------------|
| 35.00 | 37.00 | 12 | 48.00 ***** |
| 37.00 | 39.00 | 11 | 44.00 ***** |
| 39.00 | 41.00 | 2 | 8.00 **** |

CLASS

CLASS NO. 6 SITE NO. 1 BAND NO.

SITE IS 5 BY 5 CENTERED ON: X 86 Y 139

R4 R5 R6 R7 R8

137 34 36 37 41 36
 138 35 37 36 39 34
 139 37 37 35 34 34
 140 34 37 34 34 35
 141 34 39 34 34 35

MEAN: 37.4 VARIANCE: 1.2 STD: 1.1
 MIN: 34.0 MAX: 39.0 RANGE: 4.0

HISTOGRAM

| LOW | HIGH | PTS | % |
|-------|-------|-----|-------------|
| 34.00 | 36.00 | 24 | 96.00 ***** |
| 36.00 | 38.00 | 1 | 4.00 ** |

CLASS
 CLASS NO. 6 SITE NO. 1 BAND NO. 06

STIP IS 5 BY 5 CENTERED ON: 2 6c 5 13c

| | B4 | B5 | B6 | B7 | B8 |
|-----|----|----|----|----|----|
| 137 | 0 | 27 | 79 | 94 | 87 |
| 138 | 0 | 47 | 63 | 42 | 47 |
| 139 | 0 | 65 | 5 | 28 | 26 |
| 140 | 0 | 78 | 24 | 41 | 44 |
| 141 | 0 | 67 | 66 | 70 | 41 |

MEAN: 44.4 VARIANCE: 89.4 STD: 9.46
 MIN: 0.0 MAX: 94.0 RANGE: 94.0

HISTOGRAM

| LOW | HIGH | FREQ | % |
|-------|-------|------|-------------|
| 0.00 | 2.00 | 5 | 20.00 ***** |
| 2.00 | 4.00 | 0 | 0.00 |
| 4.00 | 6.00 | 0 | 0.00 |
| 6.00 | 8.00 | 0 | 0.00 |
| 8.00 | 10.00 | 0 | 0.00 |
| 10.00 | 12.00 | 0 | 0.00 |
| 12.00 | 14.00 | 0 | 0.00 |
| 14.00 | 16.00 | 0 | 0.00 |
| 16.00 | 18.00 | 0 | 0.00 |
| 18.00 | 20.00 | 0 | 0.00 |
| 20.00 | 22.00 | 0 | 0.00 |
| 22.00 | 24.00 | 0 | 0.00 |
| 24.00 | 26.00 | 1 | 4.00 **** |
| 26.00 | 28.00 | 1 | 4.00 **** |
| 28.00 | 30.00 | 0 | 0.00 |
| 30.00 | 32.00 | 0 | 0.00 |
| 32.00 | 34.00 | 0 | 0.00 |
| 34.00 | 36.00 | 1 | 4.00 |
| 36.00 | 38.00 | 0 | 0.00 |
| 38.00 | 40.00 | 0 | 0.00 |
| 40.00 | 42.00 | 3 | 12.00 ***** |
| 42.00 | 44.00 | 1 | 4.00 ** |
| 44.00 | 46.00 | 0 | 0.00 |
| 46.00 | 48.00 | 1 | 4.00 ** |
| 48.00 | 50.00 | 1 | 4.00 ** |
| 50.00 | 52.00 | 1 | 4.00 ** |
| 52.00 | 54.00 | 0 | 0.00 |
| 54.00 | 56.00 | 0 | 0.00 |
| 56.00 | 58.00 | 0 | 0.00 |
| 58.00 | 60.00 | 0 | 0.00 |
| 60.00 | 62.00 | 1 | 4.00 ** |
| 62.00 | 64.00 | 0 | 0.00 |
| 64.00 | 66.00 | 1 | 4.00 ** |
| 66.00 | 68.00 | 1 | 4.00 ** |
| 68.00 | 70.00 | 1 | 4.00 ** |
| 70.00 | 72.00 | 0 | 0.00 |
| 72.00 | 74.00 | 0 | 0.00 |
| 74.00 | 76.00 | 0 | 0.00 |
| 76.00 | 78.00 | 1 | 4.00 ** |
| 78.00 | 80.00 | 1 | 4.00 ** |
| 80.00 | 82.00 | 0 | 0.00 |
| 82.00 | 84.00 | 1 | 4.00 ** |
| 84.00 | 86.00 | 0 | 0.00 |
| 86.00 | 88.00 | 1 | 4.00 ** |
| 88.00 | 90.00 | 0 | 0.00 |
| 90.00 | 92.00 | 0 | 0.00 |
| 92.00 | 94.00 | 1 | 4.00 ** |

CLASS SITE B
 CLASS NO. 7 SITE NO. 1 BAND NO.04
 SITE IS 5 BY 5 CENTERED ON: X 103 Y 43

101 102 103 104 105

41 37 37 37 37 37
 42 38 38 38 38 38
 43 38 38 38 38 38
 44 37 37 37 37 37
 45 37 37 37 37 37

MEAN: 37.4 VARIANCE: 0.2 STD: 0.5
 MIN: 37.0 MAX: 38.0 RANGE: 1.0

HISTOGRAM

| LOW | HIGH | PTS | % |
|-------|-------|----------|-------|
| 37.00 | 39.00 | 25100.00 | ***** |

CLASS SITE B
 CLASS NO. 7 SITE NO. 1 BAND NO.05
 SITE IS 5 BY 5 CENTERED ON: X 103 Y 43

101 102 103 104 105

41 42 42 42 39 39
 42 44 44 44 44 44
 43 44 44 44 44 44
 44 39 39 42 42 42
 45 39 39 39 42 42

MEAN: 41.8 VARIANCE: 4.6 STD: 2.2
 MIN: 39.0 MAX: 44.0 RANGE: 5.0

HISTOGRAM

| LOW | HIGH | PTS | % |
|-------|-------|----------|-------|
| 39.00 | 41.00 | 8 32.00 | ***** |
| 41.00 | 43.00 | 7 28.00 | ***** |
| 43.00 | 45.00 | 10 40.00 | ***** |

CLASS SITE B
 CLASS NO. 7 SITE NO. 1 BAND NO.06
 SITE IS 5 BY 5 CENTERED ON: X 103 Y 43

101 102 103 104 105

41 45 40 40 43 43
 42 41 41 41 41 41
 43 41 41 41 41 41
 44 41 43 43 45 45
 45 41 43 43 45 45

MEAN: 42.2 VARIANCE: 2.9 STD: 1.7
 MIN: 40.0 MAX: 45.0 RANGE: 5.0

HISTOGRAM

| LOW | HIGH | PTS | % |
|-------|-------|----------|-------|
| 40.00 | 42.00 | 14 56.00 | ***** |
| 42.00 | 44.00 | 6 24.00 | ***** |
| 44.00 | 46.00 | 5 20.00 | ***** |

CLASS SITE B
 CLASS NO. 7 SITE NO. 1 BAND NO.07
 SITE IS 5 BY 5 CENTERED ON: X 103 Y 43

101 102 103 104 105

41 46 46 46 46 46
 42 46 46 46 46 46
 43 46 46 46 46 46
 44 46 46 46 46 46
 45 46 46 46 46 46

MEAN: 47.5 VARIANCE: 0.8 STD: 0.9
 MIN: 46.0 MAX: 48.0 RANGE: 2.0

HISTOGRAM

| LOW | HIGH | PTS | % |
|-------|-------|----------|-------|
| 46.00 | 48.00 | 25100.00 | ***** |

CLASS
 CLASS NO. 7 SITE NO. 1 BAND NO. 06

SITE IS 5 BY 5 CENTERED ON: > 103 Y 40

101 102 104 104 105

| | | | | | |
|----|----|----|----|----|----|
| 41 | 50 | 40 | 54 | 42 | 73 |
| 42 | 73 | 41 | 39 | 28 | 59 |
| 43 | 61 | 43 | 79 | 59 | 60 |
| 44 | 53 | 65 | 66 | 36 | 90 |
| 45 | 35 | 56 | 35 | 48 | 75 |

MEAN: 54.5 VARIANCE: 246.8 STD: 15.7
 MIN: 28.0 MAX: 90.0 RANGE: 62.0

HISTOGRAM

| BIN | RANGE | FREQ | % |
|-------|-------|------|-----------|
| 30.00 | 30.00 | 1 | 4.00 ** |
| 32.00 | 32.00 | 0 | 0.00 |
| 34.00 | 34.00 | 0 | 0.00 |
| 36.00 | 36.00 | 2 | 8.00 **** |
| 38.00 | 38.00 | 1 | 4.00 ** |
| 40.00 | 40.00 | 1 | 4.00 ** |
| 42.00 | 42.00 | 2 | 8.00 **** |
| 44.00 | 44.00 | 0 | 0.00 |
| 46.00 | 46.00 | 0 | 0.00 |
| 48.00 | 48.00 | 1 | 4.00 ** |
| 50.00 | 50.00 | 1 | 4.00 ** |
| 52.00 | 52.00 | 0 | 0.00 |
| 54.00 | 54.00 | 2 | 8.00 **** |
| 56.00 | 56.00 | 2 | 8.00 **** |
| 58.00 | 58.00 | 0 | 0.00 |
| 60.00 | 60.00 | 2 | 8.00 **** |
| 62.00 | 62.00 | 1 | 4.00 ** |
| 64.00 | 64.00 | 0 | 0.00 |
| 66.00 | 66.00 | 2 | 8.00 **** |
| 68.00 | 68.00 | 0 | 0.00 |
| 70.00 | 70.00 | 0 | 0.00 |
| 72.00 | 72.00 | 0 | 0.00 |
| 74.00 | 74.00 | 2 | 8.00 **** |
| 76.00 | 76.00 | 1 | 4.00 ** |
| 78.00 | 78.00 | 0 | 0.00 |
| 80.00 | 80.00 | 1 | 4.00 ** |
| 82.00 | 82.00 | 0 | 0.00 |
| 84.00 | 84.00 | 0 | 0.00 |
| 86.00 | 86.00 | 0 | 0.00 |
| 88.00 | 88.00 | 0 | 0.00 |
| 90.00 | 90.00 | 1 | 4.00 ** |

CLASS SITE 9
 CLASS NO. 8 SITE NO. 1 BAND NO.04

SITE IS 9 BY 9 CENTERED ON: X 173 Y 104

169 170 171 172 173 174 175 176 177

| | | | | | | | | | |
|-----|----|----|----|----|----|----|----|----|----|
| 100 | 33 | 33 | 33 | 33 | 33 | 33 | 33 | 30 | 30 |
| 101 | 33 | 33 | 33 | 33 | 33 | 33 | 33 | 30 | 30 |
| 102 | 35 | 35 | 35 | 33 | 33 | 35 | 35 | 35 | 35 |
| 103 | 35 | 35 | 35 | 33 | 33 | 35 | 35 | 35 | 35 |
| 104 | 35 | 33 | 33 | 33 | 33 | 33 | 33 | 33 | 33 |
| 105 | 35 | 33 | 33 | 33 | 33 | 33 | 33 | 33 | 33 |
| 106 | 32 | 32 | 32 | 35 | 35 | 35 | 35 | 35 | 35 |
| 107 | 32 | 32 | 32 | 35 | 35 | 35 | 35 | 35 | 35 |
| 108 | 34 | 34 | 34 | 34 | 34 | 31 | 31 | 31 | 31 |

MEAN: 33.4 VARIANCE: 2.0 STD: 1.4
 MIN: 30.0 MAX: 35.0 RANGE: 5.0

HISTOGRAM

| LOW | HIGH | PTS | % |
|-------|-------|-----|-------------|
| 30.00 | 32.00 | 14 | 17.28 ***** |
| 32.00 | 34.00 | 39 | 48.15 ***** |
| 34.00 | 36.00 | 28 | 34.57 ***** |

CLASS SITE 9
 CLASS NO. 8 SITE NO. 1 BAND NO.05

SITE IS 9 BY 9 CENTERED ON: X 173 Y 104

169 170 171 172 173 174 175 176 177

| | | | | | | | | | |
|-----|----|----|----|----|----|----|----|----|----|
| 100 | 35 | 35 | 35 | 33 | 33 | 35 | 35 | 35 | 35 |
| 101 | 35 | 35 | 35 | 33 | 33 | 35 | 35 | 35 | 35 |
| 102 | 34 | 34 | 34 | 33 | 33 | 36 | 36 | 34 | 34 |
| 103 | 34 | 34 | 34 | 33 | 33 | 36 | 36 | 34 | 34 |
| 104 | 37 | 35 | 35 | 33 | 33 | 35 | 35 | 35 | 35 |
| 105 | 3 | 35 | 35 | 33 | 33 | 35 | 35 | 35 | 35 |
| 106 | 34 | 34 | 34 | 35 | 35 | 35 | 35 | 34 | 34 |
| 107 | 34 | 34 | 34 | 35 | 35 | 35 | 35 | 34 | 34 |
| 108 | 36 | 36 | 36 | 34 | 34 | 34 | 34 | 34 | 34 |

MEAN: 34.5 VARIANCE: 0.9 STD: 0.9
 MIN: 33.0 MAX: 37.0 RANGE: 4.0

HISTOGRAM

| LOW | HIGH | PTS | % |
|-------|-------|-----|-------------|
| 33.00 | 35.00 | 72 | 88.89 ***** |
| 35.00 | 37.00 | 9 | 11.11 ***** |

CLASS SITE 9
 CLASS NO. 8 SITE NO. 1 BAND NO.06

SITE IS 9 BY 9 CENTERED ON: X 173 Y 104

169 170 171 172 173 174 175 176 177

| | | | | | | | | | |
|-----|----|----|----|----|----|----|----|----|----|
| 100 | 33 | 33 | 33 | 34 | 34 | 33 | 33 | 34 | 33 |
| 101 | 33 | 33 | 33 | 34 | 34 | 33 | 33 | 33 | 33 |
| 102 | 35 | 33 | 33 | 31 | 31 | 35 | 35 | 33 | 33 |
| 103 | 35 | 33 | 33 | 31 | 31 | 35 | 35 | 33 | 33 |
| 104 | 35 | 32 | 32 | 32 | 32 | 32 | 32 | 32 | 32 |
| 105 | 35 | 32 | 32 | 32 | 32 | 32 | 32 | 32 | 32 |
| 106 | 33 | 33 | 34 | 35 | 35 | 33 | 33 | 35 | 35 |
| 107 | 33 | 33 | 33 | 35 | 35 | 33 | 33 | 35 | 35 |
| 108 | 33 | 33 | 33 | 33 | 33 | 33 | 33 | 36 | 36 |

MEAN: 33.2 VARIANCE: 1.4 STD: 1.2
 MIN: 31.0 MAX: 36.0 RANGE: 5.0

HISTOGRAM

| LOW | HIGH | PTS | % |
|-------|-------|-----|-------------|
| 31.00 | 34.00 | 59 | 72.84 ***** |
| 33.00 | 35.00 | 20 | 24.69 ***** |
| 35.00 | 37.00 | 2 | 2.47 ***** |

CLASS SITE 9
 CLASS NO. 8 SITE NO. 1 BAND NO. 0

SITE IS 9 BY 9 CENTERED ON: X 173 Y 104

169 170 171 172 173 174 175 176 177

| | | | | | | | | | |
|-----|----|----|----|----|----|----|----|----|----|
| 100 | 38 | 36 | 36 | 28 | 28 | 30 | 30 | 30 | 30 |
| 101 | 38 | 36 | 36 | 28 | 28 | 30 | 30 | 30 | 30 |
| 102 | 30 | 35 | 35 | 30 | 30 | 30 | 30 | 30 | 30 |
| 103 | 30 | 35 | 35 | 30 | 30 | 30 | 30 | 30 | 30 |
| 104 | 37 | 30 | 30 | 28 | 28 | 30 | 30 | 32 | 32 |
| 105 | 37 | 30 | 30 | 28 | 28 | 30 | 30 | 32 | 32 |
| 106 | 28 | 30 | 30 | 30 | 30 | 30 | 30 | 28 | 28 |
| 107 | 28 | 30 | 30 | 30 | 30 | 30 | 30 | 28 | 28 |
| 108 | 30 | 30 | 30 | 30 | 30 | 30 | 30 | 32 | 32 |

MEAN: 30.0 VARIANCE: 1.8 STD: 1.3
 MIN: 28.0 MAX: 32.0 RANGE: 4.0

HISTOGRAM

| LOW | HIGH | PTS | % |
|-------|-------|-----|-------------|
| 28.00 | 30.00 | 65 | 80.25 ***** |
| 30.00 | 32.00 | 16 | 19.75 ***** |

CLASS
 CL-55 8 SITE NO. 1 RANT NO.08

SITE IS 9 BY 9 CENTERED ON: X 173 Y 104

169 170 171 172 173 174 175 176 177

| | | | | | | | | | |
|-----|----|----|----|----|----|----|----|----|----|
| 169 | 44 | 41 | 81 | 14 | 20 | 21 | 40 | 21 | 10 |
| 170 | 37 | 31 | 81 | 11 | 20 | 21 | 31 | 21 | 41 |
| 171 | 34 | 40 | 45 | 17 | 13 | 31 | 16 | 17 | 29 |
| 172 | 20 | 44 | 18 | 15 | 20 | 56 | 31 | 31 | 14 |
| 173 | 40 | 24 | 30 | 36 | 28 | 28 | 16 | 31 | 54 |
| 174 | 11 | 38 | 24 | 36 | 14 | 44 | 31 | 21 | 10 |
| 175 | 11 | 44 | 40 | 20 | 44 | 24 | 11 | 21 | 19 |
| 176 | 44 | 18 | 14 | 18 | 48 | 30 | 61 | 40 | 80 |
| 177 | 20 | 11 | 12 | 14 | 12 | 20 | 21 | 34 | 10 |

MEAN: 32.4 VARIANCE: 311.4 STD: 17.6
 MIN: 11.0 MAX: 85.0 RANGE: 74.0

HISTOGRAM

| FROM | TO | FREQ | Z |
|-------|-------|------|-----------|
| 11.00 | 13.00 | 6 | 7.41 *** |
| 13.00 | 15.00 | 5 | 6.17 *** |
| 15.00 | 17.00 | 5 | 6.17 *** |
| 17.00 | 19.00 | 6 | 7.41 *** |
| 19.00 | 21.00 | 6 | 7.41 *** |
| 21.00 | 23.00 | 5 | 6.17 *** |
| 23.00 | 25.00 | 5 | 6.17 *** |
| 25.00 | 27.00 | 3 | 3.70 * |
| 27.00 | 29.00 | 0 | 0.00 |
| 29.00 | 31.00 | 1 | 8.64 **** |
| 31.00 | 33.00 | 1 | 1.23 |
| 33.00 | 35.00 | 4 | 4.94 ** |
| 35.00 | 37.00 | 4 | 3.68 ** |
| 37.00 | 39.00 | 1 | 1.23 |
| 39.00 | 41.00 | 4 | 4.94 ** |
| 41.00 | 43.00 | 1 | 1.23 |
| 43.00 | 45.00 | 2 | 2.47 * |
| 45.00 | 47.00 | 4 | 4.94 ** |
| 47.00 | 49.00 | 1 | 1.23 |
| 49.00 | 51.00 | 0 | 0.00 |
| 51.00 | 53.00 | 0 | 0.00 |
| 53.00 | 55.00 | 1 | 1.23 |
| 55.00 | 57.00 | 1 | 1.23 |
| 57.00 | 59.00 | 1 | 1.23 |
| 59.00 | 61.00 | 2 | 2.47 * |
| 61.00 | 63.00 | 1 | 1.23 |
| 63.00 | 65.00 | 0 | 0.00 |
| 65.00 | 67.00 | 0 | 0.00 |
| 67.00 | 69.00 | 0 | 0.00 |
| 69.00 | 71.00 | 1 | 1.23 |
| 71.00 | 73.00 | 0 | 0.00 |
| 73.00 | 75.00 | 0 | 0.00 |
| 75.00 | 77.00 | 1 | 1.23 |
| 77.00 | 79.00 | 1 | 1.23 |
| 79.00 | 81.00 | 1 | 1.23 |
| 81.00 | 83.00 | 0 | 0.00 |
| 83.00 | 85.00 | 1 | 1.23 |

CLASS SITE R1
CLASS NO. 10 SITE NO. 1 BAND NO.04

SITE IS 5 BY 3 CENTERED ON: X 225 Y 39

223 224 225 226 227

| | | | | | |
|----|----|----|----|----|----|
| 38 | 40 | 43 | 43 | 43 | 43 |
| 39 | 40 | 43 | 43 | 43 | 43 |
| 40 | 37 | 39 | 39 | 37 | 37 |

MEAN: 40.9 VARIANCE: 6.4 STD: 2.5
MIN: 37.0 MAX: 43.0 RANGE: 6.0

HISTOGRAM

| LOW | HIGH | PTS | % |
|-------|-------|-----|-------------|
| 37.00 | 39.00 | 5 | 33.33 ***** |
| 39.00 | 41.00 | 2 | 13.33 ***** |
| 41.00 | 43.00 | 8 | 53.33 ***** |

CLASS SITE R1
CLASS NO. 10 SITE NO. 1 BAND NO.05

SITE IS 5 BY 3 CENTERED ON: X 225 Y 39

223 224 225 226 227

| | | | | | |
|----|----|----|----|----|----|
| 38 | 49 | 49 | 49 | 49 | 49 |
| 39 | 49 | 49 | 49 | 49 | 49 |
| 40 | 42 | 42 | 42 | 39 | 39 |

MEAN: 46.3 VARIANCE: 16.8 STD: 4.1
MIN: 39.0 MAX: 49.0 RANGE: 10.0

HISTOGRAM

| LOW | HIGH | PTS | % |
|-------|-------|-----|-------------|
| 39.00 | 41.00 | 2 | 13.33 ***** |
| 41.00 | 43.00 | 3 | 20.00 ***** |
| 43.00 | 45.00 | 0 | 0.00 |
| 45.00 | 47.00 | 0 | 0.00 |
| 47.00 | 49.00 | 10 | 66.67 ***** |

CLASS SITE R1
CLASS NO. 10 SITE NO. 1 BAND NO.06

SITE IS 5 BY 3 CENTERED ON: X 225 Y 39

223 224 225 226 227

| | | | | | |
|----|----|----|----|----|----|
| 38 | 47 | 50 | 50 | 47 | 47 |
| 39 | 47 | 50 | 50 | 47 | 47 |
| 40 | 40 | 45 | 45 | 43 | 43 |

MEAN: 46.5 VARIANCE: 8.7 STD: 2.9
MIN: 40.0 MAX: 50.0 RANGE: 10.0

HISTOGRAM

| LOW | HIGH | PTS | % |
|-------|-------|-----|-------------|
| 40.00 | 42.00 | 1 | 6.67 *** |
| 42.00 | 44.00 | 2 | 13.33 ***** |
| 44.00 | 46.00 | 2 | 13.33 ***** |
| 46.00 | 48.00 | 4 | 40.00 ***** |
| 48.00 | 50.00 | 4 | 26.67 ***** |

CLASS SITE R1
CLASS NO. 10 SITE NO. 1 BAND NO.07

SITE IS 5 BY 3 CENTERED ON: X 225 Y 39

223 224 225 226 227

| | | | | | |
|----|----|----|----|----|----|
| 38 | 40 | 44 | 44 | 40 | 40 |
| 39 | 40 | 44 | 44 | 40 | 40 |
| 40 | 38 | 36 | 36 | 36 | 36 |

MEAN: 39.9 VARIANCE: 9.4 STD: 3.1
MIN: 36.0 MAX: 44.0 RANGE: 8.0

HISTOGRAM

| LOW | HIGH | PTS | % |
|-------|-------|-----|-------------|
| 36.00 | 38.00 | 5 | 33.33 ***** |
| 38.00 | 40.00 | 6 | 40.00 ***** |
| 40.00 | 42.00 | 0 | 0.00 |
| 42.00 | 44.00 | 4 | 26.67 ***** |

CLASS
 CLASS NO. 10 SITE NO. 1 BAND NO.08

SITE IS 5 BY 3 CENTERED ON: X 225 Y 39

223 244 225 226 227

38 0 0 0 0 0
 39 30 24 31 20 59
 40 25 27 27 24 32

MEAN: 19.5 VARIANCE: 286.1 STD: 17.0
 MIN: 0.0 MAX: 59.0 RANGE: 59.0

HISTOGRAM

| LOW | HIGH | PTS | 2 |
|-------|-------|-----|-------------|
| 0.00 | 2.00 | 5 | 37.73 ***** |
| 2.00 | 4.00 | 0 | 0.00 |
| 4.00 | 6.00 | 0 | 0.00 |
| 6.00 | 8.00 | 0 | 0.00 |
| 8.00 | 10.00 | 0 | 0.00 |
| 10.00 | 12.00 | 0 | 0.00 |
| 12.00 | 14.00 | 0 | 0.00 |
| 14.00 | 16.00 | 0 | 0.00 |
| 16.00 | 18.00 | 0 | 0.00 |
| 18.00 | 20.00 | 1 | 6.67 *** |
| 20.00 | 22.00 | 0 | 0.00 |
| 22.00 | 24.00 | 2 | 13.33 ***** |
| 24.00 | 26.00 | 1 | 6.67 *** |
| 26.00 | 28.00 | 2 | 13.33 ***** |
| 28.00 | 30.00 | 1 | 6.67 *** |
| 30.00 | 32.00 | 2 | 13.33 ***** |
| 32.00 | 34.00 | 0 | 0.00 |
| 34.00 | 36.00 | 0 | 0.00 |
| 36.00 | 38.00 | 0 | 0.00 |
| 38.00 | 40.00 | 0 | 0.00 |
| 40.00 | 42.00 | 0 | 0.00 |
| 42.00 | 44.00 | 0 | 0.00 |
| 44.00 | 46.00 | 0 | 0.00 |
| 46.00 | 48.00 | 0 | 0.00 |
| 48.00 | 50.00 | 0 | 0.00 |
| 50.00 | 52.00 | 0 | 0.00 |
| 52.00 | 54.00 | 0 | 0.00 |
| 54.00 | 56.00 | 0 | 0.00 |
| 56.00 | 58.00 | 0 | 0.00 |
| 58.00 | 60.00 | 1 | 6.67 *** |

CLASS SITE 65.35
 CLASS NO. 11 SITE NO. 1 BAND NO.04

SITE IS 9 R1 9 CENTERED ON: X 253 Y 91

249 250 251 252 253 254 255 256 257

| | | | | | | | | | |
|----|----|----|----|----|----|----|----|----|----|
| R7 | 34 | 34 | 34 | 34 | 34 | 34 | 34 | 34 | 34 |
| R8 | 34 | 34 | 34 | 34 | 34 | 34 | 34 | 34 | 34 |
| R9 | 34 | 34 | 34 | 34 | 34 | 34 | 34 | 34 | 34 |
| R0 | 34 | 38 | 38 | 38 | 38 | 35 | 35 | 35 | 35 |
| R1 | 34 | 38 | 38 | 38 | 39 | 35 | 35 | 35 | 35 |
| R2 | 34 | 35 | 35 | 33 | 33 | 35 | 35 | 33 | 33 |
| R3 | 35 | 35 | 35 | 33 | 33 | 35 | 35 | 33 | 33 |
| R4 | 35 | 35 | 35 | 35 | 35 | 35 | 35 | 35 | 35 |
| R5 | 35 | 35 | 35 | 35 | 35 | 35 | 35 | 35 | 35 |

MEAN: 34.9 VARIANCE: 1.7 STD: 1.3
 MIN: 33.0 MAX: 38.0 RANGE: 5.0

HISTOGRAM

| LOW | HIGH | FIS | % |
|-------|-------|-----|-------------|
| 34.00 | 35.00 | 66 | 81.48 ***** |
| 35.00 | 37.00 | 7 | 8.64 **** |
| 37.00 | 39.00 | 8 | 9.88 **** |

CLASS SITE 60.35
 CLASS NO. 11 SITE NO. 1 BAND NO.05

SITE IS 9 R1 9 CENTERED ON: X 253 Y 91

249 250 251 252 253 254 255 256 257

| | | | | | | | | | |
|----|----|----|----|----|----|----|----|----|----|
| R7 | 38 | 38 | 38 | 38 | 38 | 38 | 38 | 41 | 41 |
| R8 | 37 | 37 | 37 | 37 | 37 | 35 | 35 | 37 | 37 |
| R9 | 37 | 37 | 37 | 37 | 37 | 35 | 35 | 37 | 37 |
| R0 | 36 | 39 | 39 | 39 | 39 | 36 | 36 | 36 | 36 |
| R1 | 36 | 39 | 39 | 39 | 39 | 36 | 36 | 36 | 36 |
| R2 | 39 | 39 | 39 | 37 | 37 | 37 | 37 | 35 | 35 |
| R3 | 39 | 39 | 39 | 37 | 37 | 37 | 37 | 35 | 35 |
| R4 | 40 | 37 | 37 | 37 | 37 | 40 | 40 | 40 | 40 |
| R5 | 40 | 37 | 37 | 37 | 37 | 40 | 40 | 40 | 40 |

MEAN: 37.6 VARIANCE: 2.5 STD: 1.6
 MIN: 35.0 MAX: 41.0 RANGE: 6.0

HISTOGRAM

| LOW | HIGH | FIS | % |
|-------|-------|-----|-------------|
| 35.00 | 37.00 | 48 | 59.26 ***** |
| 37.00 | 39.00 | 21 | 25.93 ***** |
| 39.00 | 41.00 | 12 | 14.81 ***** |

CLASS SITE 65.35
 CLASS NO. 11 SITE NO. 1 BAND NO.04

SITE IS 9 R1 9 CENTERED ON: X 253 Y 91

249 250 251 252 253 254 255 256 257

| | | | | | | | | | |
|----|----|----|----|----|----|----|----|----|----|
| R7 | 36 | 38 | 38 | 38 | 38 | 38 | 38 | 38 | 38 |
| R8 | 34 | 40 | 40 | 38 | 38 | 38 | 38 | 36 | 36 |
| R9 | 34 | 40 | 40 | 38 | 38 | 38 | 38 | 36 | 36 |
| R0 | 35 | 35 | 35 | 37 | 37 | 35 | 35 | 37 | 37 |
| R1 | 35 | 35 | 35 | 37 | 37 | 35 | 35 | 37 | 37 |
| R2 | 39 | 39 | 39 | 35 | 35 | 37 | 37 | 35 | 35 |
| R3 | 39 | 39 | 39 | 35 | 35 | 37 | 37 | 35 | 35 |
| R4 | 39 | 39 | 39 | 39 | 39 | 39 | 39 | 39 | 39 |
| R5 | 39 | 39 | 39 | 39 | 39 | 39 | 39 | 39 | 39 |

MEAN: 37.3 VARIANCE: 2.8 STD: 1.7
 MIN: 34.0 MAX: 40.0 RANGE: 6.0

HISTOGRAM

| LOW | HIGH | FIS | % |
|-------|-------|-----|-------------|
| 34.00 | 38.00 | 25 | 30.86 ***** |
| 36.00 | 37.00 | 32 | 39.50 ***** |
| 38.00 | 40.00 | 24 | 29.63 ***** |

CLASS SITE 60.35
 CLASS NO. 11 SITE NO. 1 BAND NO.07

SITE IS 9 R1 9 CENTERED ON: X 253 Y 91

249 250 251 252 253 254 255 256 257

| | | | | | | | | | |
|----|----|----|----|----|----|----|----|----|----|
| R7 | 32 | 34 | 34 | 32 | 32 | 32 | 32 | 34 | 34 |
| R8 | 32 | 32 | 32 | 32 | 32 | 34 | 34 | 34 | 34 |
| R9 | 32 | 32 | 32 | 32 | 32 | 34 | 34 | 34 | 34 |
| R0 | 32 | 32 | 32 | 32 | 32 | 32 | 32 | 34 | 34 |
| R1 | 32 | 32 | 32 | 32 | 32 | 32 | 32 | 34 | 34 |
| R2 | 32 | 32 | 32 | 30 | 30 | 34 | 34 | 32 | 32 |
| R3 | 32 | 32 | 32 | 30 | 30 | 34 | 34 | 32 | 32 |
| R4 | 32 | 32 | 32 | 32 | 32 | 32 | 32 | 32 | 32 |
| R5 | 32 | 32 | 32 | 32 | 32 | 32 | 32 | 32 | 32 |

MEAN: 32.4 VARIANCE: 1.0 STD: 1.0
 MIN: 30.0 MAX: 34.0 RANGE: 4.0

HISTOGRAM

| LOW | HIGH | FIS | % |
|-------|-------|-----|-------------|
| 30.00 | 32.00 | 61 | 75.31 ***** |
| 32.00 | 34.00 | 20 | 24.69 ***** |

0140
 CHANNEL 13 SITE NO. 1 BAND NUMBER
 SITE IS 9 BY 9 CENTERED ON X 200 Y 91

| | | | | | | | | | |
|----|-----|-----|-----|-----|-----|-----|-----|-----|-----|
| | 249 | 250 | 251 | 252 | 253 | 254 | 255 | 256 | 257 |
| 51 | 61 | 53 | 61 | 33 | 61 | 89 | 67 | 81 | 81 |
| 46 | 53 | 47 | 47 | 34 | 56 | 70 | 49 | 50 | 50 |
| 34 | 57 | 71 | 34 | 26 | 70 | 48 | 91 | 50 | 50 |
| 67 | 108 | 106 | 81 | 91 | 77 | 50 | 41 | 34 | 34 |
| 38 | 54 | 97 | 94 | 123 | 100 | 94 | 83 | 84 | 84 |
| 50 | 55 | 57 | 50 | 51 | 65 | 61 | 81 | 100 | 100 |
| 50 | 30 | 61 | 58 | 101 | 118 | 114 | 91 | 100 | 100 |
| 61 | 80 | 84 | 101 | 76 | 78 | 100 | 84 | 100 | 100 |
| 76 | 28 | 47 | 61 | 76 | 77 | 50 | 81 | 100 | 100 |

MEAN 67.4 VARIANCE 531.6 STD 23.1
 MIN 24.9 MAX 118.0 RANGE 93.1

HISTOGRAM

| FROM | THRU | FREQ | % |
|--------|--------|------|----------|
| 24.90 | 30.00 | 4 | 4.94 ** |
| 30.00 | 35.00 | 0 | 0.00 |
| 35.00 | 40.00 | 4 | 4.94 ** |
| 40.00 | 45.00 | 1 | 1.23 |
| 45.00 | 50.00 | 1 | 1.23 |
| 50.00 | 55.00 | 0 | 0.00 |
| 55.00 | 60.00 | 0 | 0.00 |
| 60.00 | 65.00 | 0 | 0.00 |
| 65.00 | 70.00 | 3 | 3.70 * |
| 70.00 | 75.00 | 2 | 2.47 * |
| 75.00 | 80.00 | 3 | 3.70 * |
| 80.00 | 85.00 | 3 | 3.70 * |
| 85.00 | 90.00 | 4 | 4.94 ** |
| 90.00 | 95.00 | 1 | 1.23 |
| 95.00 | 100.00 | 4 | 4.94 ** |
| 100.00 | 105.00 | 6 | 7.41 *** |
| 105.00 | 110.00 | 0 | 0.00 |
| 110.00 | 115.00 | 0 | 0.00 |
| 115.00 | 120.00 | 4 | 4.94 ** |
| 120.00 | 125.00 | 1 | 1.23 |
| 125.00 | 130.00 | 3 | 3.70 * |
| 130.00 | 135.00 | 2 | 2.47 * |
| 135.00 | 140.00 | 2 | 2.47 * |
| 140.00 | 145.00 | 2 | 2.47 * |
| 145.00 | 150.00 | 1 | 1.23 |
| 150.00 | 155.00 | 1 | 1.23 |
| 155.00 | 160.00 | 1 | 1.23 |
| 160.00 | 165.00 | 1 | 1.23 |
| 165.00 | 170.00 | 0 | 0.00 |
| 170.00 | 175.00 | 0 | 0.00 |
| 175.00 | 180.00 | 2 | 2.47 * |
| 180.00 | 185.00 | 3 | 3.70 * |
| 185.00 | 190.00 | 2 | 2.47 * |
| 190.00 | 195.00 | 3 | 3.70 * |
| 195.00 | 200.00 | 2 | 2.47 * |
| 200.00 | 205.00 | 1 | 1.23 |
| 205.00 | 210.00 | 1 | 1.23 |
| 210.00 | 215.00 | 1 | 1.23 |
| 215.00 | 220.00 | 0 | 0.00 |
| 220.00 | 225.00 | 0 | 0.00 |
| 225.00 | 230.00 | 0 | 0.00 |
| 230.00 | 235.00 | 1 | 1.23 |
| 235.00 | 240.00 | 0 | 0.00 |
| 240.00 | 245.00 | 0 | 0.00 |
| 245.00 | 250.00 | 0 | 0.00 |
| 250.00 | 255.00 | 1 | 1.23 |

CLASS SITE 70.25
CLASS NO. 12 SITE NO. 1 BAND NO.04

SITE IS 3 BY 3 CENTERED ON: X 292 Y 282

291 292 293

281 27 29 29
282 29 28 28
283 29 28 28

MEAN: 28.4 VARIANCE: 0.5 STD: 0.7
MIN: 27.0 MAX: 29.0 RANGE: 2.0

HISTOGRAM

| LOW | HIGH | FIS | % |
|-------|-------|-----|--------------|
| 27.00 | 29.00 | 9 | 100.00 ***** |

CLASS SITE 70.25
CLASS NO. 12 SITE NO. 1 BAND NO.05

SITE IS 3 BY 3 CENTERED ON: X 292 Y 282

291 292 293

281 27 29 29
282 26 26 26
283 26 26 26

MEAN: 26.8 VARIANCE: 1.7 STD: 1.3
MIN: 26.0 MAX: 29.0 RANGE: 3.0

HISTOGRAM

| LOW | HIGH | FIS | % |
|-------|-------|-----|-------------|
| 26.00 | 26.00 | 7 | 77.78 ***** |
| 28.00 | 30.00 | 2 | 22.22 ***** |

CLASS SITE 70.25
CLASS NO. 12 SITE NO. 1 BAND NO.06

SITE IS 3 BY 3 CENTERED ON: X 292 Y 282

291 292 293

281 28 28 28
282 28 28 28
283 28 28 28

MEAN: 28.0 VARIANCE: 4.0 STD: 2.0
MIN: 28.0 MAX: 28.0 RANGE: 0.0

HISTOGRAM

| LOW | HIGH | FIS | % |
|-------|-------|-----|-------------|
| 28.00 | 28.00 | 7 | 77.78 ***** |
| 29.00 | 29.00 | 0 | 0.00 |
| 30.00 | 30.00 | 2 | 22.22 ***** |

CLASS SITE 70.25
CLASS NO. 12 SITE NO. 1 BAND NO.07

SITE IS 3 BY 3 CENTERED ON: X 292 Y 282

291 292 293

281 29 28 28
282 29 28 28
283 29 28 28

MEAN: 29.0 VARIANCE: 2.0 STD: 1.4
MIN: 28.0 MAX: 29.0 RANGE: 1.0

HISTOGRAM

| LOW | HIGH | FIS | % |
|-------|-------|-----|-------------|
| 28.00 | 28.00 | 7 | 77.78 ***** |
| 29.00 | 29.00 | 2 | 22.22 ***** |

CLASS
 CLASS NO. 12 SITE NO. 1 BAND NO.0E
 SITE IS 3 F1 3 CENTERED ON: X 292 Y 282
 291 292 293

281 29 100 57
 292 48 67 72
 293 77 26 52

MEAN: 58.7 VARIANCE: 473.5 STD: 21.8
 MIN: 29.0 MAX: 101.0 RANGE: 72.0

HISTOGRAM

| LOW | HIGH | FTS | % |
|--------|--------|-----|-------------|
| 28.00 | 30.00 | 1 | 11.11 ***** |
| 30.00 | 32.00 | 0 | 0.00 |
| 32.00 | 34.00 | 0 | 0.00 |
| 34.00 | 36.00 | 0 | 0.00 |
| 36.00 | 38.00 | 1 | 11.11 ***** |
| 38.00 | 40.00 | 0 | 0.00 |
| 40.00 | 42.00 | 0 | 0.00 |
| 42.00 | 44.00 | 1 | 11.11 ***** |
| 44.00 | 46.00 | 0 | 0.00 |
| 46.00 | 48.00 | 0 | 0.00 |
| 48.00 | 50.00 | 0 | 0.00 |
| 50.00 | 52.00 | 1 | 11.11 ***** |
| 52.00 | 54.00 | 0 | 0.00 |
| 54.00 | 56.00 | 0 | 0.00 |
| 56.00 | 58.00 | 1 | 11.11 ***** |
| 58.00 | 60.00 | 0 | 0.00 |
| 60.00 | 62.00 | 0 | 0.00 |
| 62.00 | 64.00 | 0 | 0.00 |
| 64.00 | 66.00 | 1 | 11.11 ***** |
| 66.00 | 68.00 | 0 | 0.00 |
| 68.00 | 70.00 | 1 | 11.11 ***** |
| 70.00 | 72.00 | 1 | 11.11 ***** |
| 72.00 | 74.00 | 0 | 0.00 |
| 74.00 | 76.00 | 0 | 0.00 |
| 76.00 | 78.00 | 0 | 0.00 |
| 78.00 | 80.00 | 0 | 0.00 |
| 80.00 | 82.00 | 0 | 0.00 |
| 82.00 | 84.00 | 0 | 0.00 |
| 84.00 | 86.00 | 0 | 0.00 |
| 86.00 | 88.00 | 0 | 0.00 |
| 88.00 | 90.00 | 0 | 0.00 |
| 90.00 | 92.00 | 0 | 0.00 |
| 92.00 | 94.00 | 0 | 0.00 |
| 94.00 | 96.00 | 0 | 0.00 |
| 96.00 | 98.00 | 0 | 0.00 |
| 98.00 | 100.00 | 0 | 0.00 |
| 100.00 | 102.00 | 1 | 11.11 ***** |

CLASS SITE 704F
 CLASS NO. 13 SITE NO. 1 BAND NO.06

SITE IS 5 BY 5 CENTERED ON: X 326 Y 314

326 327 328 329 330

| | | | | | |
|-----|----|----|----|----|----|
| 312 | 23 | 23 | 21 | 21 | 23 |
| 313 | 23 | 24 | 21 | 21 | 23 |
| 314 | 25 | 25 | 23 | 23 | 25 |
| 315 | 25 | 25 | 23 | 23 | 25 |
| 316 | 25 | 25 | 25 | 25 | 25 |

MEAN: 23.6 VARIANCE: 2.2 STD: 1.5
 MIN: 21.0 MAX: 25.0 RANGE: 4.0

HISTOGRAM
 LOW HIGH PTS %
 21.00 23.00 14 56.00 *****
 23.00 25.00 11 44.00 *****

CLASS SITE 704F
 CLASS NO. 13 SITE NO. 1 BAND NO.04

SITE IS 5 BY 5 CENTERED ON: X 328 Y 314

326 327 328 329 330

| | | | | | |
|-----|----|----|----|----|----|
| 312 | 27 | 27 | 27 | 27 | 27 |
| 313 | 27 | 27 | 27 | 27 | 27 |
| 314 | 28 | 28 | 27 | 27 | 27 |
| 315 | 28 | 28 | 27 | 27 | 27 |
| 316 | 27 | 27 | 27 | 27 | 27 |

MEAN: 27.2 VARIANCE: 0.1 STD: 0.4
 MIN: 27.0 MAX: 28.0 RANGE: 1.0

HISTOGRAM
 LOW HIGH PTS %
 27.00 29.00 25 100.00 *****

CLASS
 CLASS NO. 13 SITE NO. 1 BAND NO.07

SITE IS 5 BY 5 CENTERED ON: X 328 Y 314

326 327 328 329 330

| | | | | | |
|-----|----|----|----|----|----|
| 312 | 20 | 20 | 18 | 18 | 20 |
| 313 | 20 | 20 | 18 | 18 | 20 |
| 314 | 20 | 20 | 22 | 22 | 22 |
| 315 | 20 | 20 | 22 | 22 | 22 |
| 316 | 20 | 20 | 20 | 20 | 20 |

MEAN: 20.2 VARIANCE: 1.6 STD: 1.3
 MIN: 18.0 MAX: 22.0 RANGE: 4.0

HISTOGRAM
 LOW HIGH PTS %
 18.00 20.00 19 76.00 *****
 20.00 22.00 6 24.00 *****

CLASS SITE 704F
 CLASS NO. 13 SITE NO. 1 BAND NO.05

SITE IS 5 BY 5 CENTERED ON: X 328 Y 314

326 327 328 329 330

| | | | | | |
|-----|----|----|----|----|----|
| 312 | 25 | 25 | 23 | 23 | 25 |
| 313 | 25 | 25 | 23 | 23 | 25 |
| 314 | 24 | 24 | 24 | 24 | 24 |
| 315 | 24 | 24 | 24 | 24 | 24 |
| 316 | 24 | 24 | 26 | 26 | 26 |

MEAN: 24.3 VARIANCE: 0.8 STD: 0.9
 MIN: 23.0 MAX: 26.0 RANGE: 3.0

HISTOGRAM
 LOW HIGH PTS %
 23.00 25.00 22 88.00 *****
 25.00 27.00 3 12.00 *****

CLASS

CLASS NO. 13 SITE NO. 1 BAND NO. 0P

SITE IS 5 BY 5 CENTERED ON: X 328 Y 314

306 327 328 329 330

| | | | | | |
|-----|-----|----|----|----|----|
| 311 | 97 | 28 | 90 | 71 | 98 |
| 313 | 127 | 93 | 78 | 67 | 36 |
| 314 | 29 | 53 | 24 | 59 | 86 |
| 315 | 89 | 33 | 46 | 43 | 22 |
| 316 | 102 | 85 | 92 | 95 | 40 |

MEAN: 69.7 VARIANCE: 915.7 STD: 30.4
 MIN: 22.0 MAX: 127.0 RANGE: 105.0

HISTOGRAM

| LOW | HIGH | PTS | % |
|--------|--------|-----|-----------|
| 22.00 | 24.00 | 2 | 8.00 **** |
| 24.00 | 26.00 | 0 | 0.00 |
| 26.00 | 28.00 | 1 | 4.00 ** |
| 28.00 | 30.00 | 1 | 4.00 ** |
| 30.00 | 32.00 | 0 | 0.00 |
| 32.00 | 34.00 | 1 | 4.00 ** |
| 34.00 | 36.00 | 0 | 0.00 |
| 36.00 | 38.00 | 1 | 4.00 ** |
| 38.00 | 40.00 | 1 | 4.00 ** |
| 40.00 | 42.00 | 0 | 0.00 |
| 42.00 | 44.00 | 1 | 4.00 ** |
| 44.00 | 46.00 | 1 | 4.00 ** |
| 46.00 | 48.00 | 0 | 0.00 |
| 48.00 | 50.00 | 0 | 0.00 |
| 50.00 | 52.00 | 0 | 0.00 |
| 52.00 | 54.00 | 1 | 4.00 ** |
| 54.00 | 56.00 | 0 | 0.00 |
| 56.00 | 58.00 | 0 | 0.00 |
| 58.00 | 60.00 | 1 | 4.00 ** |
| 60.00 | 62.00 | 0 | 0.00 |
| 62.00 | 64.00 | 0 | 0.00 |
| 64.00 | 66.00 | 0 | 0.00 |
| 66.00 | 68.00 | 0 | 0.00 |
| 68.00 | 70.00 | 0 | 0.00 |
| 70.00 | 72.00 | 1 | 4.00 ** |
| 72.00 | 74.00 | 0 | 0.00 |
| 74.00 | 76.00 | 0 | 0.00 |
| 76.00 | 78.00 | 1 | 4.00 ** |
| 78.00 | 80.00 | 0 | 0.00 |
| 80.00 | 82.00 | 0 | 0.00 |
| 82.00 | 84.00 | 0 | 0.00 |
| 84.00 | 86.00 | 1 | 4.00 ** |
| 86.00 | 88.00 | 2 | 8.00 **** |
| 88.00 | 90.00 | 2 | 8.00 **** |
| 90.00 | 92.00 | 1 | 4.00 ** |
| 92.00 | 94.00 | 1 | 4.00 ** |
| 94.00 | 96.00 | 1 | 4.00 ** |
| 96.00 | 98.00 | 2 | 8.00 **** |
| 98.00 | 100.00 | 0 | 0.00 |
| 100.00 | 102.00 | 1 | 4.00 ** |
| 102.00 | 104.00 | 0 | 0.00 |
| 104.00 | 106.00 | 0 | 0.00 |
| 106.00 | 108.00 | 0 | 0.00 |
| 108.00 | 110.00 | 0 | 0.00 |
| 110.00 | 112.00 | 0 | 0.00 |
| 112.00 | 114.00 | 0 | 0.00 |
| 114.00 | 116.00 | 0 | 0.00 |
| 116.00 | 118.00 | 0 | 0.00 |
| 118.00 | 120.00 | 0 | 0.00 |
| 120.00 | 122.00 | 0 | 0.00 |
| 122.00 | 124.00 | 0 | 0.00 |
| 124.00 | 126.00 | 0 | 0.00 |
| 126.00 | 128.00 | 1 | 4.00 ** |

CLASS SITE 704D
 CLASS NO. 14 SITE NO. 1 BAND NO.04

SITE IS 5 BY 5 CENTERED ON: X 321 Y 328

| | | | | | |
|-----|-----|-----|-----|-----|-----|
| | 319 | 320 | 321 | 322 | 323 |
| 326 | 31 | 31 | 31 | 34 | 34 |
| 327 | 31 | 31 | 31 | 34 | 34 |
| 328 | 30 | 34 | 34 | 30 | 30 |
| 329 | 30 | 34 | 34 | 30 | 30 |
| 330 | 30 | 33 | 33 | 30 | 30 |

MEAN: 31.8 VARIANCE: 3.1 STD: 1.8
 MIN: 30.0 MAX: 34.0 RANGE: 4.0

HISTOGRAM

| LOW | HIGH | FIS | % |
|-------|-------|-----|-------------|
| 30.00 | 32.00 | 17 | 40.00 ***** |
| 32.00 | 34.00 | 10 | 40.00 ***** |

CLASS SITE 704D
 CLASS NO. 14 SITE NO. 1 BAND NO.05

SITE IS 5 BY 5 CENTERED ON: X 321 Y 328

| | | | | | |
|-----|-----|-----|-----|-----|-----|
| | 319 | 320 | 321 | 322 | 323 |
| 326 | 32 | 32 | 32 | 34 | 34 |
| 327 | 32 | 32 | 32 | 34 | 34 |
| 328 | 31 | 33 | 33 | 33 | 33 |
| 329 | 31 | 33 | 33 | 33 | 33 |
| 330 | 30 | 33 | 33 | 30 | 30 |

MEAN: 32.4 VARIANCE: 1.5 STD: 1.2
 MIN: 30.0 MAX: 34.0 RANGE: 4.0

HISTOGRAM

| LOW | HIGH | FIS | % |
|-------|-------|-----|-------------|
| 30.00 | 32.00 | 11 | 44.00 ***** |
| 32.00 | 34.00 | 14 | 56.00 ***** |

CLASS SITE 704D
 CLASS NO. 14 SITE NO. 1 BAND NO.06

SITE IS 5 BY 5 CENTERED ON: X 321 Y 328

| | | | | | |
|-----|-----|-----|-----|-----|-----|
| | 319 | 320 | 321 | 322 | 323 |
| 326 | 30 | 31 | 31 | 31 | 31 |
| 327 | 30 | 31 | 31 | 31 | 31 |
| 328 | 30 | 33 | 33 | 30 | 30 |
| 329 | 30 | 33 | 33 | 30 | 30 |
| 330 | 32 | 32 | 32 | 30 | 30 |

MEAN: 31.0 VARIANCE: 1.2 STD: 1.1
 MIN: 30.0 MAX: 33.0 RANGE: 3.0

HISTOGRAM

| LOW | HIGH | FIS | % |
|-------|-------|-----|-------------|
| 30.00 | 32.00 | 21 | 84.00 ***** |
| 32.00 | 34.00 | 4 | 16.00 ***** |

CLASS
 CLASS NO. 14 SITE NO. 1 BAND NO.07

SITE IS 5 BY 5 CENTERED ON: X 321 Y 328

| | | | | | |
|-----|-----|-----|-----|-----|-----|
| | 319 | 320 | 321 | 322 | 323 |
| 326 | 28 | 28 | 28 | 28 | 28 |
| 327 | 28 | 28 | 28 | 28 | 28 |
| 328 | 26 | 28 | 28 | 26 | 26 |
| 329 | 26 | 28 | 28 | 26 | 26 |
| 330 | 26 | 28 | 28 | 28 | 28 |

MEAN: 27.4 VARIANCE: 0.8 STD: 0.9
 MIN: 26.0 MAX: 28.0 RANGE: 2.0

HISTOGRAM

| LOW | HIGH | FIS | % |
|-------|-------|-----|--------------|
| 26.00 | 28.00 | 25 | 100.00 ***** |

CLIFF NO. 14 SITE NO. 1 BANTON JOB
 108 15 2 H 5 CENTERED ON: > 321 Y 326

319 320 321 322 323

| | | | | | |
|-----|-----|-----|-----|----|----|
| 326 | 64 | 107 | 45 | 68 | 47 |
| 402 | 71 | 81 | 92 | 66 | 71 |
| 319 | 87 | 58 | 86 | 72 | 68 |
| 324 | 121 | 70 | 107 | 71 | 46 |
| 330 | 56 | 61 | 85 | 40 | 66 |

MEAN 70.8 VARIANCE: 400.9 SITE 1001
 STD 20.0 MAX 125.0 RANGE 88.0

Histogram

| Bin | From | To | Freq | % |
|--------|--------|---------|------|-------------|
| 31.00 | 35.00 | 40.00 | 1 | 4.00 ** |
| 35.00 | 40.00 | 45.00 | 2 | 8.00 **** |
| 40.00 | 45.00 | 45.00 | 0 | 0.00 |
| 45.00 | 45.00 | 50.00 | 1 | 4.00 ** |
| 50.00 | 50.00 | 55.00 | 1 | 4.00 ** |
| 55.00 | 55.00 | 60.00 | 0 | 0.00 |
| 60.00 | 60.00 | 65.00 | 0 | 0.00 |
| 65.00 | 65.00 | 70.00 | 2 | 8.00 **** |
| 70.00 | 70.00 | 75.00 | 0 | 0.00 |
| 75.00 | 75.00 | 80.00 | 0 | 0.00 |
| 80.00 | 80.00 | 85.00 | 0 | 0.00 |
| 85.00 | 85.00 | 90.00 | 2 | 8.00 **** |
| 90.00 | 90.00 | 95.00 | 1 | 4.00 ** |
| 95.00 | 95.00 | 100.00 | 7 | 28.00 ***** |
| 100.00 | 100.00 | 105.00 | 1 | 4.00 ** |
| 105.00 | 105.00 | 110.00 | 5 | 20.00 ***** |
| 110.00 | 110.00 | 115.00 | 0 | 0.00 |
| 115.00 | 115.00 | 120.00 | 0 | 0.00 |
| 120.00 | 120.00 | 125.00 | 0 | 0.00 |
| 125.00 | 125.00 | 130.00 | 0 | 0.00 |
| 130.00 | 130.00 | 135.00 | 0 | 0.00 |
| 135.00 | 135.00 | 140.00 | 0 | 0.00 |
| 140.00 | 140.00 | 145.00 | 0 | 0.00 |
| 145.00 | 145.00 | 150.00 | 0 | 0.00 |
| 150.00 | 150.00 | 155.00 | 0 | 0.00 |
| 155.00 | 155.00 | 160.00 | 0 | 0.00 |
| 160.00 | 160.00 | 165.00 | 0 | 0.00 |
| 165.00 | 165.00 | 170.00 | 0 | 0.00 |
| 170.00 | 170.00 | 175.00 | 0 | 0.00 |
| 175.00 | 175.00 | 180.00 | 0 | 0.00 |
| 180.00 | 180.00 | 185.00 | 0 | 0.00 |
| 185.00 | 185.00 | 190.00 | 0 | 0.00 |
| 190.00 | 190.00 | 195.00 | 0 | 0.00 |
| 195.00 | 195.00 | 200.00 | 0 | 0.00 |
| 200.00 | 200.00 | 205.00 | 0 | 0.00 |
| 205.00 | 205.00 | 210.00 | 0 | 0.00 |
| 210.00 | 210.00 | 215.00 | 0 | 0.00 |
| 215.00 | 215.00 | 220.00 | 0 | 0.00 |
| 220.00 | 220.00 | 225.00 | 0 | 0.00 |
| 225.00 | 225.00 | 230.00 | 0 | 0.00 |
| 230.00 | 230.00 | 235.00 | 0 | 0.00 |
| 235.00 | 235.00 | 240.00 | 0 | 0.00 |
| 240.00 | 240.00 | 245.00 | 0 | 0.00 |
| 245.00 | 245.00 | 250.00 | 0 | 0.00 |
| 250.00 | 250.00 | 255.00 | 0 | 0.00 |
| 255.00 | 255.00 | 260.00 | 0 | 0.00 |
| 260.00 | 260.00 | 265.00 | 0 | 0.00 |
| 265.00 | 265.00 | 270.00 | 0 | 0.00 |
| 270.00 | 270.00 | 275.00 | 0 | 0.00 |
| 275.00 | 275.00 | 280.00 | 0 | 0.00 |
| 280.00 | 280.00 | 285.00 | 0 | 0.00 |
| 285.00 | 285.00 | 290.00 | 0 | 0.00 |
| 290.00 | 290.00 | 295.00 | 0 | 0.00 |
| 295.00 | 295.00 | 300.00 | 0 | 0.00 |
| 300.00 | 300.00 | 305.00 | 0 | 0.00 |
| 305.00 | 305.00 | 310.00 | 0 | 0.00 |
| 310.00 | 310.00 | 315.00 | 0 | 0.00 |
| 315.00 | 315.00 | 320.00 | 0 | 0.00 |
| 320.00 | 320.00 | 325.00 | 0 | 0.00 |
| 325.00 | 325.00 | 330.00 | 0 | 0.00 |
| 330.00 | 330.00 | 335.00 | 0 | 0.00 |
| 335.00 | 335.00 | 340.00 | 0 | 0.00 |
| 340.00 | 340.00 | 345.00 | 0 | 0.00 |
| 345.00 | 345.00 | 350.00 | 0 | 0.00 |
| 350.00 | 350.00 | 355.00 | 0 | 0.00 |
| 355.00 | 355.00 | 360.00 | 0 | 0.00 |
| 360.00 | 360.00 | 365.00 | 0 | 0.00 |
| 365.00 | 365.00 | 370.00 | 0 | 0.00 |
| 370.00 | 370.00 | 375.00 | 0 | 0.00 |
| 375.00 | 375.00 | 380.00 | 0 | 0.00 |
| 380.00 | 380.00 | 385.00 | 0 | 0.00 |
| 385.00 | 385.00 | 390.00 | 0 | 0.00 |
| 390.00 | 390.00 | 395.00 | 0 | 0.00 |
| 395.00 | 395.00 | 400.00 | 0 | 0.00 |
| 400.00 | 400.00 | 405.00 | 0 | 0.00 |
| 405.00 | 405.00 | 410.00 | 0 | 0.00 |
| 410.00 | 410.00 | 415.00 | 0 | 0.00 |
| 415.00 | 415.00 | 420.00 | 0 | 0.00 |
| 420.00 | 420.00 | 425.00 | 0 | 0.00 |
| 425.00 | 425.00 | 430.00 | 0 | 0.00 |
| 430.00 | 430.00 | 435.00 | 0 | 0.00 |
| 435.00 | 435.00 | 440.00 | 0 | 0.00 |
| 440.00 | 440.00 | 445.00 | 0 | 0.00 |
| 445.00 | 445.00 | 450.00 | 0 | 0.00 |
| 450.00 | 450.00 | 455.00 | 0 | 0.00 |
| 455.00 | 455.00 | 460.00 | 0 | 0.00 |
| 460.00 | 460.00 | 465.00 | 0 | 0.00 |
| 465.00 | 465.00 | 470.00 | 0 | 0.00 |
| 470.00 | 470.00 | 475.00 | 0 | 0.00 |
| 475.00 | 475.00 | 480.00 | 0 | 0.00 |
| 480.00 | 480.00 | 485.00 | 0 | 0.00 |
| 485.00 | 485.00 | 490.00 | 0 | 0.00 |
| 490.00 | 490.00 | 495.00 | 0 | 0.00 |
| 495.00 | 495.00 | 500.00 | 0 | 0.00 |
| 500.00 | 500.00 | 505.00 | 0 | 0.00 |
| 505.00 | 505.00 | 510.00 | 0 | 0.00 |
| 510.00 | 510.00 | 515.00 | 0 | 0.00 |
| 515.00 | 515.00 | 520.00 | 0 | 0.00 |
| 520.00 | 520.00 | 525.00 | 0 | 0.00 |
| 525.00 | 525.00 | 530.00 | 0 | 0.00 |
| 530.00 | 530.00 | 535.00 | 0 | 0.00 |
| 535.00 | 535.00 | 540.00 | 0 | 0.00 |
| 540.00 | 540.00 | 545.00 | 0 | 0.00 |
| 545.00 | 545.00 | 550.00 | 0 | 0.00 |
| 550.00 | 550.00 | 555.00 | 0 | 0.00 |
| 555.00 | 555.00 | 560.00 | 0 | 0.00 |
| 560.00 | 560.00 | 565.00 | 0 | 0.00 |
| 565.00 | 565.00 | 570.00 | 0 | 0.00 |
| 570.00 | 570.00 | 575.00 | 0 | 0.00 |
| 575.00 | 575.00 | 580.00 | 0 | 0.00 |
| 580.00 | 580.00 | 585.00 | 0 | 0.00 |
| 585.00 | 585.00 | 590.00 | 0 | 0.00 |
| 590.00 | 590.00 | 595.00 | 0 | 0.00 |
| 595.00 | 595.00 | 600.00 | 0 | 0.00 |
| 600.00 | 600.00 | 605.00 | 0 | 0.00 |
| 605.00 | 605.00 | 610.00 | 0 | 0.00 |
| 610.00 | 610.00 | 615.00 | 0 | 0.00 |
| 615.00 | 615.00 | 620.00 | 0 | 0.00 |
| 620.00 | 620.00 | 625.00 | 0 | 0.00 |
| 625.00 | 625.00 | 630.00 | 0 | 0.00 |
| 630.00 | 630.00 | 635.00 | 0 | 0.00 |
| 635.00 | 635.00 | 640.00 | 0 | 0.00 |
| 640.00 | 640.00 | 645.00 | 0 | 0.00 |
| 645.00 | 645.00 | 650.00 | 0 | 0.00 |
| 650.00 | 650.00 | 655.00 | 0 | 0.00 |
| 655.00 | 655.00 | 660.00 | 0 | 0.00 |
| 660.00 | 660.00 | 665.00 | 0 | 0.00 |
| 665.00 | 665.00 | 670.00 | 0 | 0.00 |
| 670.00 | 670.00 | 675.00 | 0 | 0.00 |
| 675.00 | 675.00 | 680.00 | 0 | 0.00 |
| 680.00 | 680.00 | 685.00 | 0 | 0.00 |
| 685.00 | 685.00 | 690.00 | 0 | 0.00 |
| 690.00 | 690.00 | 695.00 | 0 | 0.00 |
| 695.00 | 695.00 | 700.00 | 0 | 0.00 |
| 700.00 | 700.00 | 705.00 | 0 | 0.00 |
| 705.00 | 705.00 | 710.00 | 0 | 0.00 |
| 710.00 | 710.00 | 715.00 | 0 | 0.00 |
| 715.00 | 715.00 | 720.00 | 0 | 0.00 |
| 720.00 | 720.00 | 725.00 | 0 | 0.00 |
| 725.00 | 725.00 | 730.00 | 0 | 0.00 |
| 730.00 | 730.00 | 735.00 | 0 | 0.00 |
| 735.00 | 735.00 | 740.00 | 0 | 0.00 |
| 740.00 | 740.00 | 745.00 | 0 | 0.00 |
| 745.00 | 745.00 | 750.00 | 0 | 0.00 |
| 750.00 | 750.00 | 755.00 | 0 | 0.00 |
| 755.00 | 755.00 | 760.00 | 0 | 0.00 |
| 760.00 | 760.00 | 765.00 | 0 | 0.00 |
| 765.00 | 765.00 | 770.00 | 0 | 0.00 |
| 770.00 | 770.00 | 775.00 | 0 | 0.00 |
| 775.00 | 775.00 | 780.00 | 0 | 0.00 |
| 780.00 | 780.00 | 785.00 | 0 | 0.00 |
| 785.00 | 785.00 | 790.00 | 0 | 0.00 |
| 790.00 | 790.00 | 795.00 | 0 | 0.00 |
| 795.00 | 795.00 | 800.00 | 0 | 0.00 |
| 800.00 | 800.00 | 805.00 | 0 | 0.00 |
| 805.00 | 805.00 | 810.00 | 0 | 0.00 |
| 810.00 | 810.00 | 815.00 | 0 | 0.00 |
| 815.00 | 815.00 | 820.00 | 0 | 0.00 |
| 820.00 | 820.00 | 825.00 | 0 | 0.00 |
| 825.00 | 825.00 | 830.00 | 0 | 0.00 |
| 830.00 | 830.00 | 835.00 | 0 | 0.00 |
| 835.00 | 835.00 | 840.00 | 0 | 0.00 |
| 840.00 | 840.00 | 845.00 | 0 | 0.00 |
| 845.00 | 845.00 | 850.00 | 0 | 0.00 |
| 850.00 | 850.00 | 855.00 | 0 | 0.00 |
| 855.00 | 855.00 | 860.00 | 0 | 0.00 |
| 860.00 | 860.00 | 865.00 | 0 | 0.00 |
| 865.00 | 865.00 | 870.00 | 0 | 0.00 |
| 870.00 | 870.00 | 875.00 | 0 | 0.00 |
| 875.00 | 875.00 | 880.00 | 0 | 0.00 |
| 880.00 | 880.00 | 885.00 | 0 | 0.00 |
| 885.00 | 885.00 | 890.00 | 0 | 0.00 |
| 890.00 | 890.00 | 895.00 | 0 | 0.00 |
| 895.00 | 895.00 | 900.00 | 0 | 0.00 |
| 900.00 | 900.00 | 905.00 | 0 | 0.00 |
| 905.00 | 905.00 | 910.00 | 0 | 0.00 |
| 910.00 | 910.00 | 915.00 | 0 | 0.00 |
| 915.00 | 915.00 | 920.00 | 0 | 0.00 |
| 920.00 | 920.00 | 925.00 | 0 | 0.00 |
| 925.00 | 925.00 | 930.00 | 0 | 0.00 |
| 930.00 | 930.00 | 935.00 | 0 | 0.00 |
| 935.00 | 935.00 | 940.00 | 0 | 0.00 |
| 940.00 | 940.00 | 945.00 | 0 | 0.00 |
| 945.00 | 945.00 | 950.00 | 0 | 0.00 |
| 950.00 | 950.00 | 955.00 | 0 | 0.00 |
| 955.00 | 955.00 | 960.00 | 0 | 0.00 |
| 960.00 | 960.00 | 965.00 | 0 | 0.00 |
| 965.00 | 965.00 | 970.00 | 0 | 0.00 |
| 970.00 | 970.00 | 975.00 | 0 | 0.00 |
| 975.00 | 975.00 | 980.00 | 0 | 0.00 |
| 980.00 | 980.00 | 985.00 | 0 | 0.00 |
| 985.00 | 985.00 | 990.00 | 0 | 0.00 |
| 990.00 | 990.00 | 995.00 | 0 | 0.00 |
| 995.00 | 995.00 | 1000.00 | 0 | 0.00 |

CLASS SITE 83.7
CLASS NO. 15 SITE NO. 1 BAND NO.06

SITE IS 5 BY 5 CENTERED ON: X 106 Y 60

104 105 106 107 108

58 35 35 36 36 37
59 35 35 36 36 37
60 34 34 34 34 36
61 34 34 34 34 36
62 34 34 34 34 34

MEAN: 34.9 VARIANCE: 1.3 STD: 1.1
MIN: 32.0 MAX: 36.0 RANGE: 4.0

HISTOGRAM

LOW HIGH PTS %
32.00 34.00 15 40.00 *****
34.00 36.00 10 40.00 *****

CLASS SITE 83.7
CLASS NO. 15 SITE NO. 1 BAND NO.06

SITE IS 5 BY 5 CENTERED ON: X 106 Y 60

104 105 106 107 108

58 40 40 37 37 37
59 40 40 37 37 37
60 38 34 34 34 36
61 34 34 34 34 36
62 38 38 38 38 38

MEAN: 36.6 VARIANCE: 4.7 STD: 2.2
MIN: 34.0 MAX: 40.0 RANGE: 6.0

HISTOGRAM

LOW HIGH PTS %
34.00 36.00 10 40.00 *****
36.00 38.00 11 44.00 *****
38.00 40.00 4 16.00 *****

CLASS SITE 83.7
CLASS NO. 15 SITE NO. 1 BAND NO.06

SITE IS 5 BY 5 CENTERED ON: X 106 Y 60

104 105 106 107 108

58 37 37 37 37 37
59 37 37 37 37 37
60 36 36 36 36 36
61 36 36 36 36 36
62 36 36 36 36 36

MEAN: 36.4 VARIANCE: 0.2 STD: 0.5
MIN: 36.0 MAX: 37.0 RANGE: 1.0

HISTOGRAM

LOW HIGH PTS %
36.00 37.00 25 100.00 *****

CLASS SITE 83.7
CLASS NO. 15 SITE NO. 1 BAND NO.07

SITE IS 5 BY 5 CENTERED ON: X 106 Y 60

104 105 106 107 108

58 32 32 32 32 34
59 32 32 32 32 34
60 32 32 32 32 34
61 32 32 32 32 34
62 32 32 32 32 34

MEAN: 31.8 VARIANCE: 1.1 STD: 1.1
MIN: 30.0 MAX: 34.0 RANGE: 4.0

HISTOGRAM

LOW HIGH PTS %
30.00 32.00 39 92.00 *****
32.00 34.00 2 8.00 *****

CLASS

CLASS NO. 15 SITE NO. 1 BAND NO.06

SITE IS 5 BY 5 CENTERED ON: X 106 Y 60

104 105 106 107 108

| | | | | | |
|----|----|----|----|----|----|
| 58 | 45 | 27 | 85 | 50 | 76 |
| 59 | 93 | 70 | 56 | 46 | 58 |
| 60 | 66 | 58 | 24 | 43 | 41 |
| 61 | 44 | 67 | 39 | 03 | 41 |
| 62 | 81 | 60 | 51 | 70 | 40 |

MEAN: 55.8 VARIANCE: 277.0 STD: 16.6
 MIN: 26.0 MAX: 93.0 RANGE: 67.0

HISTOGRAM

| LOW | HIGH | FREQ | % |
|-------|-------|------|------------|
| 26.00 | 28.00 | 2 | 6.00 **** |
| 28.00 | 30.00 | 0 | 0.00 |
| 30.00 | 32.00 | 0 | 0.00 |
| 32.00 | 34.00 | 0 | 0.00 |
| 34.00 | 36.00 | 0 | 0.00 |
| 36.00 | 38.00 | 0 | 0.00 |
| 38.00 | 40.00 | 1 | 4.00 ** |
| 40.00 | 42.00 | 1 | 4.00 ** |
| 42.00 | 44.00 | 1 | 4.00 ** |
| 44.00 | 46.00 | 4 | 16.00 **** |
| 46.00 | 48.00 | 0 | 0.00 |
| 48.00 | 50.00 | 1 | 4.00 ** |
| 50.00 | 52.00 | 2 | 8.00 **** |
| 52.00 | 54.00 | 1 | 4.00 ** |
| 54.00 | 56.00 | 1 | 4.00 ** |
| 56.00 | 58.00 | 2 | 8.00 **** |
| 58.00 | 60.00 | 0 | 0.00 |
| 60.00 | 62.00 | 2 | 8.00 **** |
| 62.00 | 64.00 | 0 | 0.00 |
| 64.00 | 66.00 | 1 | 4.00 ** |
| 66.00 | 68.00 | 0 | 0.00 |
| 68.00 | 70.00 | 2 | 8.00 **** |
| 70.00 | 72.00 | 1 | 4.00 ** |
| 72.00 | 74.00 | 0 | 0.00 |
| 74.00 | 76.00 | 0 | 0.00 |
| 76.00 | 78.00 | 0 | 0.00 |
| 78.00 | 80.00 | 0 | 0.00 |
| 80.00 | 82.00 | 1 | 4.00 ** |
| 82.00 | 84.00 | 0 | 0.00 |
| 84.00 | 86.00 | 1 | 4.00 ** |
| 86.00 | 88.00 | 0 | 0.00 |
| 88.00 | 90.00 | 0 | 0.00 |
| 90.00 | 92.00 | 0 | 0.00 |
| 92.00 | 94.00 | 1 | 4.00 ** |

REFERENCES CITED

- Allen, C. C., 1978, Desert varnish of the Sonoran desert--optical and electron microanalysis: *Jour. of Geology*, v. 86, pp. 743-752.
- Attema, B. P. W., L. G. den Hollander, Th. A. de Boer, D. Venk, W. J. Bradus, G. P. de Loor, H. van Kasteren, and J. van Kuilenburg, 1974, Radar cross sections of vegetation canopies determined by monostatic and bistatic scatterometry: *in* Environmental Research Institute of Michigan, Proceedings of the 9th Symposium on Remote Sensing of Environment, v. II, pp. 1457-1465.
- Ballew, G. I., 1975, A method for converting LANDSAT-1 MSS data to reflectance by means of ground calibration sites: Stanford Remote Sensing Lab Tech. Rep. 75-7, pp. 285-379.
- Bard, J. C., F. Asaro, and R. F. Heizer, 1978, Perspectives on the dating of prehistoric great basin petroglyphs by neutron activation analysis: *Archaeometry* 20, pp. 85-88.
- Bauman, A. J., 1976, Desert varnish and marine ferromanganese oxide nodules: congeneric phenonema: *Nature*, v. 259, pp. 387-388.
- Baumgardner, M. F., C. J. Johannsen, and S. J. Kristoff, 1969, Multi-spectral studies of soils and clay minerals: Proceedings of the German Soil Sci. Soc. Meetings, Hannover, West Germany, Sept.
- Beaumont, P., 1968, Salt weathering on the margin of the Great Ravin, Iran: *Geological Society of America Bulletin*, v. 79, pp. 1683-1684.
- Beckmann, P. and A. Spizzichino, 1963, The scattering of electromagnetic waves from rough surfaces: *McMillan*, New York, 128 pp.
- Billings, W. D. and R. J. Morris, 1951, Reflection of visible and infrared radiation from leaves of different ecological groups: *American Journal of Botany*, v. 38, pp. 327-331.
- Birkeland, P. W., 1974, Pedology, weathering, and geomorphological research: *Oxford University Press*, London, p. 285.
- Blake, W. P., 1904, Origin of pebble covered plains in desert regions: *Transactions of the American Institute of Mining Engineers*, v. 34, pp. 161-162.

- Blanchard, A. J., 1979, Realistic Earth/Land Radar Models: in Radar Geology: An Assessment, Report of Radar Geology Workshop, Snowmass, Colorado, July 16-20, 1979, NASA, JPL Publication 80-61, pp. 200-222.
- Bowers, S. A. and R. J. Hanks, 1965, Reflection of radiant energy from soils: Soil Sci. v. 100, pp. 130-138.
- Brennan, P. A. and J. C. Quade, 1967, Mechanical measurements of surface roughness, 1/10th to 100 mm: University of Nevada, NASA Tech. Letter 5.
- Brown, D. E., 1973. The natural vegetation communities of Arizona: Arizona Resource Information System Map, 1:500,000.
- Brown, W. M. and L. J. Porcello, 1969, An introduction to synthetic-aperture radar: IEEE Spectrum, v. 6, pp. 57-62.
- Bull, W. B., 1974, Geomorphic tectonic analysis of the vidal region. Information concerning site characteristics, Vidal Nuclear Generation Station: Southern California Edison Company, 1975, Appendix 2.5B, 66 pp.
- Bull, W. B., 1978, Personal communication: Professor, Department of Geology, University of Arizona, Tucson, Arizona.
- Bull, W. B., 1981, Personal communication, Professor, Department of Geology, University of Arizona, Tucson, Arizona.
- Bull, W. B., in preparation, Tectonic and climatic geomorphology of arid regions, Professor, Department of Geology, University of Arizona, Tucson, Arizona.
- Burns, R. G. and W. S. Fyfe, 1967, Crystal field theory and geochemistry of transition elements: Researches in Geochemistry, v. 2, p. 259.
- Carlton, S. G. and O. R. Mitchell, 1977, Image segmentation using texture and grey level: Proceedings IEEE Pattern Recognition and Image Processing, pp. 387-391.
- Chavez, P., Jr., 1979, Automatic shading correction and speckle noise mapping/removal techniques for radar image data: Presented at Radar Geology Workshop, Snowmass, Colorado, July 18.
- Chepil, W. S., 1950, Properties of soil which influence wind erosion: the governing principles of surface roughness: Soil Science, v. 69, pp. 149-162.

- Colwell, R. N., 1978, Interpretability of vegetation resources on various image types acquired from earth orbiting spacecraft: *Journal Applied Photo. Engineering*, v. 4, no. 3, pp. 107-117.
- Condit, H. R., 1970, The spectral reflectance of American soils: *Journal of Photogrammetric Engineering*, v. 36, pp. 955-966.
- Conners, R. W., and C. A. Harlow, 1980, A theoretical comparison of textural algorithms: *IEEE Transactions on Pattern Analysis and Machine Intelligence*, v. PAM1-2, no. 3, pp. 204-222.
- Cooke, R. U., 1970. Stone pavements in deserts: *Annals of the Association of American Geographers*, v. 60, pp. 560-577.
- Cooke, R. U. and A. Warren, 1973. *Geomorphology in deserts*: University of California Press, Berkeley, California, 374 pp.
- Cosgriff, R. L., W. H. Peake and R. C. Taylor, 1960, Terrain scattering properties for sensor system design (Terrain Handbook II): *Ohio State University, Columbus, Engineering Experiment Station Bulletin*, 181, v. 29, no. 3, 118 pp.
- Crowe, B. M., 1978, Cenozoic volcanic geology and probable age of inception of basin-range faulting in southeastern Chocolate Mountains, California: *Geological Society of America Bulletin*, v. 89, pp. 251-264.
- Crown, P. H. and S. Pawluck, 1974, Spectral signatures from selected soils in Edmonton-Vegreville area: in *Proceedings of the 2nd Canadian Symposium on Remote Sensing*, University of Guelph, Guelph, Ontario, Canada, v. II, pp. 449-462.
- Curcio, J. A., 1961, Evaluation of atmospheric aerosol particle size distribution from scattering measurement in visible and infrared: *Journal of the Optical Society of America*, v. 51, pp. 548-551.
- Daily, M., C. Elachi, T. Farr, W. Stromberg, S. Williams and G. Schaber, 1978, Application of multispectral radar and Landsat imagery to geologic mapping in Death Valley: *Jet Propulsion Publication* 78-19, 47 pp.
- Deane, R. A. and A. R. Domville, 1972, Side-looking radar systems and their potential application to earth-resource surveys--radar scattering from natural surfaces: *European Space Research Organization*. ESTEC Contract Report No. 1537/71 CR-137, 47 pp.
- Denny, C. S., 1965, Alluvial fans in the Death Valley regions, California and Nevada: *U.S. Geological Survey Professional Paper* 446, 62 pp.

- Dorn, R. I., 1980, A biological model of rock varnish formation: Abstracts, Pacific Division, American Association for the Advancement of Science, University of California, Davis, June 22-27, p. 50.
- Dorn, R. I. and T. M. Oberlander, 1981, Rock varnish origin, characteristics, and usage: Unpublished report, University of California, Berkeley, 20 pp.
- Eberly, L. D. and T. B. Stanley, 1978, Cenozoic stratigraphy and geologic history of southwestern Arizona: Geological Society of America Bulletin, v. 89, pp. 921-940.
- Ehleringer, J. R. and O. Björkman, 1978, Pubescence and leaf spectral characteristics in a desert shrub, Encelia farinosa: Oecologia, v. 36, pp. 151-162.
- Engel, C. G. and R. F. Sharp, 1958. Chemical data on desert varnish: Geological Society of America Bulletin, v. 69, pp. 487-518.
- Estes, J. E. and D. S. Simonett, 1975. Fundamentals of image interpretation, Chapter 14: in R. G. Reeves, Manual of Remote Sensing, American Society of Photogrammetry, pp. 869-1106.
- Evans, W. E., 1974, Marking ERTS images with a small mirror reflector: Journal of Photogrammetric Engineering, v. 40, pp. 665-671.
- Everett, J. and D. S. Simonett, 1976. Principles, concepts, and philosophical problems in remote sensing: in J. Lintz, Jr. and D. S. Simonett, eds., Remote Sensing of Environment, Addison-Wesley Publications, pp. 85-127.
- Fasler, F., 1980, Texture measurements from SEASAT-SAR image for urban land use interpretation: in American Society of Photogrammetry, Fall Technical Meeting, October, pp. PS-2-B-1, PS-2-B-10.
- Fenneman, H. M., 1931, Physiography of western United States: McGraw Hill, New York, 543 pp.
- Fleischhauer, L. H., 1978, Characteristics and identification of Quaternary fluvial deposits: in R. Gerson, W. B. Bull, L. H. Fleischhauer, L. R. McHargue, L. Mayer, E. H. H. Shih, and W. C. Tucker, Jr., Origin and distribution of gravel in stream systems of arid regions: University of Arizona, Department of Geosciences, v. 1, pp. 5-1, 5-22, Tucson, Arizona.

- Frye, J. C. and H. B. Willman, 1962, Morphostratigraphic units in Pleistocene stratigraphy: American Association of Petroleum Geologists Bulletin, v. 46, pp. 112-113.
- Gates, D. M., H. J. Keegan, J. C. Schleiter and V. R. Weidner, 1965, Spectral properties of plants: Applied Optics, v. 4, pp. 11-20.
- Gile, I. H., F. F. Peterson and R. B. Grossman, 1966, Morphological and genetic sequences of carbonate accumulation in desert soils: Soil Science, v. 101, no. 5, pp. 347-360.
- Goudie, A. S., 1978, Dust storms and their geomorphological implications: Journal of Arid Environments, v. 1, pp. 291-310.
- Goetz, A. F. H., 1976, Remote sensing geology--Landsat and beyond: Proceedings of Caltech/JPL Conference on Image Processing Technology, Data Sources, and Software for Commercial and Scientific Applications, Jet Propulsion Laboratory, Sp. 43-30, pp. 8-1, 8-8.
- Goodwin, A. J. H., 1960, Chemical alteration (patination of stone): in The application of quantitative methods in archaeology: Viking Viking Publication in Anthropology, v. 28, pp. 300-324.
- Haralick, R. M., 1979, Statistical and structural approaches to texture: Proceedings of IEEE, v. 67, no. 5, pp. 786-804.
- Haralick, R. M., K. Shanmugam and I. Dinstein, 1973, Textural features for image classification: IEEE Transactions on Systems, Man and Cybernetics, v. SMC-3, pp. 610-621.
- Harding, L., 1980, Petrology and tectonic setting of the Livingston Hills formation, Yuma County, Arizona: in J. P. Jenney and C. Stone, eds., Studies in western Arizona: Arizona Geological Society Digest, v. XII, pp. 135-146.
- Hayden, J. D., 1976, Pre-altithermal archaeology in the Sierra Pinacate, Sonora, Mexico: American Antiquities, v. 41, no. 3, pp. 274-288.
- Hipp, J. E., 1974. Soil electromagnetic parameters as functions of frequency, soil density, and soil moisture: Proceedings IEEE, v. 62, no. 1, pp. 98-103.
- Hoffer, R. M. and C. J. Johannsen, 1969, Ecological potentials in spectral signature analysis: in P. Johnson, ed., Remote Sensing in Ecology, University of Georgia Press, Athens, pp. 1-16.

- Honey, R. F., A. Prelat and R. J. P. Lyon, 1974, Stansort: Stanford Remote Sensing Laboratory pattern recognition and classification system, Proceedings of the 9th International Symposium on Remote Sensing of the Environment, ERIM, Ann Arbor, Michigan, pp. 857-905.
- Hooke, R. L., H. Yang and P. W. Weiblen, 1969, Desert varnish: an electron microprobe study: *Journal of Geology*, v. 77, pp. 275-288.
- Hsu, S. Y., 1978, Texture-tone analysis for automated land-use mapping: *Photogrammetric Engineering and Remote Sensing*, v. 44, no. 11, pp. 1393-1404.
- Hsu, S. Y., 1979, The Mahalanobis classifier with the generalized inverse approach for automated analysis of imagery texture data: *Computer Graphics and Image Processing*, v. 9, pp. 117-134.
- Hunt, C. B., 1954, Desert varnish: *Science*, v. 120, pp. 183-184.
- Hunt, C. B., 1961, Stratigraphy of desert varnish: U.S. Geological Survey Professional Paper 424-B, 194 pp.
- Hunt, G. R., 1977, Spectral signatures of particulate minerals in the visible and near infrared: *Geophysics*, v. 42, no. 3, pp. 501-513.
- Irons, J. R. and G. W. Peterson, 1981, Texture transforms of remote sensing data: *Remote Sensing of Environment*, v. 11, pp. 359-370.
- Jacobsen, M. R. and R. D. Lamoreaux, 1979, Instrumentation for the evaluation of selective surfaces at the University of Arizona: Proceedings of the 2nd Annual Conference on Absorber Surfaces for Solar Receivers, Boulder, Colorado, 24-25 January, 11 pp.
- Janza, F. J., 1975, Interaction mechanisms, Chapter 4: in R. G. Reeves, ed., *Manual of remote sensing*: American Society of Photogrammetry, v. 7, pp. 75-179.
- Janza, F. J., 1976, Passive microwave systems, Chapter 6: in T. Lintz, Jr. and D. S. Simonett, eds., *Remote sensing of environment*: Addison-Wesley, Reading, Massachusetts, pp. 194-233.
- Jensen, J. R., 1979, Spectral and textural features to classify elusive land cover at the urban fringe: *Professional Geographer*, v. 31, no. 4, pp. 400-409.
- Jensen, J. R. and D. L. Toll, 1982, Detecting residential land-use development at the urban fringe: *Photogrammetric Engineering and Remote Sensing*, v. 48, no. 14, pp. 629-643.

- Jessup, R. W., 1960, The stony tableland soils of the southeastern portion of the Australian arid zone and their evolutionary history: *Journal of Soil Science*, v. 11, pp. 188-196.
- Kearney, T. H., R. H. Pebbles and collaborators, 1960, *Arizona flora*: University of California Press, Berkeley, California, 1081 pp.
- Kristoff, S. J. and A. L. Zachary, 1974, Mapping soil features from multispectral scanner data: *Journal of Photogrammetric Engineering*, v. 40, pp. 1427-1434.
- Laudermilk, A. C., 1931, On the origin of desert varnish, *American Journal of Science*, v. 221, pp. 51-66.
- Lowdermilk, W. C. and H. L. Sundling, 1950, Erosional pavement, its formation and significance: *Transactions of the American Geophysical Union*, v. 31, pp. 96-100.
- Lowe, C. H. and D. E. Brown, 1973. The natural vegetation of Arizona: Arizona Resource Information System Cooperative Publication No. 2, 53 pp.
- Lundien, J. R., 1966, Terrain analysis by electromagnetic means: Radar responses to laboratory-prepared soil samples: U.S. Army Corps of Engineers, Waterways Experimental Station Technical Report 3-639, Report No. 2, 55 pp.
- Lynch, D., 1979, Personal communication: Research Associate, Department of Geology, University of Arizona, Tucson, Arizona.
- MacDonald, H. C., 1969 Geologic evaluation of radar imagery from Darien Province, Panama: *Modern Geology*, v. 7, pp. 1-64.
- MacDonald, H. C. and W. P. Waite, 1973, Imaging radars provide terrain texture and roughness parameters in semi-arid environments: *Modern Geology*, v. 4, pp. 145-158.
- Marsh, S. E. and R. J. P. Lyon, 1980, Quantitative relationships of near surface spectra to Landsat radiometer data: *Remote Sensing of Environment* (Elsevier), v. 10, pp. 241-261.
- Mathews, H. L., R. L. Cunningham and G. W. Petersen, 1973, Spectral reflectance of selected Pennsylvania soils: *Soil Science Society of America Proceedings*, v. 37, pp. 421-424.

- McGinnies, W. G., E. F. Haase, L. K. Lepley, J. S. Conn, H. B. Musick and K. E. Foster, 1974, A study to explore the use of orbital remote sensing to determine native arid plant distribution: Office of Arid Lands Studies, University of Arizona, Tucson, Arizona, 36 pp.
- McHargue, L. R., 1981, Late Quaternary deposition and pedogenesis on the Aguila Mountains piedmont, southwestern Arizona: Unpublished M.S. thesis, University of Arizona, Tucson, Arizona, 132 pp.
- McIntyre, D. S., 1958, Soil splash and the formation of surface crusts by raindrop impact: *Soil Science*, v. 85, pp. 261-266.
- Meigs, P., 1953, World distribution of arid and semiarid homoclimates: in UNESCO, *Reviews of Research on arid zone hydrology*: UNESCO, Paris, pp. 203-209.
- Merrill, B. P., 1898, Desert varnish: *United States Geological Survey Bulletin*, v. 150, pp. 389-391.
- Mitchell, O. R., C. R. Myers and W. Boyne, 1977, A max-min measure for image texture analysis: *IEEE Transactions on Computers*, pp. 408-414.
- Mooney, H. A., J. Ehleringer and O. Björkman, 1977, The energy balance of leaves of the evergreen desert shrub Atriplex hymenelytra: *Oecologia*, v. 29, pp. 301-310.
- Moore, R. K., 1975, Microwave remote sensors, Chapter 9: in R. G. Reeves, ed., *Manual of Remote Sensing: American Society of Photogrammetry*, v. 1, pp. 399-537.
- Moore, R. K., 1976, Active microwave systems, Chapter 7: in T. Lintz, Jr. and R. S. Simonett, eds., *Remote Sensing of Environment: Addison-Wesley Publishers, Reading, Massachusetts*, pp. 234-290.
- Musick, B. H., 1975. Barrenness of desert pavement in Yuma County, Arizona: *Journal of the Arizona Academy of Sciences*, v. 10, pp. 24-28.
- Musick, H. B., W. McGinnes, E. Haase and L. K. Lepley, 1973, ERTS-1 imagery and native plant distributions: *Proceedings of the 4th Annual Conference on Remote Sensing in Arid Lands*, pp. 338-346.
- Nassau, K., 1980, The causes of color: *Scientific American*, v. 243, no. 4, pp. 124-154.

- National Aeronautics and Space Administration, 1972, Data users handbook: ERTS Document No. 715d4249, Goddard Space Flight Center, Greenbelt, Maryland.
- Norwood, V. T., 1974. Balance between resolution and signal-to-noise ratio in scanner design for earth resources systems: SPIE Proceedings, Scanners and Images for Earth Observations, 51, 37.
- Palmer, J. M., 1979, Report of calibration no. 79-0001 on radiometrics model RMR-10 multispectral radiometer serial no. 1001: Radiometrics, unpublished report, Research Associate, Optical Sciences, University of Arizona, Tucson, Arizona, 8 pp.
- Parry, J. T., 1977, Interpretation techniques for X-band SLAR: 4th Canadian Symposium on Remote Sensing, Quebec City, May, Canadian Aeronautics and Space Institute, Ottawa, Canada, pp. 376-394.
- Peake, W. H. and T. L. Oliver, 1971, The response of terrestrial surfaces at microwave frequencies: United States Air Force Avionics Laboratory Report AFAC-TR-70-301, 255 pp.
- Perry, R. S. and J. B. Adams, 1978, Desert varnish: Evidence for cyclic deposition of manganese: Nature, v. 276, pp. 489-451.
- Peterson, F. P., 1980, Holocene soil formation under sodium salt influence in a playa-margin environment: Quaternary Research, v. 13. 172-186.
- Piech, K. R. and J. E. Walker, 1974, Interpretation of soils: Journal of Photogrammetric Engineering, v. 40, pp. 87-94.
- Potter, R. M. and G. R. Rossman, 1977, Desert varnish: importance of clay minerals: Science, v. 196, pp. 1446-1448.
- Reeves, R. G., ed., 1975, Manual of remote sensing: American Society of Photogrammetry, 2 vols., 2123 pp.
- Reynolds, S., B. Scarborough and D. Lynch, 1980, Personal communications: Arizona Bureau of Geology and Mineral Technology, Tucson, Arizona.
- Richardson, A. J. and C. L. Wiegand, 1977, Distinguishing vegetation from soil background: Photogrammetric Engineering and Remote Sensing, v. 43, pp. 721-726.

- Richardson, M. L., S. D. Clemmons and J. C. Walker, 1979, Soil survey of Santa Cruz and parts of Cochise and Pima Counties, Arizona: United States Department of Agriculture, Soil Conservation Service, and Forest Service and Agricultural Experiment Station, 104 pp. and maps.
- Sabins, F. F., Jr., 1978, Remote sensing principles and interpretation: W. H. Freeman and Company, San Francisco, 426 pp.
- Salisbury, J. W. and G. R. Hunt, 1974, Remote sensing of rock type in the visible and near-infrared: in Proceedings of the 9th International Symposium on Remote Sensing of Environment, Environmental Research Institute of Michigan, v. VIII, pp. 1953-1958.
- Schaber, G. G., G. L. Berlin and W. E. Brown, Jr., 1976, Variation in surface roughness within Death Valley, California: Geologic evaluation of 25 cm-wavelength radar images: Geological Society of America Bulletin, v. 87, pp. 29-41.
- Scheffer, F., R. Meyer and E. Kalk, 1963, Biologische Ursachen der Wustenlackbildung: Zeitschrift für Geomorphologie, v. 7, pp. 112-119.
- Schenker, A. R., 1977, Particle size distribution of late Cenozoic gravels on an arid region piedmont, Gila Mountain, Arizona: University of Arizona, unpublished M.A. thesis, 118 pp.
- Schowengerdt, R. A., 1978, Landsat digital image preprocessing/utility software documentation: Applied Remote Sensing Program, unpublished document, University of Arizona, Tucson, Arizona, 13 pp.
- Schowengerdt, R. A., 1979, Calscan users manual: University of Arizona, unpublished document, Tucson, Arizona, 43 pp.
- Schreier, H., 1977, Quantitative predictions of chemical soil conditions from multispectral airborne ground and laboratory measurements: in 4th Canadian Symposium on Remote Sensing, Canadian Aeronautics and Space Institute, Ottawa, Ontario, Canada, K1P, 5A5, pp. 106-108.
- Schuchman, R. and R. T. Lowry, 1977, Vegetation classification with digital X-band and L-band dual polarized SAR imagery: 4th Canadian Symposium on Remote Sensing, Quebec City, May, Canadian Aeronautics and Space Institute, Ottawa, Canada, pp. 444-458.
- Sellers, W. D. and R. H. Hill, 1974, eds., Arizona Climate 1931-1972: University of Arizona Press, p. 516.

- Shafiqullah, M., P. E. Damon, D. J. Lynch, S. J. Reynolds, W. A. Rehrig and R. H. Raymond, 1980, K-Ar geochronology and geologic history of southwestern Arizona and adjacent areas: in J. P. Jenney and C. Stone, eds., Studies in western Arizona: Arizona Geological Society Digest, v. XII, pp. 201-242.
- Sharon, D., 1962. On the nature of hamadas in Israel: Zeitschrift für Geomorphologie, v. 6, pp. 129-147.
- Sherman, J. W., III, 1970, Aperture-antenna analysis: in M. I. Skolnik, ed., RADAR Handbook: McGraw Hill, pp. 9-25.
- Shih, E. H. H., 1982, Documentation of DIAL programs in [302, 304]: University of Arizona, Office of Arid Lands Studies, unpublished report.
- Siegel, H. J., P. H. Swain and B. W. Smith, 1980, Parallel processing implementation of a contextual classifier for multispectral remote sensing data: in IEEE, 1980 Machine Processing of Remotely Sensed Data Symposium, IEEE CH1533-9, pp. 19-29.
- Simonett, D. S., 1968, Land evaluation studies with remote sensors in the infrared and radar regions: in J. A. Stewart, ed., Land evaluation: MacMillan, New York, pp. 349-366.
- Sinclair, T. R., M. M. Schreiber and R. M. Hoffer, 1973, Diffuse reflectance hypothesis for the pathway of solar radiation through leaves: Agronomy Journal, v. 65, pp. 276-283.
- Slater, P. N., 1980a, MRS "proof of concept" study on atmospheric corrections, atmospheric corrections using an orbital pointable imaging system: NASA Report No. TR1653, p. 80.
- Slater, P. N., 1980b, Remote sensing optics and optical systems: Addison-Wesley, London, p. 575.
- Springer, M. E., 1958, Desert pavement and vesicular layer of some soils of the desert on the Lahonton Basin, Nevada: Proceedings of the Soil Science Society of America, v. 22, pp. 63-66.
- Swain, P. H., 1978, Fundamentals of pattern recognition in remote sensing: in P. Swain and S. M. Davis, eds., Remote sensing: the quantitative approach: McGraw-Hill, Inc., New York, pp. 136-186.
- Swain, P. H. and S. M. Davis, eds., 1978, Remote sensing: the quantitative approach: McGraw-Hill, Inc., New York.

- Symmons, P. M. and C. F. Hemming, 1968, A note on wind-stable stone-mantles in the southern Sahara: *Geography Journal*, v. 134, pp. 60-69.
- Taranik, J. V., 1978, Characteristics of the Landsat system multispectral data system: U. S. Geological Survey, Open File Report 78-187, 76 pp.
- Tilton, J. C., P. H. Swain and S. B. Vardeman, 1980, Context distribution estimation for contextual classification of multispectral image data: *in* IEEE, 1980 Machine Processing of Remotely Sensed Data Symposium, IEEE CH1533-9, pp. 171-180.
- Tomiyasu, K., 1978, Tutorial review of synthetic-aperture radar (SAR) with applications to imaging of the ocean surface: *Proceedings, IEEE*, v. 66, no. 5, pp. 563-583.
- Tou, J. T. and R. C. Gonzalez, 1974, *Pattern recognition principles*: Addison-Wesley, Reading, Massachusetts.
- United States Department of Agriculture, Soil Conservation Service, 1975, *Soil Taxonomy*: USDA, SCS, Agriculture Handbook No. 436, 754 pp.
- University of Arizona, 1981a, *SADIE 2.4 Image processing software users manual*, 183 pp.
- University of Arizona, 1981b, *DIAL users guide*, 81 pp.
- Valenzuela, G. R., 1967, Depolarization of EM waves by slightly rough surfaces: *IEEE Transactions on Antennas and Propagation*, AP-15, pp. 552.
- Valenzuela, G. R., 1968, Scattering of electromagnetic waves from a tilted slightly rough surface: *Radio Science*, v. 3, pp. 1057-1066.
- Weszka, J., C. Dyer and A. Rosenfeld, 1976, A comparative study of texture measures for terrain classification: *IEEE Transactions, Systems, Man and Cybernetics*, SMC-6, pp. 269-285.
- Wiersma, D. J. and D. Landgrebe, 1976, The use of spatial characteristics for the improvement of multispectral classification of remotely sensed data: *Proceedings of the 1976 Symposium on Machine Processing of Remotely Sensed Data*, West Lafayette, Indiana, June 29-July, IEEE No. 76CH1103-1 MPRSD, pp. 2A-18, 2A-26.

- Wilson, E. D., 1933, Geology and mineral deposits of southern Yuma County: University of Arizona and the Arizona Bureau of Mines, Geological Series No. 7, Bulletin 134.
- Wilson, E. D., 1960, Geologic map of Yuma County, Arizona: Arizona Bureau of Mines and University of Arizona, Map, 1:375,000.
- Wilson, E. D., R. T. Moore and J. R. Cooper, 1969, Geologic map of Arizona: Arizona Bureau of Mines and U.S. Geological Survey, 1:500,000.
- Yaalon, D. H. and J. Dan, 1974. Accumulation and distribution of loess-derived deposits in the semidesert and desert fringe areas of Israel: Zeitschrift für Geomorphologie, N. F. Suppl. Bd., pp. 91-105.
- Yaalon, D. H. and E. Ganor, 1973, The influence of dust on soils during the Quaternary: Soil Science, v. 116, pp. 146-155.

Wilson, E. D., 1911. Geology and mineral resources of southern Texas. Country University of Arkansas and the National Bureau of Geology. Geological Survey No. 7. Bulletin 134.

Wilson, E. D., 1916. Geologic map of Iowa County, Arkansas. Bureau of Mines and Geology of Arkansas, pp. 1:125,000.

Wilson, E. D., E. T. Howe and A. E. Cooper, 1919. Geologic map of Arkansas. Bureau of Mines and Geology of Arkansas, pp. 1:100,000.

Yarrow, W. W. and A. Dyer, 1914. Accumulation and distribution of lead-zinc deposits in the sedimentary and igneous belts of Iowa. Iowa Geological Survey, Bulletin No. 1. pp. 1-100.

Yarrow, W. W. and E. Dyer, 1915. The influence of lead on zinc in the sedimentary belt of Iowa. Iowa Geological Survey, Bulletin No. 2. pp. 1-100.



3 9001 01470 5696